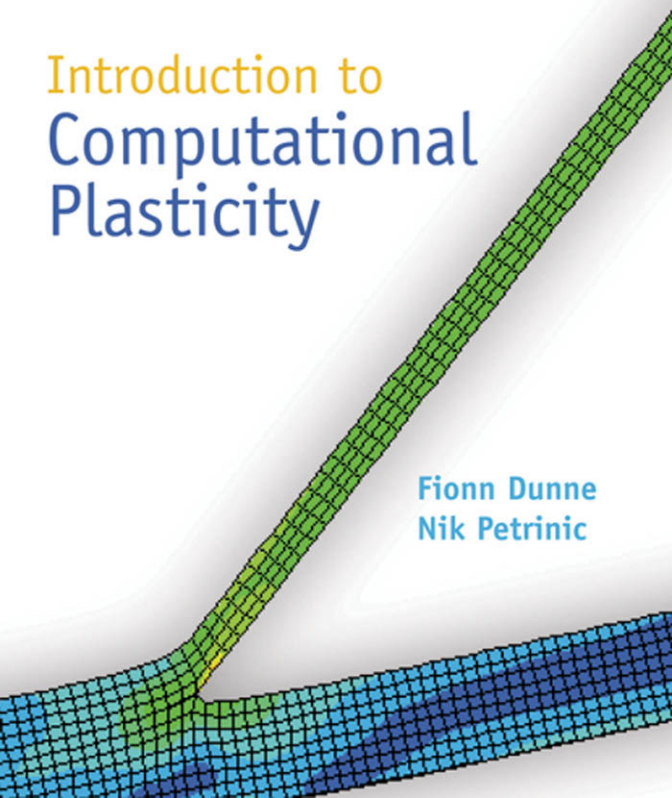


OXFORD

Introduction to
Computational
Plasticity

Fionn Dunne
Nik Petrinic



Introduction to Computational Plasticity

This page intentionally left blank

Introduction to Computational Plasticity

FIONN DUNNE AND NIK PETRINIC

*Department of Engineering Science
Oxford University, UK*

OXFORD
UNIVERSITY PRESS

OXFORD

UNIVERSITY PRESS

Great Clarendon Street, Oxford OX2 6DP

Oxford University Press is a department of the University of Oxford.
It furthers the University's objective of excellence in research, scholarship,
and education by publishing worldwide in

Oxford New York

Auckland Cape Town Dar es Salaam Hong Kong Karachi
Kuala Lumpur Madrid Melbourne Mexico City Nairobi
New Delhi Shanghai Taipei Toronto

With offices in

Argentina Austria Brazil Chile Czech Republic France Greece
Guatemala Hungary Italy Japan Poland Portugal Singapore
South Korea Switzerland Thailand Turkey Ukraine Vietnam

Oxford is a registered trade mark of Oxford University Press
in the UK and in certain other countries

Published in the United States
by Oxford University Press Inc., New York

© Oxford University Press, 2005

The moral rights of the authors have been asserted
Database right Oxford University Press (maker)

First published 2005
Reprinted 2006 (with corrections)

All rights reserved. No part of this publication may be reproduced,
stored in a retrieval system, or transmitted, in any form or by any means,
without the prior permission in writing of Oxford University Press,
or as expressly permitted by law, or under terms agreed with the appropriate
reprographics rights organization. Enquiries concerning reproduction
outside the scope of the above should be sent to the Rights Department,
Oxford University Press, at the address above

You must not circulate this book in any other binding or cover
and you must impose the same condition on any acquirer

British Library Cataloguing in Publication Data
(Data available)

Library of Congress Cataloging in Publication Data
(Data available)

Typeset by Newgen Imaging Systems (P) Ltd., Chennai, India
Printed in Great Britain
on acid-free paper by
Biddles Ltd, King's Lynn

ISBN 0-19-856826-6 (Hbk) 978-0-19-856826-1

3 5 7 9 10 8 6 4 2

To Hannah and Roberta, with love

This page intentionally left blank

Preface

The intention of this book is to bridge the gap between undergraduate texts in engineering plasticity and the many excellent books in computational plasticity aimed at more senior graduate students, researchers, and practising engineers working in solid mechanics. The book is in two parts. The first introduces microplasticity and covers continuum plasticity, the kinematics of large deformations and continuum mechanics, the finite element method, implicit and explicit integration of plasticity constitutive equations, and the implementation of the constitutive equations, and the associated material Jacobian, into finite element software. In particular, the implementation into the commercial code ABAQUS is addressed (and to help, we provide a range of ABAQUS material model UMATs), together, importantly, with the tests necessary to verify the implementation. Our intention, wherever possible, is to develop a good physical feel for the plasticity models and equations described by considering, at every stage, the simplification of the equations to uniaxial conditions. In addition, we hope to provide a reasonably physical understanding of some of the large deformation quantities (such as the continuum spin) and concepts (such as objectivity) which are often unfamiliar to many undergraduate engineering students who demand more than just a mathematical description.

The second part of the book introduces a range of plasticity models including those for superplasticity, porous plasticity, creep, cyclic plasticity, and thermo-mechanical fatigue (TMF). We also describe a number of practical applications of the plasticity models introduced to demonstrate the reasonable maturity of continuum plasticity in engineering practice.

We hope, above all, that this book will help all those—undergraduates, graduates, researchers, and practising engineers—who need to move on from knowledge of undergraduate plasticity to modern practice in computational plasticity. Our aims have been to encourage development of understanding, and ease of passage to the more advanced texts on computational plasticity.

This page intentionally left blank

Contents

Acknowledgements **xii**

Notation **xiii**

Part I. Microplasticity and continuum plasticity

1. Microplasticity	3
1.1 Introduction	3
1.2 Crystal slip	5
1.3 Critical resolved shear stress	7
1.4 Dislocations	8
Further reading	10
2. Continuum plasticity	11
2.1 Introduction	11
2.2 Some preliminaries	11
2.3 Yield criterion	17
2.4 Isotropic hardening	23
2.5 Kinematic hardening	27
2.6 Combined isotropic and kinematic hardening	36
2.7 Viscoplasticity and creep	38
Further reading	45
3. Kinematics of large deformations and continuum mechanics	47
3.1 Introduction	47
3.2 The deformation gradient	48
3.3 Measures of strain	49
3.4 Interpretation of strain measures	52
3.5 Polar decomposition	57

x Contents

3.6	Velocity gradient, rate of deformation, and continuum spin	60
3.7	Elastic–plastic coupling	66
3.8	Objective stress rates	69
3.9	Summary	81
	Further reading	82
4.	The finite element method for static and dynamic plasticity	83
4.1	Introduction	83
4.2	Hamilton’s principle	84
4.3	Introduction to the finite element method	96
4.4	Finite element equilibrium equations	100
4.5	Integration of momentum balance and equilibrium equations	136
	Further reading	142
5.	Implicit and explicit integration of von Mises plasticity	143
5.1	Introduction	143
5.2	Implicit and explicit integration of constitutive equations	143
5.3	Material Jacobian	150
5.4	Kinematic hardening	154
5.5	Implicit integration in viscoplasticity	161
5.6	Incrementally objective integration for large deformations	167
	Further reading	168
6.	Implementation of plasticity models into finite element code	169
6.1	Introduction	169
6.2	Elasticity implementation	170
6.3	Verification of implementations	171
6.4	Isotropic hardening plasticity implementation	172
6.5	Large deformation implementations	176
6.6	Elasto-viscoplasticity implementation	180

Part II. Plasticity models

7.	Superplasticity	185
7.1	Introduction	185
7.2	Some properties of superplastic alloys	185

7.3	Constitutive equations for superplasticity	189
7.4	Multiaxial constitutive equations and applications	192
	References	197
8.	Porous plasticity	199
8.1	Introduction	199
8.2	Finite element implementation of the porous material constitutive equations	201
8.3	Application to consolidation of Ti–MMCs	205
	References	207
9.	Creep in an aero-engine combustor material	209
9.1	Introduction	209
9.2	Physically based constitutive equations	209
9.3	Multiaxial implementation into ABAQUS	212
	References	217
	Appendix 9.1	218
10.	Cyclic plasticity, creep, and TMF	219
10.1	Introduction	219
10.2	Constitutive equations for cyclic plasticity	219
10.3	Constitutive equations for C263 undergoing TMF	222
	References	227
Appendix A:	Elements of tensor algebra	229
	Differentiation	231
	The chain rule	232
	Rotation	233
Appendix B:	Fortran coding available via the OUP website	235
Index		239

Acknowledgements

The authors would like to express their sincere gratitude to Esteban Busso for reading a draft and providing many helpful comments and suggestions, to Paul Buckley for the provision of the figures in Chapter 1, and to Jinguo Lin for permission to use Figures 7.9–7.14.

The authors acknowledge, with gratitude, permission granted to reproduce the following figures:

Figures 7.9–7.14: Elsevier Ltd, Oxford, UK.

Figures 8.1–8.6: Institute of Materials Communications Ltd, London, UK.

Figures 9.1–9.4, 10.1–10.3: Elsevier Ltd, Oxford, UK.

Notation

- Regular italic typeface (v, σ, \dots): scalars, scalar functions.
- Bold italic typeface ($\mathbf{P}, \mathbf{v}, \mathbf{A}, \boldsymbol{\sigma}, \dots$): points, vectors, tensors, vector and tensor functions.
- Helvetica bold italic typeface ($\mathbf{C}, \mathbf{c}, \mathbf{l}, \dots$): fourth order tensors.

Operations

$f(\cdot)$	function of (\cdot)
$\det[\cdot]$	determinant of $[\cdot]$
$\text{Tr}[\cdot]$	trace of $[\cdot]$
$\ln(\cdot)$	logarithm of (\cdot)
$\Delta[\cdot]$	increment of $[\cdot]$
$\frac{\partial}{\partial x}[\cdot]$	partial derivative of $[\cdot]$ with respect to x
$\nabla(\cdot) = \text{grad}[\cdot]$	gradient of $[\cdot]$
$\text{div}[\cdot] = \text{tr}[\nabla(\cdot)]$	divergence of $[\cdot]$
$\mathbf{x} \cdot \mathbf{y}$	scalar product of vectors
$\mathbf{x} \otimes \mathbf{y}$	dyadic product of vectors
$\boldsymbol{\sigma} : \boldsymbol{\varepsilon}$	double contraction of tensors
$ \mathbf{u} = \sqrt{\mathbf{u} \cdot \mathbf{u}}$	norm of vector
$ \mathbf{A} = \sqrt{\mathbf{A} : \mathbf{A}}$	norm of tensor

Some commonly used notation

\mathbf{C}	fourth-order tensor of material constants
\mathbf{D}	rate of deformation tensor
\mathbf{E}	Lagrangian strain tensor
E	Young's modulus
$\boldsymbol{\varepsilon}$	strain tensor

xiv Notation

F	deformation gradient
f	force vector field
ρ	density
I	second-order identity tensor
J	Jacobian
K	stiffness matrix
M	mass matrix
ν	Poisson's ratio
P	material particle
P	material point $\in \mathcal{R}^n$
R	rotation tensor
\mathcal{R}	real set
σ	Cauchy stress tensor
t	time
t	surface traction vector
u	displacement vector field
\dot{u}	velocity vector field
\ddot{u}	acceleration vector field
W	work

Part I. Microplasticity and continuum plasticity

This page intentionally left blank

1. Microplasticity

1.1 Introduction

This chapter briefly introduces the origins of yield and plastic flow, and in particular, attempts to explain the usual assumptions in simple continuum plasticity of isotropy, incompressibility, and independence of hydrostatic stress. While short, we introduce grains, crystal slip, slip systems, resolved shear stress, and dislocations; the minimum knowledge of microplasticity for users of continuum plasticity.

The origin of plasticity in crystalline materials is crystal slip. Metals are usually polycrystalline; that is, made up of many crystals in which atoms are stacked in a regular array. A typical micrograph for a polycrystalline nickel-base superalloy is shown in Fig. 1.1 in which the ‘crystal’ or grain boundaries can be seen. The grain size is about 100 μm . The grain boundaries demarcate regions of different crystallographic orientation.

If we represent the crystallographic structure of a tiny region of a single grain by planes of atoms, as shown in Fig. 1.2(a), we can then visualize plastic deformation taking place as shown in Fig. 1.2(a) and (b); this is crystallographic slip. Unlike elastic deformation, involving only the stretching of interatomic bonds, slip requires the breaking and re-forming of interatomic bonds and the motion of one plane of atoms relative to another. After shearing the crystal from configuration 1.2(a) to configuration 1.2(b), the structure is unchanged except at the extremities of the crystal.

A number of very important phenomena in macroscopic plasticity become apparent from just two Figs 1.1 and 1.2:

- (1) plastic slip does not lead to volume change; this is the incompressibility condition of plasticity;
- (2) plastic slip is a shearing process; hydrostatic stress, at the macrolevel, can often be assumed not to influence slip;
- (3) in a polycrystal, plastic yielding is often an isotropic process.

As we will see later, the incompressibility condition is very important in macro-scale plasticity and manifests itself at the heart of constitutive equations for plasticity.

4 Microplasticity

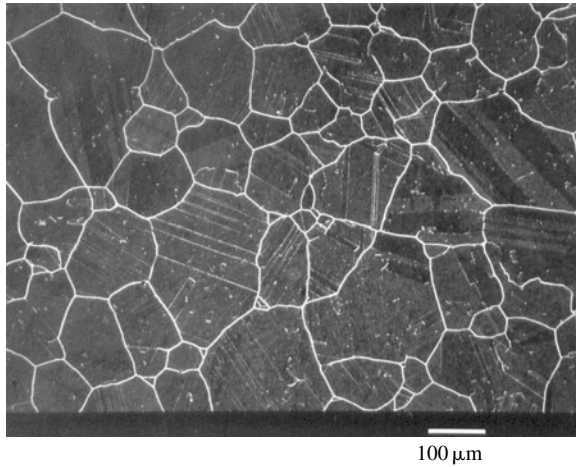


Fig. 1.1 Micrograph of polycrystal nickel-base alloy C263.

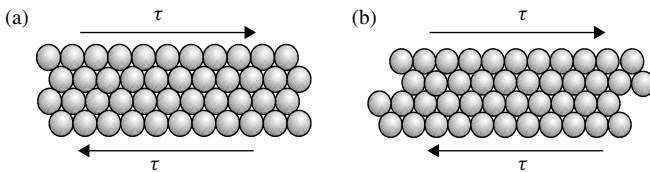


Fig. 1.2 Schematic representation of the crystallographic structure within a single grain undergoing slip.

However, not all plastic deformation processes are incompressible. A porous metal, for example, under compressive load may undergo plastic deformation during which the pores reduce in size. Consequently, there is a change of volume and a dependence on hydrostatic stress. However, the volume change does not originate from the plastic slip process itself, but from the pore closure.

The fact that plastic slip is a shearing process gives more information about the nature of yielding; in principle, it tells us that plastic deformation is independent of hydrostatic stress (pressure). For non-porous metals, this is one of the cornerstones of yield criteria. The von Mises criterion, for example, is one in which the initiation of macroscale yield is quite independent of hydrostatic stress. If we take a sample of the theoretical material shown schematically in Fig. 1.2(a) and submerge it to an ever deeper depth in an imaginary sea of water, the hydrostatic stress becomes ever larger but causes no more than the atoms in the theoretical material to come closer together. It will never in itself be able to generate the shearing necessary for crystallographic slip.

Figure 1.1 shows a micrograph of a polycrystal. If we assume that there is no preferred crystallographic orientation, but that the orientation changes randomly from one

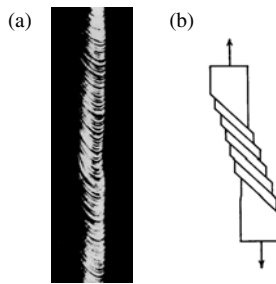


Fig. 1.3 (a) Photograph of a single zinc crystal and (b) a schematic diagram representing single slip in a single crystal.

grain to the next, and if our sample of material contains a sufficiently large number of grains, we can get a reasonable physical feel that macroscale yielding of the material will be isotropic. This is a further cornerstone of the von Mises yield criterion.

1.2 Crystal slip

The evidence for crystal slip being the origin of plasticity comes from mechanical tests carried out on *single crystals* of metals.

The single crystal of zinc shown in Fig. 1.3(a) is a few millimetres in width and has been loaded beyond yield in tension. The planes that can be seen are those on which slip has occurred resulting from many hundreds of dislocations running through the crystal and emerging at the edge. Each dislocation contributes just one Burger's vector of relative displacement, but with many such dislocations, the displacements become large. Figure 1.3(b) shows schematically what is happening in Fig. 1.3(a). The ends of the test sample have not been constrained in the lateral directions. It can be seen that single slip in this case leads to the horizontal displacement of one end relative to the other. Had this test been carried out in a conventional uniaxial testing machine, the lateral motion would have been prevented. In order to retain compatibility, then, with the imposed axial displacement, the slip planes would have to rotate towards the loading direction. The uniaxial loading therefore leads not only to crystallographic slip, but also to rotation of the crystallographic lattice.

1.2.1 Slip systems: slip directions and slip normals

Observations on single crystals show that slip tends to occur preferentially on certain crystal planes and in certain specific crystal directions. The combination of a slip

6 Microplasticity

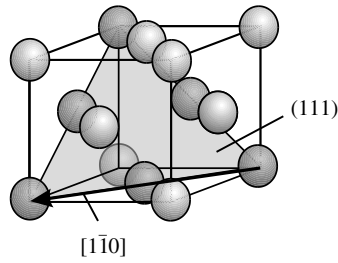


Fig. 1.4 The particular slip system $(111)[\bar{1}\bar{1}0]$ in an fcc lattice.

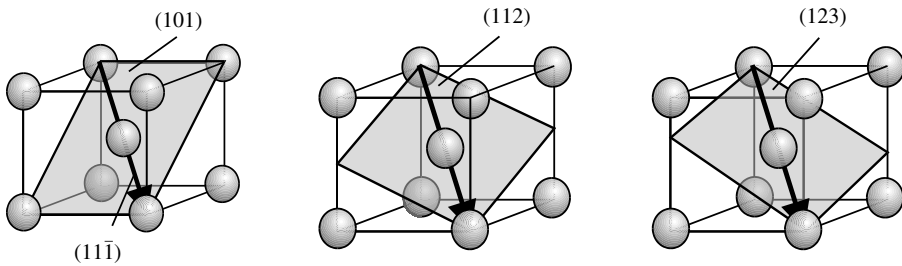


Fig. 1.5 Slip systems in bcc materials.

plane and a slip direction is called a slip system. These tend to be the most densely packed planes and the directions in which the atoms are packed closest together. This is explained in terms of dislocations. In face centred cubic (fcc) materials, the most densely packed planes are the diagonal planes of the unit cell. In fact the crystal is ‘close-packed’ in these planes; the observed slip systems are shown in Fig. 1.4.

The full family of slip systems in such crystals may be written as $\langle 1\bar{1}0 \rangle \{111\}$. There are 12 such systems in an fcc crystal (four planes each with three directions).

In body centre cubic (bcc) crystals, there are several planes that are of similar density of packing, and hence there are several families of planes on which slip occurs. However, there is no ambiguity about the slip direction, since the atoms are closest along the $[11\bar{1}]$ direction and those equivalent to it. The slip systems observed in bcc crystals are shown in Fig. 1.5.

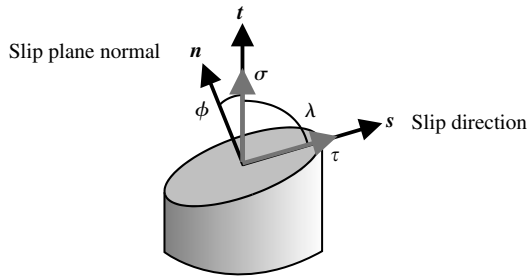
Thus, there are three families of slip systems operative:

$$\langle 11\bar{1} \rangle \{101\}; \quad \langle 11\bar{1} \rangle \{112\}; \quad \langle 11\bar{1} \rangle \{123\}.$$

Table 1.1 shows the slip systems found in single crystals of some of the important fcc and bcc pure metals together with the resolved shear stress required to cause slip—the critical resolved shear stress (CRSS).

Table 1.1 Slip systems and CRSS for some pure metals.

Metal	Structure	Slip systems	CRSS (MPa)
Cu	fcc	$\langle 1\bar{1}0 \rangle \{111\}$	0.64
Al	fcc	$\langle 1\bar{1}0 \rangle \{111\}$	0.40
Ni	fcc	$\langle 1\bar{1}0 \rangle \{111\}$	5.8
α -Fe	bcc	$\langle 11\bar{1} \rangle \{101\}$, $\langle 11\bar{1} \rangle \{112\}$, $\langle 11\bar{1} \rangle \{123\}$	32
Mo	bcc	$\langle 11\bar{1} \rangle \{101\}$	50
Ta	bcc	$\langle 11\bar{1} \rangle \{101\}$, $\langle 11\bar{1} \rangle \{112\}$, $\langle 11\bar{1} \rangle \{123\}$	50

**Fig. 1.6** A single crystal containing slip plane with normal n , slip direction s , and loaded in direction t .

1.3 Critical resolved shear stress

Suppose a single crystal in the shape of a rod is tested in tension. The axis of the rod is parallel to unit vector t . The crystal has an active *slip plane*, normal in direction of unit vector n . It has an active *slip direction* parallel to unit vector s , as shown in Fig. 1.6.

When the applied tensile stress is σ , the shear stress acting on the slip plane and in the slip direction is τ which may be found as follows: if the cross-sectional area of the rod is A , the force in the slip direction is $A\sigma \cos \lambda$ and it acts on an area $A/\cos \phi$ of the slip plane. Hence the resolved shear stress is

$$\tau = \sigma \cos \phi \cos \lambda = \sigma (\mathbf{t} \cdot \mathbf{n})(\mathbf{t} \cdot \mathbf{s}). \quad (1.1)$$

Slip will take place on the slip system, that is, the crystal will yield, when τ reaches the CRSS. This is known as Schmid's law. The data shown in Fig. 1.7 were obtained from tensile tests on cadmium single crystals which are hexagonal close packed (hcp). The measured yield stress depends upon the angle between the tensile loading direction and the basal plane. The minimum stress to cause yield occurs when the tensile axis is 45° to this plane, that is, when the shear stress is maximized. Schmid's law provides a good explanation for the observed behaviour.

8 Microplasticity

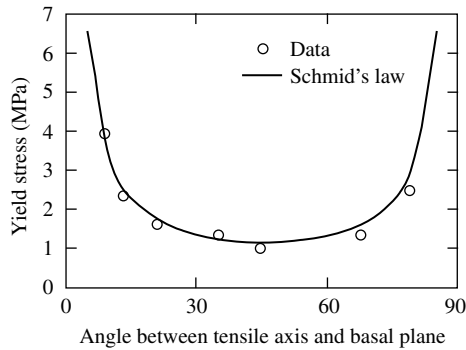


Fig. 1.7 The dependence of yield stress on the angle between the tensile axis and basal plane in an hcp cadmium single crystal.

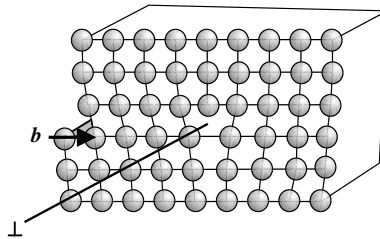


Fig. 1.8 An edge dislocation.

1.4 Dislocations

The theoretical shear strength of a crystal, calculated assuming that the shear is homogeneous (the entire crystal shears simultaneously on one plane), is given by

$$\tau_{\text{th}} = \frac{G}{2\pi}.$$

The expected shear strength is therefore very large; many orders of magnitude greater than the CRSS values are shown in Table 1.1. The assumption of homogeneous shear is, of course, wrong and plastic deformation in crystals normally occurs by the movement of the line defects known as *dislocations*, that are usually present in large numbers. The glide of a dislocation involves only very local rearrangements of atoms close to it, and requires a stress much lower than τ_{th} , thereby explaining the low observed values of CRSS.

Each dislocation is associated with a unit of slip displacement given by the *Burgers vector* \mathbf{b} . Since the dislocation is a *line* defect, there are two extreme cases. Figure 1.8 shows a schematic representation of an edge dislocation.

In this case the Burgers vector \mathbf{b} is *perpendicular* to the line of the dislocation, and the dislocation corresponds to the edge of a missing half-plane of atoms. Thus \mathbf{b} and

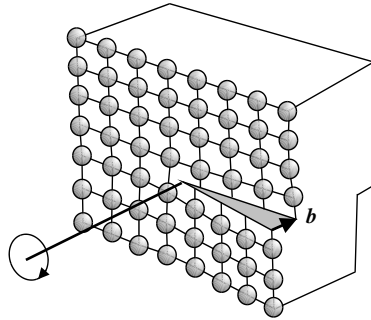


Fig. 1.9 A screw dislocation.

the dislocation line define a plane: a specific slip plane. If l is a unit vector parallel to the dislocation line, then

$$s = \frac{\mathbf{b}}{|\mathbf{b}|} \quad \text{and} \quad \mathbf{n} = \frac{\mathbf{b} \times \mathbf{l}}{|\mathbf{b}|}. \quad (1.2)$$

Figure 1.9 shows a schematic representation of a screw dislocation. This is the other extreme case where the Burger's vector is parallel to the dislocation line. The dislocation itself corresponds to a line of scissors-like shearing of the crystal. It follows from the fact that \mathbf{b} is parallel to l , that, although the slip direction s is defined, the slip plane \mathbf{n} is not. Hence, a screw dislocation can cause slip on any slip plane containing l . Dislocations are therefore vital in understanding yield and plastic flow.

We have said nothing about the important role of dislocations in strain hardening and softening. Nor have we discussed the effect of temperature on diffusivity which influences or controls many plastic deformation mechanisms including thermally activated dislocation climb leading to recovery, vacancy core and boundary diffusion, and grain boundary sliding. All of these subjects can be found in existing materials text books, some of which are listed below. Our aim has been to include sufficient material on microplasticity to ensure that the physical bases of at least some of the assumptions made in macrolevel continuum plasticity are understood.

There have been many developments over the last 25 years in physically based microplasticity modelling, including the development of time-independent and rate-dependent crystal plasticity. Here, for a given crystallographic lattice (e.g. fcc), using finite element techniques, the resolved shear stresses on all slip systems can be determined to find the active slip systems. Within either a time-independent or rate-dependent formulation, the slip on each active system can be determined from which the overall total deformation can be found. Such models are being used successfully for the plastic and creep deformation of single crystal materials which find application in aero-engines. The modelling of single crystal components has become

10 Microplasticity

possible with the development of high-performance computing. More recently, using finite element techniques, polycrystal plasticity models have been developed. Here, the understanding of microplasticity discussed above is also employed and again, as in single crystal plasticity, the active slip systems can be identified and the corresponding slips determined to give the overall deformation within a given grain. This is now done for all the grains in the polycrystal, which all have their own measured or specified crystallographic orientations, subject to the requirements of equilibrium and compatibility which are imposed within the finite element method. In order to do this, it is necessary to generate many finite elements within each grain. It is clear that for large numbers of grains, such polycrystal plasticity modelling becomes untenable. The consequence is that while desirable, it is not (for the foreseeable future) going to be feasible to carry out polycrystal plasticity modelling at the engineering component level. Currently, and for many years to come, the plastic deformation occurring in both the processing to produce engineering components, and occurring under in-service conditions at localized regions of a component, will continue to be modelled using continuum-level plasticity. This is particularly so in engineering industry where pressures of time and cost demand rapid analyses. We will now, therefore, leave microplasticity and address, in the remainder of the book, continuum-level plasticity.

Further reading

- Dieter, G.E. (1988). *Mechanical Metallurgy*. McGraw-Hill Book Co., London.
- Meyers, M.A., Armstrong, R.W., and Kirchner, H.O.K. (1999). *Mechanics and Materials. Fundamentals and Linkages*. John Wiley & Sons Inc., New York.

2. Continuum plasticity

2.1 Introduction

This chapter introduces the fundamentals of time-independent and rate-dependent continuum, or phenomenological plasticity: multiaxial yield, normality hypothesis, consistency condition, isotropic and kinematic hardening, and simple constitutive equations for viscoplasticity and creep. We assume throughout the chapter that we are dealing with small strain problems in the absence of large rigid body rotations. The kinematics of large deformations are left until the following chapter.

2.2 Some preliminaries

2.2.1 Strain decomposition

Figure 2.1 shows the idealized stress–strain behaviour which might be obtained from a purely uniaxial tensile test. Plasticity commences at a uniaxial stress of σ_y , after which the material strain hardens. It is called hardening because the stress is increasing relative to perfect plastic behaviour, also shown in the figure. If, at a strain of ε , the loading were to be reversed, the material would cease to deform plastically (at least in the absence of time-dependent effects) and would show a linearly decreasing stress with strain such that the gradient of this part of the stress–strain curve would

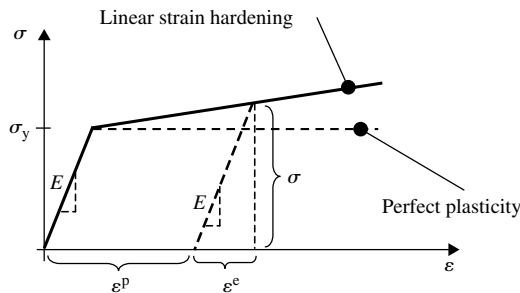


Fig. 2.1 The classical decomposition of strain into elastic and plastic parts.

12 Continuum plasticity

again be the Young's modulus, E , shown in Fig. 2.1. Once a stress of zero is achieved (provided the material remains elastic on full reversal of the load), the strain remaining in the test specimen is the plastic strain, ε^P . The recovered strain, ε^e , is the elastic strain and it can be seen that the total strain, ε , is the sum of the two

$$\varepsilon = \varepsilon^e + \varepsilon^P. \quad (2.1)$$

This is called the classical additive decomposition of strain. It is also apparent from Fig. 2.1 that the stress achieved at a strain of ε is given by

$$\sigma = E\varepsilon^e = E(\varepsilon - \varepsilon^P). \quad (2.2)$$

In many practical situations, particularly in materials processing operations such as forging or superplastic forming, for example, the strains achieved can be very large indeed, and of order 1–4. Compare the magnitude of this strain with that of typical elastic strains of order 0.001 (the 0.1% proof strain) which are generated in metals, even in forming processes (you can estimate this from the measured forces to give a stress, and the elastic strains are of order σ/E). In such circumstances, it is entirely reasonable to make the assumption that $\varepsilon^e \approx 0$ so that $\varepsilon^P \approx \varepsilon$.

2.2.2 Incompressibility condition

We saw in Chapter 1 that plastic deformation satisfies the incompressibility condition; that is, the deformation takes place without volume change. The consequence of this is that the sum of the plastic strain rate components is zero:

$$\dot{\varepsilon}_X^P + \dot{\varepsilon}_Y^P + \dot{\varepsilon}_Z^P = 0. \quad (2.3)$$

This is easily verified by considering a cube of material, with dimensions shown in Fig. 2.2, which undergoes purely plastic, uniform deformation (or simply argue that the strains are very large so that the elastic components are negligibly small).

Constancy of volume requires

$$xyz = x_0y_0z_0.$$

Differentiating both sides with respect to time, and dividing by xyz gives

$$\frac{\dot{x}}{x} + \frac{\dot{y}}{y} + \frac{\dot{z}}{z} = 0. \quad (2.4)$$

The strains are defined by

$$\varepsilon_X = \ln \left(\frac{x}{x_0} \right)$$

and similarly for ε_Y and ε_Z , and the strain rate in the Y -direction is therefore

$$\dot{\varepsilon}_Y = \frac{1}{y} \dot{y}.$$

Equation (2.4) is therefore the incompressibility condition given in Equation (2.3).

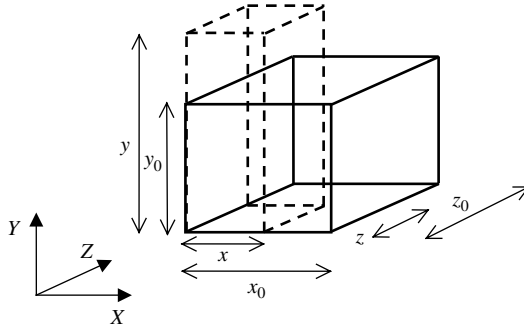


Fig. 2.2 An element of material undergoing plastic, incompressible, elongation in the Y -direction.

2.2.3 Effective stress and plastic strain rate

Identifying the yield condition for uniaxial, monotonically increasing load is straightforward:

If $\sigma < \sigma_y$ then the material is elastic,

If $\sigma \geq \sigma_y$ then the material has yielded.

It is not quite so straightforward for a multiaxial stress state; that is, one in which more than one direct stress exists. A whole range of multiaxial yield criteria exist. The most commonly used in engineering practice, particularly for computational analysis, is that of von Mises (to which we will return later), which relies on the knowledge of an effective stress, sometimes called (von Mises) equivalent stress. In terms of principal stresses, the effective stress is defined as

$$\sigma_e = \frac{1}{\sqrt{2}} [(\sigma_1 - \sigma_2)^2 + (\sigma_2 - \sigma_3)^2 + (\sigma_3 - \sigma_1)^2]^{1/2}, \quad (2.5)$$

or in terms of direct and shear stresses,

$$\sigma_e = \left[\frac{3}{2} (\sigma_{11}^2 + \sigma_{22}^2 + \sigma_{33}^2 + 2\sigma_{12}^2 + 2\sigma_{23}^2 + 2\sigma_{31}^2) \right]^{1/2}, \quad (2.6)$$

where we use the numerical subscripts 1, 2, and 3 in an equivalent way to X , Y , and Z to indicate direction. σ_e is, of course, a scalar quantity and its origin lies in the postulate that yielding occurs when a critical elastic shear energy is achieved. Mohr's circle tells us that in a given plane, the maximum shear stress is $\tau = (\sigma_1 - \sigma_2)/2$ so that with $\gamma = \tau/G$, the elastic shear energy per unit volume is $\tau\gamma/2 = \tau^2/2G = (\sigma_1 - \sigma_2)^2/8G$. The origin of the terms in Equation (2.5) then becomes apparent. An effective plastic strain rate, \dot{p} , is defined, similarly, as

$$\dot{p} = \frac{\sqrt{2}}{3} [(\dot{\epsilon}_1^p - \dot{\epsilon}_2^p)^2 + (\dot{\epsilon}_2^p - \dot{\epsilon}_3^p)^2 + (\dot{\epsilon}_3^p - \dot{\epsilon}_1^p)^2]^{1/2}. \quad (2.7)$$

14 Continuum plasticity

Writing the stress and plastic strain rate tensors (dropping the superscript p on the plastic strain rate components) as

$$\boldsymbol{\sigma} = \begin{pmatrix} \sigma_{11} & \sigma_{12} & \sigma_{13} \\ \sigma_{21} & \sigma_{22} & \sigma_{23} \\ \sigma_{31} & \sigma_{32} & \sigma_{33} \end{pmatrix} \quad \text{and} \quad \dot{\boldsymbol{\epsilon}} = \begin{pmatrix} \dot{\epsilon}_{11} & \dot{\epsilon}_{12} & \dot{\epsilon}_{13} \\ \dot{\epsilon}_{21} & \dot{\epsilon}_{22} & \dot{\epsilon}_{23} \\ \dot{\epsilon}_{31} & \dot{\epsilon}_{32} & \dot{\epsilon}_{33} \end{pmatrix} \quad (2.8)$$

then the effective stress and plastic strain rate may be written as

$$\begin{aligned} \sigma_e &= \left(\frac{3}{2} \boldsymbol{\sigma}' : \boldsymbol{\sigma}' \right)^{1/2} \\ \dot{p} &= \left(\frac{2}{3} \dot{\boldsymbol{\epsilon}}^p : \dot{\boldsymbol{\epsilon}}^p \right)^{1/2} \approx \left(\frac{2}{3} \dot{\boldsymbol{\epsilon}} : \dot{\boldsymbol{\epsilon}} \right)^{1/2} \end{aligned} \quad (2.9)$$

in which $\boldsymbol{\sigma}'$ is the deviatoric stress given by

$$\boldsymbol{\sigma}' = \boldsymbol{\sigma} - \frac{1}{3} \text{Tr}(\boldsymbol{\sigma}) \mathbf{I}, \quad (2.10)$$

for example

$$\begin{aligned} \sigma'_{11} &= \sigma_{11} - \frac{1}{3}(\sigma_{11} + \sigma_{22} + \sigma_{33}) \\ &= \frac{2}{3}\sigma_{11} - \frac{1}{3}(\sigma_{22} + \sigma_{33}) \end{aligned}$$

and

$$\sigma'_{12} = \sigma_{12} - 0 \equiv \sigma_{12}.$$

The deviatoric stress can be seen to be the difference between the stress and the mean stress, $\sigma_m = \frac{1}{3}(\sigma_{11} + \sigma_{22} + \sigma_{33})$; the latter is often called the hydrostatic stress. The symbol ‘:’ in Equations (2.9) is called the double contracted product, or double dot product, of two second-order tensors, which will be defined a little later in the chapter. The equations in (2.9) for the effective stress and plastic strain rates are a useful and compact way of writing the equations given in (2.5) and (2.7), respectively.

The coefficients in Equations (2.5) and (2.7) (and equivalently in Equations (2.9)) are chosen to ensure that under purely uniaxial loading, the effective stress σ_e is identical to the uniaxial stress and the effective plastic strain rate, \dot{p} , is identical to the uniaxial plastic strain rate.

Let us look at this in detail for the case in which a test specimen is loaded uniaxially upto large plastic strain (so that $\epsilon^e \ll \epsilon^p$, and $\epsilon \approx \epsilon^p$) under an applied stress σ_{11} , shown schematically in Fig. 2.3. We will now use Equation (2.9) to determine the effective stress and plastic strain rate.

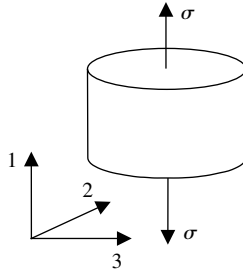


Fig. 2.3 Uniaxial loading of a schematic test piece.

In these circumstances, $\sigma_{11} = \sigma$, $\sigma_{22} = \sigma_{33} = 0$, and all the shear components are zero. The incompressibility condition leads to the requirement that

$$\dot{\epsilon}_{11} + \dot{\epsilon}_{22} + \dot{\epsilon}_{33} = 0. \quad (2.11)$$

Because of symmetry, $\dot{\epsilon}_{22} = \dot{\epsilon}_{33}$ so that incompressibility gives $\dot{\epsilon}_{22} = \dot{\epsilon}_{33} = -\frac{1}{2}\dot{\epsilon}_{11} = -\frac{1}{2}\dot{\epsilon}$. The deviatoric stress components can be determined using Equation (2.10) as

$$\begin{aligned} \sigma'_{11} &= \sigma_{11} - \frac{1}{3}(\sigma_{11} + \sigma_{22} + \sigma_{33}) \\ &= \frac{2}{3}\sigma_{11} \\ \sigma'_{22} &= \sigma_{22} - \frac{1}{3}(\sigma_{11} + \sigma_{22} + \sigma_{33}) \\ &= -\frac{1}{3}\sigma_{11}. \end{aligned}$$

Similarly,

$$\sigma'_{33} = -\frac{1}{3}\sigma_{11}$$

and

$$\sigma'_{12} = \sigma'_{23} = \sigma'_{33} = 0$$

so that the deviatoric stress tensor becomes, for uniaxial loading,

$$\boldsymbol{\sigma}' = \begin{pmatrix} \frac{2}{3}\sigma_{11} & 0 & 0 \\ 0 & -\frac{1}{3}\sigma_{11} & 0 \\ 0 & 0 & -\frac{1}{3}\sigma_{11} \end{pmatrix}. \quad (2.12)$$

We can now use Equation (2.9) to determine the effective stress for this trivial case, but we first need to find the contracted tensor product, $\boldsymbol{\sigma}' : \boldsymbol{\sigma}'$. This is defined, for two

16 Continuum plasticity

second-order tensors, \mathbf{A} and \mathbf{B} , by

$$\mathbf{A} : \mathbf{B} = \sum_{i=1}^n \sum_{j=1}^n A_{ij} B_{ij}. \quad (2.13)$$

That is, multiply component by component and sum the terms to give a scalar quantity. $\boldsymbol{\sigma}' : \boldsymbol{\sigma}'$ is therefore given by

$$\boldsymbol{\sigma}' : \boldsymbol{\sigma}' = \frac{4}{9}\sigma_{11}^2 + \frac{1}{9}\sigma_{11}^2 + \frac{1}{9}\sigma_{11}^2 = \frac{6}{9}\sigma_{11}^2 \equiv \frac{2}{3}\sigma^2$$

and so

$$\sigma_e = \left(\frac{3}{2} \boldsymbol{\sigma}' : \boldsymbol{\sigma}' \right)^{1/2} = \left(\frac{3}{2} \frac{2}{3} \sigma^2 \right)^{1/2} \equiv \sigma.$$

For a uniaxial stress state, therefore, $\sigma_e \equiv \sigma$. Let us follow the same procedure for the effective plastic strain rate.

With the incompressibility condition and symmetry conditions discussed above the plastic strain rate tensor becomes

$$\dot{\boldsymbol{\epsilon}} = \begin{pmatrix} \dot{\epsilon}_{11} & 0 & 0 \\ 0 & -\frac{1}{2}\dot{\epsilon}_{11} & 0 \\ 0 & 0 & -\frac{1}{2}\dot{\epsilon}_{11} \end{pmatrix} = \begin{pmatrix} \dot{\epsilon} & 0 & 0 \\ 0 & -\frac{1}{2}\dot{\epsilon} & 0 \\ 0 & 0 & -\frac{1}{2}\dot{\epsilon} \end{pmatrix}$$

so that

$$\begin{aligned} \dot{p} &= \left(\frac{2}{3} \dot{\boldsymbol{\epsilon}} : \dot{\boldsymbol{\epsilon}} \right)^{1/2} = \left[\frac{2}{3} \left(\dot{\epsilon}^2 + \frac{1}{4}\dot{\epsilon}^2 + \frac{1}{4}\dot{\epsilon}^2 \right) \right]^{1/2} \\ &= \left[\frac{2}{3} \frac{3}{2} \dot{\epsilon}^2 \right]^{1/2} = \dot{\epsilon}. \end{aligned}$$

For uniaxial loading, therefore, $\dot{p} = \dot{\epsilon}$. Note that the plastic strain rates appearing in Equation (2.9) are not given as deviatoric quantities, that is, $\boldsymbol{\epsilon}'$. This is because the plastic strain rate components are, in themselves, deviatoric due to the incompressibility condition. For example, consider the deviatoric component $\dot{\epsilon}'_{11}$ of plastic strain rate.

$$\dot{\epsilon}'_{11} = \dot{\epsilon}_{11} - \frac{1}{3}(\dot{\epsilon}_{11} + \dot{\epsilon}_{22} + \dot{\epsilon}_{33}).$$

Because of the incompressibility condition, therefore,

$$\dot{\epsilon}'_{11} \equiv \dot{\epsilon}_{11}.$$

2.3 Yield criterion

Only the von Mises yield criterion is considered here. There are many others including that of Tresca and the Gurson model for porous materials. In Chapter 1, we saw that there were several general requirements for yield in isotropic, non-porous materials. Let f be a yield function such that $f = 0$ is our yield criterion. Then:

1. Yield is independent of the hydrostatic stress.

Since f is independent of σ_m , it must be expressible in terms of the deviatoric stresses σ'_i ($i = 1, \dots, 3$) alone.

2. Yield in polycrystalline metals can be taken to be isotropic (provided we are concerned with yield in a volume of material containing many grains) and must therefore be independent of the labelling of the axes.

Thus f must be a *symmetric* function of σ'_i ($i = 1, \dots, 3$).

3. Yield stresses measured in compression have the same magnitude as yield stresses measured in tension.

Thus f must be an *even* function of σ'_i ($i = 1, \dots, 3$).

The von Mises yield function is defined by

$$f = \sigma_e - \sigma_y = \left(\frac{3}{2} \boldsymbol{\sigma}' : \boldsymbol{\sigma}' \right)^{1/2} - \sigma_y \quad (2.14)$$

and, with reference to Equation (2.5), it can be seen that it satisfies the three requirements given above. The yield criterion is given by

$$\begin{aligned} f < 0: & \text{Elastic deformation} \\ f = 0: & \text{Plastic deformation.} \end{aligned} \quad (2.15)$$

The second stress invariant, J_2 , is defined as $J_2 = (\frac{1}{2} \boldsymbol{\sigma} : \boldsymbol{\sigma})^{1/2}$ and it is for this reason that plastic flow based on the von Mises yield criterion is often referred to as J_2 plasticity. Geometrically, Equation (2.14) corresponds to a cylinder in three-dimensional principal stress space with axis lying along the line $\sigma_1 = \sigma_2 = \sigma_3$. It is apparent from this that hydrostatic stress has no effect on yield according to the von Mises criterion. Even infinite, but equal, principal stresses σ_1 , σ_2 , and σ_3 will never cause yield, since σ_e remains zero (see Equation (2.5)) and $f < 0$.

Let us consider the yield function in two-dimensional principal stress space by putting $\sigma_3 = 0$ and so imposing conditions of plane stress. Geometrically, this corresponds to finding the intersection between the von Mises cylinder and the plane $\sigma_3 = 0$.

18 Continuum plasticity

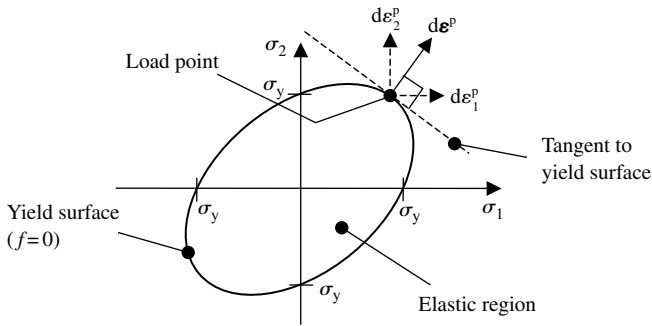


Fig. 2.4 The von Mises yield surface for conditions of plane stress, showing the increment in plastic strain, $d\epsilon^P$, in a direction normal to the tangent to the surface.

From Equations (2.14) and (2.5),

$$\begin{aligned} f &= \sigma_e - \sigma_y = \left(\frac{3}{2} \boldsymbol{\sigma} : \boldsymbol{\sigma} \right)^{1/2} - \sigma_y \\ &= \frac{1}{\sqrt{2}} [(\sigma_1 - \sigma_2)^2 + (\sigma_2 - \sigma_3)^2 + (\sigma_3 - \sigma_1)^2]^{1/2} - \sigma_y, \end{aligned}$$

which for plane stress, at yield, becomes

$$f = \frac{1}{\sqrt{2}} [(\sigma_1 - \sigma_2)^2 + \sigma_2^2 + \sigma_1^2]^{1/2} - \sigma_y = 0 \quad (2.16)$$

so

$$\sigma_1^2 - \sigma_1 \sigma_2 + \sigma_2^2 = \sigma_y^2,$$

which is the equation of an ellipse. The yield criterion is shown, for plane stress, in Fig. 2.4. Naturally, when $\sigma_1 = 0$, $\sigma_2 = \sigma_y$ at yield and similarly for the other points where the ellipse intersects the lines $\sigma_1 = 0$ and $\sigma_2 = 0$.

2.3.1 The normality hypothesis of plasticity

We have now looked at the conditions necessary to initiate yielding. The question then is what happens after that if loading continues? After yield comes plastic flow and the normality hypothesis of plasticity enables us to determine the ‘direction’ of flow. For what is termed associated flow, the hypothesis states that the increment in the plastic strain tensor is in a direction (i.e. relative to the principal stress directions) which is normal to the tangent to the yield surface at the load point. This is shown schematically in Fig. 2.4, but may be written in terms of the yield function, f , as

$$d\boldsymbol{\epsilon}^P = d\lambda \frac{\partial f}{\partial \boldsymbol{\sigma}} \quad \text{or} \quad \dot{\boldsymbol{\epsilon}}^P = \dot{\lambda} \frac{\partial f}{\partial \boldsymbol{\sigma}}. \quad (2.17)$$

In these expressions, the *direction* of the plastic strain increment (or equivalently, plastic strain rate) is given by $\partial f / \partial \boldsymbol{\sigma}$ while the magnitude is determined, for the plastic strain rate, by $\dot{\lambda}$. This is called the plastic multiplier which we shall return to later.

In order to look at this in more detail, and to make understanding easier, let us write the plastic strain rate and stress tensors in vector form (using what is known as Voigt notation, which we shall address in greater depth in Chapter 4). We will continue to consider principal components only, for the time being. Then for plane stress,

$$\boldsymbol{\sigma} = \begin{pmatrix} \sigma_1 \\ \sigma_2 \end{pmatrix}.$$

Note that the vector representation of the stress, $\boldsymbol{\sigma}$, is not italicized. This is the convention to be adopted throughout the book for stress and strain: an italicized bold $\boldsymbol{\sigma}$ and $\boldsymbol{\varepsilon}$ indicates a tensor, a non-italicized bold symbol a vector, or Voigt notation. The yield function f , written in terms of principal stresses is, from Equation (2.16)

$$f = \frac{1}{\sqrt{2}}[(\sigma_1 - \sigma_2)^2 + \sigma_2^2 + \sigma_1^2]^{1/2} - \sigma_y = 0,$$

and we can then determine the direction of plastic flow from Equation (2.17) as

$$\frac{\partial f}{\partial \boldsymbol{\sigma}} = \text{grad}(f) = \begin{pmatrix} \frac{\partial f}{\partial \sigma_1} \\ \frac{\partial f}{\partial \sigma_2} \end{pmatrix} = \begin{pmatrix} \frac{1}{2}(\sigma_1^2 - \sigma_1\sigma_2 + \sigma_2^2)^{-1/2}(2\sigma_1 - \sigma_2) \\ \frac{1}{2}(\sigma_1^2 - \sigma_1\sigma_2 + \sigma_2^2)^{-1/2}(2\sigma_2 - \sigma_1) \end{pmatrix},$$

which has direction $\begin{pmatrix} 2\sigma_1 - \sigma_2 \\ -\sigma_1 + 2\sigma_2 \end{pmatrix}$. This is normal to the yield surface at all points (e.g. choose $\sigma_1 = \sigma_2 = \alpha$, say, and the direction of the normal is clearly along the line $\sigma_1 = \sigma_2$). Let us now derive the plastic strain increment using the normality hypothesis with the von Mises yield criterion given in Equation (2.14), but using the other expression for effective stress for three-dimensions given in Equation (2.5). We will look at just one component, namely $d\varepsilon_1^p$, to see the general pattern emerge. From Equation (2.17), the first component of direction of plastic flow is given by

$$\begin{aligned} \frac{\partial f}{\partial \sigma_1} &= \frac{1}{2} \frac{1}{\sqrt{2}} [(\sigma_1 - \sigma_2)^2 + (\sigma_2 - \sigma_3)^2 + (\sigma_3 - \sigma_1)^2]^{-1/2} [2(\sigma_1 - \sigma_2) - 2(\sigma_3 - \sigma_1)] \\ &= \frac{(3/2)[\sigma_1 - (1/3)(\sigma_1 + \sigma_2 + \sigma_3)]}{\sigma_e} \end{aligned}$$

so

$$\frac{\partial f}{\partial \sigma_1} = \frac{3}{2} \frac{\sigma_1'}{\sigma_e}$$

20 Continuum plasticity

remembering the definition of deviatoric stress given in Equation (2.10). Similar results are obtained for the other components so that Equation (2.17) may be rewritten, for the von Mises yield criterion, as

$$d\boldsymbol{\epsilon}^P = d\lambda \frac{\partial f}{\partial \boldsymbol{\sigma}} = \frac{3}{2} d\lambda \frac{\boldsymbol{\sigma}'}{\sigma_e} \quad (2.18)$$

in which the stress and strain are now written as tensor quantities. Let us now look at the meaning of the plastic multiplier (at least, that is, for a von Mises material). We can use the expression for effective plastic strain rate in Equation (2.9) to write a similar expression for the increment in effective plastic strain as

$$dp = \left(\frac{2}{3} d\boldsymbol{\epsilon}^P : d\boldsymbol{\epsilon}^P \right)^{1/2}. \quad (2.19)$$

If we substitute Equation (2.18) into (2.19) we obtain

$$dp = \left(\frac{2}{3} \frac{3}{2} d\lambda \frac{\boldsymbol{\sigma}'}{\sigma_e} : \frac{3}{2} d\lambda \frac{\boldsymbol{\sigma}'}{\sigma_e} \right)^{1/2} = d\lambda \frac{((3/2)\boldsymbol{\sigma}' : \boldsymbol{\sigma}')^{1/2}}{\sigma_e}$$

so that with Equation (2.9) we obtain

$$dp = d\lambda \quad (2.20)$$

and similarly,

$$\dot{p} = \dot{\lambda}. \quad (2.21)$$

So, for a von Mises material, the plastic multiplier, $d\lambda$, turns out simply to be the increment in effective plastic strain. We can then rewrite the flow rule in Equation (2.18) as

$$d\boldsymbol{\epsilon}^P = \frac{3}{2} dp \frac{\boldsymbol{\sigma}'}{\sigma_e}. \quad (2.22)$$

In order for Equation (2.22) to be useful to us, we need to be able to calculate the increment in effective plastic strain, dp , or equivalently, the plastic multiplier, so that with prescribed loading, we can then calculate the increment in plastic strain components. We will address this next.

2.3.2 Consistency condition

Let us consider the case of uniaxial, tensile loading, for which the stress path taken relative to the yield surface is shown in Fig. 2.5.

Starting from zero stress, σ_2 then increases while the material deforms elastically until the load point (i.e. the point in stress space corresponding to the current loading) meets the yield surface at $\sigma_2 = \sigma_y$. At this point, the material behaves plastically,

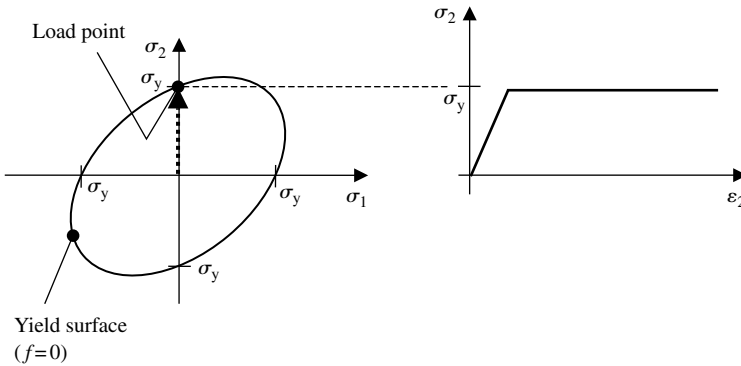


Fig. 2.5 The von Mises yield surface for plane stress and the corresponding stress–strain curve obtained for uniaxial straining in the 2-direction.

with no hardening, as shown in the resulting stress–strain curve in Fig. 2.5. With further plastic deformation, the load point remains on the yield surface and the stress remains constant and equal to σ_y . The requirement for the load point to remain on the yield surface during plastic deformation (at least, that is, for time-independent plasticity—we will look at viscoplasticity later) is called the consistency condition, and it is this that enables us to determine the plastic multiplier, or equivalently for a von Mises material, the increment in effective plastic strain.

The yield function given in Equation (2.14) includes a dependence on the stress components and the yield stress, σ_y . We will see later, when considering hardening, that the yield stress can increase (and sometimes decrease), and does so often as a function of effective plastic strain, p . It is therefore convenient to write the yield function as

$$f(\boldsymbol{\sigma}, p) = \sigma_e - \sigma_y = \sigma_e(\boldsymbol{\sigma}) - \sigma_y(p) = 0. \quad (2.23)$$

The consistency condition is written, for an incremental change in stress and effective plastic strain

$$f(\boldsymbol{\sigma} + d\boldsymbol{\sigma}, p + dp) = 0. \quad (2.24)$$

We can expand this as

$$f(\boldsymbol{\sigma} + d\boldsymbol{\sigma}, p + dp) = f(\boldsymbol{\sigma}, p) + \frac{\partial f}{\partial \boldsymbol{\sigma}} : d\boldsymbol{\sigma} + \frac{\partial f}{\partial p} dp. \quad (2.25)$$

Note that all terms in the equation are scalar. Let us work in principal stress space only. The advantage of this is simplicity; the disadvantage is that we ignore the complicating features of dealing with tensor versus engineering strain components. However, this will be dealt with in Chapters 4–6. We will therefore store stress and strain principal components as vectors, in Voigt notation, as discussed above. The product

22 Continuum plasticity

$\partial f / \partial \boldsymbol{\sigma} : d\boldsymbol{\sigma}$ then becomes the scalar (dot) product, $(\partial f / \partial \boldsymbol{\sigma}) \cdot d\boldsymbol{\sigma}$ of two vectors (this is only true in principal stress space, as we shall see later) which gives a scalar. Combining Equations (2.23)–(2.25) gives

$$\frac{\partial f}{\partial \boldsymbol{\sigma}} \cdot d\boldsymbol{\sigma} + \frac{\partial f}{\partial p} dp = 0. \quad (2.26)$$

We can use Hooke's law in incremental form to relate the stress and elastic strains, written as column vectors, by

$$d\boldsymbol{\sigma} = \mathbf{C} d\boldsymbol{\epsilon}^e = \mathbf{C}(d\boldsymbol{\epsilon} - d\boldsymbol{\epsilon}^p) \quad (2.27)$$

in which \mathbf{C} is the elastic stiffness matrix. We will use the most general form for the plastic strain increment, given in Equation (2.17), for now, but simplify for the case of the von Mises yield criterion later.

Substituting (2.17) into (2.27) gives

$$d\boldsymbol{\sigma} = \mathbf{C} \left(d\boldsymbol{\epsilon} - d\lambda \frac{\partial f}{\partial \boldsymbol{\sigma}} \right) \quad (2.28)$$

and (2.28) into (2.26)

$$\frac{\partial f}{\partial \boldsymbol{\sigma}} \cdot \mathbf{C} \left(d\boldsymbol{\epsilon} - d\lambda \frac{\partial f}{\partial \boldsymbol{\sigma}} \right) + \frac{\partial f}{\partial p} dp = 0. \quad (2.29)$$

We can obtain the most general form for dp , that is, without assuming a von Mises material for the time being, by using Equations (2.17) and (2.19) to give

$$dp = \left(\frac{2}{3} d\boldsymbol{\epsilon}^p : d\boldsymbol{\epsilon}^p \right)^{1/2} = \left(\frac{2}{3} d\lambda \frac{\partial f}{\partial \boldsymbol{\sigma}} : d\lambda \frac{\partial f}{\partial \boldsymbol{\sigma}} \right)^{1/2} = \left(\frac{2}{3} d\lambda \frac{\partial f}{\partial \boldsymbol{\sigma}} \cdot d\lambda \frac{\partial f}{\partial \boldsymbol{\sigma}} \right)^{1/2} \quad (2.30)$$

for principal stress space, in which the contracted tensor product simplifies to the scalar product. Substituting (2.30) into (2.29) and rearranging gives the plastic multiplier $d\lambda$

$$d\lambda = \frac{(\partial f / \partial \boldsymbol{\sigma}) \cdot \mathbf{C} d\boldsymbol{\epsilon}}{(\partial f / \partial \boldsymbol{\sigma}) \cdot \mathbf{C} (\partial f / \partial \boldsymbol{\sigma}) - (\partial f / \partial p) ((2/3) (\partial f / \partial \boldsymbol{\sigma}) \cdot (\partial f / \partial \boldsymbol{\sigma}))^{1/2}}. \quad (2.31)$$

The stress increment can then be determined by substituting (2.31) into (2.28) to give

$$\begin{aligned} d\boldsymbol{\sigma} &= \mathbf{C} \left(d\boldsymbol{\epsilon} - \frac{\partial f}{\partial \boldsymbol{\sigma}} \frac{(\partial f / \partial \boldsymbol{\sigma}) \cdot \mathbf{C} d\boldsymbol{\epsilon}}{(\partial f / \partial \boldsymbol{\sigma}) \cdot \mathbf{C} (\partial f / \partial \boldsymbol{\sigma}) - (\partial f / \partial p) ((2/3) (\partial f / \partial \boldsymbol{\sigma}) \cdot (\partial f / \partial \boldsymbol{\sigma}))^{1/2}} \right) \\ &= \left(\mathbf{C} - \mathbf{C} \frac{\partial f}{\partial \boldsymbol{\sigma}} \frac{(\partial f / \partial \boldsymbol{\sigma}) \cdot \mathbf{C}}{(\partial f / \partial \boldsymbol{\sigma}) \cdot \mathbf{C} (\partial f / \partial \boldsymbol{\sigma}) - (\partial f / \partial p) ((2/3) (\partial f / \partial \boldsymbol{\sigma}) \cdot (\partial f / \partial \boldsymbol{\sigma}))^{1/2}} \right) d\boldsymbol{\epsilon} \end{aligned} \quad (2.32)$$

or

$$d\boldsymbol{\sigma} = \mathbf{C}_{ep} d\boldsymbol{\varepsilon}. \quad (2.33)$$

\mathbf{C}_{ep} is called the tangential stiffness matrix. In the absence of plastic deformation, $d\lambda = 0$, and in this case, $\mathbf{C}_{ep} \equiv \mathbf{C}$, the elastic stiffness matrix. In the case of plastic deformation, with knowledge of the total strain increment, the stress increment can be obtained from Equation (2.32). Before looking at the plastic multiplier in more detail, to gain better physical insight, we will first introduce isotropic hardening.

2.4 Isotropic hardening

Many metals, when deformed plastically, harden; that is, the stress required to cause further plastic deformation increases, often as a function of accumulated plastic strain, p , which can be written as

$$p = \int dp = \int \dot{p} dt, \quad (2.34)$$

where \dot{p} and dp are given in (2.9) and (2.19), respectively. A uniaxial stress–strain curve with non-linear hardening is shown in Fig. 2.6 together with schematic representations of the initial and subsequent yield surfaces. In this instance, the subsequent yield surface is shown expanded compared with the original. When the expansion is uniform in all directions in stress space, the hardening is referred to as *isotropic*. Let us just consider what happens in going from elastic behaviour to plastic, hardening behaviour in Fig. 2.6.

Loading is in the 2-direction, so the load point moves in the σ_2 direction from zero until it meets the initial yield surface at $\sigma_2 = \sigma_y$. Yield occurs at this point. In order

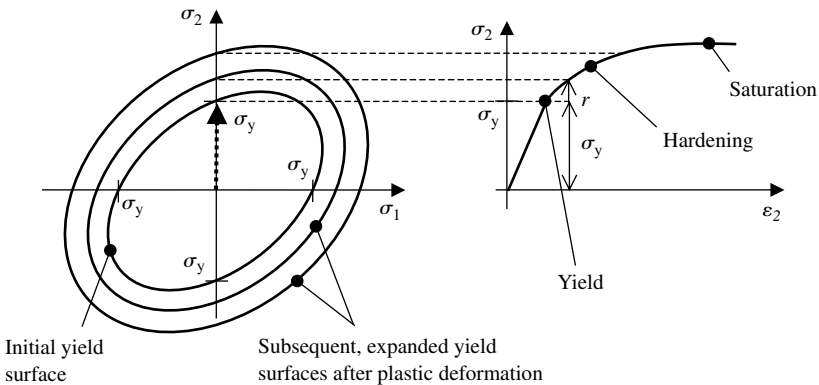


Fig. 2.6 Isotropic hardening, in which the yield surface expands with plastic deformation, and the corresponding uniaxial stress–strain curve.

24 Continuum plasticity

for hardening to take place, and for the load point to stay on the yield surface (the consistency condition requires this), the yield surface must expand as σ_2 increases, shown in Fig. 2.6. The amount of expansion is often taken to be a function of accumulated plastic strain, p , and for this case, the yield function becomes that given in (2.23),

$$f(\boldsymbol{\sigma}, p) = \sigma_e - \sigma_y(p) = 0, \quad (2.35)$$

where $\sigma_y(p)$ might be of the form

$$\sigma_y(p) = \sigma_{y0} + r(p) \quad (2.36)$$

in which σ_{y0} is the initial yield stress and $r(p)$ is called the isotropic hardening function. There are many forms used for $r(p)$ but a common one is

$$\dot{r}(p) = b(Q - r)\dot{p} \quad \text{or} \quad dr(p) = b(Q - r) dp \quad (2.37)$$

in which b and Q are material constants, which gives an exponential shape to the uniaxial stress–strain curve which *saturates* with increasing plastic strain, since integrating (2.37) with initial condition $r(0) = 0$, gives

$$r(p) = Q(1 - e^{-bp}). \quad (2.38)$$

Q is the saturated value of r so that the peak stress achieved with this kind of hardening, from Equation (2.36), is therefore $(\sigma_{y0} + Q)$. The constant b determines the rate at which saturation is achieved. Figure 2.6 shows an example of the uniaxial stress–strain behaviour predicted using this kind of isotropic hardening function.

Let us now consider a slightly simpler form of isotropic hardening and determine the plastic multiplier in Equation (2.31) and hence the stress increments in (2.32).

2.4.1 Linear isotropic hardening

We write the linear isotropic hardening function as

$$dr(p) = h dp \quad (2.39)$$

in which h is a constant. With this hardening, we expect the uniaxial stress–strain curve to look like that shown in Fig. 2.7. For uniaxial conditions, $dp = d\varepsilon^p$, and referring to Figs 2.6 and 2.7, the stress increase due to isotropic hardening is just dr , so using Equation (2.39) we may write

$$d\varepsilon^p = \frac{d\sigma}{h}$$

and, of course, the increment in elastic strain is just

$$d\varepsilon^e = \frac{d\sigma}{E}$$

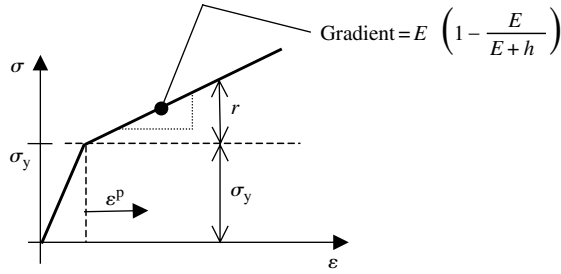


Fig. 2.7 Stress–strain curve for linear strain hardening with $dr = h d\varepsilon^p$.

so that the total strain is

$$d\varepsilon = \frac{d\sigma}{E} + \frac{d\sigma}{h} = d\sigma \left(\frac{E + h}{Eh} \right),$$

giving

$$d\sigma = E \left(1 - \frac{E}{E + h} \right) d\varepsilon.$$

The plastic multiplier has been derived, in Equation (2.31), in terms of the total strain increment. This is the most appropriate form when considering the development of computational techniques, including the finite element method in which, often, the total strain increments are provided, step by step, and it is then necessary to calculate the corresponding stress increments. However, in order to obtain better physical insight into the process, it is more appropriate (and simpler) to write the plastic multiplier in terms of a known stress increment. In this section, we will obtain the plastic multiplier in terms of the stress increment so that we can then examine the equations for a simple uniaxial problem using the von Mises yield criterion in Section 2.4.2.

Now, returning to the plastic multiplier and combining Equations (2.26) and (2.30), we obtain

$$\frac{\partial f}{\partial \boldsymbol{\sigma}} \cdot d\boldsymbol{\sigma} + \frac{\partial f}{\partial p} dp = \frac{\partial f}{\partial \boldsymbol{\sigma}} \cdot d\boldsymbol{\sigma} + \frac{\partial f}{\partial p} d\lambda \left(\frac{2}{3} \frac{\partial f}{\partial \boldsymbol{\sigma}} \cdot \frac{\partial f}{\partial \boldsymbol{\sigma}} \right) = 0. \quad (2.40)$$

Rearranging (2.40) gives the plastic multiplier, but now in terms of the stress increment, $d\boldsymbol{\sigma}$, as

$$d\lambda = \frac{-(\partial f / \partial \boldsymbol{\sigma}) \cdot d\boldsymbol{\sigma}}{(\partial f / \partial p) \left(\frac{2}{3} (\partial f / \partial \boldsymbol{\sigma}) \cdot (\partial f / \partial \boldsymbol{\sigma}) \right)}. \quad (2.41)$$

2.4.2 Uniaxial loading with linear isotropic hardening

Let us consider purely uniaxial loading, in the 1-direction, for a material that yields according to the von Mises criterion. In other words, we will apply a stress σ_1 in the

26 Continuum plasticity

1-direction, and all other stresses are zero. For simplicity, we will continue to work in principal stress space and represent the stresses in Voigt notation; that is, the stress is written in vector form as

$$\boldsymbol{\sigma} = \begin{bmatrix} \sigma_1 \\ \sigma_2 \\ \sigma_3 \end{bmatrix}.$$

We will now determine the plastic multiplier using Equation (2.41). We will consider the denominator first. With the hardening function given in (2.39), the yield function becomes

$$f(\boldsymbol{\sigma}, p) = \sigma_e(\boldsymbol{\sigma}) - \sigma_y(p) = \sigma_e(\boldsymbol{\sigma}) - \sigma_{y0} - r(p) = 0 \quad (2.42)$$

from which we can obtain

$$\frac{\partial f}{\partial p} = -\frac{\partial r}{\partial p} = -h. \quad (2.43)$$

For the von Mises yield criterion, $\partial f/\partial \boldsymbol{\sigma}$ can be obtained using Equation (2.18), with the deviatoric stress components taken from (2.12), as

$$\frac{\partial f}{\partial \boldsymbol{\sigma}} = \frac{3}{2} \frac{\boldsymbol{\sigma}'}{\sigma_e} = \frac{3}{2} \frac{1}{\sigma_1} \begin{bmatrix} \frac{2}{3}\sigma_1 \\ -\frac{1}{3}\sigma_1 \\ -\frac{1}{3}\sigma_1 \end{bmatrix} = \begin{bmatrix} 1 \\ -\frac{1}{2} \\ -\frac{1}{2} \end{bmatrix}$$

so that

$$\frac{\partial f}{\partial p} \left(\frac{2}{3} \frac{\partial f}{\partial \boldsymbol{\sigma}} \cdot \frac{\partial f}{\partial \boldsymbol{\sigma}} \right) = -h \left(\frac{2}{3} \begin{bmatrix} 1 \\ -\frac{1}{2} \\ -\frac{1}{2} \end{bmatrix} \cdot \begin{bmatrix} 1 \\ -\frac{1}{2} \\ -\frac{1}{2} \end{bmatrix} \right)^{1/2} = -h. \quad (2.44)$$

The numerator can be determined as follows:

$$-\frac{\partial f}{\partial \boldsymbol{\sigma}} \cdot d\boldsymbol{\sigma} = - \begin{bmatrix} 1 \\ -\frac{1}{2} \\ -\frac{1}{2} \end{bmatrix} \cdot \begin{bmatrix} d\sigma_1 \\ d\sigma_2 \\ d\sigma_3 \end{bmatrix} = - \begin{bmatrix} 1 \\ -\frac{1}{2} \\ -\frac{1}{2} \end{bmatrix} \cdot \begin{bmatrix} d\sigma_1 \\ 0 \\ 0 \end{bmatrix} = d\sigma_1 \quad (2.45)$$

and substituting (2.44) and (2.45) into (2.41) gives the plastic multiplier as

$$d\lambda = \frac{d\sigma_1}{h}. \quad (2.46)$$

For a von Mises material, under uniaxial loading, therefore,

$$d\lambda = dp = d\varepsilon_1^p = \frac{d\sigma_1}{h}. \quad (2.47)$$

This is telling us that the increment in stress for unit increase in plastic strain is h . This arises because we chose linear hardening with gradient h . We know, of course,

that because we are considering uniaxial loading and the incompressibility condition applies, the other plastic strain increments must be

$$d\varepsilon_2^p = d\varepsilon_3^p = -\frac{1}{2} d\varepsilon_1^p = -\frac{1}{2} \frac{d\sigma_1}{h}. \quad (2.48)$$

We can, of course, obtain the other plastic strain components formally from Equation (2.17) as

$$d\boldsymbol{\varepsilon}^p = d\lambda \frac{\partial f}{\partial \boldsymbol{\sigma}} = \frac{d\sigma_1}{h} \begin{bmatrix} 1 \\ -\frac{1}{2} \\ -\frac{1}{2} \end{bmatrix} \quad (2.49)$$

in agreement with (2.48).

The total strain increment in the loading direction is given by

$$d\varepsilon_1 = d\varepsilon_1^e + d\varepsilon_1^p = \frac{d\sigma_1}{E} + \frac{d\sigma_1}{h}. \quad (2.50)$$

Rearranging (2.50), and omitting the subscript 1 to indicate the uniaxial loading direction, gives

$$d\sigma = E \left(1 - \frac{E}{E+h} \right) d\varepsilon, \quad (2.51)$$

which is what we obtained earlier for linear strain hardening shown in Fig. 2.7. Equation (2.51) shows the linear hardening obtained, under uniaxial loading, for the isotropic hardening model chosen in Equation (2.39). If we choose perfect plasticity, that is, with no hardening ($h = 0$), Equation (2.51) gives a stress increment of zero.

The plastic multiplier can, using (2.51) and (2.46), be rewritten as

$$d\lambda = \frac{E}{E+h} d\varepsilon_1. \quad (2.52)$$

2.5 Kinematic hardening

In the case of monotonically increasing loading, it is often reasonable to assume that any hardening that occurs is isotropic. For the case of reversed loading, however, this is often not appropriate. Consider a material which hardens isotropically, shown schematically in Fig. 2.8. At a strain of ε_i , corresponding to load point (1) shown in the figure, the load is reversed so that the material behaves elastically (the stress is now lower than the yield stress) and linear stress–strain behaviour results up until load point (2). At this point, the load point is again on the expanded yield surface, and any further increase in load results in plastic deformation. Figure 2.8(b) shows that isotropic hardening leads to a very large elastic region, on reversed loading, which is often not what would be seen in experiments. In fact, a much smaller elastic region

28 Continuum plasticity

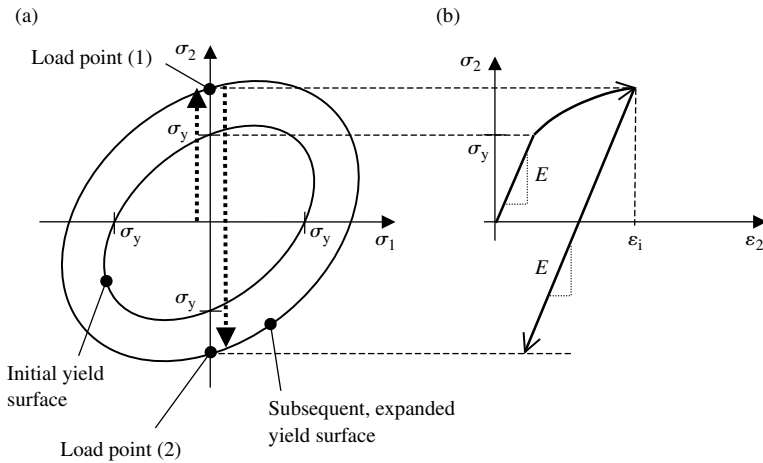


Fig. 2.8 Reversed loading with isotropic hardening showing (a) the yield surface and (b) the resulting stress–strain curve.

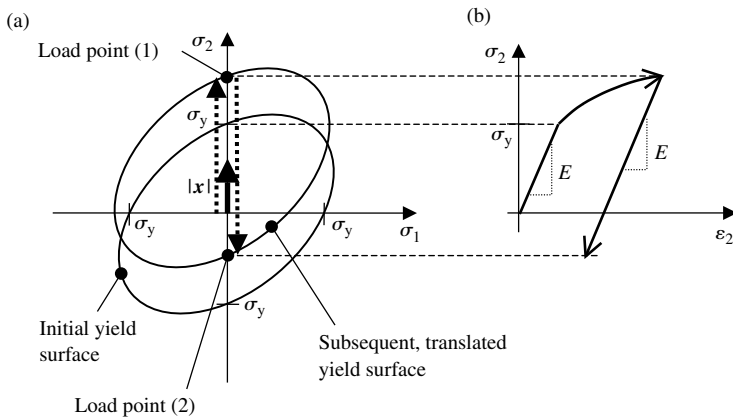


Fig. 2.9 Kinematic hardening showing (a) the translation, $|x|$ of the yield surface with plastic strain, and (b) the resulting stress–strain curve with shifted yield stress in compression—the Bauschinger effect.

is expected and this results from what is often called the *Bauschinger* effect, and kinematic hardening. In kinematic hardening, the yield surface translates in stress space, rather than expanding. This is shown in Fig. 2.9.

In Fig. 2.9(a), the stress increases until the yield stress, σ_y , is achieved. With continued loading, the material deforms plastically and the yield surface translates. When load point (1) is achieved, the load is reversed so that the material deforms elastically until point (2) is achieved when the load point is again in contact with the yield surface. The elastic region is much smaller than that for isotropic hardening shown in Fig. 2.8(b). In fact, for the kinematic hardening in Fig. 2.9, the elastic region

is of size $2\sigma_y$ whereas for the isotropic hardening, it is $2(\sigma_y + r)$. In the case of plastic flow with kinematic hardening, note that the consistency condition still holds; the load point must always lie on the yield surface during plastic flow. In addition, normality still holds; the increment in plastic strain has direction normal to the tangent to the yield surface at the load point.

The yield function describing the yield surface must now also depend on the location of the surface in stress space. Consider the initial yield surface shown in Fig. 2.9. Under applied loading and plastic deformation, the surface translates to the new location shown such that the initial centre point has been translated by $|\mathbf{x}|$. We now need to determine the stresses relative to the new yield surface centre to check for yield. In the absence of kinematic hardening, the yield function written in terms of tensor stresses is

$$f = \sigma_e - \sigma_y = \left(\frac{3}{2} \boldsymbol{\sigma}' : \boldsymbol{\sigma}' \right)^{1/2} - \sigma_y.$$

With kinematic hardening, however, it is

$$f = \left(\frac{3}{2} (\boldsymbol{\sigma}' - \mathbf{x}') : (\boldsymbol{\sigma}' - \mathbf{x}') \right)^{1/2} - \sigma_y \quad (2.53)$$

in which \mathbf{x} is the kinematic hardening variable and is often called a *back stress*. Because it is a variable defined in stress space, it has the same components as stress, and we can write it as a tensor, or, using Voigt notation, as a vector. In order to understand Equation (2.53), let us consider purely uniaxial loading with linear kinematic hardening.

2.5.1 Kinematic hardening under uniaxial loading

We will take the increment in kinematic hardening to be proportional to the increment in plastic strain, hence

$$d\mathbf{x} = \frac{2}{3} c d\boldsymbol{\epsilon}^P \quad \text{or equivalently,} \quad \dot{\mathbf{x}} = \frac{2}{3} c \dot{\boldsymbol{\epsilon}}^P \quad (2.54)$$

in which c is a material constant, and the coefficient of $\frac{2}{3}$ will be discussed below. This is called Prager linear hardening. Equation (2.54) has the similarity with isotropic hardening, that the hardening variable depends linearly on the plastic strain. The major difference is that isotropic hardening is described by a scalar variable, r , whereas for kinematic hardening, the hardening variable (or back stress) is a tensor, just as for stress. Because of the incompressibility condition, we know that the plastic strain increment is a deviatoric quantity, that is

$$d\boldsymbol{\epsilon}^{P'} = d\boldsymbol{\epsilon}^P - \frac{1}{3} \text{Tr}(d\boldsymbol{\epsilon}^P) \mathbf{1} \equiv d\boldsymbol{\epsilon}^P. \quad (2.55)$$

30 Continuum plasticity

From Equation (2.54), $d\mathbf{x}$ is therefore also a deviatoric quantity so that for uniaxial loading in the 1-direction, we may write

$$\mathbf{x} = \mathbf{x}' = \begin{pmatrix} x_{11} & 0 & 0 \\ 0 & x_{22} & 0 \\ 0 & 0 & x_{33} \end{pmatrix} = \begin{pmatrix} x_{11} & 0 & 0 \\ 0 & -\frac{1}{2}x_{11} & 0 \\ 0 & 0 & -\frac{1}{2}x_{11} \end{pmatrix}. \quad (2.56)$$

The *magnitude* or *norm* of \mathbf{x} is defined by

$$x = |\mathbf{x}| = (\mathbf{x} : \mathbf{x})^{1/2} \quad (2.57)$$

$$\begin{aligned} &= \left[\begin{pmatrix} x_{11} & 0 & 0 \\ 0 & -\frac{1}{2}x_{11} & 0 \\ 0 & 0 & -\frac{1}{2}x_{11} \end{pmatrix} : \begin{pmatrix} x_{11} & 0 & 0 \\ 0 & -\frac{1}{2}x_{11} & 0 \\ 0 & 0 & -\frac{1}{2}x_{11} \end{pmatrix} \right]^{1/2} \\ &= \left[\left(x_{11}^2 + \frac{1}{4}x_{11}^2 + \frac{1}{4}x_{11}^2 \right) \right]^{1/2} = \left| \frac{3}{2}x_{11} \right| \end{aligned} \quad (2.58)$$

so the uniaxial component of \mathbf{x} , that is x_{11} , is $\frac{2}{3}$ times the magnitude of \mathbf{x} . Bear in mind that under uniaxial loading, the effective stress is identical to the uniaxial applied stress, and the effective plastic strain increment is identical to the uniaxial plastic strain increment. Note also that like the plastic strain, uniaxial loading leads to the development of not only the uniaxial component of \mathbf{x} , but also the other direct components as well. This is because \mathbf{x} depends directly on the plastic strain, given in its evolution equation in (2.54). Consider now the components of $d\mathbf{x}$, for uniaxial loading, in Equation (2.54).

$$d\mathbf{x} = \begin{pmatrix} dx_{11} & 0 & 0 \\ 0 & -\frac{1}{2}dx_{11} & 0 \\ 0 & 0 & -\frac{1}{2}dx_{11} \end{pmatrix} = \frac{2}{3}c \begin{pmatrix} d\varepsilon_{11}^p & 0 & 0 \\ 0 & -\frac{1}{2}d\varepsilon_{11}^p & 0 \\ 0 & 0 & -\frac{1}{2}d\varepsilon_{11}^p \end{pmatrix}$$

so that

$$dx_{11} = \frac{2}{3}c d\varepsilon_{11}^p \equiv \frac{2}{3}c dp. \quad (2.59)$$

It is often simpler, and in particular, for uniaxial loading, to write the equations in terms of the magnitude of \mathbf{x} rather than the loading direction component. Combining Equations (2.59) and (2.58), therefore, gives

$$d\mathbf{x} = c d\varepsilon_{11}^p \equiv c dp, \quad (2.60)$$

which is why the coefficient of $\frac{2}{3}$ appears in Equation (2.55).

We may now determine the terms necessary for the yield function in Equation (2.53) for uniaxial loading as

$$\boldsymbol{\sigma}' - \mathbf{x}' = \begin{pmatrix} \frac{2}{3}\sigma_{11} - x_{11} & 0 & 0 \\ 0 & -\frac{1}{2}(\frac{2}{3}\sigma_{11} - x_{11}) & 0 \\ 0 & 0 & -\frac{1}{2}(\frac{2}{3}\sigma_{11} - x_{11}) \end{pmatrix} \quad (2.61)$$

which can be written in terms of the magnitude, x , of the back stress as

$$\boldsymbol{\sigma}' - \mathbf{x}' = \frac{2}{3} \begin{pmatrix} \sigma_{11} - x & 0 & 0 \\ 0 & -\frac{1}{2}(\sigma_{11} - x) & 0 \\ 0 & 0 & -\frac{1}{2}(\sigma_{11} - x) \end{pmatrix}$$

so that

$$\begin{aligned} (\boldsymbol{\sigma}' - \mathbf{x}') : (\boldsymbol{\sigma}' - \mathbf{x}') &= \frac{4}{9} \begin{pmatrix} (\sigma_{11} - x) & 0 & 0 \\ 0 & -\frac{1}{2}(\sigma_{11} - x) & 0 \\ 0 & 0 & -\frac{1}{2}(\sigma_{11} - x) \end{pmatrix} \\ &\quad : \begin{pmatrix} (\sigma_{11} - x) & 0 & 0 \\ 0 & -\frac{1}{2}(\sigma_{11} - x) & 0 \\ 0 & 0 & -\frac{1}{2}(\sigma_{11} - x) \end{pmatrix} \\ &= \left[\frac{4}{9}(\sigma_{11} - x)^2 + \frac{1}{9}(\sigma_{11} - x)^2 + \frac{1}{9}(\sigma_{11} - x)^2 \right] \\ &= \frac{2}{3}(\sigma_{11} - x)^2 \end{aligned}$$

so that

$$f = \left(\frac{3}{2}(\boldsymbol{\sigma}' - \mathbf{x}') : (\boldsymbol{\sigma}' - \mathbf{x}') \right)^{1/2} - \sigma_y = |\sigma_{11} - x| - \sigma_y = 0. \quad (2.62)$$

Because we are considering here only uniaxial loading, σ_{11} is just the uniaxial stress, σ , so Equation (2.62) can be written

$$f = |\sigma - x| - \sigma_y = 0. \quad (2.63)$$

The physical interpretation of Equation (2.63) can be seen in Fig. 2.9. Plastic deformation leads to the translation of the yield surface in stress space. Under uniaxial conditions, therefore, further yield occurs if $|\sigma - x|$ is equal to the yield stress, σ_y .

There are many forms of kinematic hardening available. What often distinguishes them is how the direction of translation of the yield surface is chosen, and the rate of its evolution as a function of the plastic strain. We shall now look at what is often called Armstrong–Frederick, or Chaboche non-linear kinematic hardening.

32 Continuum plasticity

2.5.2 Non-linear kinematic hardening

In its multiaxial form, the increment, $d\mathbf{x}$, in the back stress is given by

$$d\mathbf{x} = \frac{2}{3}c d\boldsymbol{\varepsilon}^P - \gamma \mathbf{x} d\rho \quad (2.64)$$

or equivalently,

$$\dot{\mathbf{x}} = \frac{2}{3}c\dot{\boldsymbol{\varepsilon}}^P - \gamma \mathbf{x}\dot{\rho} \quad (2.65)$$

in which γ is a further material constant. In its uniaxial form, for monotonically increasing plastic strain, Equation (2.64) may be written in terms of the magnitude, x , as

$$dx = c d\varepsilon^P - \gamma x d\varepsilon^P,$$

which can be integrated, taking x to be 0 at $\varepsilon^P = 0$, to give

$$x = \frac{c}{\gamma}(1 - e^{-\gamma\varepsilon^P}). \quad (2.66)$$

The resulting form of the stress–strain curve, for this non-linear kinematic hardening, is shown together with the translated yield surface, in Fig. 2.10. As the plastic strain increases, so the back stress, x , in Equation (2.66) saturates to the value c/γ giving a maximum saturated stress of $\sigma_y + c/\gamma$. The constant γ is the *time constant* and determines the rate of saturation of stress. c/γ determines the magnitude. We will now examine the flow rule for kinematic hardening.

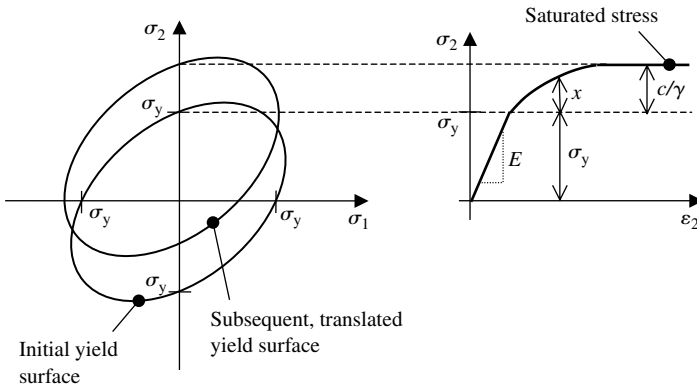


Fig. 2.10 Non-linear kinematic hardening and the resulting non-linear hardening stress–strain curve which saturates at stress c/γ .

2.5.3 Flow rule with kinematic hardening

We will use the normality hypothesis in Equation (2.17) together with the yield function in (2.53) to determine the flow rule for plastic deformation with kinematic hardening. First, let us write the yield function, f , as

$$\begin{aligned} f &= \left(\frac{3}{2} (\boldsymbol{\sigma}' - \mathbf{x}') : (\boldsymbol{\sigma}' - \mathbf{x}') \right)^{1/2} - \sigma_y \\ &= J(\boldsymbol{\sigma}' - \mathbf{x}') - \sigma_y. \end{aligned} \quad (2.67)$$

The normality hypothesis then gives

$$d\boldsymbol{\varepsilon}^P = d\lambda \frac{\partial f}{\partial \boldsymbol{\sigma}} = d\lambda \frac{3}{2} \frac{\boldsymbol{\sigma}' - \mathbf{x}'}{J(\boldsymbol{\sigma}' - \mathbf{x}')}. \quad (2.68)$$

We now need to use the consistency condition to determine the plastic multiplier. First, let us use Equation (2.68) just to show that

$$dp = \left(\frac{2}{3} d\boldsymbol{\varepsilon}^P : d\boldsymbol{\varepsilon}^P \right)^{1/2} = d\lambda \frac{[(3/2)(\boldsymbol{\sigma}' - \mathbf{x}') : (\boldsymbol{\sigma}' - \mathbf{x}')]^{1/2}}{J(\boldsymbol{\sigma}' - \mathbf{x}')} = d\lambda \quad (2.69)$$

for the case of kinematic hardening with a von Mises yield criterion. The yield function depends upon the stress, $\boldsymbol{\sigma}$, and the back stress, \mathbf{x} , which are both tensor quantities. However, for simplicity, we shall now work in principal stress space again, and use Voigt notation. The consistency condition becomes

$$\frac{\partial f}{\partial \boldsymbol{\sigma}} \cdot d\boldsymbol{\sigma} + \frac{\partial f}{\partial \mathbf{x}} \cdot d\mathbf{x} = 0, \quad (2.70)$$

which, when combined with Hooke's law in (2.27), the normality hypothesis in (2.17), and Equation (2.69) gives

$$\begin{aligned} \frac{\partial f}{\partial \boldsymbol{\sigma}} \cdot \mathbf{C} \left(d\boldsymbol{\varepsilon} - d\lambda \frac{\partial f}{\partial \boldsymbol{\sigma}} \right) + \frac{\partial f}{\partial \mathbf{x}} \cdot \left(\frac{2}{3} c d\boldsymbol{\varepsilon}^P - \gamma \mathbf{x} d\lambda \right) \\ = \frac{\partial f}{\partial \boldsymbol{\sigma}} \cdot \mathbf{C} \left(d\boldsymbol{\varepsilon} - d\lambda \frac{\partial f}{\partial \boldsymbol{\sigma}} \right) + \frac{\partial f}{\partial \mathbf{x}} \cdot \left(\frac{2}{3} c d\lambda \frac{\partial f}{\partial \boldsymbol{\sigma}} - \gamma \mathbf{x} d\lambda \right) = 0 \end{aligned}$$

so that

$$d\lambda = \frac{(\partial f / \partial \boldsymbol{\sigma}) \cdot \mathbf{C} d\boldsymbol{\varepsilon}}{(\partial f / \partial \boldsymbol{\sigma}) \cdot \mathbf{C} (\partial f / \partial \boldsymbol{\sigma}) + \gamma (\partial f / \partial \mathbf{x}) \cdot \mathbf{x} - (2/3)c (\partial f / \partial \mathbf{x}) \cdot (\partial f / \partial \boldsymbol{\sigma})} \quad (2.71)$$

and the plastic strain increment is

$$d\boldsymbol{\varepsilon}^P = \frac{(\partial f / \partial \boldsymbol{\sigma}) \cdot \mathbf{C} d\boldsymbol{\varepsilon}}{(\partial f / \partial \boldsymbol{\sigma}) \cdot \mathbf{C} (\partial f / \partial \boldsymbol{\sigma}) + \gamma (\partial f / \partial \mathbf{x}) \cdot \mathbf{x} - (2/3)c (\partial f / \partial \mathbf{x}) \cdot (\partial f / \partial \boldsymbol{\sigma})} \frac{\partial f}{\partial \boldsymbol{\sigma}} \quad (2.72)$$

34 Continuum plasticity

and so the stress increment can be obtained from Equation (2.27). We will simplify this to the case of uniaxial loading to interpret the terms in Section 2.5.4, but first, we will start by obtaining the plastic multiplier in terms of stress rather than strain increments.

Starting from the consistency condition in (2.70) gives

$$\frac{\partial f}{\partial \boldsymbol{\sigma}} \cdot d\boldsymbol{\sigma} + \frac{\partial f}{\partial \mathbf{x}} \cdot d\mathbf{x} = \frac{\partial f}{\partial \boldsymbol{\sigma}} \cdot d\boldsymbol{\sigma} + \frac{\partial f}{\partial \mathbf{x}} \cdot \left(\frac{2}{3}c d\boldsymbol{\varepsilon}^p - \gamma \mathbf{x} dp \right) = 0. \quad (2.73)$$

From the yield function in (2.67), $\partial f/\partial \mathbf{x} = -(\partial f/\partial \boldsymbol{\sigma})$ and $dp = d\lambda$ and with (2.68), (2.73) becomes

$$\frac{\partial f}{\partial \boldsymbol{\sigma}} \cdot d\boldsymbol{\sigma} - \frac{\partial f}{\partial \boldsymbol{\sigma}} \cdot \left(\frac{2}{3}c d\lambda \frac{\partial f}{\partial \boldsymbol{\sigma}} - \gamma \mathbf{x} d\lambda \right) = 0$$

so that

$$d\lambda = \frac{-(\partial f/\partial \boldsymbol{\sigma}) \cdot d\boldsymbol{\sigma}}{\gamma(\partial f/\partial \boldsymbol{\sigma}) \cdot \mathbf{x} - (2/3)c(\partial f/\partial \boldsymbol{\sigma}) \cdot (\partial f/\partial \boldsymbol{\sigma})}. \quad (2.74)$$

We will examine this for uniaxial loading in a von Mises material in the following section.

2.5.4 Simple uniaxial loading

For uniaxial loading, we can determine the terms in the denominator of Equation (2.74) as follows:

$$\gamma \frac{\partial f}{\partial \boldsymbol{\sigma}} \cdot \mathbf{x} - \frac{2}{3}c \frac{\partial f}{\partial \boldsymbol{\sigma}} \cdot \frac{\partial f}{\partial \boldsymbol{\sigma}} = \gamma \begin{bmatrix} 1 \\ -\frac{1}{2} \\ -\frac{1}{2} \end{bmatrix} \cdot \begin{bmatrix} x_1 \\ x_2 \\ x_3 \end{bmatrix} - \frac{2}{3}c \begin{bmatrix} 1 \\ -\frac{1}{2} \\ -\frac{1}{2} \end{bmatrix} \cdot \begin{bmatrix} 1 \\ -\frac{1}{2} \\ -\frac{1}{2} \end{bmatrix}. \quad (2.75)$$

We know that \mathbf{x} is a deviatoric quantity so that for uniaxial loading in the 1-direction,

$$x_2 = x_3 = -\frac{1}{2}x_1$$

so that Equation (2.75) becomes just $\frac{3}{2}\gamma x_1 - c$. Now, we can write $x_1 = \frac{2}{3}x$ so that this becomes $\gamma x - c$. The numerator in (2.74) is, as before, just $-d\sigma_1$ so that the plastic multiplier for uniaxial loading is just

$$d\lambda = \frac{d\sigma_1}{c - \gamma x}. \quad (2.76)$$

In a similar manner to that for the isotropic hardening example, we can obtain the uniaxial stress increment as

$$d\boldsymbol{\sigma} = E \left(1 - \frac{E}{E + c - \gamma x} \right) d\boldsymbol{\varepsilon}. \quad (2.77)$$

Let us look at this in a little more detail. If the material behaviour is purely elastic, then the plastic multiplier is zero and the right-hand term in the bracket is zero so that (2.77) simply reduces to

$$d\sigma = E d\varepsilon.$$

If we have elastic, perfectly plastic behaviour, that is, no strain hardening, then $c = \gamma = 0$ and then (2.77) tells us that during plastic deformation, the increment in stress is zero. If the material undergoes linear kinematic hardening, that is, $\gamma = 0$, the stress–strain relation during plasticity becomes

$$d\sigma = E \left(1 - \frac{E}{E + c} \right) d\varepsilon \quad (2.78)$$

which is linear during plastic deformation since c is constant. This equation for linear kinematic hardening and that for linear isotropic hardening in Equation (2.51) can be seen to be near identical. The two types of hardening are in fact the same for monotonically increasing loading (provided $c = h$) and only differ under uniaxial conditions on a load reversal when the Bauschinger effect becomes important.

If, finally, the material undergoes non-linear kinematic hardening, the back stress, x , increases according to its evolution equation, (2.64), so that the stress increment progressively decreases until saturation is achieved at which point, no further stress increase occurs. This can be seen by substituting the equation for x , given in (2.66), into (2.77) to give

$$\begin{aligned} d\sigma &= E \left(1 - \frac{E}{E + c - \gamma x} \right) d\varepsilon \\ &= E \left(1 - \frac{E}{E + c - \gamma[(c/\gamma)(1 - e^{-\gamma\varepsilon^p})]} \right) d\varepsilon = E \left(1 - \frac{E}{E + ce^{-\gamma\varepsilon^p}} \right) d\varepsilon. \end{aligned}$$

As the plastic strain increases, so the exponential term diminishes until ultimately, the material becomes perfectly plastic with $d\sigma = 0$.

Before finishing this section, Equation (2.77) demonstrates quite nicely the incremental nature of plasticity. Let us consider first the case of elasticity only. Equation (2.77) gives

$$d\sigma = E d\varepsilon,$$

where $d\varepsilon = d\varepsilon^e$. Integrating this equation is clearly possible such that at any particular value of elastic strain, the stress can be calculated. This is simply not possible for the case of plasticity, for which all we can do (normally) is consider increments in stress resulting from an increment in strain. This follows from Equation (2.77) since x itself depends upon strain, so that the increment in stress varies from step to step. The increment in stress, and indeed plastic strain, often depend then, in plasticity, on the *history* of prior deformation. Plasticity must, in general, therefore, be considered to be an incremental process.

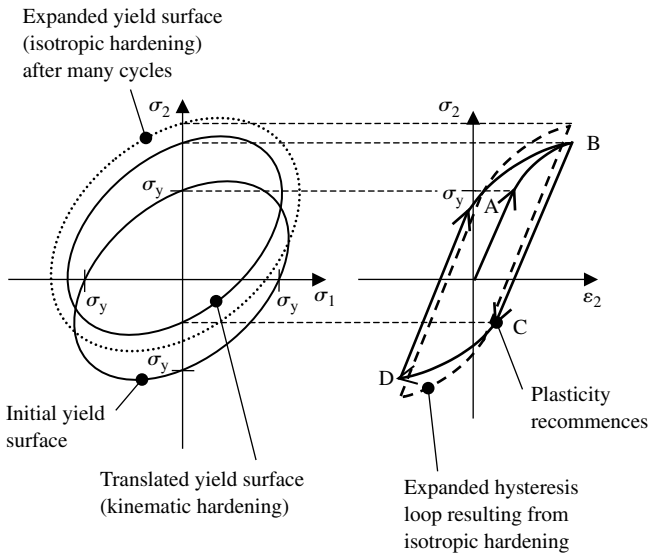


Fig. 2.11 Combined kinematic and isotropic hardening.

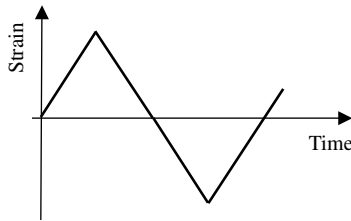


Fig. 2.12 Strain imposed resulting in cyclic plasticity shown in Fig. 2.11.

2.6 Combined isotropic and kinematic hardening

We will consider, finally, materials which harden both kinematically and isotropically. This is particularly appropriate for applications to cyclic plasticity where within an individual cycle, kinematic hardening is the dominant hardening process such that the Bauschinger effect can be represented, but over (normally) quite large numbers of cycles, the material also hardens isotropically such that the peak tension and compression stresses in a given cycle increase from one cycle to the next until saturation is achieved. Such a process is represented schematically in Fig. 2.11. Starting from the point of zero stress and strain, the material is subjected to the strain shown in Fig. 2.12. The stress increases until yield is achieved at point A, and the material kinematically hardens leading to the translation of the yield surface, as shown in Fig. 2.11. Once the peak strain is achieved, the strain reversal occurs so that the material becomes elastic

at point B. Elastic deformation continues until the load point reaches the yield surface again at point C where plasticity recommences until the next strain reversal at point D. The yield surface is translated again because of the kinematic hardening. The stress–strain loop BCDB produced in this way is called a *hysteresis loop*. If, in addition to the kinematic hardening, the material also isotropically hardens, then superimposed upon the translation of the yield surface is a progressive expansion, shown by the broken line hysteresis loop in Fig. 2.11. This process, by which the peak stress and strain in a hysteresis loop increase, due to isotropic hardening, is often called cyclic hardening, as it often occurs from cycle to cycle over many cycles. Kinematic hardening, on the other hand, occurs within each cycle.

We will consider the case of non-linear kinematic and isotropic hardening, given by Equations (2.64) and (2.37), respectively. In order to determine the plastic multiplier, we will use the consistency condition as before. The yield function, for combined kinematic and isotropic hardening, depends on the stress, back stress, and accumulated plastic strain as follows

$$f = J(\boldsymbol{\sigma}' - \mathbf{x}') - r(p) - \sigma_y \quad (2.79)$$

so that the consistency condition becomes

$$\frac{\partial f}{\partial \boldsymbol{\sigma}} \cdot d\boldsymbol{\sigma} + \frac{\partial f}{\partial \mathbf{x}} \cdot d\mathbf{x} + \frac{\partial f}{\partial p} dp = 0. \quad (2.80)$$

Substituting for $d\boldsymbol{\sigma}$ and $d\mathbf{x}$ from Equations (2.27) and (2.64) and writing $\partial f/\partial p = -(\partial r/\partial p)$ from (2.79), together with (2.37) gives

$$\frac{\partial f}{\partial \boldsymbol{\sigma}} \cdot \mathbf{C}(d\boldsymbol{\epsilon} - d\boldsymbol{\epsilon}^p) + \frac{\partial f}{\partial \mathbf{x}} \cdot \left(\frac{2}{3}c d\boldsymbol{\epsilon}^p - \gamma \mathbf{x} dp \right) - b(Q - r(p)) dp = 0. \quad (2.81)$$

Following the procedure for isotropic and kinematic hardening, (2.81) can be rearranged to give the plastic multiplier. Assuming von Mises behaviour, $dp = d\lambda$, and substituting for $d\boldsymbol{\epsilon}^p$ from (2.17), gives the plastic multiplier as

$$d\lambda = \frac{(\partial f/\partial \boldsymbol{\sigma}) \cdot \mathbf{C} d\boldsymbol{\epsilon}}{(\partial f/\partial \boldsymbol{\sigma}) \cdot \mathbf{C}(\partial f/\partial \boldsymbol{\sigma}) - \gamma(\partial f/\partial \boldsymbol{\sigma}) \cdot \mathbf{x} + (2/3)c(\partial f/\partial \boldsymbol{\sigma}) \cdot (\partial f/\partial \boldsymbol{\sigma}) + b(Q - r(p))}. \quad (2.82)$$

In a similar manner as before, we can determine the plastic multiplier in terms of the increment of stress, rather than strain, as follows. Equation (2.80) is written as

$$\frac{\partial f}{\partial \boldsymbol{\sigma}} \cdot d\boldsymbol{\sigma} + \frac{\partial f}{\partial \mathbf{x}} \cdot \left(\frac{2}{3}c d\boldsymbol{\epsilon}^p - \gamma \mathbf{x} dp \right) - b(Q - r(p)) dp = 0$$

38 Continuum plasticity

so that the plastic multiplier becomes

$$d\lambda = \frac{(\partial f/\partial \boldsymbol{\sigma}) \cdot d\boldsymbol{\sigma}}{(2/3)c(\partial f/\partial \boldsymbol{\sigma}) \cdot (\partial f/\partial \boldsymbol{\sigma}) - \gamma(\partial f/\partial \boldsymbol{\sigma}) \cdot \mathbf{x} + b(Q - r(p))}. \quad (2.83)$$

As in previous examples, we can reduce this to the form for uniaxial loading of a von Mises material and obtain for the uniaxial stress increment

$$d\sigma = E \left(1 - \frac{E}{E + c - \gamma x + b(Q - r(p))} \right) d\varepsilon. \quad (2.84)$$

2.7 Viscoplasticity and creep

So far, we have considered time-independent plasticity only; that is, the stress–strain behaviour has been assumed to be independent of the rate of loading, whether strain or stress controlled. The plasticity of materials which do exhibit rate effects is called *viscoplasticity*. We shall see that the same formalism for viscoplasticity is also appropriate for creep—the time dependent, irreversible deformation of a material under load. The usual convention for terminology is that viscoplasticity describes rate-dependent plasticity in which crystallographic slip is the dominant deformation process, though likely enhanced by thermally-activated processes such as diffusion-activated dislocation climb. *Creep* is normally used to describe low strain rate, time-dependent irreversible deformation which is either diffusion controlled, or influenced by diffusion, though there may well be crystallographic slip still occurring.

In viscoplasticity, the elastic–plastic strain decomposition still holds, and yield is determined as for time-independent plasticity with a yield function. In addition, the plastic flow rule is obtained as before using the normality hypothesis of plasticity, and once yielding has occurred, the material may harden isotropically or kinematically. An important difference occurs, however, in that the consistency condition is no longer formally applied so that the load point may now lie outside of the yield surface. As a result, some viscoplasticity models are referred to as *over-stress* models. We shall start by addressing uniaxial loading in the 1-direction, as before, for conditions of plane stress.

Figure 2.13 shows schematically the material’s stress–strain response and the corresponding yield surface which we assume to expand due to linear isotropic hardening. At load point (1) shown on the yield surface in Fig. 2.13(a) and at the corresponding point on the uniaxial stress–strain curve in Fig. 2.13(b), for the case of time-independent plasticity, the stress achieved is the yield stress, σ_y , together with the contribution from the linear isotropic hardening, $r(p)$ so that

$$\sigma = \sigma_y + r(p).$$

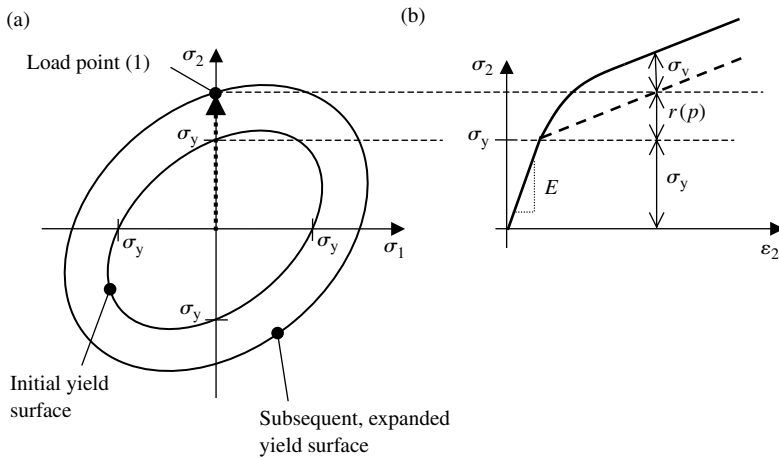


Fig. 2.13 (a) The von Mises yield surface in plane stress for viscoplasticity with linear isotropic hardening, with viscous (over-stress) stress σ_v , and (b), the corresponding stress strain curve.

The resulting stress–strain curve is that shown by the broken line in Fig. 2.13(b). However, for the case of viscoplasticity, the stress is augmented by the *viscous stress*, σ_v , also shown schematically in Fig. 2.13(b) by the solid line. There are many types of equations used to represent the viscous stress, but they often contain a dependence on the effective plastic strain rate (which for uniaxial conditions is identical to the uniaxial plastic strain rate), \dot{p} . This, of course, is how the strain rate dependence of the plasticity is introduced. Let us consider the commonly used power law function

$$\sigma_v = K\dot{p}^m \quad (2.85)$$

in which K and m are material constants. The constant m is called the material's *strain rate sensitivity*. From Fig. 2.13(b), the stress–strain curve which includes the rate-dependence of stress is therefore

$$\sigma = \sigma_y + r(p) + \sigma_v = \sigma_y + r(p) + K\dot{p}^m. \quad (2.86)$$

In viscoplasticity, the uniaxial stress depends on the yield stress, the hardening of the yield stress, and the plastic strain rate. The stress response is, therefore, strain rate dependent. For this reason, viscoplasticity is sometimes referred to as time-dependent plasticity or rate-dependent plasticity. Let us consider the uniaxial behaviour described by Equation (2.86) in a little more detail, but to simplify, let us assume perfect plasticity so that there is no isotropic hardening and $r(p) = 0$. In this case, the equation becomes

$$\sigma = \sigma_y + K\dot{p}^m. \quad (2.87)$$

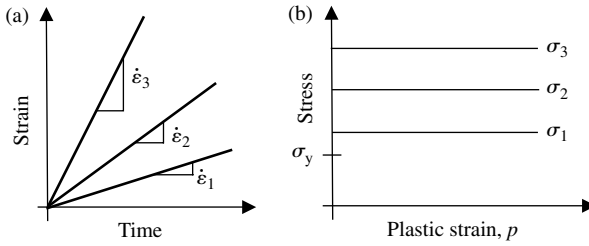


Fig. 2.14 (a) Applied strain and (b) the resulting rate-dependent stress response.

If we apply strain controlled loading to the uniaxial sample, as shown in Fig. 2.14(a), at a range of different strain rates as shown, the stress response (for given σ_y , K , and m) as a function of the plastic strain is shown in Fig. 2.14(b).

The strain rate dependence of stress is clear and for the three strain rates applied, the corresponding stresses are given by Equation (2.87). Once yield is achieved, for uniaxial perfect plasticity, since $d\sigma = 0$, $dp = d\epsilon$, or equivalently, $\dot{p} = \dot{\epsilon}$ so that the stresses are

$$\begin{aligned} \sigma_1 &= \sigma_y + K \dot{\epsilon}_1^m, \\ \sigma_2 &= \sigma_y + K \dot{\epsilon}_2^m, \\ \sigma_3 &= \sigma_y + K \dot{\epsilon}_3^m. \end{aligned} \tag{2.88}$$

Many materials exhibit strain rate-dependent plasticity, but unlike the stress–strain curves in Fig. 2.14, would also show isotropic or kinematic hardening. Let us return to the case of isotropic hardening given in Equation (2.86). We can rearrange the equation to give

$$\dot{p} = \left(\frac{\sigma - r - \sigma_y}{K} \right)^{1/m}. \tag{2.89}$$

If in addition to isotropic hardening, kinematic hardening also occurs, Equation (2.89) becomes

$$\dot{p} = \left(\frac{\sigma - x - r - \sigma_y}{K} \right)^{1/m}. \tag{2.90}$$

Equations (2.89) and (2.90) are *constitutive equations* relating uniaxial plastic strain rate to uniaxial stress, and which depend upon *internal variables*; the isotropic hardening, r , and the kinematic hardening, x . For a von Mises material, the uniaxial stress is identical to the effective stress and similarly for the effective plastic strain rate. Equation (2.90) can therefore be written

$$\dot{p} = \left(\frac{J(\sigma' - x') - r - \sigma_y}{K} \right)^{1/m}. \tag{2.91}$$

In viscoplasticity, we need a constitutive equation, such as (2.91), which relates the effective plastic strain rate to the stress and internal hardening variables. This replaces the consistency condition in time-independent plasticity, which forces the load point to stay on the yield surface during plastic deformation. In viscoplasticity, the load point may lie outside the yield surface because of the viscous or over-stress. In addition to the viscoplastic constitutive equation, as before, we make use of the normality hypothesis and the elastic constitutive equation; namely Hooke's law. For viscoplasticity, we write the normality hypothesis, from Equation (2.17), as

$$\dot{\boldsymbol{\epsilon}}^P = \dot{\lambda} \frac{\partial f}{\partial \boldsymbol{\sigma}}. \quad (2.92)$$

The yield function is, from Section 2.6,

$$f = J(\boldsymbol{\sigma}' - \mathbf{x}') - r(p) - \sigma_y \quad (2.93)$$

so that

$$\frac{\partial f}{\partial \boldsymbol{\sigma}} = \frac{3}{2} \frac{\boldsymbol{\sigma}' - \mathbf{x}'}{J(\boldsymbol{\sigma}' - \mathbf{x}')}$$

and

$$\dot{\boldsymbol{\epsilon}}^P = \frac{3}{2} \dot{\lambda} \frac{\boldsymbol{\sigma}' - \mathbf{x}'}{J(\boldsymbol{\sigma}' - \mathbf{x}')}. \quad (2.94)$$

We showed in Section 2.5.3 that for a von Mises material, $dp = d\lambda$, or equivalently $\dot{p} = \dot{\lambda}$ so that (2.94) becomes

$$\dot{\boldsymbol{\epsilon}}^P = \frac{3}{2} \dot{p} \frac{\boldsymbol{\sigma}' - \mathbf{x}'}{J(\boldsymbol{\sigma}' - \mathbf{x}')}. \quad (2.95)$$

We may now combine the constitutive equation given in (2.91) with (2.95) to give the plastic flow rule for viscoplasticity with isotropic and kinematic hardening as

$$\dot{\boldsymbol{\epsilon}}^P = \frac{3}{2} \left(\frac{J(\boldsymbol{\sigma}' - \mathbf{x}') - r - \sigma_y}{K} \right)^{1/m} \frac{\boldsymbol{\sigma}' - \mathbf{x}'}{J(\boldsymbol{\sigma}' - \mathbf{x}')}. \quad (2.96)$$

To complete the model, we need the evolution equations for the isotropic and kinematic hardening variables r and \mathbf{x} , and the rate form of Hooke's law.

From Section 2.4, Equation (2.37) and Section 2.5.2, Equation (2.65), the hardening rates are given by

$$\dot{r}(p) = b(Q - r)\dot{p}, \quad (2.97)$$

$$\dot{\mathbf{x}} = \frac{2}{3} c \dot{\boldsymbol{\epsilon}}^P - \gamma \mathbf{x} \dot{p} \quad (2.98)$$

and we will now write Hooke's law in terms of tensor rather than vector strain terms as

$$\dot{\boldsymbol{\sigma}} = 2G\dot{\boldsymbol{\epsilon}}^e + \lambda \text{Tr}(\dot{\boldsymbol{\epsilon}}^e)\mathbf{I}, \quad (2.99)$$

42 Continuum plasticity

where

$$\dot{\boldsymbol{\epsilon}}^e = \dot{\boldsymbol{\epsilon}} - \dot{\boldsymbol{\epsilon}}^p \quad (2.100)$$

and in which G is the shear modulus, λ the Lamé constant given by

$$\lambda = \frac{E\nu}{(1-2\nu)(1+\nu)}$$

and \mathbf{I} is the identity tensor given by

$$\mathbf{I} = \begin{pmatrix} 1 & 0 & 0 \\ 0 & 1 & 0 \\ 0 & 0 & 1 \end{pmatrix}.$$

Equations (2.96)–(2.100) form the complete elastic–viscoplastic model. At a given time, t , with knowledge of the current total strain rate, $\dot{\boldsymbol{\epsilon}}$ and the hardening variables r and \mathbf{x} , together with the stress, $\boldsymbol{\sigma}$, these equations enable the stresses at the end of a given step forward in time to be determined. We will address this in a later chapter, but for now, let us examine the equations for a simple problem of uniform, uniaxial, and axisymmetric *upsetting*.

2.7.1 Uniform, uniaxial, and axisymmetric compression

Upsetting is the name given to the open-die forging of cylindrical billets of material. We will consider the uniaxial compression of a cylinder between two platens such that the frictional effects on the contacting surfaces are negligible so that the cylinder remains under uniform, uniaxial compression. The process is shown schematically in Fig. 2.15.

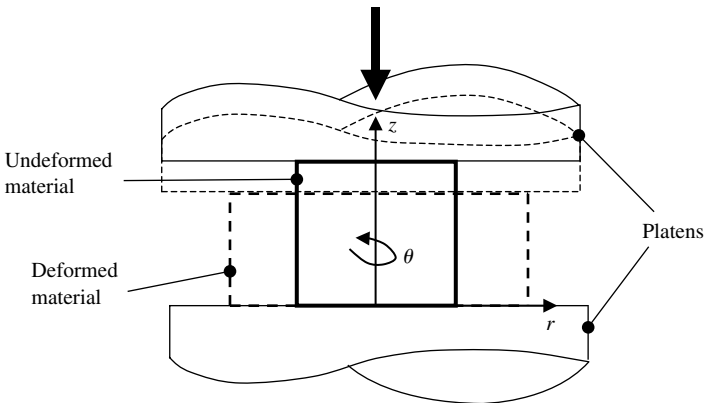


Fig. 2.15 Frictionless, uniaxial compression representing open-die forging.

We will consider constant strain rate-controlled loading and write the plastic strain rates as

$$\dot{\boldsymbol{\epsilon}}^p = \begin{pmatrix} \dot{\epsilon}_{rr}^p & \dot{\epsilon}_{rz}^p & 0 \\ \dot{\epsilon}_{rz}^p & \dot{\epsilon}_{zz}^p & 0 \\ 0 & 0 & \dot{\epsilon}_{\theta\theta}^p \end{pmatrix}. \quad (2.101)$$

Because we are assuming friction to be negligible, the shear terms are zero. The boundary conditions give us that

$$\sigma_{rr} = \sigma_{\theta\theta} = \sigma_{rz} = 0$$

so that the stress and deviatoric stress tensors for the problem become

$$\boldsymbol{\sigma} = \begin{pmatrix} 0 & 0 & 0 \\ 0 & \sigma_{zz} & 0 \\ 0 & 0 & 0 \end{pmatrix}, \quad \boldsymbol{\sigma}' = \begin{pmatrix} -\frac{1}{3}\sigma_{zz} & 0 & 0 \\ 0 & \frac{2}{3}\sigma_{zz} & 0 \\ 0 & 0 & -\frac{1}{3}\sigma_{zz} \end{pmatrix}. \quad (2.102)$$

We will now use Equation (2.96) to determine the plastic strain rate components for the problem.

Under this loading,

$$J(\boldsymbol{\sigma}' - \mathbf{x}') = \sigma_{zz} - x \quad (2.103)$$

and from Section 2.5.1,

$$\boldsymbol{\sigma}' - \mathbf{x}' = \frac{2}{3} \begin{pmatrix} -\frac{1}{2}(\sigma_{zz} - x) & 0 & 0 \\ 0 & \sigma_{zz} - x & 0 \\ 0 & 0 & -\frac{1}{2}(\sigma_{zz} - x) \end{pmatrix} \quad (2.104)$$

so that (2.96) becomes

$$\begin{pmatrix} \dot{\epsilon}_{rr}^p & \dot{\epsilon}_{rz}^p & 0 \\ \dot{\epsilon}_{rz}^p & \dot{\epsilon}_{zz}^p & 0 \\ 0 & 0 & \dot{\epsilon}_{\theta\theta}^p \end{pmatrix} = \frac{3}{2} \left(\frac{|\sigma_{zz} - x| - r - \sigma_y}{K} \right)^{1/m} \\ \times \frac{1}{|\sigma_{zz} - x|} \frac{2}{3} \begin{pmatrix} -\frac{1}{2}(\sigma_{zz} - x) & 0 & 0 \\ 0 & \sigma_{zz} - x & 0 \\ 0 & 0 & -\frac{1}{2}(\sigma_{zz} - x) \end{pmatrix}$$

which reduces to

$$\begin{pmatrix} \dot{\epsilon}_{rr}^p & \dot{\epsilon}_{rz}^p & 0 \\ \dot{\epsilon}_{rz}^p & \dot{\epsilon}_{zz}^p & 0 \\ 0 & 0 & \dot{\epsilon}_{\theta\theta}^p \end{pmatrix} = \left(\frac{|\sigma_{zz} - x| - r - \sigma_y}{K} \right)^{1/m} \begin{pmatrix} -\frac{1}{2} & 0 & 0 \\ 0 & 1 & 0 \\ 0 & 0 & -\frac{1}{2} \end{pmatrix}. \quad (2.105)$$

44 Continuum plasticity

We may now look at individual components of the plastic strain rate. We see that

$$\dot{\epsilon}_{zz}^p = \left(\frac{|\sigma_{zz} - x| - r - \sigma_y}{K} \right)^{1/m} \quad (2.106)$$

which is, of course, just what we would get for purely uniaxial loading, and Equation (2.105) also shows that

$$\dot{\epsilon}_{rr}^p = \dot{\epsilon}_{\theta\theta}^p = -\frac{1}{2}\dot{\epsilon}_{zz}^p = -\frac{1}{2} \left(\frac{|\sigma_{zz} - x| - r - \sigma_y}{K} \right)^{1/m}$$

demonstrating that the incompressibility condition of plasticity is satisfied.

2.7.2 Power-law creep

Let us look at one further case in which we assume there to be neither isotropic nor kinematic hardening. Equation (2.96) then becomes, for the plastic strain rate,

$$\dot{\epsilon}^p = \frac{3}{2} \left(\frac{J(\boldsymbol{\sigma}') - \sigma_y}{K} \right)^{1/m} \frac{\boldsymbol{\sigma}'}{J(\boldsymbol{\sigma}')} \quad (2.107)$$

and $J(\boldsymbol{\sigma}') = \sigma_e$ so the equation reduces further to

$$\dot{\epsilon}^p = \frac{3}{2} \left(\frac{\sigma_e - \sigma_y}{K} \right)^{1/m} \frac{\boldsymbol{\sigma}'}{\sigma_e}. \quad (2.108)$$

Often in creep problems, where the time-dependent deformation is not dependent upon yield, creep deformation is assumed to occur with the application of a non-zero stress. For creep problems, therefore, Equation (2.108) is often written

$$\dot{\epsilon}^c = \frac{3}{2} \left(\frac{\sigma_e}{K} \right)^{1/m} \frac{\boldsymbol{\sigma}'}{\sigma_e} = \frac{3}{2} A (\sigma_e)^n \frac{\boldsymbol{\sigma}'}{\sigma_e} = \frac{3}{2} A \sigma_e^{n-1} \boldsymbol{\sigma}' \quad (2.109)$$

which is the multiaxial form of Norton's creep law, where A and n are material constants. For uniaxial loading, it reduces to

$$\dot{\epsilon}^c = \frac{3}{2} A \sigma_e^{n-1} \frac{2}{3} \sigma = A \sigma^n.$$

For completeness, we can write out Equation (2.109) in full component form as

$$\begin{pmatrix} \dot{\epsilon}_{xx}^c & \dot{\epsilon}_{xy}^c & \dot{\epsilon}_{xz}^c \\ \dot{\epsilon}_{yx}^c & \dot{\epsilon}_{yy}^c & \dot{\epsilon}_{yz}^c \\ \dot{\epsilon}_{zx}^c & \dot{\epsilon}_{zy}^c & \dot{\epsilon}_{zz}^c \end{pmatrix} = \frac{3}{2} A \sigma_e^{n-1} \begin{pmatrix} \sigma'_{xx} & \sigma'_{xy} & \sigma'_{xz} \\ \sigma'_{yx} & \sigma'_{yy} & \sigma'_{yz} \\ \sigma'_{zx} & \sigma'_{zy} & \sigma'_{zz} \end{pmatrix} \quad (2.110)$$

in which the stress and strain rate tensors are symmetric.

2.7.3 Potential and yield function equivalence

In the last example, we saw how the plastic strain rate, based on the normality hypothesis together with an appropriate constitutive equation for plastic strain rate, was determined for viscoplasticity, but then reduced to Norton's law for creep deformation. Because creep processes may occur independently of plastic yielding, it is not appropriate to use a yield surface, in the conventional sense discussed earlier. Instead, a potential function is defined from which creep strain rates are determined.

We will define a potential, ϕ , such that

$$\phi = \frac{\dot{\epsilon}_0 \sigma_0}{n+1} \left(\frac{\sigma_e}{\sigma_0} \right)^{n+1} \quad (2.111)$$

in which $\dot{\epsilon}_0$ and σ_0 are material constants with units of strain rate and stress, respectively. The potential function, ϕ , therefore has units of Joules per second per unit volume. It therefore represents an energy per second per unit volume.

The plastic (creep) strain rate is determined from

$$\dot{\epsilon}^c = \frac{\partial \phi}{\partial \sigma} \quad (2.112)$$

giving

$$\dot{\epsilon}^c = \frac{3}{2} \frac{\dot{\epsilon}_0 \sigma_0}{\sigma_0^{n+1}} \sigma_e^{n-1} \sigma' = \frac{3}{2} A \sigma_e^{n-1} \sigma', \quad (2.113)$$

which is identical to Equation (2.109). The potential function, ϕ , in creep plays a similar role to the yield function in plasticity. In fact, often the yield function is considered to be a potential function. The surfaces in stress space represented by ϕ are often called equipotential surfaces; the energy per second per unit volume is the same at each point on the potential surface, just as the value of σ_e takes the same value on every point of a yield surface in plasticity.

Further reading

- Dieter, G.E. (1988). *Mechanical Metallurgy*. McGraw-Hill Book Co., London.
- Hill, R. (1998). *The Mathematical Theory of Plasticity*. OUP (Oxford Classics Series). (first published in 1950).
- Khan, A.S. and Huang, S. (1995). *Continuum Theory of Plasticity*. John Wiley & Sons Inc, New York.
- Lemaitre, J. and Chaboche, J.-L. (1990). *Mechanics of Solid Materials*. CUP, Cambridge, UK.
- Lubarda, V.A. (2002). *Elastoplasticity Theory*. CRC Press, Florida, USA.

This page intentionally left blank

3. Kinematics of large deformations and continuum mechanics

3.1 Introduction

The strains, be they elastic or plastic, which most engineering components undergo in service are usually small, that is, <0.001 (or 0.1%). At yield, for example, a nickel alloy may have undergone a strain of about $\sigma_y/E \sim 0.002$ and it is hoped that this occurs rarely in nickel-based alloy aero-engine components in service! During manufacture, however, the strains may be much bigger; the forging of an aero-engine compressor disc, for example, requires strains in excess of 2.0 (i.e. $>200\%$). This is three orders of magnitude larger than the strain needed to cause yield. In manufacturing processes, another very important feature is material rotation. Deformation processing leading to large plastic strains often also leads to large *rigid body rotations*. The bending of a circular plate, to large deformation, is an example which shows the rigid body rotation. Figure 3.1 shows the result of applying a large downward displacement at the centre of an initially horizontal, simply supported circular disc. Only one half of the disc section is shown. While the displacements and rigid body rotations can be very large, the strains remain quite small.

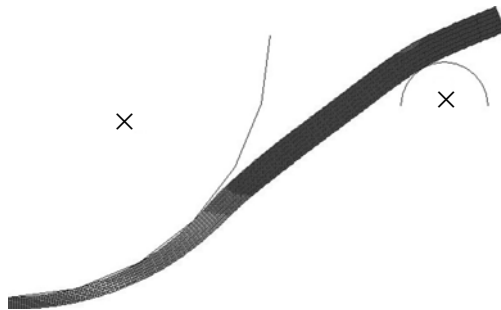


Fig. 3.1 Simulated large elastic–plastic deformation of an initially horizontal, simply supported circular plate. Only one half of the plate section is shown.

Towards the outer edge of the disc, where it is supported, the finite element simulation shows that the strains generated are quite small, but that because of the disc bending, the rigid body rotations are very large. Generally, deformation comprises of *stretch*, *rigid body rotation*, and *translation*. The stretch provides the shape change. The rigid body rotation neither contributes to shape change nor to internal stress. Because a translation does not lead to a change in stress state, we will not address it in detail here. In this chapter, we will give an introduction to measures of large deformation, rigid body rotation, elastic–plastic coupling in large deformation, stress rates, and what is called *material objectivity*, or *frame indifference*. Later chapters dealing with the implementation of plasticity models into finite element code will rely on the material covered here and in Chapter 2.

3.2 The deformation gradient

In order to look at deformation, let us consider a small lump of imaginary material which is yet to be loaded so that it is in the *undeformed* (or *initial*) *configuration* (or *state*). This is shown schematically as state A in Fig. 3.2.

We will now apply a load to the material in state A so that it deforms to that shown in state B, the *deformed* or *current configuration*. We will assume that the material undergoes combined stretch (i.e. relative elongations with respect to the three orthogonal axes), rigid body rotation, and translation. We will measure all quantities relative to the global XYZ axes, often known as the *material coordinate system*. Consider an infinitesimal line, PQ , or vector, dX , embedded in the material in the undeformed configuration. The position of point P is given by vector X , relative to the material reference frame. The line PQ undergoes deformation from state A to the deformed

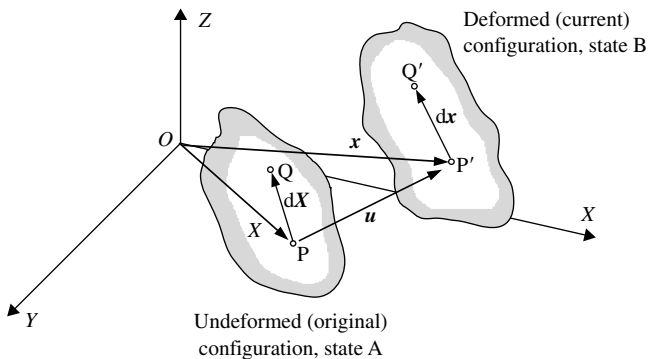


Fig. 3.2 An element of material in the reference or undeformed configuration undergoing deformation to the deformed or current configuration.

configuration in state B. In doing so, point P has been translated by \mathbf{u} to point P'. Relative to the material reference frame, point P' is given by vector \mathbf{x} where

$$\mathbf{x} = \mathbf{X} + \mathbf{u}. \quad (3.1)$$

The infinitesimal vector $d\mathbf{X}$ is transformed to its deformed state, $d\mathbf{x}$, by the *deformation gradient*, \mathbf{F} , where

$$d\mathbf{x} = \mathbf{F} d\mathbf{X}. \quad (3.2)$$

We can write this in component form as

$$\begin{pmatrix} dx \\ dy \\ dz \end{pmatrix} = \begin{pmatrix} F_{xx} & F_{xy} & F_{xz} \\ F_{yx} & F_{yy} & F_{yz} \\ F_{zx} & F_{zy} & F_{zz} \end{pmatrix} \begin{pmatrix} dX \\ dY \\ dZ \end{pmatrix} = \begin{pmatrix} \frac{\partial x}{\partial X} & \frac{\partial x}{\partial Y} & \frac{\partial x}{\partial Z} \\ \frac{\partial y}{\partial X} & \frac{\partial y}{\partial Y} & \frac{\partial y}{\partial Z} \\ \frac{\partial z}{\partial X} & \frac{\partial z}{\partial Y} & \frac{\partial z}{\partial Z} \end{pmatrix} \begin{pmatrix} dX \\ dY \\ dZ \end{pmatrix} \quad (3.3)$$

or

$$\mathbf{F} = \frac{\partial \mathbf{x}}{\partial \mathbf{X}}. \quad (3.4)$$

The deformation gradient, \mathbf{F} , provides a complete description of deformation (excluding translations) which includes stretch as well as rigid body rotation. Rigid body rotation does not contribute to shape or size change, or internal stress. In solving problems, it is necessary to separate out the stretch from the rigid body rotation contained within \mathbf{F} . In the following sections, we will see examples of stretch, rigid body rotation, and their combination, and how they are described by the deformation gradient.

3.3 Measures of strain

Let us consider the length, ds , of the line $d\mathbf{x}$ in the deformed configuration. We may write

$$\begin{aligned} ds^2 &= d\mathbf{x} \cdot d\mathbf{x} = (\mathbf{F} d\mathbf{X}) \cdot (\mathbf{F} d\mathbf{X}) = d\mathbf{X}^T \mathbf{F}^T \mathbf{F} d\mathbf{X} \\ &= d\mathbf{X}^T \left(\frac{\partial \mathbf{x}}{\partial \mathbf{X}} \right)^T \frac{\partial \mathbf{x}}{\partial \mathbf{X}} d\mathbf{X} = d\mathbf{X}^T \mathbf{C} d\mathbf{X} \end{aligned}$$

so that

$$\mathbf{C} = \mathbf{F}^T \mathbf{F}. \quad (3.5)$$

\mathbf{C} is called the (left) Cauchy–Green tensor. Consider also the length, dS , of the element, $d\mathbf{X}$, in the undeformed state:

$$dS^2 = d\mathbf{X}^T d\mathbf{X}. \quad (3.6)$$

50 Large deformations and continuum mechanics

Now

$$d\mathbf{x} = \mathbf{F} d\mathbf{X}$$

so

$$d\mathbf{X} = \mathbf{F}^{-1} d\mathbf{x}.$$

Substituting into Equation (3.6) gives

$$dS^2 = (\mathbf{F}^{-1} d\mathbf{x})^T \mathbf{F}^{-1} d\mathbf{x} = d\mathbf{x}^T (\mathbf{F}^{-1})^T \mathbf{F}^{-1} d\mathbf{x} = d\mathbf{x}^T \mathbf{B}^{-1} d\mathbf{x},$$

where

$$\mathbf{B}^{-1} = (\mathbf{F}^{-1})^T \mathbf{F}^{-1} \quad (3.7)$$

and \mathbf{B} is called the (right) Cauchy–Green tensor. Both \mathbf{B} and \mathbf{C} are in fact measures of stretch as we will now see.

A measure of the stretch is given by the difference in lengths of the lines PQ and P'Q' in Fig. 3.2 in the undeformed and deformed configurations, respectively. We can write

$$ds^2 - dS^2 = d\mathbf{x} \cdot d\mathbf{x} - d\mathbf{x} \cdot \mathbf{B}^{-1} d\mathbf{x} = d\mathbf{x} \cdot (\mathbf{I} - \mathbf{B}^{-1}) d\mathbf{x} \quad (3.8)$$

in which \mathbf{I} is the identity tensor. It can be seen, therefore, that \mathbf{B} is related to the change in length of the line; in other words, a measure of stretch. It is independent of rigid body rotation because the orientations of the lines in the undeformed and deformed configurations are irrelevant. If ds and dS are the same length, then there is no stretch and

$$ds^2 - dS^2 = 0.$$

From Equation (3.8), this means that

$$\mathbf{B} = \mathbf{I} \quad (3.9)$$

and there is no stretch, so that in this instance, the deformation gradient contains only rigid body rotation. The Cauchy–Green tensor, \mathbf{B} , could itself be used as a measure of strain, since it is independent of rigid body rotation, but depends upon the stretch. This is an important criterion for any strain measure in large deformation analysis in which rigid body rotation occurs. A strain which depends upon rigid body rotation would not be appropriate since it would give a different measure of the strain depending upon orientation. However, the Cauchy–Green tensor given in (3.9) contains non-zero components even though the stretch is zero. An alternative and more appropriate strain measure called the Almansi strain was introduced:

$$\mathbf{e} = \frac{1}{2}(\mathbf{I} - \mathbf{B}^{-1}) \quad (3.10)$$

so that for zero stretch,

$$\mathbf{e} = 0.$$

This strain measure behaves more like familiar strains, such as engineering strain, since for zero stretch, it gives us strain components of zero.

A further measure of strain is the logarithmic, or true strain defined as

$$\boldsymbol{\varepsilon} = -\frac{1}{2} \ln \mathbf{B}^{-1}, \quad (3.11)$$

which we shall consider in more detail later. In determining the change of length of the line OP, we could have chosen the original configuration to work in as follows:

$$\begin{aligned} ds^2 - dS^2 &= d\mathbf{x}^T d\mathbf{x} - d\mathbf{X}^T d\mathbf{X} = (\mathbf{F} d\mathbf{X})^T \mathbf{F} d\mathbf{X} - d\mathbf{X}^T d\mathbf{X} \\ &= d\mathbf{X} \mathbf{F}^T \mathbf{F} d\mathbf{X} - d\mathbf{X}^T d\mathbf{X} = d\mathbf{X}^T (\mathbf{F}^T \mathbf{F} - \mathbf{I}) d\mathbf{X} \\ &= d\mathbf{X}^T (\mathbf{C} - \mathbf{I}) d\mathbf{X} = d\mathbf{X}^T (2\mathbf{E}) d\mathbf{X}, \end{aligned}$$

where

$$\mathbf{E} = \frac{1}{2} (\mathbf{C} - \mathbf{I}) = \frac{1}{2} (\mathbf{F}^T \mathbf{F} - \mathbf{I}). \quad (3.12)$$

\mathbf{E} is called the large strain or the *Green–Lagrange strain tensor*. We can make this look a little more familiar, perhaps, by combining Equations (3.4) for \mathbf{F} and (3.1) for \mathbf{x}

$$\mathbf{F} = \frac{\partial \mathbf{x}}{\partial \mathbf{X}} = \frac{\partial (\mathbf{u} + \mathbf{X})}{\partial \mathbf{X}} = \frac{\partial \mathbf{u}}{\partial \mathbf{X}} + \mathbf{I}$$

and then substituting into (3.12) to give

$$\begin{aligned} \mathbf{E} &= \frac{1}{2} (\mathbf{F}^T \mathbf{F} - \mathbf{I}) = \frac{1}{2} \left(\left[\frac{\partial \mathbf{u}}{\partial \mathbf{X}} + \mathbf{I} \right]^T \left[\frac{\partial \mathbf{u}}{\partial \mathbf{X}} + \mathbf{I} \right] - \mathbf{I} \right) \\ &= \frac{1}{2} \left(\frac{\partial \mathbf{u}}{\partial \mathbf{X}} + \left(\frac{\partial \mathbf{u}}{\partial \mathbf{X}} \right)^T + \left(\frac{\partial \mathbf{u}}{\partial \mathbf{X}} \right)^T \frac{\partial \mathbf{u}}{\partial \mathbf{X}} \right). \end{aligned} \quad (3.13)$$

If we ignore the second-order term, this reduces to

$$\mathbf{E} = \frac{1}{2} \left(\frac{\partial \mathbf{u}}{\partial \mathbf{X}} + \left(\frac{\partial \mathbf{u}}{\partial \mathbf{X}} \right)^T \right). \quad (3.14)$$

We will examine this and other strains for simple uniaxial loading in Section 3.4. Before doing so, let us examine the symmetry of the strain quantities presented above.

The symmetric part of a tensor, \mathbf{A} , is given by

$$\text{sym}(\mathbf{A}) = \frac{1}{2} (\mathbf{A} + \mathbf{A}^T) \quad (3.15)$$

and the antisymmetric or skew symmetric (or sometimes simply skew) part of \mathbf{A} by

$$\text{asym}(\mathbf{A}) = \frac{1}{2} (\mathbf{A} - \mathbf{A}^T). \quad (3.16)$$

52 Large deformations and continuum mechanics

To be pedantic, let us write out the symmetric and antisymmetric parts of the 2×2 matrix \mathbf{A} given by

$$\mathbf{A} = \begin{pmatrix} a_{11} & a_{12} \\ a_{21} & a_{22} \end{pmatrix}$$

in which $a_{12} \neq a_{21}$.

$$\text{sym}(\mathbf{A}) = \begin{pmatrix} a_{11} & \frac{a_{12} + a_{21}}{2} \\ \frac{a_{12} + a_{21}}{2} & a_{22} \end{pmatrix}$$

and

$$\text{asym}(\mathbf{A}) = \begin{pmatrix} 0 & \frac{a_{12} - a_{21}}{2} \\ -\frac{a_{12} - a_{21}}{2} & 0 \end{pmatrix}.$$

Clearly, $\text{sym}(\mathbf{A})$ is symmetric and the leading diagonal of an antisymmetric tensor always contains zeros. Let us now consider the quantity $\mathbf{F}^T \mathbf{F}$ which appears above in a number of strain quantities:

$$\text{sym}(\mathbf{F}^T \mathbf{F}) = \frac{1}{2}[\mathbf{F}^T \mathbf{F} + (\mathbf{F}^T \mathbf{F})^T] = \mathbf{F}^T \mathbf{F}$$

and

$$\text{asym}(\mathbf{F}^T \mathbf{F}) = \frac{1}{2}[\mathbf{F}^T \mathbf{F} - (\mathbf{F}^T \mathbf{F})^T] = 0.$$

We see, therefore, that $\mathbf{F}^T \mathbf{F}$ is a symmetric tensor so that, in fact, the quantities \mathbf{B}^{-1} , \mathbf{C} , $\boldsymbol{\varepsilon}$, and \mathbf{E} are all themselves symmetric. In general, \mathbf{F} will not necessarily be symmetric. If it is, the deformation it represents is made only up of stretch.

3.4 Interpretation of strain measures

Let us determine the deformation gradient for the simple case of a uniaxial rod which is subjected, first to purely rigid body rotation and then to uniaxial stretch and then consider some of the measures of deformation and strain introduced in Section 3.3.

3.4.1 Rigid body rotation only

Figure 3.3 shows a rod lying along the Y -axis which undergoes a clockwise rotation about the Z -axis of angle θ . There is no stretch imposed, so the deformation gradient is simply the rotation matrix, \mathbf{R} , given by

$$\mathbf{F} = \mathbf{R} = \begin{pmatrix} \cos \theta & -\sin \theta & 0 \\ \sin \theta & \cos \theta & 0 \\ 0 & 0 & 1 \end{pmatrix}. \quad (3.17)$$

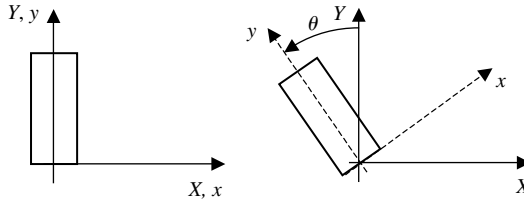


Fig. 3.3 A rod undergoing rigid body rotation through angle θ .

The uppercase letters in Fig. 3.3, XY , refer to the material reference frame directions. Also shown in the figure is a coordinate system which rotates with the deforming material (in this case, the rotating rod). We will generally use lowercase letters, xy , to indicate the reference frame which rotates with the material. This is called the *co-rotational reference frame*.

We can now determine the Cauchy–Green tensor, \mathbf{B}^{-1} , and the strain quantities. From Equation (3.7),

$$\begin{aligned}\mathbf{B}^{-1} &= (\mathbf{F}^{-1})^T \mathbf{F}^{-1} = \begin{pmatrix} \cos \theta & -\sin \theta & 0 \\ \sin \theta & \cos \theta & 0 \\ 0 & 0 & 1 \end{pmatrix} \begin{pmatrix} \cos \theta & \sin \theta & 0 \\ -\sin \theta & \cos \theta & 0 \\ 0 & 0 & 1 \end{pmatrix} \\ &= \begin{pmatrix} 1 & 0 & 0 \\ 0 & 1 & 0 \\ 0 & 0 & 1 \end{pmatrix}.\end{aligned}$$

The tensor \mathbf{B}^{-1} is found to be the identity tensor for rigid body rotation because there is no stretch. Measures of deformation that are appropriate for large deformations with rigid body rotation must have this property: that they depend upon the stretch but are independent of the rigid body rotation. The Almansi strain, from (3.10), is

$$\mathbf{e} = \frac{1}{2}(\mathbf{I} - \mathbf{B}^{-1}) = 0$$

and the true strain, (3.11), is given by

$$\boldsymbol{\varepsilon} = \frac{1}{2} \ln \mathbf{B}^{-1} = 0.$$

Similarly, the Green strain is

$$\mathbf{E} = \frac{1}{2}(\mathbf{F}^T \mathbf{F} - \mathbf{I}) = 0.$$

We see that the three strain measures give zero for the case of rigid body rotation. Before moving away from rotation, it is important to note that a rotation tensor, such as \mathbf{R} , is always orthogonal, that is,

$$\mathbf{R}\mathbf{R}^T = \mathbf{I} \quad (3.18)$$

54 Large deformations and continuum mechanics

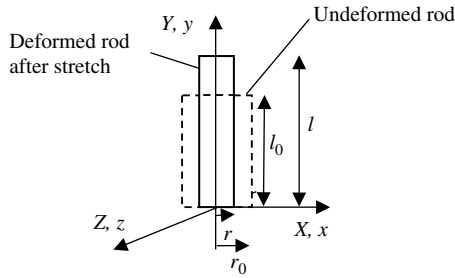


Fig. 3.4 A rod undergoing pure stretch in the absence of rigid body rotation.

so that

$$\mathbf{R}^T = \mathbf{R}^{-1}.$$

We will make much use of this property in the subsequent sections.

3.4.2 Uniaxial stretch

Let us now consider uniaxial stretch of the circular rod in the Y -direction. This is shown schematically in Fig. 3.4. Note that because there is no rotation in this case, the co-rotational reference frame is directionally coincident with the material reference frame.

For the uniaxial stretch shown, the *stretch ratios*, λ , are

$$\lambda_x = \frac{r}{r_0}, \quad \lambda_y = \frac{l}{l_0}, \quad \lambda_z = \frac{r}{r_0}. \quad (3.19)$$

Let us consider the case of large strain such that the elastic strains can be ignored. For large plastic deformation, the incompressibility condition written in terms of stretches is

$$\lambda_x \lambda_y \lambda_z = 1 \quad (3.20)$$

so that

$$\lambda_x = \lambda_z \equiv \frac{1}{\sqrt{\lambda_y}}$$

and therefore

$$\lambda_x = \lambda_z = \left(\frac{l}{l_0}\right)^{-1/2}. \quad (3.21)$$

Considering the stretch along the Y -axis, any point, Y , lying on the undeformed rod becomes the point $y = \lambda_y Y$ on the deformed rod. The deformation can therefore be represented by

$$x = \lambda_x X, \quad y = \lambda_y Y, \quad z = \lambda_z Z$$

so that

$$\frac{\partial x}{\partial X} = \lambda_x, \quad \frac{\partial y}{\partial Y} = \lambda_y, \quad \frac{\partial z}{\partial Z} = \lambda_z$$

and

$$\frac{\partial x}{\partial Y} = \frac{\partial x}{\partial Z} = 0 \text{ etc.}$$

The deformation gradient can then be determined using Equation (3.3),

$$\mathbf{F} = \frac{\partial \mathbf{x}}{\partial \mathbf{X}} = \begin{pmatrix} \frac{\partial x}{\partial X} & \frac{\partial x}{\partial Y} & \frac{\partial x}{\partial Z} \\ \frac{\partial y}{\partial X} & \frac{\partial y}{\partial Y} & \frac{\partial y}{\partial Z} \\ \frac{\partial z}{\partial X} & \frac{\partial z}{\partial Y} & \frac{\partial z}{\partial Z} \end{pmatrix} = \begin{pmatrix} \lambda_x & 0 & 0 \\ 0 & \lambda_y & 0 \\ 0 & 0 & \lambda_z \end{pmatrix}$$

and with (3.19) and (3.21)

$$\mathbf{F} = \begin{pmatrix} \left(\frac{l}{l_0}\right)^{-1/2} & 0 & 0 \\ 0 & \left(\frac{l}{l_0}\right) & 0 \\ 0 & 0 & \left(\frac{l}{l_0}\right)^{-1/2} \end{pmatrix}.$$

We first notice that \mathbf{F} is symmetric so that

$$\mathbf{F}^T = \mathbf{F}$$

and therefore represents stretch only. Let us examine the various deformation and strain tensors.

The inverse of \mathbf{F} is

$$\mathbf{F}^{-1} = \begin{pmatrix} \left(\frac{l}{l_0}\right)^{1/2} & 0 & 0 \\ 0 & \left(\frac{l}{l_0}\right)^{-1} & 0 \\ 0 & 0 & \left(\frac{l}{l_0}\right)^{1/2} \end{pmatrix}$$

so the Cauchy–Green tensor is given by

$$\mathbf{B}^{-1} = (\mathbf{F}^{-1})^T \mathbf{F}^{-1} = \mathbf{F}^{-1} \mathbf{F}^{-1} = \begin{pmatrix} \frac{l}{l_0} & 0 & 0 \\ 0 & \left(\frac{l}{l_0}\right)^{-2} & 0 \\ 0 & 0 & \frac{l}{l_0} \end{pmatrix}.$$

56 Large deformations and continuum mechanics

The true plastic strain is, therefore,

$$\boldsymbol{\varepsilon} = -\frac{1}{2} \ln \mathbf{B}^{-1} = -\frac{1}{2} \ln \begin{pmatrix} \frac{l}{l_0} & 0 & 0 \\ 0 & \left(\frac{l}{l_0}\right)^{-2} & 0 \\ 0 & 0 & \frac{l}{l_0} \end{pmatrix} = \begin{pmatrix} -\frac{1}{2} \ln \frac{l}{l_0} & 0 & 0 \\ 0 & \ln \frac{l}{l_0} & 0 \\ 0 & 0 & -\frac{1}{2} \ln \frac{l}{l_0} \end{pmatrix}. \quad (3.22)$$

We see that the true strain components are $\varepsilon_{xx} = \varepsilon_{zz} = -\frac{1}{2} \ln(l/l_0) = -\frac{1}{2} \varepsilon_{yy}$ and $\varepsilon_{yy} = \ln(l/l_0)$, as we would expect for uniaxial plasticity conditions. Before leaving the true strain, note that we needed to take the logarithm of the Cauchy–Green tensor which we did by operating on the leading diagonal alone. We were able to do this in this case because the leading diagonal terms happen, in this simple case, to be the principal parts of the tensor (i.e. the eigenvalues).

In general, in order to carry out an operation, p , on tensor \mathbf{A} having a linearly independent set of eigenvectors, we need to diagonalize the tensor and operate on the principal values. In practice, this means transforming the tensor into its principal coordinates, by finding the eigenvalues and eigenvectors of \mathbf{A} , operating on it and transforming it back. If the modal matrix (i.e. the matrix containing the eigenvectors of \mathbf{A}) is written as \mathbf{M} , and the diagonal matrix (i.e. the matrix containing the eigenvalues of \mathbf{A} along the leading diagonal) as $\hat{\mathbf{A}}$, then \mathbf{A} can be written

$$\mathbf{A} = \mathbf{M} \hat{\mathbf{A}} \mathbf{M}^{-1}$$

so that we operate on \mathbf{A} to give $p(\mathbf{A})$ as follows

$$p(\mathbf{A}) = \mathbf{M} p(\hat{\mathbf{A}}) \mathbf{M}^{-1}, \quad (3.23)$$

where the operation p is carried out only on the leading diagonal terms. For example,

$$\ln(\mathbf{A}) = \mathbf{M} \ln(\hat{\mathbf{A}}) \mathbf{M}^{-1}.$$

In Equation (3.22), the modal matrix of \mathbf{B}^{-1} in this case is just the identity matrix and its diagonal matrix $\hat{\mathbf{B}}^{-1}$ is the same as \mathbf{B}^{-1} so that

$$\ln(\mathbf{B}^{-1}) = \mathbf{M} \ln(\hat{\mathbf{B}}^{-1}) \mathbf{M}^{-1} = \mathbf{I} \ln(\mathbf{B}^{-1}) \mathbf{I}^{-1} = \ln(\mathbf{B}^{-1}).$$

Let us finally determine the Green strain first from (3.12) and second directly from the displacements using (3.14).

Using (3.12), we need

$$\mathbf{F}^T \mathbf{F} = \begin{pmatrix} \left(\frac{r}{r_0}\right)^2 & 0 & 0 \\ 0 & \left(\frac{l}{l_0}\right)^2 & 0 \\ 0 & 0 & \left(\frac{r}{r_0}\right)^2 \end{pmatrix} \approx \begin{pmatrix} 1 + \frac{2\Delta r}{r_0} & 0 & 0 \\ 0 & 1 + \frac{2\Delta l}{l_0} & 0 \\ 0 & 0 & 1 + \frac{2\Delta r}{r_0} \end{pmatrix}$$

if we write $r = r_0 + \Delta r$ and assume that the strains are small, so that

$$\mathbf{E} = \frac{1}{2} \left[\begin{pmatrix} 1 + \frac{2\Delta r}{r_0} & 0 & 0 \\ 0 & 1 + \frac{2\Delta l}{l_0} & 0 \\ 0 & 0 & 1 + \frac{2\Delta r}{r_0} \end{pmatrix} - \begin{pmatrix} 1 & 0 & 0 \\ 0 & 1 & 0 \\ 0 & 0 & 1 \end{pmatrix} \right] = \begin{pmatrix} \frac{\Delta r}{r_0} & 0 & 0 \\ 0 & \frac{\Delta l}{l_0} & 0 \\ 0 & 0 & \frac{\Delta r}{r_0} \end{pmatrix}.$$

We see that the components of the Green strain are therefore approximately the engineering strain components. If we now start from (3.14) in which we have also neglected second-order terms, we need the displacements, \mathbf{u} , which are given by

$$\mathbf{u}_x = (r - r_0) \frac{X}{r_0}, \quad \mathbf{u}_y = (l - l_0) \frac{Y}{l_0}, \quad \mathbf{u}_z = (r - r_0) \frac{Z}{r_0}$$

so that

$$\frac{\partial \mathbf{u}}{\partial \mathbf{X}} = \begin{pmatrix} \frac{\Delta r}{r_0} & 0 & 0 \\ 0 & \frac{\Delta l}{l_0} & 0 \\ 0 & 0 & \frac{\Delta r}{r_0} \end{pmatrix} \quad \text{and} \quad \mathbf{E} = \frac{1}{2} \left(\frac{\partial \mathbf{u}}{\partial \mathbf{X}} + \left(\frac{\partial \mathbf{u}}{\partial \mathbf{X}} \right)^T \right) = \begin{pmatrix} \frac{\Delta r}{r_0} & 0 & 0 \\ 0 & \frac{\Delta l}{l_0} & 0 \\ 0 & 0 & \frac{\Delta r}{r_0} \end{pmatrix}$$

as before.

We have looked at a number of examples in which stretch and rigid body rotation have taken place exclusively. We will now look at how to separate them in cases where they occur simultaneously, using the *polar decomposition theorem*.

3.5 Polar decomposition

Recall that the deformation at any material point can be considered to comprise three parts:

- (1) rigid body translation (which we do not need to consider here);
- (2) rigid body rotation;
- (3) stretch.

58 Large deformations and continuum mechanics

The polar decomposition theorem states that any non-singular, second-order tensor can be decomposed uniquely into the product of an orthogonal tensor (a rotation), and a symmetric tensor (stretch).

The deformation gradient is a non-singular, second-order tensor and can therefore be written as

$$\mathbf{F} = \mathbf{R}\mathbf{U} = \mathbf{V}\mathbf{R}, \quad (3.24)$$

where \mathbf{R} is an orthogonal ($\mathbf{R}^T\mathbf{R} = \mathbf{I}$) rotation tensor, and \mathbf{U} and \mathbf{V} are symmetric ($\mathbf{U} = \mathbf{U}^T$) stretch tensors.

Using the polar decomposition theorem, we can now examine in more detail the right and left Cauchy–Green deformation tensors. From Equation (3.7),

$$\begin{aligned} \mathbf{B}^{-1} &= (\mathbf{F}^{-1})^T\mathbf{F}^{-1} = [(\mathbf{V}\mathbf{R})^{-1}]^T(\mathbf{V}\mathbf{R})^{-1} = (\mathbf{R}^{-1}\mathbf{V}^{-1})^T\mathbf{R}^{-1}\mathbf{V}^{-1} \\ &= (\mathbf{V}^{-1})^T(\mathbf{R}^{-1})^T\mathbf{R}^{-1}\mathbf{V}^{-1} = (\mathbf{V}^{-1})^T\mathbf{V}^{-1} \end{aligned}$$

since \mathbf{R} is orthogonal

$$\mathbf{B}^{-1} = \mathbf{V}^{-1}\mathbf{V}^{-1} = (\mathbf{V}^{-1})^2,$$

where the squaring operation is carried out on the diagonalized form of \mathbf{V}^{-1} . This confirms, therefore, that \mathbf{B} is a measure of deformation that depends on stretch only, and is independent of the rigid body rotation, \mathbf{R} .

Similarly, for \mathbf{C} ,

$$\begin{aligned} \mathbf{C} &= \mathbf{F}^T\mathbf{F} = (\mathbf{R}\mathbf{U})^T\mathbf{R}\mathbf{U} = \mathbf{U}^T\mathbf{R}^T\mathbf{R}\mathbf{U} \\ &= \mathbf{U}^T\mathbf{U} \quad \text{since } \mathbf{R} \text{ is orthogonal} \\ &= \mathbf{U}^2 \quad \text{since } \mathbf{U} \text{ is symmetric.} \end{aligned}$$

The true strain rate can now be written in terms of \mathbf{V} since

$$\boldsymbol{\epsilon} = -\frac{1}{2} \ln \mathbf{B}^{-1} = -\frac{1}{2} \ln (\mathbf{V}^{-1})^2 = \ln \mathbf{V}, \quad (3.25)$$

which is also independent of the rigid body rotation and dependent on the stretch alone. Let us have a look at a problem in which both stretch and rigid body rotation occur together: the problem of simple shear.

3.5.1 Simple shear

Figure 3.5 shows schematically the simple shear by δ , in two dimensions, of a unit square.

We can represent the deformation, which transforms a point (X, Y) in the undeformed configuration to (x, y) in the deformed configuration, by

$$x = X + \delta Y, \quad y = Y$$

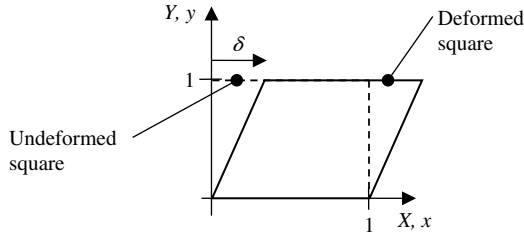


Fig. 3.5 A unit square undergoing simple shear.

so that

$$\frac{\partial x}{\partial X} = 1, \quad \frac{\partial x}{\partial Y} = \delta, \quad \frac{\partial y}{\partial X} = 0, \quad \frac{\partial y}{\partial Y} = 1.$$

The deformation gradient is, therefore,

$$\mathbf{F} = \begin{pmatrix} 1 & \delta \\ 0 & 1 \end{pmatrix}.$$

We can then determine the Cauchy–Green tensor, \mathbf{C} , from

$$\mathbf{C} = \mathbf{F}^T \mathbf{F} = \begin{pmatrix} 1 & 0 \\ \delta & 1 \end{pmatrix} \begin{pmatrix} 1 & \delta \\ 0 & 1 \end{pmatrix} = \begin{pmatrix} 1 & \delta \\ \delta & 1 + \delta^2 \end{pmatrix}. \quad (3.26)$$

Note the symmetry of this deformation tensor. We can use the polar decomposition theorem to separate out the stretch and rigid body rotation contained in the deformation gradient. Let us set

$$\mathbf{U} = \begin{pmatrix} U_{xx} & U_{xy} \\ U_{yx} & U_{yy} \end{pmatrix} \quad \mathbf{R} = \begin{pmatrix} \cos \varphi & \sin \varphi \\ -\sin \varphi & \cos \varphi \end{pmatrix} \quad (3.27)$$

so that

$$\mathbf{F} = \mathbf{R}\mathbf{U} \quad \text{gives} \quad \begin{pmatrix} 1 & \delta \\ 0 & 1 \end{pmatrix} = \begin{pmatrix} \cos \varphi & \sin \varphi \\ -\sin \varphi & \cos \varphi \end{pmatrix} \begin{pmatrix} U_{xx} & U_{xy} \\ U_{yx} & U_{yy} \end{pmatrix}. \quad (3.28)$$

Solving for the stretches in terms of δ and φ gives

$$\mathbf{U} = \begin{pmatrix} \cos \varphi & \sin \varphi \\ \sin \varphi & \cos \varphi + \delta \sin \varphi \end{pmatrix}$$

and substituting back into (3.28) gives

$$\sin \varphi = \frac{\delta}{\sqrt{2^2 + \delta^2}} \quad \text{and} \quad \cos \varphi = \frac{2}{\sqrt{2^2 + \delta^2}}$$

so that

$$\mathbf{R} = \frac{1}{\sqrt{2^2 + \delta^2}} \begin{pmatrix} 2 & \delta \\ -\delta & 2 \end{pmatrix} \quad (3.29)$$

and

$$\mathbf{U} = \frac{1}{\sqrt{2^2 + \delta^2}} \begin{pmatrix} 2 & \delta \\ \delta & 2 + \delta^2 \end{pmatrix}. \quad (3.30)$$

Comparing Equations (3.30) and (3.26), and with a little algebra confirms that $\mathbf{C} = \mathbf{U}^2$. \mathbf{U} is the symmetric stretch and Equation (3.29) shows that the rigid body rotation is non-zero. It is useful to examine why this is. It may not be obvious that the deformation corresponding to simple shear shown in Fig. 3.5 leads to a rigid body rotation. Let us first determine the Green–Lagrange strain for this deformation. Using Equation (3.12),

$$\mathbf{E} = \frac{1}{2}(\mathbf{F}^T \mathbf{F} - \mathbf{I}) = \frac{1}{2}(\mathbf{C} - \mathbf{I}) = \frac{1}{2} \left(\begin{pmatrix} 1 & \delta \\ \delta & 1 + \delta^2 \end{pmatrix} - \begin{pmatrix} 1 & 0 \\ 0 & 1 \end{pmatrix} \right) = \frac{1}{2} \begin{pmatrix} 0 & \delta \\ \delta & \delta^2 \end{pmatrix}. \quad (3.31)$$

From Equation (3.29), or from the components of strain in Equation (3.31), we see that the principal stretch directions rotate as the simple shear proceeds. That is, the ‘material axes’ rotate relative to the direction of the applied deformation.

The polar decomposition theorem is fundamental to large deformation kinematics and we shall return to it in subsequent sections.

3.6 Velocity gradient, rate of deformation, and continuum spin

We have so far considered stretch, rigid body rotation, measures of strain, and the polar decomposition theorem which enables us to separate out stretch and rotation. All the quantities considered have been independent of time. However, many plasticity formulations (viscoplasticity is an obvious case) are developed in terms of rate quantities and it is necessary, therefore, to consider how the quantities already discussed can be put in rate form. Often, in fact, even rate-independent plasticity models are written in rate form for implementation into finite element code. This is easy to understand given that plasticity is an incremental process; rather than deal with increments in plastic strain, it is often more convenient to work with the equivalent quantity, plastic strain rate.

Consider a spatially varying *velocity field*, that is, one for which the material point velocities vary spatially. The increment in velocity, $d\mathbf{v}$, occurring over an incremental change in position, $d\mathbf{x}$, in the deformed configuration, may be written as

$$d\mathbf{v} = \frac{\partial \mathbf{v}}{\partial \mathbf{x}} d\mathbf{x}.$$

The *velocity gradient* describes the spatial rate of change of the velocity and is given by

$$\mathbf{L} = \frac{\partial \mathbf{v}}{\partial \mathbf{x}}. \quad (3.32)$$

Consider the time rate of change of the deformation gradient:

$$\dot{\mathbf{F}} = \frac{\partial}{\partial t} \left(\frac{\partial \mathbf{x}}{\partial \mathbf{X}} \right) = \frac{\partial \mathbf{v}}{\partial \mathbf{X}} = \frac{\partial \mathbf{v}}{\partial \mathbf{x}} \frac{\partial \mathbf{x}}{\partial \mathbf{X}} = \mathbf{L}\mathbf{F}$$

or

$$\mathbf{L} = \dot{\mathbf{F}}\mathbf{F}^{-1}. \quad (3.33)$$

The velocity gradient, therefore, maps the deformation gradient onto the rate of change of the deformation gradient.

The velocity gradient can be decomposed into symmetric (stretch related) and antisymmetric (rotation related) parts:

$$\mathbf{L} = \text{sym}(\mathbf{L}) + \text{asym}(\mathbf{L}),$$

where

$$\text{sym}(\mathbf{L}) = \frac{1}{2}(\mathbf{L} + \mathbf{L}^T) \quad (3.34)$$

and

$$\text{asym}(\mathbf{L}) = \frac{1}{2}(\mathbf{L} - \mathbf{L}^T). \quad (3.35)$$

The symmetric part is called the *rate of deformation*, \mathbf{D} , and the antisymmetric part the *continuum spin*, \mathbf{W} , so that

$$\mathbf{L} = \mathbf{D} + \mathbf{W}, \quad (3.36)$$

where the rate of deformation

$$\mathbf{D} = \frac{1}{2}(\mathbf{L} + \mathbf{L}^T) \quad (3.37)$$

and the continuum spin is given by

$$\mathbf{W} = \frac{1}{2}(\mathbf{L} - \mathbf{L}^T). \quad (3.38)$$

We shall now examine both quantities, the rate of deformation and the continuum spin, for some simple examples, including uniaxial stretch and purely rigid body rotation in order to gain a physical feel for these quantities.

3.6.1 Rigid body rotation and continuum spin

We have previously looked at the rigid body rotation of a uniaxial rod. Figure 3.3 shows this schematically. We will now look not only at the rigid body rotation, but also the rate at which it occurs. Consider the rotation of the rod shown in Fig. 3.3,

62 Large deformations and continuum mechanics

at time t making an angle θ with the Y -axis, with no stretch, rotating at constant rate $\dot{\theta}$. The deformation gradient at any instant is given by

$$\mathbf{F} = \begin{pmatrix} \cos \theta & -\sin \theta & 0 \\ \sin \theta & \cos \theta & 0 \\ 0 & 0 & 1 \end{pmatrix} \quad (3.39)$$

so that the rate of change of deformation gradient is

$$\dot{\mathbf{F}} = \dot{\theta} \begin{pmatrix} -\sin \theta & -\cos \theta & 0 \\ \cos \theta & -\sin \theta & 0 \\ 0 & 0 & 0 \end{pmatrix}. \quad (3.40)$$

In order to determine the velocity gradient, we need the inverse of \mathbf{F} which we can obtain from (3.39) as

$$\mathbf{F}^{-1} (= \mathbf{F}^T \text{ in this case}) = \begin{pmatrix} \cos \theta & \sin \theta & 0 \\ -\sin \theta & \cos \theta & 0 \\ 0 & 0 & 1 \end{pmatrix}.$$

We may then determine the velocity gradient using Equation (3.33) as

$$\mathbf{L} = \dot{\mathbf{F}}\mathbf{F}^{-1} = \dot{\theta} \begin{pmatrix} -\sin \theta & -\cos \theta & 0 \\ \cos \theta & -\sin \theta & 0 \\ 0 & 0 & 0 \end{pmatrix} \begin{pmatrix} \cos \theta & \sin \theta & 0 \\ -\sin \theta & \cos \theta & 0 \\ 0 & 0 & 1 \end{pmatrix} = \dot{\theta} \begin{pmatrix} 0 & -1 & 0 \\ 1 & 0 & 0 \\ 0 & 0 & 0 \end{pmatrix}.$$

The transpose of \mathbf{L} is

$$\mathbf{L}^T = \dot{\theta} \begin{pmatrix} 0 & 1 & 0 \\ -1 & 0 & 0 \\ 0 & 0 & 0 \end{pmatrix}$$

so that the deformation gradient is given by

$$\mathbf{D} = \frac{1}{2}(\mathbf{L} + \mathbf{L}^T) = \dot{\theta} \begin{pmatrix} 0 & 0 & 0 \\ 0 & 0 & 0 \\ 0 & 0 & 0 \end{pmatrix} = \mathbf{0}$$

and the continuum spin is

$$\mathbf{W} = \frac{1}{2}(\mathbf{L} - \mathbf{L}^T) = \dot{\theta} \begin{pmatrix} 0 & -1 & 0 \\ 1 & 0 & 0 \\ 0 & 0 & 0 \end{pmatrix}. \quad (3.41)$$

That is, there is no stretch rate contributing to the velocity gradient so that the rate of deformation is zero, but rigid body rotation occurs so that the continuum spin is non-zero. Let us now examine the significance of the continuum spin for the case of rigid body rotation of the uniaxial rod without stretch.

Consider the rate of rotation, $\dot{\mathbf{R}}$, given by

$$\dot{\mathbf{R}} = \dot{\theta} \begin{pmatrix} -\sin \theta & -\cos \theta & 0 \\ \cos \theta & -\sin \theta & 0 \\ 0 & 0 & 0 \end{pmatrix}. \quad (3.42)$$

Next, consider the product of \mathbf{W} and \mathbf{R}

$$\mathbf{WR} = \dot{\theta} \begin{pmatrix} 0 & -1 & 0 \\ 1 & 0 & 0 \\ 0 & 0 & 0 \end{pmatrix} \begin{pmatrix} \cos \theta & -\sin \theta & 0 \\ \sin \theta & \cos \theta & 0 \\ 0 & 0 & 1 \end{pmatrix} = \dot{\theta} \begin{pmatrix} -\sin \theta & -\cos \theta & 0 \\ \cos \theta & -\sin \theta & 0 \\ 0 & 0 & 0 \end{pmatrix}.$$

That is, for this particular case of rigid body rotation only, we see that

$$\dot{\mathbf{R}} = \mathbf{WR} \quad (3.43)$$

so that \mathbf{W} is the tensor that maps \mathbf{R} onto $\dot{\mathbf{R}}$. Remembering that \mathbf{R} is orthogonal so that $\mathbf{R}^{-1} = \mathbf{R}^T$, \mathbf{W} can be written for this simple case as

$$\mathbf{W} = \dot{\mathbf{R}}\mathbf{R}^T. \quad (3.44)$$

The spin is not itself, therefore, a rate of rotation, but it is closely related to it. Let us use the polar decomposition theorem to examine the continuum spin in a little more detail and more generally, and introduce the angular velocity tensor.

3.6.2 Angular velocity tensor

From Equation (3.38), the continuum spin is given by

$$\mathbf{W} = \frac{1}{2}(\mathbf{L} - \mathbf{L}^T)$$

so substituting for the velocity gradient from (3.33) gives

$$\mathbf{W} = \frac{1}{2}(\dot{\mathbf{F}}\mathbf{F}^{-1} - (\dot{\mathbf{F}}\mathbf{F}^{-1})^T) = \frac{1}{2}(\dot{\mathbf{F}}\mathbf{F}^{-1} - (\mathbf{F}^{-1})^T\dot{\mathbf{F}}^T).$$

If we now substitute for \mathbf{F} using the polar decomposition theorem in (3.24), after a little algebra we obtain

$$\mathbf{W} = \frac{1}{2}[\dot{\mathbf{R}}\mathbf{R}^T - \mathbf{R}\dot{\mathbf{R}}^T + \mathbf{R}(\dot{\mathbf{U}}\mathbf{U}^{-1} - (\dot{\mathbf{U}}\mathbf{U}^{-1})^T)\mathbf{R}^T]. \quad (3.45)$$

We will simplify this further by considering the product

$$\mathbf{R}\mathbf{R}^T = \mathbf{I},$$

which we can differentiate with respect to time to give

$$\dot{\mathbf{R}}\mathbf{R}^T + \mathbf{R}\dot{\mathbf{R}}^T = 0$$

64 Large deformations and continuum mechanics

so that

$$\dot{\mathbf{R}}\mathbf{R}^T = -\mathbf{R}\dot{\mathbf{R}}^T = -(\dot{\mathbf{R}}\mathbf{R}^T)^T. \quad (3.46)$$

We see, therefore, that $\dot{\mathbf{R}}\mathbf{R}^T$ is antisymmetric, since any tensor \mathbf{Z} for which $\mathbf{Z} = -\mathbf{Z}^T$ is antisymmetric because

$$\text{sym}(\mathbf{Z}) = \frac{1}{2}(\mathbf{Z} + \mathbf{Z}^T) = \frac{1}{2}(\mathbf{Z} - \mathbf{Z}) = 0.$$

Substituting (3.46) into (3.45) gives

$$\mathbf{W} = \dot{\mathbf{R}}\mathbf{R}^T + \frac{1}{2}\mathbf{R}(\dot{\mathbf{U}}\mathbf{U}^{-1} - (\dot{\mathbf{U}}\mathbf{U}^{-1})^T)\mathbf{R}^T \quad (3.47)$$

or

$$\mathbf{W} = \boldsymbol{\Omega} + \frac{1}{2}\mathbf{R}(\dot{\mathbf{U}}\mathbf{U}^{-1} - (\dot{\mathbf{U}}\mathbf{U}^{-1})^T)\mathbf{R}^T = \boldsymbol{\Omega} + \mathbf{R} \text{asym}(\dot{\mathbf{U}}\mathbf{U}^{-1})\mathbf{R}^T \quad (3.48)$$

in which $\boldsymbol{\Omega} = \dot{\mathbf{R}}\mathbf{R}^T$ is called the *angular velocity tensor* which depends only on the rigid body rotation and its rate of change and is independent of the stretch. If we consider a deformation comprising of rigid body rotation only, as we did in Section 3.6.1, or if the stretch is negligibly small, then Equation (3.48) simply reduces to

$$\mathbf{W} = \boldsymbol{\Omega} = \dot{\mathbf{R}}\mathbf{R}^T \quad (3.49)$$

as we saw in Equation (3.44). In general, the angular velocity tensor and continuum spin are not the same; Equation (3.48) shows that they differ depending on the stretch, \mathbf{U} . Both \mathbf{W} and $\boldsymbol{\Omega}$ are important when considering *objective stress rates*, as we shall see in Section 3.8. We will look at one further simple example in which we examine in particular the rate of deformation and the continuum spin; that of uniaxial stretch with no rigid body rotation.

3.6.3 Uniaxial stretch

We considered the uniaxial elongation of a rod lying along the Y -direction earlier (see Fig. 3.4) for which we obtained the deformation gradient, assuming purely plastic deformation and the incompressibility condition, in terms of the current, l , and original, l_0 , rod lengths as

$$\mathbf{F} = \begin{pmatrix} \left(\frac{l}{l_0}\right)^{-1/2} & 0 & 0 \\ 0 & \frac{l}{l_0} & 0 \\ 0 & 0 & \left(\frac{l}{l_0}\right)^{-1/2} \end{pmatrix}.$$

We will now determine the rate of deformation and continuum spin for the case of uniaxial stretch. Differentiating the deformation gradient gives

$$\dot{\mathbf{F}} = \begin{pmatrix} -\frac{1}{2} \left(\frac{l}{l_0}\right)^{-3/2} \frac{1}{l_0} \dot{l} & 0 & 0 \\ 0 & \frac{\dot{l}}{l_0} & 0 \\ 0 & 0 & -\frac{1}{2} \left(\frac{l}{l_0}\right)^{-3/2} \frac{\dot{l}}{l_0} \end{pmatrix}$$

and

$$\mathbf{F}^{-1} = \begin{pmatrix} \left(\frac{l}{l_0}\right)^{1/2} & 0 & 0 \\ 0 & \left(\frac{l}{l_0}\right)^{-1} & 0 \\ 0 & 0 & \left(\frac{l}{l_0}\right)^{1/2} \end{pmatrix}$$

so that the velocity gradient is

$$\mathbf{L} = \dot{\mathbf{F}}\mathbf{F}^{-1} = \begin{pmatrix} -\frac{1}{2} \left(\frac{l}{l_0}\right)^{-1} \frac{\dot{l}}{l_0} & 0 & 0 \\ 0 & \frac{\dot{l}}{l_0} \left(\frac{l}{l_0}\right)^{-1} & 0 \\ 0 & 0 & -\frac{1}{2} \left(\frac{l}{l_0}\right)^{-1} \frac{\dot{l}}{l_0} \end{pmatrix} = \frac{\dot{l}}{l} \begin{pmatrix} -\frac{1}{2} & 0 & 0 \\ 0 & 1 & 0 \\ 0 & 0 & -\frac{1}{2} \end{pmatrix}.$$

This is a symmetric quantity and therefore equal to the rate of deformation. In addition, its antisymmetric part is zero so that the continuum spin is zero. Formally,

$$\mathbf{D} = \frac{1}{2}(\mathbf{L} + \mathbf{L}^T) = \frac{\dot{l}}{l} \begin{pmatrix} -\frac{1}{2} & 0 & 0 \\ 0 & 1 & 0 \\ 0 & 0 & -\frac{1}{2} \end{pmatrix}, \quad (3.50)$$

$$\mathbf{W} = \frac{1}{2}(\mathbf{L} - \mathbf{L}^T) = 0.$$

There is, therefore, no rigid body rotation occurring; just stretch. Let us look at the rate of deformation for this case of uniaxial stretch.

For uniaxial stretch in the Y -direction, the true plastic strain components are given by

$$\varepsilon_{yy} = \ln \frac{l}{l_0}, \quad \varepsilon_{xx} = \varepsilon_{zz} = -\frac{1}{2}\varepsilon_{yy}$$

66 Large deformations and continuum mechanics

so that the strain rates are

$$\dot{\epsilon}_{yy} = \frac{\dot{l}}{l}, \quad \dot{\epsilon}_{xx} = \dot{\epsilon}_{zz} = -\frac{1}{2} \frac{\dot{l}}{l} \quad \text{and} \quad \dot{\epsilon}_{xy} = \dot{\epsilon}_{yz} = \dot{\epsilon}_{zx} = 0.$$

Examination of the components of the deformation gradient in (3.50) shows, therefore, that \mathbf{D} , for this case, can be rewritten

$$\mathbf{D} = \begin{pmatrix} \dot{\epsilon}_{xx} & 0 & 0 \\ 0 & \dot{\epsilon}_{yy} & 0 \\ 0 & 0 & \dot{\epsilon}_{zz} \end{pmatrix}. \quad (3.51)$$

For uniaxial stretch, therefore, in the absence of a rigid body rotation, it can be seen that the rate of deformation is identical to the true strain rate. This is not generally the case; it happens to be so for this example because there is no rigid body rotation. However, the example gives us a reasonable feel for what kind of measure the rate of deformation is.

We now return to the consideration of elastic–plastic material behaviour under large deformation conditions. We will consider cases in which the elastic strains, while not negligible, can always be assumed to be small compared with the plastic strains.

3.7 Elastic–plastic coupling

Consider now an imaginary lump of material in the undeformed configuration, shown in Fig. 3.6. The material contains a line vector, $d\mathbf{X}$. As before, after deformation

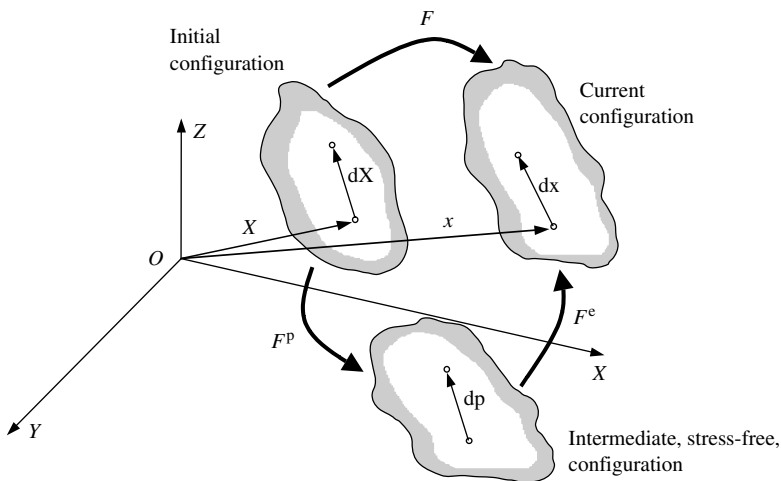


Fig. 3.6 Schematic diagram showing an element of a material in the initial and current configurations and in the intermediate, stress-free, configuration.

to the deformed or current configuration, the line vector is transformed to $d\mathbf{x}$. The transformation mapping of $d\mathbf{X}$ to $d\mathbf{x}$ is, of course, the deformation gradient, \mathbf{F} . We now introduce what is called the intermediate configuration. In transforming from the initial to deformed configuration, the line vector $d\mathbf{X}$ has undergone elastic and plastic deformation. The intermediate configuration is that in which line vector $d\mathbf{x}$ has been unloaded to a stress-free state; this is an imaginary state corresponding to one in which $d\mathbf{X}$ in the undeformed configuration has undergone purely plastic deformation to become $d\mathbf{p}$ in the intermediate configuration. The transformation mapping of $d\mathbf{X}$ to $d\mathbf{p}$ is the *plastic deformation gradient* so that

$$d\mathbf{p} = \mathbf{F}^p d\mathbf{X}$$

and the plastic deformation gradient is defined as

$$\mathbf{F}^p = \frac{\partial \mathbf{p}}{\partial \mathbf{X}}. \quad (3.52)$$

In the current configuration $d\mathbf{p}$ is deformed into $d\mathbf{x}$ by the elastic deformation so that

$$d\mathbf{x} = \mathbf{F}^e d\mathbf{p}$$

and the elastic deformation gradient is defined as

$$\mathbf{F}^e = \frac{\partial \mathbf{x}}{\partial \mathbf{p}}. \quad (3.53)$$

We may then write

$$d\mathbf{x} = \mathbf{F}^e d\mathbf{p} = \mathbf{F}^e \mathbf{F}^p d\mathbf{X}$$

so that

$$\mathbf{F} = \mathbf{F}^e \mathbf{F}^p. \quad (3.54)$$

This is the classical *multiplicative decomposition* of the deformation gradient into elastic and plastic parts, due to Erastus Lee.

Note that for general inhomogeneous plastic deformation, unloading a body will not generally lead to uniform zero stress; rather a residual stress field exists. Considering a finite number of material points within a continuum, at each point an unstressed configuration can be obtained, but \mathbf{F}^p and \mathbf{F}^e are, strictly, no longer pointwise continuous. Within the context of a finite element analysis, however, in which a discretization is necessary and the discontinuity of stress and strain resulting from the discretization is the norm, this is not a problem. In addition, note that the intermediate configuration described by \mathbf{p} is, in general, not uniquely determined since an arbitrary rigid body rotation can be superimposed on it, still leaving it unstressed. In Equation (3.54), both the elastic and plastic deformation gradients may contain both stretch and rigid body rotation.

68 Large deformations and continuum mechanics

However, in order to overcome the uniqueness problem, often, by convention, all the rigid body rotation is lumped into the plastic deformation gradient, \mathbf{F}^p , such that the elastic deformation gradient, \mathbf{F}^e , includes stretch only (no rigid body rotation). As a result, \mathbf{F}^e is written

$$\mathbf{F}^e = \mathbf{V}^e \quad (\text{symmetric stretch})$$

and so

$$\mathbf{F}^p = \mathbf{V}^p \mathbf{R}$$

in which \mathbf{R} is the equivalent total rigid body rotation. With this convention, let us now look at the velocity gradient and address the decomposition of the elastic and plastic rates of deformation.

3.7.1 Velocity gradient and elastic and plastic rates of deformation

We will now determine the velocity gradient in terms of the elastic and plastic deformation gradient decomposition given in (3.54). The velocity gradient is given by

$$\begin{aligned} \mathbf{L} &= \dot{\mathbf{F}}\mathbf{F}^{-1} = \frac{\partial}{\partial t}(\mathbf{F}^e\mathbf{F}^p)(\mathbf{F}^e\mathbf{F}^p)^{-1} = (\mathbf{F}^e\dot{\mathbf{F}}^p + \dot{\mathbf{F}}^e\mathbf{F}^p)\mathbf{F}^{p-1}\mathbf{F}^{e-1} \\ &= \dot{\mathbf{F}}^e\mathbf{F}^{e-1} + \mathbf{F}^e\dot{\mathbf{F}}^p\mathbf{F}^{p-1}\mathbf{F}^{e-1} = \dot{\mathbf{V}}^e\mathbf{V}^{e-1} + \mathbf{V}^e\dot{\mathbf{F}}^p\mathbf{F}^{p-1}\mathbf{V}^{e-1}. \end{aligned}$$

Now,

$$\begin{aligned} \mathbf{L}^e &= \dot{\mathbf{V}}^e\mathbf{V}^{e-1} = \mathbf{D}^e + \mathbf{W}^e \\ \mathbf{L}^p &= \dot{\mathbf{F}}^p\mathbf{F}^{p-1} = \mathbf{D}^p + \mathbf{W}^p \end{aligned}$$

so

$$\mathbf{L} = \mathbf{L}^e + \mathbf{V}^e\mathbf{L}^p\mathbf{V}^{e-1} = \mathbf{D}^e + \mathbf{W}^e + \mathbf{V}^e\mathbf{D}^p\mathbf{V}^{e-1} + \mathbf{V}^e\mathbf{W}^p\mathbf{V}^{e-1}. \quad (3.55)$$

Now,

$$\mathbf{D} = \text{sym}(\mathbf{L}) \quad \mathbf{W} = \text{asym}(\mathbf{L}).$$

Therefore, using Equation (3.55),

$$\mathbf{D} = \mathbf{D}^e + \text{sym}(\mathbf{V}^e\mathbf{D}^p\mathbf{V}^{e-1}) + \text{sym}(\mathbf{V}^e\mathbf{W}^p\mathbf{V}^{e-1}) \quad (3.56)$$

and

$$\mathbf{W} = \mathbf{W}^e + \text{asym}(\mathbf{V}^e\mathbf{D}^p\mathbf{V}^{e-1}) + \text{asym}(\mathbf{V}^e\mathbf{W}^p\mathbf{V}^{e-1}). \quad (3.57)$$

In general, therefore, we see from (3.56) the result that the elastic and plastic rates of deformation are not additively decomposed, that is,

$$\mathbf{D} \neq \mathbf{D}^e + \mathbf{D}^p.$$

This is unlike the additive decomposition of elastic and plastic strain rates for the case of small deformation theory, given in Equation (2.1). However, if the elastic strains are small, then

$$\mathbf{V}^e = \mathbf{V}^{e-1} \approx \mathbf{I}.$$

Also, $\text{sym}(\mathbf{D}^P) = \mathbf{D}^P$, $\text{sym}(\mathbf{W}^P) = 0$, since rate of deformation and spin are symmetric and antisymmetric, respectively. Hence, for small elastic stretches ($\mathbf{V}^e \approx \mathbf{I}$), from Equations (3.56) and (3.57),

$$\mathbf{D} = \mathbf{D}^e + \mathbf{D}^P \quad (3.58)$$

and

$$\mathbf{W} = \mathbf{W}^e + \mathbf{W}^P. \quad (3.59)$$

This is an important and well-known result and we will shortly see that Equation (3.58) is often used in the implementation of plasticity models into finite element code. The plastic rate of deformation, \mathbf{D}^P , like the plastic strain rate in small strain theory, is specified by a constitutive equation. Often, in finite element implementations, the total rate of deformation, \mathbf{D} , is known such that if \mathbf{D}^P is specified by a constitutive equation, then \mathbf{D}^e can be determined using (3.58) so that the stress rate may be determined using Hooke's law. Once we know the stress rate, we can integrate over time to determine stress. This brings us to the final step in our brief examination of continuum mechanics. We need to address stress rate and how to determine it in a material undergoing rigid body rotation with respect to a fixed coordinate system. We will do this in Section 3.8, and then summarize the most important steps required in going from knowledge of deformation to determination of stress, before introducing finite element methods in Chapter 4.

3.8 Objective stress rates

The primary focus of this section is stress rate, but before looking at this, we need to look at what is called *material objectivity*. We will start not by considering stress rate, but by something more familiar; transformation of stress.

3.8.1 Principle of material objectivity or frame indifference

Consider the transformation of the stress tensor, $\boldsymbol{\sigma}$, which undergoes a rotation through θ relative to the (XYZ) coordinate system. The stress transformation equations, or Mohr's circle, tell us that the transformed stresses, $\boldsymbol{\sigma}'$, with respect to the

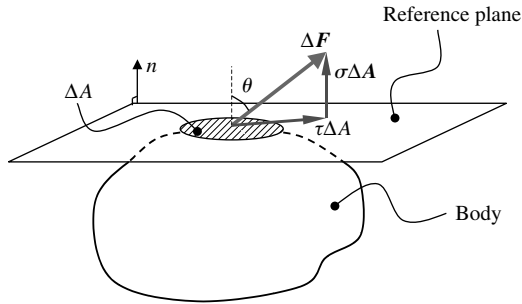


Fig. 3.7 Schematic diagram showing a body cut by a plane with normal \mathbf{n} generating an area of intersection of ΔA , subjected to resultant force $\Delta \mathbf{F}$.

(XYZ) coordinate system become

$$\begin{aligned} \sigma'_{XX} &= \sigma_{XX} \cos^2 \theta + 2\sigma_{XY} \sin \theta \cos \theta + \sigma_{YY} \sin^2 \theta \\ \sigma'_{YY} &= \sigma_{XX} \sin^2 \theta - 2\sigma_{XY} \sin \theta \cos \theta + \sigma_{YY} \cos^2 \theta \\ \sigma'_{XY} &= (\sigma_{YY} - \sigma_{XX}) \sin \theta \cos \theta + \sigma_{XY}(\cos^2 \theta - \sin^2 \theta). \end{aligned} \tag{3.60}$$

The last of the three equations enables us to determine the direction of the principal axes, relative to the applied stress direction, and of course, the principal stresses. It does this because along the principal directions, $\sigma'_{XY} = 0$ so that

$$\tan 2\theta = \frac{\sigma_{XY}}{\sigma_{XX} - \sigma_{YY}}. \tag{3.61}$$

We will look at an alternative way of dealing with stress (and indeed, other tensor quantities such as strain) transformation. In order to do this, we need to introduce the *stress vector* or *surface traction*.

3.8.1.1 The stress vector or traction. Figure 3.7 shows a lump of material, making up a body which has been cut by a plane with normal direction \mathbf{n} , with an infinitesimal area of intersection, ΔA .

Under uniform stress state, the resultant force acting on the area ΔA is $\Delta \mathbf{F}$. The stress vector acting on the area ΔA is defined by

$$\mathbf{t} = \left(\frac{\Delta \mathbf{F}}{\Delta A} \right)_{\Delta A \rightarrow 0}. \tag{3.62}$$

By definition, \mathbf{t} is a vector quantity with normal, σ , and shear, τ , components, as shown in Fig. 3.7. We will now look at how the stress vector, \mathbf{t} , on a particular plane with normal \mathbf{n} is related to the stress tensor, $\boldsymbol{\sigma}$. Consider the three orthogonal planes shown in Fig. 3.8(a) and the resulting plane ABC, reproduced in Fig. 3.8(b).

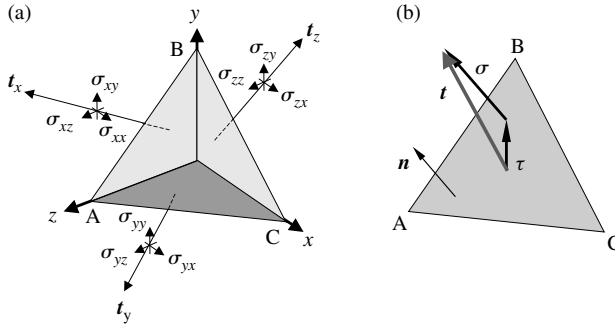


Fig. 3.8 Schematic diagram showing (a) the stress vectors acting on three orthogonal planes with components in the x -, y -, and z -directions shown and (b) the resultant stress vector acting on plane ABC which has normal n , with components $n = [n_x \ n_y \ n_z]^T$.

On each of the orthogonal planes in Fig. 3.8(a), a stress vector acts. For example, on plane 'x', that is, the plane orthogonal to the x -direction, the stress vector is t_x . The stress vectors acting on the three orthogonal planes have components given by

$$t_x = \begin{bmatrix} \sigma_{xx} \\ \sigma_{xy} \\ \sigma_{xz} \end{bmatrix}, \quad t_y = \begin{bmatrix} \sigma_{yx} \\ \sigma_{yy} \\ \sigma_{yz} \end{bmatrix}, \quad t_z = \begin{bmatrix} \sigma_{zx} \\ \sigma_{zy} \\ \sigma_{zz} \end{bmatrix}. \quad (3.63)$$

The convention is that on plane 'x', the stress components are labelled σ_{xx} in the x -direction, σ_{xy} in the y -direction, and so on. If the area of plane ABC is A , then the areas of the three orthogonal planes are given by

$$A_x = \begin{bmatrix} 1 \\ 0 \\ 0 \end{bmatrix} \cdot An = An_x, \quad A_y = \begin{bmatrix} 0 \\ 1 \\ 0 \end{bmatrix} \cdot An = An_y, \quad A_z = \begin{bmatrix} 0 \\ 0 \\ 1 \end{bmatrix} \cdot An = An_z. \quad (3.64a)$$

By consideration of equilibrium, the resultant force on plane ABC must be balanced by the forces on the three orthogonal planes so that

$$tA = t_x A_x + t_y A_y + t_z A_z = \begin{bmatrix} \sigma_{xx} \\ \sigma_{xy} \\ \sigma_{xz} \end{bmatrix} An_x + \begin{bmatrix} \sigma_{yx} \\ \sigma_{yy} \\ \sigma_{yz} \end{bmatrix} An_y + \begin{bmatrix} \sigma_{zx} \\ \sigma_{zy} \\ \sigma_{zz} \end{bmatrix} An_z. \quad (3.64b)$$

Therefore

$$t = \begin{bmatrix} \sigma_{xx} \\ \sigma_{xy} \\ \sigma_{xz} \end{bmatrix} n_x + \begin{bmatrix} \sigma_{yx} \\ \sigma_{yy} \\ \sigma_{yz} \end{bmatrix} n_y + \begin{bmatrix} \sigma_{zx} \\ \sigma_{zy} \\ \sigma_{zz} \end{bmatrix} n_z = \begin{pmatrix} \sigma_{xx} & \sigma_{xy} & \sigma_{xz} \\ \sigma_{yx} & \sigma_{yy} & \sigma_{yz} \\ \sigma_{zx} & \sigma_{zy} & \sigma_{zz} \end{pmatrix} \begin{bmatrix} n_x \\ n_y \\ n_z \end{bmatrix} \quad (3.65)$$

72 Large deformations and continuum mechanics

remembering that for reasons of moment, or rotational equilibrium, the stress tensor is symmetric so that $\sigma_{xy} = \sigma_{yx}$ etc. Equation (3.65) can be written in a simple way as

$$\mathbf{t} = \boldsymbol{\sigma} \mathbf{n}. \quad (3.66)$$

3.8.1.2 Transformation of stress. Let us now return to the problem of transformation of stress. Consider the stress vector, \mathbf{t} , acting on a surface with normal \mathbf{n} . At the point of interest, the stress is fully described by the tensor $\boldsymbol{\sigma}$. Under some rotation, \mathbf{R} , the stress vector \mathbf{t} is transformed to \mathbf{t}' acting on a plane with normal \mathbf{n}' , and similarly, the stress $\boldsymbol{\sigma}$ is transformed to $\boldsymbol{\sigma}'$ such that

$$\mathbf{t} = \boldsymbol{\sigma} \mathbf{n} \quad \text{and} \quad \mathbf{t}' = \boldsymbol{\sigma}' \mathbf{n}'.$$

Under rotation, \mathbf{R} , the vectors \mathbf{t} and \mathbf{n} transform according to

$$\mathbf{t}' = \mathbf{R} \mathbf{t} \quad \text{and} \quad \mathbf{n}' = \mathbf{R} \mathbf{n}$$

which give

$$\mathbf{t}' = \mathbf{R} \boldsymbol{\sigma} \mathbf{n} \quad \text{and} \quad \mathbf{n} = \mathbf{R}^T \mathbf{n}'.$$

Combining these gives

$$\mathbf{t}' = \mathbf{R} \boldsymbol{\sigma} \mathbf{R}^T \mathbf{n}'$$

but

$$\mathbf{t}' = \boldsymbol{\sigma}' \mathbf{n}'$$

so that finally

$$\boldsymbol{\sigma}' = \mathbf{R} \boldsymbol{\sigma} \mathbf{R}^T. \quad (3.67)$$

We see, therefore, that unlike a vector, the stress tensor, $\boldsymbol{\sigma}$, transforms according to Equation (3.67). To see what this means in detail, let us consider the two-dimensional transformation giving Equations (3.60). The rotation matrix, \mathbf{R} , corresponding to the rotation of θ is

$$\mathbf{R} = \begin{pmatrix} \cos \theta & -\sin \theta \\ \sin \theta & \cos \theta \end{pmatrix}$$

so that

$$\boldsymbol{\sigma}' = \begin{pmatrix} \cos \theta & -\sin \theta \\ \sin \theta & \cos \theta \end{pmatrix} \begin{pmatrix} \sigma_{xx} & \sigma_{xy} \\ \sigma_{xy} & \sigma_{yy} \end{pmatrix} \begin{pmatrix} \cos \theta & \sin \theta \\ -\sin \theta & \cos \theta \end{pmatrix}.$$

Multiplying these equations will give Equation (3.60). The stress transformation equations, or Mohr's circle representation, are beautifully and succinctly summarized, therefore, in Equation (3.67). This equation also tells us how other tensor quantities (such as strain, for example) transform. More formally, a tensor, \mathbf{A} , is said to be *frame indifferent* or *objective* if it rotates according to the following:

$$\mathbf{A}' = \mathbf{Q} \mathbf{A} \mathbf{Q}^T. \quad (3.68)$$

Comparing Equation (3.67) with (3.68) shows that the Cauchy stress tensor is *objective*. Let us consider a simple example to understand what is meant by *objective*.

3.8.2 Stressed rod under rotation: co-rotational stress

Consider a rod initially lying parallel to the Y -axis, of cross-sectional area A , under constant, axial, force P , shown schematically in Fig. 3.9(a). In this configuration, with respect to the XY coordinate system, the stresses in the rod are:

$$\sigma_{XX} = 0, \quad \sigma_{YY} = \frac{P}{A}, \quad \sigma_{XY} = 0.$$

A co-rotational (xy) coordinate system has been introduced which rotates with the rod. The stresses in the rod relative to the co-rotational (xy) coordinate system initially are, similarly,

$$\sigma_{xx} = 0, \quad \sigma_{yy} = \frac{P}{A}, \quad \sigma_{xy} = 0.$$

The rod undergoes a rotation of θ as shown in Fig. 3.9(b), relative to the (XY) coordinate system. With respect to the co-rotational system, the rod is subjected to an unchanging stress in the y -direction of P/A ; all other stress components remain zero. The stresses

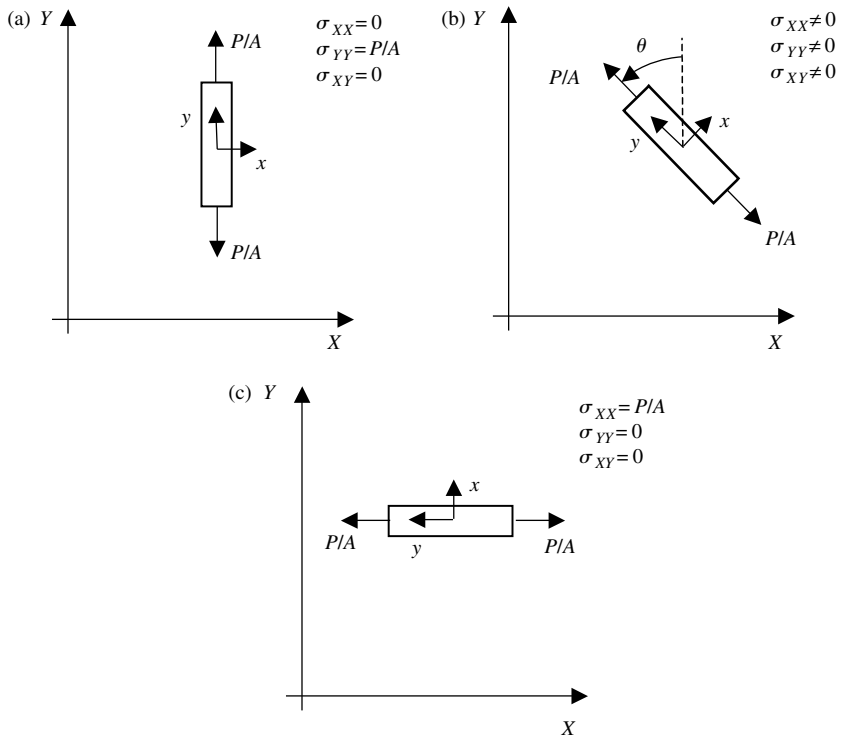


Fig. 3.9 A rod of cross-sectional area A undergoing rigid body rotation while subjected to axial force P (a) in the initial configuration, (b) having rotated through angle θ , and (c) after rotating through 90° showing the changing stresses with respect to the material (XY) reference frame.

74 Large deformations and continuum mechanics

in the rod, however, when measured with respect to the material (XY) reference frame can be seen to change. For example, when the rod has rotated through 90° as shown in Fig. 3.9(c), it lies parallel to the X -axis so that now, the stresses with respect to the material (XY) reference frame are

$$\sigma_{XX} = \frac{P}{A}, \quad \sigma_{YY} = 0, \quad \sigma_{XY} = 0.$$

They are, therefore, completely different to what they were in the initial state shown in Fig. 3.9(a). However, the stresses relative to the co-rotational system are as before; that is,

$$\sigma_{xx} = 0, \quad \sigma_{yy} = \frac{P}{A}, \quad \sigma_{xy} = 0.$$

The stresses relative to the co-rotational coordinate system, which we shall designate by $\boldsymbol{\sigma}'$, are related to those relative to the material (XY) coordinate system, which we shall designate by $\boldsymbol{\sigma}$, by

$$\boldsymbol{\sigma}' = \mathbf{R}\boldsymbol{\sigma}\mathbf{R}^T \quad (3.69)$$

in which \mathbf{R} is just the rotation matrix. $\boldsymbol{\sigma}'$ is called an objective or co-rotational stress because with respect to the co-rotational reference frame (and indeed, the material undergoing the rotation), its stress state has not changed; it has simply rotated. Note that the co-rotational stress, given in Equation (3.69) follows the requirement of objectivity given in Equations (3.67) and (3.68). The objective stress, therefore, results from the constitutive response of the material; it is independent of orientation and derives from the material response rather than the rigid body rotation.

Before addressing stress rate and its objectivity, we will first look at the objectivity, or otherwise, of a number of other important quantities in large deformation kinematics.

3.8.3 Objectivity of deformation gradient, velocity gradient, and rate of deformation

Consider the deformation gradient \mathbf{F} .

$$d\mathbf{x} = \mathbf{F} d\mathbf{X}. \quad (3.70)$$

After a transformation, \mathbf{Q} , the quantities in Equation (3.70) become $d\mathbf{x}'$, \mathbf{F}' , and $d\mathbf{X}'$ so that

$$d\mathbf{x}' = \mathbf{F}' d\mathbf{X}'. \quad (3.71)$$

Now,

$$d\mathbf{x}' = \mathbf{Q} d\mathbf{x} = \mathbf{Q}\mathbf{F} d\mathbf{X}$$

and $d\mathbf{X}$ remains unchanged under deformation, by definition, so that $d\mathbf{X}' = d\mathbf{X}$.

Therefore, from Equation (3.71),

$$\mathbf{F}' = \mathbf{Q}\mathbf{F}. \quad (3.72)$$

\mathbf{F} is, therefore, in fact objective and behaves like a vector because it is what is called a two point tensor, that is, only one of its two indices is in the spatial coordinate, x . We will now look at the objectivity of the velocity gradient, the rate of deformation, and the continuum spin.

Differentiating Equation (3.72) gives

$$\dot{\mathbf{F}}' = \dot{\mathbf{Q}}\mathbf{F} + \mathbf{Q}\dot{\mathbf{F}}$$

so that

$$\mathbf{L}' = \dot{\mathbf{F}}'\mathbf{F}'^{-1} = (\dot{\mathbf{Q}}\mathbf{F} + \mathbf{Q}\dot{\mathbf{F}})\mathbf{F}^{-1}\mathbf{Q}^{-1} = \dot{\mathbf{Q}}\mathbf{Q}^T + \mathbf{Q}\dot{\mathbf{F}}\mathbf{F}^{-1}\mathbf{Q}^T$$

and

$$\mathbf{L}' = \dot{\mathbf{Q}}\mathbf{Q}^T + \mathbf{Q}\mathbf{L}\mathbf{Q}^T. \quad (3.73)$$

Comparing with the requirement for objectivity in Equation (3.68), therefore, shows that the velocity gradient is not objective.

The transformed velocity gradient, \mathbf{L}' , from Equation (3.73) can be written

$$\mathbf{L}' = \underbrace{\frac{1}{2}\mathbf{Q}(\mathbf{L} + \mathbf{L}^T)\mathbf{Q}^T}_{\text{Symmetric}} + \underbrace{\frac{1}{2}\mathbf{Q}(\mathbf{L} - \mathbf{L}^T)\mathbf{Q}^T}_{\text{Antisymmetric}} + \dot{\mathbf{Q}}\mathbf{Q}^{-1}. \quad (3.74)$$

From Equation (3.46) we see that $\dot{\mathbf{Q}}\mathbf{Q}^T$ is antisymmetric. Therefore, from (3.74),

$$\mathbf{D}' = \text{sym}(\mathbf{L}') = \frac{1}{2}\mathbf{Q}(\mathbf{L} + \mathbf{L}^T)\mathbf{Q}^T = \mathbf{Q}\mathbf{D}\mathbf{Q}^T$$

and

$$\mathbf{W}' = \text{asym}(\mathbf{L}') = \mathbf{Q}\mathbf{W}\mathbf{Q}^T + \dot{\mathbf{Q}}\mathbf{Q}^{-1}. \quad (3.75)$$

Therefore, the deformation rate, \mathbf{D} , is objective, but the continuum spin, \mathbf{W} , is not. It is useful to ask whether this is important or not. In Sections 3.8.1 and 3.8.2, we examined the objectivity of the Cauchy stress and found that it is indeed objective. The Cauchy stress is, therefore, a quantity for which the properties are independent of the reference frame. This is very important in the development of constitutive equations. An equation which relates elastic strain to stress, for example, must be independent of the reference frame in which the relationship is used; in other words, the constitutive equation must provide information about the material response which is independent of rigid body rotation. The same holds for constitutive equations relating rate of plastic deformation (which we have just shown to be objective) to Cauchy stress (also objective), or the constitutive equation relating stress rate to elastic rate of deformation. In fact, plasticity

problems, especially within the context of finite element implementations, are often formulated in rate form. It is therefore necessary for us to address stress rate and, in particular, to examine whether stress rate is objective or otherwise. It turns out that there are many measures of objective stress rate, and we will focus on one in particular; the Jaumann stress rate.

3.8.4 Jaumann stress rate

We will examine, first, a rather contrived problem in order to get a physical feel for the meaning of the Jaumann stress rate. We will then look more generally at the objectivity of this stress rate, and finish by looking at a simple example.

Consider again a rod under axial stress σ , shown in Fig. 3.10(a). The stress tensor, with respect to the material axes is σ_t . During a time increment of Δt , the rod undergoes a rigid body rotation such that at time $t + \Delta t$, the rod lies as shown in Fig. 3.10(b) in which the co-rotational reference axes (xy) now coincide with the material reference axes (XY).

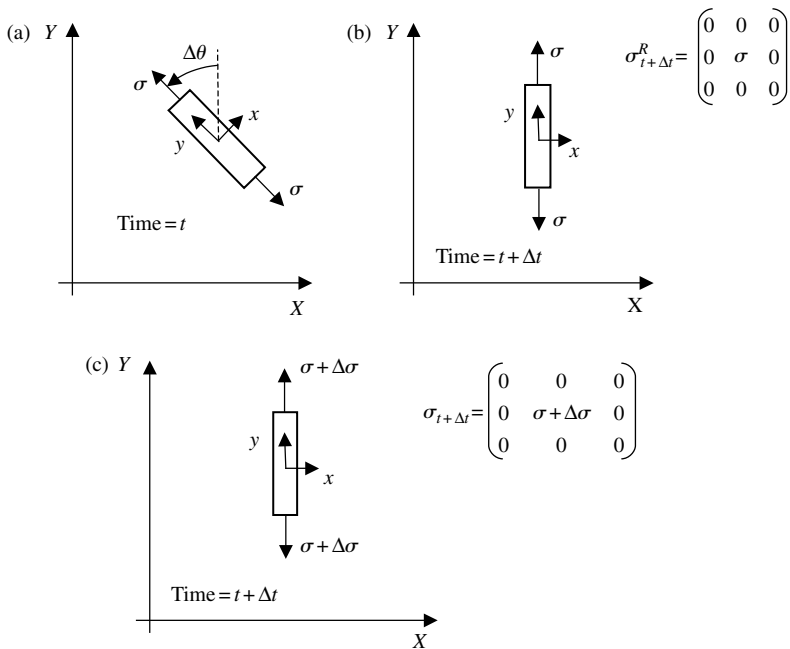


Fig. 3.10 A rod under axial stress, σ , undergoing rigid body rotation (a) at a time t , (b) at a time $t + \Delta t$ having gone through incremental rotation ΔR (corresponding to angle $\Delta\theta$ about the Z -direction) and (c) at the same time $t + \Delta t$ but having also undergone stress increment $\Delta\sigma$.

The stress tensor σ' with respect to the co-rotational reference frame is

$$\sigma'_t = \begin{pmatrix} 0 & 0 & 0 \\ 0 & \sigma & 0 \\ 0 & 0 & 0 \end{pmatrix},$$

which is obtained from

$$\sigma'_t = \Delta \mathbf{R} \sigma_t \Delta \mathbf{R}^T, \quad (3.76)$$

where $\Delta \mathbf{R}$ is the incremental rigid body rotation. Following the rigid body rotation, the rod is subjected to an additional axial stress, $\Delta \sigma$, shown in Fig. 3.10(c), so that the final stress tensor, with respect to the co-rotational frame (and the material frame since they are coincident at time $t + \Delta t$) is

$$\sigma'_{t+\Delta t} = \begin{pmatrix} 0 & 0 & 0 \\ 0 & \sigma + \Delta \sigma & 0 \\ 0 & 0 & 0 \end{pmatrix}.$$

The Cauchy stress increment with respect to the co-rotational frame may be written approximately, using Equation (2.99), as

$$\Delta \sigma' = [2GD^e + \lambda \text{Tr}(\mathbf{D}^e) \mathbf{I}] \Delta t, \quad (3.77)$$

where we have used the rate of elastic deformation in place of the elastic strain rate. The stress increment results, therefore, purely from the material's constitutive response and is co-rotational. We may then write the co-rotational stress tensor at time $t + \Delta t$ as the sum of (3.76) and (3.77) to give

$$\sigma'_{t+\Delta t} \equiv \sigma_{t+\Delta t} = \Delta \mathbf{R} \sigma_t \Delta \mathbf{R}^T + [2GD^e + \lambda \text{Tr}(\mathbf{D}^e) \mathbf{I}] \Delta t. \quad (3.78)$$

In order to investigate this further, let us consider the case in which the incremental rigid body rotation, $\Delta \mathbf{R}$, is small. We may then approximate the rotation matrix as

$$\Delta \mathbf{R} = \exp[\Delta \hat{\mathbf{r}}] \approx \mathbf{I} + \Delta \hat{\mathbf{r}}$$

in which $\Delta \hat{\mathbf{r}}$ is the associated antisymmetric tensor which is approximately given by $\mathbf{W} \Delta t$ (a full explanation for this can be found, e.g., in Belytschko *et al.*, 2000). Substituting into (3.78) then gives

$$\begin{aligned} \sigma_{t+\Delta t} &= (\mathbf{I} + \mathbf{W} \Delta t) \sigma_t (\mathbf{I} + \mathbf{W} \Delta t)^T + [2GD^e + \lambda \text{Tr}(\mathbf{D}^e) \mathbf{I}] \Delta t \\ &= \sigma_t + \sigma_t \mathbf{W}^T \Delta t + \mathbf{W} \sigma_t \Delta t + \mathbf{W} \sigma_t \mathbf{W}^T \Delta t^2 + [2GD^e + \lambda \text{Tr}(\mathbf{D}^e) \mathbf{I}] \Delta t \end{aligned}$$

so that

$$\frac{\sigma_{t+\Delta t} - \sigma_t}{\Delta t} = \sigma_t \mathbf{W}^T + \mathbf{W} \sigma_t + \sigma_t \mathbf{W} \sigma_t \Delta t + [2GD^e + \lambda \text{Tr}(\mathbf{D}^e) \mathbf{I}].$$

78 Large deformations and continuum mechanics

Now, both σ_t and $\sigma_{t+\Delta t}$ are given with respect to the material reference frame so that taking the limit, and letting $\Delta t \rightarrow 0$, gives us the *material stress rate*, $\dot{\sigma}$ as

$$\dot{\sigma} = \sigma_t W^T + W \sigma_t + 2GD^e + \lambda \text{Tr}(D^e)I$$

and as W is antisymmetric (we saw earlier that this means $W^T = -W$), we obtain

$$\dot{\sigma} = W \sigma_t - \sigma_t W + 2GD^e + \lambda \text{Tr}(D^e)I. \quad (3.79)$$

We can rewrite this as

$$\dot{\sigma} = \overset{\nabla}{\sigma} + W \sigma_t - \sigma_t W, \quad (3.80)$$

where

$$\overset{\nabla}{\sigma} = 2GD^e + \lambda \text{Tr}(D^e)I. \quad (3.81)$$

$\overset{\nabla}{\sigma}$ in Equations (3.80) and (3.81) is called the *Jaumann stress rate* and it is the stress rate that results purely from the constitutive response of the material and not from rigid body rotation. It is, therefore, as we shall see in Section 3.8.4.1, an *objective* stress rate. We may therefore use it in constitutive equations such as (3.81) in which both the Jaumann stress rate and the elastic rate of deformation are objective quantities. The material stress rate, $\dot{\sigma}$ however, does depend upon rigid body rotation. $\dot{\sigma}$ is the Cauchy stress rate with respect to the material reference frame; that is, in Figs 3.9 and 3.10, $\dot{\sigma}$ gives the stress rate with respect to the material (XY) axes. In finite element simulations, we are ordinarily interested in the stresses with respect to the material axes. Equation (3.80) is therefore important in that it enables us to determine the required stresses from knowledge of the material's constitutive response given by the Jaumann stress rate in (3.81). It is useful to remember that the stresses, σ_t , in Equation (3.80), are also given with respect to the material reference frame.

3.8.4.1 Objectivity of Jaumann stress rate. Let us now show that the Jaumann stress rate is objective. We saw earlier that a quantity A is said to be objective if it transforms according to (3.68), that is

$$A' = QAQ^T$$

and that the Cauchy stress transforms in this way ($\sigma' = Q\sigma Q^T$). Differentiating the stress with respect to time gives

$$\dot{\sigma}' = \dot{Q}\sigma Q^T + Q(\dot{\sigma}Q^T + \sigma\dot{Q}^T) = \dot{Q}\sigma Q^T + Q\dot{\sigma}Q^T + Q\sigma\dot{Q}^T. \quad (3.82)$$

We see from Equation (3.82) that the material rate of Cauchy stress is not objective (even though the stress itself is) since it does not transform according to (3.68). We saw in Section 3.8.3, Equation (3.75) that

$$W' = QWQ^T + \dot{Q}Q^{-1}.$$

Rearranging and remembering that \mathbf{Q} is orthogonal gives

$$\dot{\mathbf{Q}} = \mathbf{W}'\mathbf{Q} - \mathbf{Q}\mathbf{W} \quad (3.83)$$

so that

$$\dot{\mathbf{Q}}^T = -\mathbf{Q}^T\mathbf{W}' + \mathbf{W}\mathbf{Q}^T \quad (3.84)$$

since both \mathbf{W} and \mathbf{W}' are antisymmetric. Substituting (3.83) and (3.84) into (3.82) gives

$$\dot{\sigma}' = \mathbf{W}'\mathbf{Q}\sigma\mathbf{Q}^T - \mathbf{Q}\mathbf{W}\sigma\mathbf{Q}^T + \mathbf{Q}\dot{\sigma}\mathbf{Q}^T + \mathbf{Q}\sigma\mathbf{W}\mathbf{Q}^T - \mathbf{Q}\sigma\mathbf{Q}^T\mathbf{W}$$

so that

$$\dot{\sigma}' = \mathbf{Q}(\sigma\mathbf{W} - \mathbf{W}\sigma + \dot{\sigma})\mathbf{Q}^T + \mathbf{W}'\mathbf{Q}\sigma\mathbf{Q}^T - \mathbf{Q}\sigma\mathbf{Q}^T\mathbf{W}'. \quad (3.85)$$

Substituting for $\mathbf{Q}\sigma\mathbf{Q}^T = \sigma'$ into (3.85) gives

$$\sigma'\mathbf{W}' - \mathbf{W}'\sigma' + \dot{\sigma}' = \mathbf{Q}(\sigma\mathbf{W} - \mathbf{W}\sigma + \dot{\sigma})\mathbf{Q}^T. \quad (3.86)$$

Equation (3.86) therefore shows that the Jaumann stress rate, $\overset{\nabla}{\sigma}$, satisfies the requirement for objectivity in Equation (3.68), where

$$\overset{\nabla}{\sigma} = \dot{\sigma} + \sigma\mathbf{W} - \mathbf{W}\sigma. \quad (3.87)$$

There are objective stress rates other than that of Jaumann. Details of these may be found in many of the more advanced text books on continuum mechanics, and in particular, that of Belytschko *et al.* (2000).

3.8.4.2 Example of Jaumann stress rate for a rotating rod. We will conclude Section 3.8.4 with a simple example of a rotating rod under constant, uniaxial stress. We refer back to Fig. 3.9(b) which shows the rotating bar at an instant at which it makes an angle θ with the vertical. It is subject to a constant, uniaxial stress of P/A at all times. This, of course, gives a constant co-rotational stress (with respect to co-rotational xy -axes) of

$$\sigma' = \begin{pmatrix} 0 & 0 \\ 0 & \frac{P}{A} \end{pmatrix}. \quad (3.88)$$

The stresses with respect to the material (XY) axes, however, change with the rotation, as shown in Fig. 3.9(a)–(c). This means that there is a rate associated with each stress component which also changes with the rotation. We will now determine the stresses in the rod with respect to the material axes as it rotates. We will do this in two ways; first, we will set up the problem in rate form and integrate to obtain the stresses and second, use the standard method for transformation of stress using Equation (3.67) (or equivalently, Mohr's circle).

80 Large deformations and continuum mechanics

We may obtain the objective, or co-rotational stress rate, $\overset{\nabla}{\sigma}$, simply by differentiating (3.88) with respect to time. As the co-rotational stress is always constant, its derivative is zero, so

$$\overset{\nabla}{\sigma} = \frac{\partial}{\partial t} \begin{pmatrix} 0 & 0 \\ 0 & \frac{P}{A} \end{pmatrix} = \mathbf{0}.$$

The stress rate with respect to the original configuration, $\dot{\sigma}$, is given by rearranging (3.87)

$$\dot{\sigma} = \overset{\nabla}{\sigma} - \sigma \mathbf{W} + \mathbf{W} \sigma = \mathbf{W} \sigma - \sigma \mathbf{W}. \quad (3.89)$$

If there is no rotation, then $\mathbf{W} = 0$ and (3.89) tells us that the stress rates with respect to the material axes are also zero. However, the rod is rotating, with constant angular speed $\dot{\theta}$. We showed for this case, Equation (3.41), that this results in a continuum spin given by

$$\mathbf{W} = \dot{\theta} \begin{pmatrix} 0 & -1 \\ 1 & 0 \end{pmatrix}. \quad (3.90)$$

The stresses with respect to the material axes may be written

$$\sigma = \begin{pmatrix} \sigma_{XX} & \sigma_{XY} \\ \sigma_{XY} & \sigma_{YY} \end{pmatrix}. \quad (3.91)$$

Substituting (3.90) and (3.91) into (3.89) gives

$$\dot{\sigma} = \dot{\theta} \begin{pmatrix} -2\sigma_{XY} & \sigma_{XX} - \sigma_{YY} \\ \sigma_{XX} - \sigma_{YY} & 2\sigma_{XY} \end{pmatrix}.$$

That is

$$\frac{d\sigma_{XX}}{dt} = -2\dot{\theta}\sigma_{XY} \equiv -\frac{d\sigma_{YY}}{dt} \quad (3.92)$$

and

$$\frac{d\sigma_{XY}}{dt} = \dot{\theta}(\sigma_{XX} - \sigma_{YY}). \quad (3.93)$$

Equation (3.92) gives $\sigma_{XX} = -\sigma_{YY} + k$ where k is just a constant. The initial conditions are $\sigma_{XX}(0) = 0$, $\sigma_{YY}(0) = P/A$, $\sigma_{XY}(0) = 0$ so that $k = P/A$. Differentiating (3.93) and substituting into (3.92) and using $k = P/A$ gives

$$\frac{d^2\sigma_{XX}}{dt^2} = +4\dot{\theta}^2\sigma_{XX} = 2\dot{\theta}^2\frac{P}{A}.$$

This has general solution

$$\sigma_{XX} = A \sin 2\theta + B \cos 2\theta + \frac{P}{2A},$$

where $\theta = \dot{\theta}t$, so that with the initial conditions, the full solution is

$$\sigma_{XX} = \frac{P}{A} \sin^2 \theta, \quad \sigma_{YY} = \frac{P}{A} \cos^2 \theta, \quad \sigma_{XY} = \frac{P}{A} \sin \theta \cos \theta. \quad (3.94)$$

We see, therefore, that the stresses with respect to the material reference frame change correctly with angle θ . For example, when $\theta = 0$, $\sigma_{XX} = 0$, $\sigma_{YY} = P/A$, $\sigma_{XY} = 0$, and when $\theta = \pi/2$, $\sigma_{XX} = P/A$, $\sigma_{YY} = 0$, $\sigma_{XY} = 0$.

Finally, we will determine the same stresses using the stress transformation equation in (3.67). That is,

$$\begin{array}{ccc} \boldsymbol{\sigma}' = \mathbf{R}\boldsymbol{\sigma}\mathbf{R}^T & & \\ \uparrow & \uparrow & \\ (x, y) & (X, Y) & \\ \text{reference} & \text{reference} & \end{array}$$

so that the stresses in the material (XY) reference are given by

$$\boldsymbol{\sigma} = \begin{pmatrix} \cos \theta & \sin \theta \\ -\sin \theta & \cos \theta \end{pmatrix} \begin{pmatrix} 0 & 0 \\ 0 & P/A \end{pmatrix} \begin{pmatrix} \cos \theta & -\sin \theta \\ \sin \theta & \cos \theta \end{pmatrix} = \frac{P}{A} \begin{pmatrix} \sin^2 \theta & \sin \theta \cos \theta \\ \sin \theta \cos \theta & \cos^2 \theta \end{pmatrix},$$

which just gives the expressions in Equation (3.94).

3.9 Summary

Before leaving the kinematics of large deformations, we will summarize some of the important steps required in going from knowledge of deformation through to the determination of stresses for an elastic–plastic material undergoing large deformations. This is often required in the implementation of plasticity models into finite element code so it is something we shall return to later. We assume that any deformation taking place is such that the stretches due to elasticity are small compared with those for plasticity so that the additive decomposition of rate of deformation given in Equation (3.58) holds. We also assume full knowledge of the deformation gradient, \mathbf{F} and its rate, $\dot{\mathbf{F}}$. The steps required in determining stresses are then as follows.

1. Determine the velocity gradient

$$\mathbf{L} = \dot{\mathbf{F}}\mathbf{F}^{-1}.$$

2. Determine the rates of deformation and continuum spin

$$\mathbf{D} = \text{sym}(\mathbf{L}) = \frac{1}{2}(\mathbf{L} + \mathbf{L}^T),$$

$$\mathbf{W} = \text{asym}(\mathbf{L}) = \frac{1}{2}(\mathbf{L} - \mathbf{L}^T).$$

82 Large deformations and continuum mechanics

3. The rate of plastic deformation is specified by a constitutive equation. For example, from Chapter 2, for combined isotropic and kinematic hardening with power law dependence of effective plastic strain rate on stress, we have in the current configuration

$$D^P = \frac{3}{2} \left(\frac{J(\boldsymbol{\sigma}' - \mathbf{x}') - r - \sigma_y}{K} \right)^{1/m} \frac{\boldsymbol{\sigma}' - \mathbf{x}'}{J(\boldsymbol{\sigma}' - \mathbf{x}')}.$$

4. Determine the rate of elastic deformation

$$D^e = D - D^P.$$

5. Determine the Jaumann stress rate using the tensor form of Hooke's law, Equation (3.81), from the rate of elastic deformation

$$\overset{\nabla}{\boldsymbol{\sigma}} = 2GD^e + \lambda \text{Tr}(D^e) \mathbf{I}.$$

6. Determine the material rate of stress using (3.80)

$$\dot{\boldsymbol{\sigma}} = \overset{\nabla}{\boldsymbol{\sigma}} + \mathbf{W}\boldsymbol{\sigma} - \boldsymbol{\sigma}\mathbf{W}.$$

7. Use a numerical technique to obtain the stresses with respect to the material reference frame by integrating $\dot{\boldsymbol{\sigma}}$.

We will address all of these steps in some detail in later chapters.

Further reading

Belytschko, T., Liu, W.L., and Moran, B. (2000). *Non-linear Finite Elements for Continua and Structures*. John Wiley & Sons Inc, New York.

Khan, A.S. and Huang, S. (1995). *Continuum Theory of Plasticity*. John Wiley & Sons Inc, New York.

Lubarda, V.A. (2002). *Elastoplasticity Theory*. CRC Press, Florida, USA.

Simo, J.C. and Hughes, T.J.R. (1997). *Computational Inelasticity*. Springer-Verlag, Berlin.

4. The finite element method for static and dynamic plasticity

4.1 Introduction

There are few practical problems in plasticity which can be solved analytically. This is usually because of irregular geometry and/or complicated boundary and loading conditions. Computational mechanics, and in particular, the finite element method, enables the approximate solution of these types of problems. The important requirements of equilibrium, and compatibility, together with a material's constitutive response, enable solutions to be obtained subject to the satisfaction of initial and boundary conditions. Satisfying the requirements of equilibrium, compatibility, constitutive equations, and boundary conditions is essential for the solution of any solid mechanics problem. Within the finite element method, the body under consideration is discretized into a finite number of elements and nodes, with the latter each having a specified number of degrees of freedom. The finite element model representing the body therefore contains a finite number of degrees of freedom and the implication is that the requirement for equilibrium cannot be satisfied exactly at every point in the continuum (in what is called the *strong* sense). Instead, within the finite element technique, a *weak* formulation of equilibrium is used in which global equilibrium for the body as a whole is imposed even though this does not necessarily ensure pointwise equilibrium. Further details of strong and weak formulations are available in texts that are more specialized. A weak formulation can be obtained by consideration of the principle of virtual work, which appears in many text books, but here, we shall use *Hamilton's principle*. The advantage, as we shall see, is that the equilibrium equations of motion can be obtained in a fully unified manner, for both quasi-static and dynamic problems, and that the boundary conditions for the problem are also obtained. We shall use Hamilton's principle to obtain the equations of motion (and boundary conditions) for a number of well known discrete and continuous systems. In this way, we aim to develop a good physical feel for what the principle is doing before addressing more complicated finite element applications.

We introduce Hamilton's principle in Section 4.2. A reasonable knowledge of vector calculus is useful, but the important results are not impenetrable without it! Unfamiliar readers may like to skip on to the introduction to the finite element method in Section 4.3. Here, in keeping with the aims of this book, we address first a simple one-dimensional rod element subjected to elastic deformation alone and then very briefly look at element assemblage and some other finite element types. We then return to elastic-plastic problems and address plasticity in a one-dimensional rod element.

4.2 Hamilton's principle

Hamilton's principle, which results from conservation of energy, is one of the most general principles of mechanics. It provides a means for finding the equilibrium equations (equations of motion) of a dynamical system by determining the stationary value of a scalar integral. The principle states that the *variation* of the kinetic and potential energy plus the variation of the work done by non-conservative (external) forces acting during any time interval t_1 to t_2 must be zero. We will shortly see what is meant by variation, and of course, *non-conservative* implies forces that cannot be described by the change in a potential energy function (as can strain energy, for example), which are not already included in the potential energy term.

Let the total kinetic energy of the system be T , the potential energy of the system be U , and the work done by non-conservative forces be W . The Lagrangian, L , is defined as

$$L = T - U + W \quad (4.1)$$

and the *J-integral* is defined as

$$J = \int_{t_1}^{t_2} L \, dt = \int_{t_1}^{t_2} (T - U + W) \, dt. \quad (4.2)$$

Hamilton's principle states that the first variation (denoted by δ) of J is zero thus

$$\delta J = \int_{t_1}^{t_2} \delta L \, dt = \int_{t_1}^{t_2} \delta(T - U + W_{nc}) \, dt = 0. \quad (4.3)$$

In other words, the motion of a system between specified, realizable initial, and final conditions at times t_1 to t_2 is such that the average value of L relative to any dynamical path compatible with the physical constraints has a stationary value. An illustration of such a motion is given in Fig. 4.1 for a single degree of freedom system (SDOF).

Generally, the kinetic energy, potential energy, and work of non-conservative forces depend on some function (e.g. displacement, temperature, etc.) of time $y(t)$ which

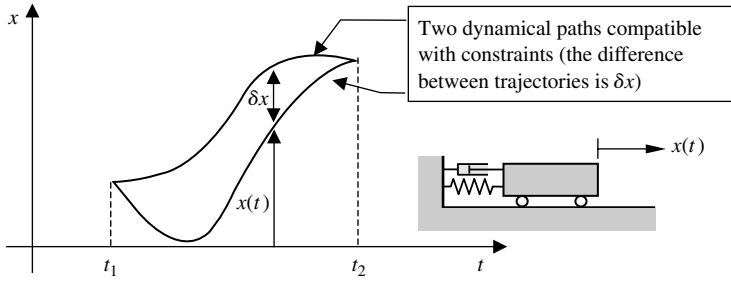


Fig. 4.1 Two dynamical paths subjected to having the same state at times t_1 and t_2 .

can be expressed as follows

$$J = \int_{t_1}^{t_2} L dt = \int_{t_1}^{t_2} L(y, y', t) dt \quad (4.4)$$

in which y' is just $\dot{y} = dy/dt$.

Hamilton's principle tells us that the dynamical path, $y(t)$, is that which leads to a stationary value of J . Let us now look at how Equation (4.4), called a functional, may be minimized by use of the *calculus of variations*.

Let $y = y(t)$ be the actual minimizing curve (as distinct from *any* admissible curve) and let

$$Y(t) = y(t) + \varepsilon \eta(t) \quad (4.5)$$

be the family of comparison curves, where $\eta(t)$ is an arbitrary function subjected to the constraint that

$$\eta(t_1) = \eta(t_2) = 0 \quad (4.6)$$

and ε is an arbitrary parameter. The corresponding J integral is

$$\bar{J}(\varepsilon) = \int_{t_1}^{t_2} L(Y, Y', t) dt \quad (4.7)$$

and its *variation* with respect to ε is

$$\frac{\partial}{\partial \varepsilon} \bar{J}(\varepsilon) = \int_{t_1}^{t_2} \left(\frac{\partial L}{\partial Y} \frac{\partial Y}{\partial \varepsilon} + \frac{\partial L}{\partial Y'} \frac{\partial Y'}{\partial \varepsilon} \right) dt. \quad (4.8)$$

For $\varepsilon = 0$, and using (4.5), this variation yields by integrating by parts, as

$$\begin{aligned} \frac{\partial}{\partial \varepsilon} \bar{J}(0) &= \int_{t_1}^{t_2} \left(\frac{\partial L}{\partial y} \eta + \frac{\partial L}{\partial y'} \eta' \right) dt = \int_{t_1}^{t_2} \frac{\partial L}{\partial y} \eta dt + \left[\frac{\partial L}{\partial y'} \eta \right]_{t_1}^{t_2} - \int_{t_1}^{t_2} \eta \frac{d}{dt} \frac{\partial L}{\partial y'} dt \\ &= \int_{t_1}^{t_2} \left(\frac{\partial L}{\partial y} - \frac{d}{dt} \frac{\partial L}{\partial y'} \right) \eta dt + \left[\frac{\partial L}{\partial y'} \eta \right]_{t_1}^{t_2}, \end{aligned}$$

86 Finite element method

which for $\eta(t_1) = \eta(t_2) = 0$ yields

$$\frac{\partial \bar{J}(0)}{\partial \varepsilon} = \int_{t_1}^{t_2} \left(\frac{\partial L}{\partial y} - \frac{d}{dt} \frac{\partial L}{\partial y'} \right) \eta \, dt. \quad (4.9)$$

Therefore, the necessary condition for minimization of J is

$$\frac{\partial \bar{J}(0)}{\partial \varepsilon} = \frac{\partial \bar{J}(\varepsilon)}{\partial \varepsilon} = 0. \quad (4.10)$$

Hence,

$$\int_{t_1}^{t_2} \left(\frac{\partial L}{\partial y} - \frac{d}{dt} \frac{\partial L}{\partial y'} \right) \eta \, dt = 0.$$

Since η is arbitrary, it follows that

$$\frac{\partial L}{\partial y} - \frac{d}{dt} \frac{\partial L}{\partial y'} = 0, \quad (4.11)$$

which is known as *Euler–Lagrange equation* and which must be satisfied for J to have a minimum.

If the function $y(t)$ is replaced by $y + \delta y$ where δy is the variation of y such that

$$\delta y(t_1) = \delta y(t_2) = 0, \quad (4.12)$$

then it follows using Taylor's theorem that

$$\begin{aligned} J(y + \delta y) &= J(y) + \int_{t_1}^{t_2} \left(\frac{\partial L}{\partial y} \delta y + \frac{\partial L}{\partial y'} (\delta y)' \right) dt \\ &+ \frac{1}{2!} \int_{t_1}^{t_2} \left(\frac{\partial^2 L}{\partial y^2} \delta y^2 + 2 \frac{\partial^2 L}{\partial y \partial y'} \delta y (\delta y)' + \frac{\partial^2 L}{\partial y'^2} (\delta y')^2 \right) dt \\ &+ \frac{1}{3!} \int_{t_1}^{t_2} \left(\delta y \frac{\partial}{\partial y} + \delta y' \frac{\partial}{\partial y'} \right)^3 L(y, y', t) \, dt + \dots \end{aligned} \quad (4.13)$$

since

$$\begin{aligned} F(x + r, y + s, z + t) &\approx F(x, y, z) + r \frac{\partial F}{\partial x} + s \frac{\partial F}{\partial y} + t \frac{\partial F}{\partial z} \\ &+ \frac{1}{2!} \left(r \frac{\partial}{\partial x} + s \frac{\partial}{\partial y} + t \frac{\partial}{\partial z} \right)^2 F(x, y, z) + \dots \end{aligned}$$

The quantity

$$\delta J = \int_{t_1}^{t_2} \left(\frac{\partial L}{\partial y} \delta y + \frac{\partial L}{\partial y'} (\delta y)' \right) dt \quad (4.14)$$

is called the *first variation* while

$$\delta^2 J = \frac{1}{2!} \int_{t_1}^{t_2} \left(\frac{\partial^2 L}{\partial y^2} \delta y^2 + 2 \frac{\partial^2 L}{\partial y \partial y'} \delta y (\delta y)' + \frac{\partial^2 L}{\partial y'^2} (\delta y')^2 \right) dt$$

is the *second variation* of J .

If the first variation is equal to zero for a particular function $y(t)$ of the admissible class, the functional $J(y)$ is said to have a *stationary value* for that particular function y . Before returning to equilibrium equations, let us look at one simple example to help understand the process of finding a stationary value.

4.2.1 Stationary value: minimizing the distance between two points

Figure 4.2 shows two points (x_1, y_1) and (x_2, y_2) which are joined by an infinite number of possible paths, $y(x)$. Only one is shown in the figure! Here note that $y(x)$ is a function only of position, x , and not time. Our aim is to use the above approach to determine that path which minimizes the distance between the two points.

An element of length dl lies on the path shown, and its length can be written as

$$dl^2 = dx^2 + dy^2 = dx^2 \left[1 + \left(\frac{dy}{dx} \right)^2 \right]$$

such that

$$dl = (1 + y'^2)^{1/2} dx$$

and finally, we obtain the functional, or J integral as

$$J = l = \int_{x_1}^{x_2} (1 + y'^2)^{1/2} dx. \quad (4.15)$$

Equation (4.15) is the functional which we wish to minimize to obtain the shortest path. We will use two approaches to do this. The first is by obtaining directly the

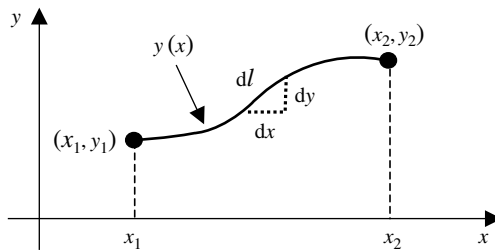


Fig. 4.2 A particular path, $y(x)$, between two points, (x_1, y_1) and (x_2, y_2) , and an element, dl , lying on the path.

88 Finite element method

stationary value of (4.15) and the second is to do the same by using the Euler–Lagrange Equation (4.11). The first variation of (4.15) is given by

$$\begin{aligned}\delta J &= \delta \int_{x_1}^{x_2} (1 + y'^2)^{1/2} dx = \int_{x_1}^{x_2} \frac{1}{2} (1 + y'^2)^{-1/2} \delta(y'^2) dx \\ &= \int_{x_1}^{x_2} (1 + y'^2)^{-1/2} y' \delta y' dx.\end{aligned}$$

Now,

$$\delta y' = \delta \left(\frac{dy}{dx} \right) = \frac{d}{dx} (\delta y)$$

so

$$\delta J = \int_{x_1}^{x_2} (1 + y'^2)^{-1/2} y' \frac{d}{dx} (\delta y) dx.$$

Integrating by parts gives

$$\delta J = [y' (1 + y'^2)^{-1/2} \delta y]_{x_1}^{x_2} - \int_{x_1}^{x_2} \frac{d}{dx} ((1 + y'^2)^{-1/2} y') \delta y dx$$

and since $\delta y(x_1) = \delta y(x_2) = 0$, and for a stationary value, we obtain

$$\delta J = - \int_{x_1}^{x_2} \frac{d}{dx} ((1 + y'^2)^{-1/2} y') \delta y dx = 0.$$

Since δy is arbitrary, we obtain the differential equation

$$\frac{d}{dx} ((1 + y'^2)^{-1/2} y') = 0, \quad (4.16)$$

which (unsurprisingly) has the solution $y = Ax + B$ in which A and B are constants of integration. We see, therefore, that the process of finding the first variation (or equivalently, the stationary value) of J , results in finding the function $y(x)$ which minimizes the functional, J . To finish off, let us do the same thing but now using the Euler–Lagrange Equation (4.11).

The functional, J , is a function of y , y' , and x and from Equation (4.15) may be written as

$$J = \int_{x_1}^{x_2} L(y, y', x) dx,$$

where $L(y, y', x) = (1 + y'^2)^{1/2}$ so the Euler–Lagrange equation becomes

$$\frac{\partial L}{\partial y} - \frac{d}{dx} \frac{\partial L}{\partial y'} = 0. \quad (4.17)$$

Now,

$$\frac{\partial L}{\partial y} = 0 \quad \text{and} \quad \frac{\partial L}{\partial y'} = \frac{1}{2} (1 + y'^2)^{-1/2} 2y'$$

and substituting into (4.17) just gives us the differential Equation (4.16) which has the solution as before.

4.2.2 Equilibrium equations

Let us now return to Hamilton's principle to see how it can be used to obtain equilibrium equations. For a solid elastic body, in the absence of body forces, the components of the Lagrangian can be expressed as follows:

$$\begin{aligned} T &= \frac{1}{2} \int_{\Omega} \rho \dot{\mathbf{u}} \cdot \dot{\mathbf{u}} \, dV, \\ U &= \frac{1}{2} \int_{\Omega} \boldsymbol{\sigma} : \boldsymbol{\epsilon} \, dV, \\ W &= \int_{\partial\Omega} \mathbf{t} \cdot \mathbf{u} \, dA \end{aligned} \quad (4.18)$$

in which \mathbf{u} and $\dot{\mathbf{u}}$ are the displacement and velocity vectors, ρ the density, \mathbf{t} the stress vector, or traction, $\boldsymbol{\sigma}$ and $\boldsymbol{\epsilon}$ the stress and strain tensors respectively, and $\partial\Omega$ and Ω are domains of area, A and volume, V , respectively. Substituting for the stress vector, \mathbf{t} , from Equation (3.66), and making use of the divergence theorem gives

$$W = \int_{\partial\Omega} \boldsymbol{\sigma} \mathbf{n} \cdot \mathbf{u} \, dA = \int_{\Omega} \operatorname{div} [\boldsymbol{\sigma} \mathbf{u}] \, dV. \quad (4.19)$$

The J integral is, therefore

$$\begin{aligned} J &= \int_{t_1}^{t_2} (T - U + W) \, dt \\ &= \int_{t_1}^{t_2} \left(\frac{1}{2} \int_{\Omega} \rho \dot{\mathbf{u}} \cdot \dot{\mathbf{u}} \, dV - \frac{1}{2} \int_{\Omega} \boldsymbol{\sigma} : \boldsymbol{\epsilon} \, dV + \int_{\Omega} \operatorname{div} [\boldsymbol{\sigma} \mathbf{u}] \, dV \right) dt. \end{aligned}$$

Taking the first variation of J gives

$$\begin{aligned} \delta J &= \int_{t_1}^{t_2} \delta(T - U + W) \, dt \\ &= \int_{t_1}^{t_2} \left(\frac{1}{2} \int_{\Omega} 2\rho \dot{\mathbf{u}} \cdot \delta \dot{\mathbf{u}} \, dV - \frac{1}{2} \int_{\Omega} (\boldsymbol{\sigma} : \delta \boldsymbol{\epsilon} + \delta \boldsymbol{\sigma} : \boldsymbol{\epsilon}) \, dV + \int_{\Omega} \operatorname{div} [\boldsymbol{\sigma} \delta \mathbf{u}] \, dV \right) dt \\ &= \int_{t_1}^{t_2} \left(\int_{\Omega} \rho \dot{\mathbf{u}} \cdot \frac{\partial}{\partial t} \delta \mathbf{u} \, dV - \int_{\Omega} \boldsymbol{\sigma} : \delta \boldsymbol{\epsilon} \, dV + \int_{\Omega} \operatorname{div} [\boldsymbol{\sigma} \delta \mathbf{u}] \, dV \right) dt = 0 \end{aligned}$$

and noting that $\operatorname{div} [\boldsymbol{\sigma} \delta \mathbf{u}] = \operatorname{div} [\boldsymbol{\sigma}] \cdot \delta \mathbf{u} + \boldsymbol{\sigma} : \nabla \delta \mathbf{u}$ and $\nabla \delta \mathbf{u} = \delta \boldsymbol{\epsilon}$ and integrating by parts gives

$$\begin{aligned} \delta J &= \int_{t_1}^{t_2} \left(- \int_{\Omega} \rho \ddot{\mathbf{u}} \cdot \delta \mathbf{u} \, dV + \int_{\Omega} \operatorname{div} \boldsymbol{\sigma} \delta \mathbf{u} \, dV \right) dt \\ &= \int_{t_1}^{t_2} \left(- \int_{\Omega} \rho \ddot{\mathbf{u}} \, dV + \int_{\Omega} \operatorname{div} \boldsymbol{\sigma} \, dV \right) \cdot \delta \mathbf{u} \, dt = 0 \end{aligned}$$

90 Finite element method

so that

$$\int_{\Omega} (-\rho \ddot{\mathbf{u}} + \text{div } \boldsymbol{\sigma}) \cdot \delta \mathbf{u} \, dV = 0 \quad (4.20)$$

and since $\delta \mathbf{u}$ is arbitrary,

$$-\rho \ddot{\mathbf{u}} + \text{div } \boldsymbol{\sigma} = 0.$$

These are the well-known equilibrium equations of stress analysis. If we consider quasi-static conditions, $\rho \ddot{\mathbf{u}} = 0$, and expand $\text{div } \boldsymbol{\sigma}$, we obtain the more familiar expressions

$$\text{div } \boldsymbol{\sigma} = \begin{bmatrix} \frac{\partial \sigma_{xx}}{\partial x} + \frac{\partial \sigma_{xy}}{\partial y} + \frac{\partial \sigma_{xz}}{\partial z} \\ \frac{\partial \sigma_{yx}}{\partial x} + \frac{\partial \sigma_{yy}}{\partial y} + \frac{\partial \sigma_{yz}}{\partial z} \\ \frac{\partial \sigma_{zx}}{\partial x} + \frac{\partial \sigma_{zy}}{\partial y} + \frac{\partial \sigma_{zz}}{\partial z} \end{bmatrix} = 0.$$

Hamilton's principle has therefore given us the very general form of the equilibrium equations of stress analysis. In addition, Equation (4.20) can be seen to be a statement of the *principle of virtual work*. The term $\int_{\Omega} (-\rho \ddot{\mathbf{u}} + \text{div } \boldsymbol{\sigma}) \, dV$ is just the residual force, \mathbf{r} , so that the expression in (4.20) is simply $\delta W = \mathbf{r} \cdot \delta \mathbf{u} = 0$. That is, in the course of an arbitrary, infinitesimal virtual displacement, $\delta \mathbf{u}$, from a position of equilibrium, the work done is zero. Hamilton's principle has therefore provided us with the condition for equilibrium and, in doing so, a statement of the principle of virtual work.

Before moving on to its application to finite elements, let us consider a few more examples, one for a discrete system, and two further continuous systems, in which we shall employ Hamilton's principle to obtain the momentum balance equations for a number of simple problems.

4.2.3 Further examples of Hamilton's principle

4.2.3.1 Discrete spring–mass problem. Consider the SDOF spring–mass system shown in Fig. 4.3. We will use Hamilton's principle to derive the equation of motion for the mass, m .

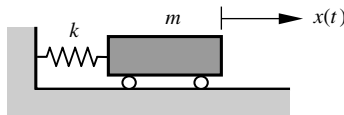


Fig. 4.3 Simple SDOF mass and spring system.

We may write expressions for the kinetic and potential energies of the system as

$$U = \frac{1}{2}kx^2, \quad T = \frac{1}{2}m\dot{x}^2.$$

The J integral may then be written, in the absence of external forces, as

$$J = \int_{t_1}^{t_2} (T - U) dt = \int_{t_1}^{t_2} \left(\frac{1}{2}m\dot{x}^2 - \frac{1}{2}kx^2 \right) dt.$$

Taking the first variation gives

$$\delta J = \frac{1}{2} \int_{t_1}^{t_2} (2m\dot{x} \delta\dot{x} - 2kx \delta x) dt = \int_{t_1}^{t_2} \left(m\dot{x} \frac{d}{dt}(\delta x) - kx \delta x \right) dt$$

and integrating by parts, we get

$$\delta J = [m\dot{x} \delta x]_{t_1}^{t_2} - \int_{t_1}^{t_2} (m\ddot{x} \delta x + kx \delta x) dt$$

and since $\delta x(t_1) = \delta x(t_2) = 0$, and δx is arbitrary,

$$\delta J = - \int_{t_1}^{t_2} (m\ddot{x} + kx) \delta x dt = 0 \quad \text{so} \quad m\ddot{x} + kx = 0.$$

Hamilton's principle has given us the governing equation of motion, or equilibrium equation, for the well known mass-spring problem.

4.2.3.2 Transverse vibration of a continuous beam. We shall next consider a continuous system and use Hamilton's principle to obtain the equations of motion for it. Figure 4.4(a) shows an elastic beam undergoing bending with deflection, y . The bending moment variation with angle, ϕ , is shown in Fig. 4.4(b) assuming elastic behaviour.

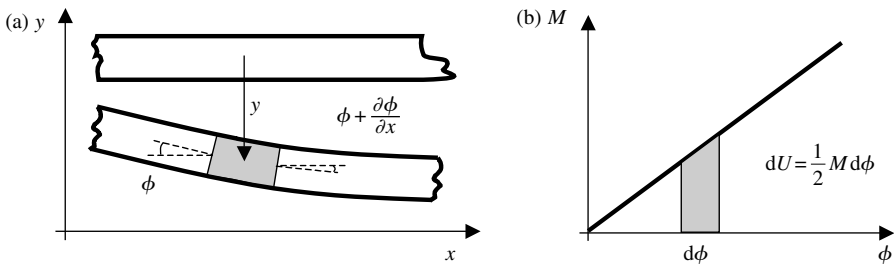


Fig. 4.4 (a) An elastic beam in bending undergoing deflection y and rotation ϕ and (b) the linear variation of bending moment M with rotation ϕ leading to stored elastic strain energy U .

92 Finite element method

The elastic strain energy stored in an element of length dx of the beam is

$$dU = \frac{1}{2} M d\phi \approx \frac{1}{2} M \frac{\partial \phi}{\partial x} dx$$

and

$$\phi = \frac{\partial y}{\partial x}$$

so that

$$dU = \frac{1}{2} M \frac{\partial^2 y}{\partial x^2} dx.$$

For an elastic beam, the bending moment is related to the deflection, y , by

$$M = EI \frac{\partial^2 y}{\partial x^2},$$

where E is Young's modulus and I is the second moment of area. Thus,

$$dU = \frac{1}{2} EI \left(\frac{\partial^2 y}{\partial x^2} \right)^2 dx$$

and finally, the potential energy for a beam of length L is

$$U = \frac{1}{2} \int_0^L EI \left(\frac{\partial^2 y}{\partial x^2} \right)^2 dx. \quad (4.21)$$

The kinetic energy, in an element of length dx , of the beam, is

$$dT = \frac{1}{2} \rho A \left(\frac{\partial y}{\partial t} \right)^2 dx$$

in which A is the beam's cross-sectional area. Hence the total system kinetic energy is

$$T = \frac{1}{2} \int_0^L \rho A \left(\frac{\partial y}{\partial t} \right)^2 dx. \quad (4.22)$$

The work done by external forces, $F(x, t)$ per unit length, is given by

$$W = \int_0^L F(x, t) y dx. \quad (4.23)$$

Consider the simply supported beam undergoing transverse vibration shown in Fig. 4.5.

We apply Hamilton's principle in the usual way. The J integral is

$$\begin{aligned} J &= \int_{t_1}^{t_2} L dt \\ &= \frac{1}{2} \int_{t_1}^{t_2} \left\{ \int_0^L \rho A \left(\frac{\partial y}{\partial t} \right)^2 dx - \int_0^L EI \left(\frac{\partial^2 y}{\partial x^2} \right)^2 dx + \int_0^L F(x, t) y dx \right\} dt. \end{aligned}$$

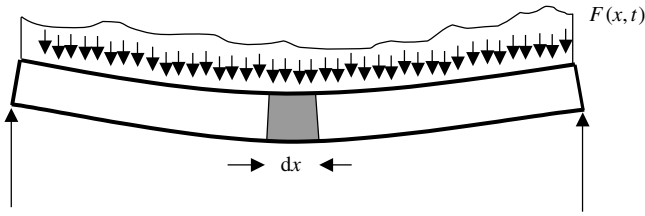


Fig. 4.5 A simply supported beam with distributed load $F(x, t)$ in transverse vibration.

We take the first variation of J to give the stationary value and equate to zero

$$\delta J = \int_{t_1}^{t_2} \delta L \, dt = 0.$$

Let us take the variation term by term. The contribution from the work done by external forces is obtained by substituting from (4.23) to give

$$\int_{t_1}^{t_2} \delta W \, dt = \int_{t_1}^{t_2} \int_0^L F(x, t) \delta y \, dx \, dt.$$

The kinetic energy term, substituting for (4.22), is

$$\begin{aligned} \int_{t_1}^{t_2} \delta T \, dt &= \frac{1}{2} \int_{t_1}^{t_2} \rho A \delta \int_0^L \left(\frac{\partial y}{\partial t} \right)^2 \, dx \, dt \\ &= \frac{1}{2} \int_{t_1}^{t_2} \rho A \int_0^L 2 \left(\frac{\partial y}{\partial t} \right) \delta \left(\frac{\partial y}{\partial t} \right) \, dx \, dt \\ &= \int_{t_1}^{t_2} \rho A \int_0^L \left(\frac{\partial y}{\partial t} \right) \delta \left(\frac{\partial y}{\partial t} \right) \, dx \, dt \\ &= \rho A \int_{t_1}^{t_2} \int_0^L \frac{\partial y}{\partial t} \frac{\partial}{\partial t} \delta y \, dx \, dt \\ &= \rho A \int_0^L \left\{ \left[\frac{\partial y}{\partial t} \delta y \right]_{t_1}^{t_2} - \int_{t_1}^{t_2} \delta y \frac{\partial^2 y}{\partial t^2} \, dt \right\} \, dx \end{aligned}$$

but

$$\delta y(t_1) = \delta y(t_2) = 0$$

thus

$$\int_{t_1}^{t_2} \delta T \, dt = -\rho A \int_0^L \int_{t_1}^{t_2} \delta y \frac{\partial^2 y}{\partial t^2} \, dt \, dx.$$

94 Finite element method

The elastic strain energy term is, using (4.21),

$$\begin{aligned}
 \int_{t_1}^{t_2} \delta U \, dt &= \frac{1}{2} \int_{t_1}^{t_2} \delta \int_0^L EI \left(\frac{\partial^2 y}{\partial x^2} \right)^2 dx \, dt = \int_{t_1}^{t_2} \int_0^L \frac{EI}{2} 2 \frac{\partial^2 y}{\partial x^2} \delta \left(\frac{\partial^2 y}{\partial x^2} \right) dx \, dt \\
 &= EI \int_{t_1}^{t_2} \int_0^L \frac{\partial^2 y}{\partial x^2} \frac{\partial^2}{\partial x^2} \delta y \, dx \, dt \\
 &= EI \int_{t_1}^{t_2} \left\{ \left[\frac{\partial^2 y}{\partial x^2} \frac{\partial}{\partial x} \delta y \right]_0^L - \int_0^L \frac{\partial^3 y}{\partial x^3} \frac{\partial}{\partial x} \delta y \, dx \right\} dt \\
 &= EI \int_{t_1}^{t_2} \left\{ \left[\frac{\partial^2 y}{\partial x^2} \frac{\partial}{\partial x} \delta y \right]_0^L - \left[\frac{\partial^3 y}{\partial x^3} \delta y \right]_0^L + \int_0^L \frac{\partial^4 y}{\partial x^4} \delta y \, dx \right\} dt.
 \end{aligned}$$

Finally, summing the terms,

$$\begin{aligned}
 \delta J &= \int_{t_1}^{t_2} \int_0^L - \left(EI \frac{\partial^4 y}{\partial x^4} + \rho A \frac{\partial^2 y}{\partial t^2} \right) \delta y \, dx \, dt \\
 &\quad - EI \int_{t_1}^{t_2} \left\{ \left[\frac{\partial^2 y}{\partial x^2} \frac{\partial}{\partial x} \delta y \right]_0^L + \left[\frac{\partial^3 y}{\partial x^3} \delta y \right]_0^L \right\} dt + \int_{t_1}^{t_2} \int_0^L F(x, t) \delta y \, dx \, dt \\
 &= \int_{t_1}^{t_2} \int_0^L - \left(EI \frac{\partial^4 y}{\partial x^4} + \rho A \frac{\partial^2 y}{\partial t^2} - F \right) \delta y \, dx \, dt \\
 &\quad + EI \int_{t_1}^{t_2} \left\{ \left[\frac{\partial^2 y}{\partial x^2} \frac{\partial}{\partial x} \delta y \right]_0^L - \left[\frac{\partial^3 y}{\partial x^3} \delta y \right]_0^L \right\} dt = 0. \tag{4.24}
 \end{aligned}$$

For δJ to be zero the integrands between 0 and L must be zero and since δy is arbitrary it follows that the individual terms in (4.24) must also vanish so that (assuming uniform, constant transverse loading, F),

$$EI \frac{\partial^4 y}{\partial x^4} + \rho A \frac{\partial^2 y}{\partial t^2} = F \tag{4.25}$$

and in addition, the boundary conditions are

$$\begin{aligned}
 \frac{\partial^2 y}{\partial x^2} \frac{\partial}{\partial x} \delta y &= 0 \quad \text{for } x = 0 \text{ and } x = L, \\
 \frac{\partial^3 y}{\partial x^3} \delta y &= 0 \quad \text{for } x = 0 \text{ and } x = L,
 \end{aligned}$$

which means

$$\begin{aligned} &\text{either } \frac{\partial^2 y}{\partial x^2} = 0 \quad \text{or} \quad \frac{\partial}{\partial x} \delta y = 0 \quad \text{for } x = 0 \text{ and } x = L \\ &\text{and} \\ &\text{either } \frac{\partial^3 y}{\partial x^3} = 0 \quad \text{or} \quad \delta y = 0 \quad \text{for } x = 0 \text{ and } x = L. \end{aligned} \tag{4.26}$$

Equation (4.25) is the equilibrium equation for the vibrating beam problem. However, note that Hamilton's principle has also given us the boundary conditions for the problem in Equations (4.26). We shall finish by looking at one further example.

4.2.3.3 Transverse vibration of a beam with axial loading. We shall now consider the previous problem but with the addition of an externally applied axial force, P , as shown in Fig. 4.6.

The axial force does work as the beam shortens due to transverse displacement (here, we are ignoring axial displacement which results from the axial strain due to the force, P). An element of the beam, ds , shortens by

$$\begin{aligned} ds - dx &= \sqrt{dx^2 + dy^2} - dx = \sqrt{1 + \left(\frac{dy}{dx}\right)^2} dx - dx \\ &= \left\{ \sqrt{1 + \left(\frac{dy}{dx}\right)^2} - 1 \right\} dx \approx \frac{1}{2} \left(\frac{dy}{dx}\right)^2 dx. \end{aligned}$$

The work done by the axial force per differential length

$$dW_P = \frac{1}{2} P \left(\frac{\partial y}{\partial x}\right)^2 dx.$$

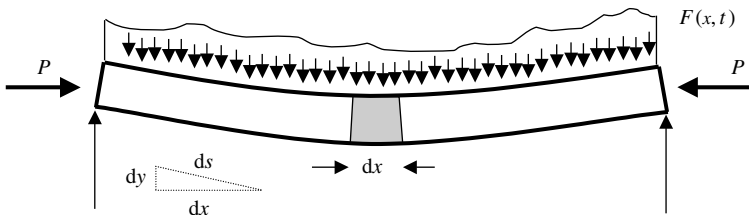


Fig. 4.6 Simply supported beam subjected to axial force P while undergoing transverse vibration.

96 Finite element method

The first variation of the work done by external forces then becomes

$$\begin{aligned} \int_{t_1}^{t_2} \delta W dt &= \int_{t_1}^{t_2} \int_0^L \left(F(x, t) \delta y + \frac{1}{2} \delta P \left(\frac{\partial y}{\partial x} \right)^2 \right) dx dt \\ &= \int_{t_1}^{t_2} \int_0^L \left(F(x, t) \delta y + P \left(\frac{\partial y}{\partial x} \right) \frac{\partial}{\partial x} \delta y \right) dx dt \\ &= \int_{t_1}^{t_2} \int_0^L \left\{ \left(F(x, t) \delta y - P \frac{\partial^2 y}{\partial x^2} \delta y \right) dx + \left[P \frac{\partial y}{\partial x} \delta y \right]_0^L \right\} dt. \end{aligned}$$

Thus, for uniform transverse loading $F(x, t) = F$, the equilibrium equation becomes

$$EI \frac{\partial^4 y}{\partial x^4} + P \frac{\partial^2 y}{\partial x^2} + \rho A \frac{\partial^2 y}{\partial t^2} = F$$

and the boundary conditions are

$$\begin{aligned} \frac{\partial^2 y}{\partial x^2} \frac{\partial}{\partial x} \delta y &= 0 \quad \text{for } x = 0 \text{ and } x = L, \\ EI \frac{\partial^3 y}{\partial x^3} + P \frac{\partial^2 y}{\partial x^2} &= 0 \quad \text{for } x = 0 \text{ and } x = L, \end{aligned}$$

which means

$$\text{either } \frac{\partial^2 y}{\partial x^2} = 0 \quad \text{or} \quad \frac{\partial}{\partial x} \delta y = 0 \quad \text{for } x = 0 \text{ and } x = L$$

and

$$\text{either } EI \frac{\partial^3 y}{\partial x^3} + P \frac{\partial^2 y}{\partial x^2} = 0 \quad \text{or} \quad \delta y = 0 \quad \text{for } x = 0 \text{ and } x = L.$$

4.3 Introduction to the finite element method

In this section, we will make use of Hamilton's principle to obtain finite element equilibrium equations which we shall then apply to some simple, uniaxial problems, before considering some further finite elements, and their application in statics and dynamics. We shall start with an introduction to the finite element method.

Figure 4.7 shows a representation of an undeformed body when the value of time is zero, which has been discretized into a finite number of tetrahedral finite elements which approximate the initial geometry of the body.

A particular, single finite element is shown which has nodes at points P_1 , P_2 , P_3 , and P_4 in the undeformed configuration. On the application of a load (which may be mechanical or thermal, for example), the body deforms (and undergoes

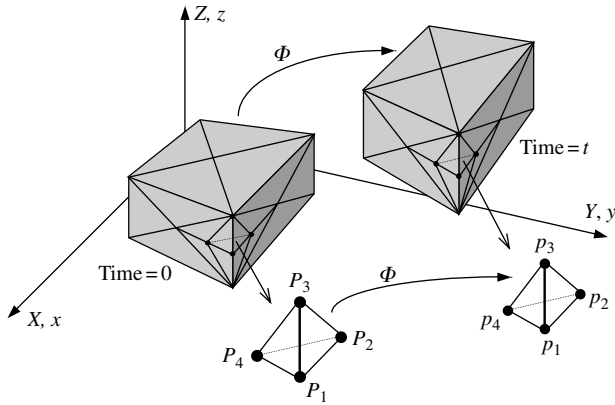


Fig. 4.7 Schematic diagram showing the finite element discretization of a body with three-dimensional tetrahedral elements.

transformation Φ) to that shown in the current configuration at time t . The nodes of the single element, after deformation, are now located at p_1 , p_2 , p_3 , and p_4 .

For simplicity, let us suppose that the quantity we are interested in determining is temperature, chosen because it is a scalar variable. The basis of the finite element method is to assign nodes to the elements and to assume that we can determine shape functions to enable interpolation to give the value of the temperature at any point within the element in terms of the nodal values of temperature. The tetrahedral element shown in the figure has four nodes. If the temperatures at the four nodes are θ_1 , θ_2 , θ_3 , and θ_4 respectively, then the temperature anywhere within the element is given by

$$\theta = N_1\theta_1 + N_2\theta_2 + N_3\theta_3 + N_4\theta_4 = \sum_{i=1}^n N_i\theta_i, \quad (4.27)$$

where N_i are called *shape (or interpolation) functions*. Let us consider in isolation the element shown in Fig. 4.7 in the deformed configuration. The element is shown in Fig. 4.8(a) with respect to the current configuration, and in (b) with respect to a local element reference frame (ξ_1, ξ_2, ξ_3) .

A transformation is clearly needed to map the element from the local reference frame to the current configuration, and similarly, from the local reference frame to the original configuration, and we shall address this later. The shape functions for this element, in terms of the local variables, are

$$N_1(\xi_1, \xi_2, \xi_3) = 1 - \xi_1 - \xi_2 - \xi_3,$$

$$N_2(\xi_1, \xi_2, \xi_3) = \xi_1,$$

$$N_3(\xi_1, \xi_2, \xi_3) = \xi_2,$$

$$N_4(\xi_1, \xi_2, \xi_3) = \xi_3.$$

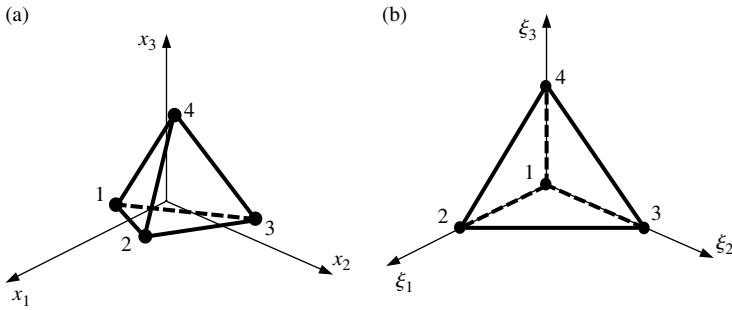


Fig. 4.8 Four-noded tetrahedral element shown with respect to (a) the current configuration and (b) the local element reference frame.

An important feature of the shape functions in the finite element method is that they generally take a value of unity at their own node and are zero at all others; at node 1, for example, $\xi_1 = \xi_2 = \xi_3 = 0$, so $N_1 = 1$. They generally sum to unity: $N_1 + N_2 + N_3 + N_4 = 1$; there are however, some special elements for which this is not the case. With knowledge of position (ξ_1, ξ_2, ξ_3) within an element, the shape functions can be used together with Equation (4.27) to determine the value of the temperature at any point within the element, given the nodal temperatures. The shape functions may be used in a similar way for any variable of interest, but often, the finite element equilibrium equations are set up with displacement as the basic quantity for which solutions are obtained. Such an approach is often referred to, therefore, as the displacement-based finite element method. We will look at a further, very simple finite element in order to examine the displacement-based approach.

Figure 4.9 shows a uniform bar under axial force P which has been discretized with a number of uniaxial truss elements. Each element has two nodes and is of length L . Each node has just one degree of freedom; namely axial displacement, u . The bar lies along the x -direction in the current configuration.

The shape functions are

$$N_1(\xi) = 1 - \xi, \quad N_2(\xi) = \xi, \quad (4.28)$$

where $\xi = x/L$ and $0 \leq \xi \leq 1$, and the element displacements are given by

$$u(\xi) = N_1 u_1 + N_2 u_2.$$

This is often written in vector form as

$$u(\xi) = \mathbf{N} \mathbf{u}_I = [N_1 \quad N_2] \begin{bmatrix} u_1 \\ u_2 \end{bmatrix}. \quad (4.29)$$

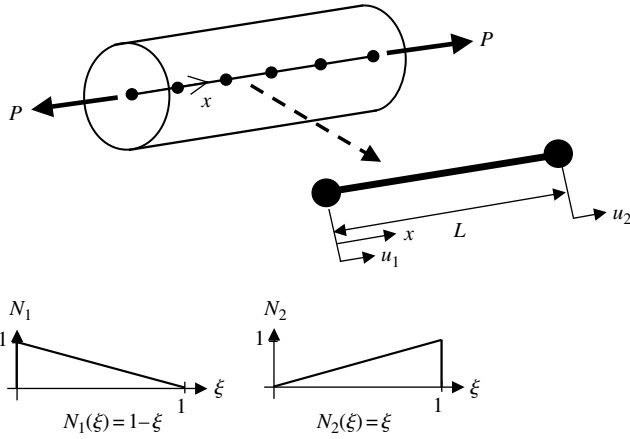


Fig. 4.9 A uniform bar discretized using uniaxial truss elements with shape functions shown.

Because we know the displacement everywhere within the element, we can determine the small strain, which, for this simple, uniaxial displacement is just

$$\begin{aligned} \varepsilon &= \frac{\partial u}{\partial x} = \begin{bmatrix} \frac{\partial N_1}{\partial x} & \frac{\partial N_2}{\partial x} \end{bmatrix} \begin{bmatrix} u_1 \\ u_2 \end{bmatrix} = \begin{bmatrix} \frac{\partial N_1}{\partial \xi} \frac{\partial \xi}{\partial x} & \frac{\partial N_2}{\partial \xi} \frac{\partial \xi}{\partial x} \end{bmatrix} \begin{bmatrix} u_1 \\ u_2 \end{bmatrix} \\ &= \frac{1}{L} \begin{bmatrix} -1 & 1 \end{bmatrix} \begin{bmatrix} u_1 \\ u_2 \end{bmatrix}. \end{aligned} \tag{4.30}$$

The derivatives of the type $\partial \xi / \partial x$ relate the current configuration to the local element reference frame and, in effect, provide the mapping of the element from the current configuration to the local element reference frame. In this case, because $\xi = x/L$, the mapping is trivial and the derivatives $\partial \xi / \partial x$ are easily obtained. We will see how to do this for more general cases a little later.

The matrix of spatial derivatives of the shape functions, given in Equation (4.30), is often referred to as the **B** matrix where for this particular element,

$$\mathbf{B} = \frac{1}{L} \begin{bmatrix} -1 & 1 \end{bmatrix}. \tag{4.31}$$

It can be seen from (4.30) that the strain is constant everywhere within the element; it is an example (as is the four-noded tetrahedron above) of a *constant strain element*. In order to progress with the analysis of the loaded bar, we need to obtain the equations of motion or equilibrium. We shall do this in a general way using Hamilton's principle, and then return to the loaded bar and to uniaxial truss elements.

4.4 Finite element equilibrium equations

4.4.1 Some preliminaries: tensor and Voigt notation, tensorial versus engineering strain

Tensorial notation is very elegant when it comes to theoretical derivations. However, for the purposes of developing numerical algorithms for implementation into computer programs, it is often more practical to work with arrays thus representing second-order tensor (strain, stress) as one-dimensional arrays and constitutive tensors (the elasticity tensor) as two-dimensional arrays.

Symmetry of stress and strain tensors is used to obtain the following (memory saving) notation (Voigt notation):

$$\boldsymbol{\sigma} = \begin{bmatrix} \sigma_{xx} & \sigma_{xy} & \sigma_{xz} \\ \sigma_{xy} & \sigma_{yy} & \sigma_{yz} \\ \sigma_{xz} & \sigma_{yz} & \sigma_{zz} \end{bmatrix} \rightarrow \boldsymbol{\sigma} = \begin{bmatrix} \sigma_{xx} \\ \sigma_{yy} \\ \sigma_{zz} \\ \sigma_{xy} \\ \sigma_{yz} \\ \sigma_{xz} \end{bmatrix}, \tag{4.32}$$

$$\boldsymbol{\epsilon} = \begin{bmatrix} \epsilon_{xx} & \epsilon_{xy} & \epsilon_{xz} \\ \epsilon_{xy} & \epsilon_{yy} & \epsilon_{yz} \\ \epsilon_{xz} & \epsilon_{yz} & \epsilon_{zz} \end{bmatrix} \rightarrow \boldsymbol{\epsilon} = \begin{bmatrix} \epsilon_{xx} \\ \epsilon_{yy} \\ \epsilon_{zz} \\ \gamma_{xy} \\ \gamma_{yz} \\ \gamma_{zx} \end{bmatrix} = \begin{bmatrix} \epsilon_{xx} \\ \epsilon_{yy} \\ \epsilon_{zz} \\ 2\epsilon_{xy} \\ 2\epsilon_{yz} \\ 2\epsilon_{zx} \end{bmatrix}. \tag{4.33}$$

Note that in vector, or Voigt notation, the shear strain components are stored as *engineering shears*, that is, twice the tensor shears. This sometimes causes confusion, so let us clarify by recalling Hooke’s law. Writing stress and elastic strain as column vectors, Hooke’s law in three dimensions becomes

$$\boldsymbol{\sigma} = \begin{bmatrix} \sigma_{xx} \\ \sigma_{yy} \\ \sigma_{zz} \\ \sigma_{xy} \\ \sigma_{yz} \\ \sigma_{xz} \end{bmatrix} = \mathbf{C} \boldsymbol{\epsilon} = \begin{bmatrix} \lambda + 2\mu & \lambda & \lambda & 0 & 0 & 0 \\ \lambda & \lambda + 2\mu & \lambda & 0 & 0 & 0 \\ \lambda & \lambda & \lambda + 2\mu & 0 & 0 & 0 \\ 0 & 0 & 0 & \mu & 0 & 0 \\ 0 & 0 & 0 & 0 & \mu & 0 \\ 0 & 0 & 0 & 0 & 0 & \mu \end{bmatrix} \begin{bmatrix} \epsilon_{xx} \\ \epsilon_{yy} \\ \epsilon_{zz} \\ \gamma_{xy} \\ \gamma_{yz} \\ \gamma_{xz} \end{bmatrix}, \tag{4.34}$$

where $\lambda = E\nu/(1 + \nu)(1 - 2\nu)$ and $\mu = G = E/2(1 + \nu)$ are the Lamé constants. Let us take one of the shear terms, for example,

$$\sigma_{xy} = \mu\gamma_{xy} \equiv \frac{E}{2(1 + \nu)}\gamma_{xy}. \quad (4.35)$$

We will now obtain the same shear stress, this time using the stress–strain tensor relation, given in Equation (2.99), that is,

$$\begin{aligned} \boldsymbol{\sigma} &= \begin{pmatrix} \sigma_{xx} & \sigma_{xy} & \sigma_{xz} \\ \sigma_{xy} & \sigma_{yy} & \sigma_{yz} \\ \sigma_{xz} & \sigma_{yz} & \sigma_{zz} \end{pmatrix} = 2G\boldsymbol{\varepsilon} + \lambda\text{Tr}(\boldsymbol{\varepsilon})\mathbf{I} \\ &= 2G \begin{pmatrix} \varepsilon_{xx} & \varepsilon_{xy} & \varepsilon_{xz} \\ \varepsilon_{xy} & \varepsilon_{yy} & \varepsilon_{yz} \\ \varepsilon_{xz} & \varepsilon_{yz} & \varepsilon_{zz} \end{pmatrix} + \lambda(\varepsilon_{xx} + \varepsilon_{yy} + \varepsilon_{zz}) \begin{pmatrix} 1 & 0 & 0 \\ 0 & 1 & 0 \\ 0 & 0 & 1 \end{pmatrix}. \end{aligned}$$

The shear stress is, therefore,

$$\sigma_{xy} = 2G\varepsilon_{xy} \equiv \frac{E}{(1 + \nu)}\varepsilon_{xy}. \quad (4.36)$$

Comparison of (4.35) and (4.36) shows that we must have

$$\gamma_{xy} = 2\varepsilon_{xy}$$

and similarly for the other shear strains. A more elegant explanation of this is as follows. Let us consider the case of pure elastic shear, as described by the stress and strain tensors

$$\boldsymbol{\sigma} = \begin{pmatrix} 0 & \sigma_{xy} & \sigma_{xz} \\ \sigma_{xy} & 0 & \sigma_{yz} \\ \sigma_{xz} & \sigma_{yz} & 0 \end{pmatrix}, \quad \boldsymbol{\varepsilon} = \begin{pmatrix} 0 & \varepsilon_{xy} & \varepsilon_{xz} \\ \varepsilon_{xy} & 0 & \varepsilon_{yz} \\ \varepsilon_{xz} & \varepsilon_{yz} & 0 \end{pmatrix}.$$

The elastic strain energy per unit volume is given by the tensor product

$$\frac{1}{2}\boldsymbol{\sigma} : \boldsymbol{\varepsilon} = \frac{1}{2} \begin{pmatrix} 0 & \sigma_{xy} & \sigma_{xz} \\ \sigma_{xy} & 0 & \sigma_{yz} \\ \sigma_{xz} & \sigma_{yz} & 0 \end{pmatrix} : \begin{pmatrix} 0 & \varepsilon_{xy} & \varepsilon_{xz} \\ \varepsilon_{xy} & 0 & \varepsilon_{yz} \\ \varepsilon_{xz} & \varepsilon_{yz} & 0 \end{pmatrix} = (\sigma_{xy}\varepsilon_{xy} + \sigma_{yz}\varepsilon_{yz} + \sigma_{xz}\varepsilon_{xz})$$

and substituting for the shear stresses using (4.36) and similar expressions gives

$$\frac{1}{2}\boldsymbol{\sigma} : \boldsymbol{\varepsilon} = \frac{E}{1 + \nu}(\varepsilon_{xy}^2 + \varepsilon_{yz}^2 + \varepsilon_{xz}^2). \quad (4.37)$$

102 Finite element method

We can also calculate the strain energy using engineering shear strain as

$$\begin{aligned} & \frac{1}{2}(\tau_{xy}\gamma_{xy} + \tau_{yz}\gamma_{yz} + \tau_{xz}\gamma_{xz}) \\ &= \frac{1}{2}G(\gamma_{xy}^2 + \gamma_{yz}^2 + \gamma_{xz}^2) = \frac{E}{4(1+\nu)}(\gamma_{xy}^2 + \gamma_{yz}^2 + \gamma_{xz}^2). \end{aligned} \quad (4.38)$$

Comparison of (4.37) and (4.38), given that the three shear strains are independent, gives

$$\gamma_{xy} = 2\varepsilon_{xy}$$

as before, and similarly for the other shear strains. The strain tensor is, of course, an objective quantity; that is, one that satisfies the criteria for objectivity discussed in Chapter 3, and this means a quantity whose properties remain unchanged under rotation. We must therefore use the tensorial shear strain components (as opposed to the engineering shear) when rotating a strain. It might be of interest to note that it is for this reason that Mohr's circle for strain is drawn in terms of $\gamma_{xy}/2 (= \varepsilon_{xy})$ rather than γ_{xy} .

We write the dot product of two first-order tensors, or vectors, as

$$\begin{aligned} \mathbf{u}^T \cdot \mathbf{v} &= u_i v_i = \sum_{i=1}^n u_i v_i, \\ \mathbf{v}^T \cdot \mathbf{u} &= v_i u_i = \sum_{i=1}^n v_i u_i \end{aligned}$$

so that

$$\mathbf{v}^T \cdot \mathbf{u} = \mathbf{u}^T \cdot \mathbf{v}.$$

If, therefore, we calculate the product of the stress vector, for example, then from (4.32),

$$\begin{aligned} \boldsymbol{\sigma}^T \cdot \boldsymbol{\sigma} &= (\sigma_{xx} \ \sigma_{yy} \ \sigma_{zz} \ \sigma_{xy} \ \sigma_{yz} \ \sigma_{xz}) \cdot (\sigma_{xx} \ \sigma_{yy} \ \sigma_{zz} \ \sigma_{xy} \ \sigma_{yz} \ \sigma_{xz})^T \\ &= \sigma_{xx}^2 + \sigma_{yy}^2 + \sigma_{zz}^2 + \sigma_{xy}^2 + \sigma_{yz}^2 + \sigma_{xz}^2. \end{aligned}$$

It is important to note that this does not give the same result as the equivalent product of the stress tensor, which is

$$\boldsymbol{\sigma} : \boldsymbol{\sigma} = \sigma_{xx}^2 + \sigma_{yy}^2 + \sigma_{zz}^2 + 2(\sigma_{xy}^2 + \sigma_{yz}^2 + \sigma_{xz}^2).$$

It is therefore necessary to take care when using the vector (Voigt) notation for stress and strain in carrying out calculations. So, for example, the *norm* of $\boldsymbol{\sigma}$, written $|\boldsymbol{\sigma}|$ is

$$|\boldsymbol{\sigma}| = (\boldsymbol{\sigma} : \boldsymbol{\sigma})^{1/2} = [\sigma_{xx}^2 + \sigma_{yy}^2 + \sigma_{zz}^2 + 2(\sigma_{xy}^2 + \sigma_{yz}^2 + \sigma_{xz}^2)]^{1/2}$$

but if we work from the stress written as a column vector, then

$$|\boldsymbol{\sigma}| = \sqrt{\boldsymbol{\sigma}^T \mathbf{S} \boldsymbol{\sigma}},$$

which includes the following scaling matrix

$$\mathbf{S} = \begin{bmatrix} 1 & 0 & 0 & 0 & 0 & 0 \\ 0 & 1 & 0 & 0 & 0 & 0 \\ 0 & 0 & 1 & 0 & 0 & 0 \\ 0 & 0 & 0 & 2 & 0 & 0 \\ 0 & 0 & 0 & 0 & 2 & 0 \\ 0 & 0 & 0 & 0 & 0 & 2 \end{bmatrix}.$$

The following are further examples of possible dangers in using Voigt notation:

1. Second invariant of deviatoric stress in tensorial notation

$$J_2 = \frac{1}{2} \boldsymbol{\sigma}' : \boldsymbol{\sigma}'$$

and its correct expression in Voigt notation

$$J_2 = \frac{1}{2} \boldsymbol{\sigma}'^T \mathbf{S} \boldsymbol{\sigma}'.$$

2. Gradient of J_2 invariant in tensorial notation

$$\frac{\partial J_2}{\partial \boldsymbol{\sigma}'} = \boldsymbol{\sigma}'$$

and its correct expression in Voigt notation

$$\frac{\partial J_2}{\partial \boldsymbol{\sigma}'} = \mathbf{S} \boldsymbol{\sigma}'.$$

3. Strain norm in tensorial notation

$$|\boldsymbol{\varepsilon}| = \sqrt{\boldsymbol{\varepsilon} : \boldsymbol{\varepsilon}}$$

and its correct expression in Voigt notation

$$|\boldsymbol{\varepsilon}| = \sqrt{\boldsymbol{\varepsilon}^T \mathbf{S}^{-1} \boldsymbol{\varepsilon}},$$

where

$$\mathbf{S}^{-1} = \begin{bmatrix} 1 & 0 & 0 & 0 & 0 & 0 \\ 0 & 1 & 0 & 0 & 0 & 0 \\ 0 & 0 & 1 & 0 & 0 & 0 \\ 0 & 0 & 0 & \frac{1}{2} & 0 & 0 \\ 0 & 0 & 0 & 0 & \frac{1}{2} & 0 \\ 0 & 0 & 0 & 0 & 0 & \frac{1}{2} \end{bmatrix}.$$

4.4.2 Finite element equations using Hamilton's principle

For the purposes of obtaining the finite element equilibrium equations, we shall confine ourselves initially to small elastic deformation problems so that we will not need to worry about the kinematics of large deformations. We will address large deformations later.

The components of the Lagrangian for a general body subject to tractions \mathbf{t} are given in Equations (4.18) using tensorial notation. We shall write them, here, using Voigt notation for a particular (the ' m 'th) finite element as follows

$$\begin{aligned} T_m &= \frac{1}{2} \int_{\Omega} \rho \dot{\mathbf{u}}^T \dot{\mathbf{u}} \, dV, \\ U_m &= \frac{1}{2} \int_{\Omega} \boldsymbol{\varepsilon}^T \boldsymbol{\sigma} \, dV, \\ W_m &= \int_{\partial\Omega} \mathbf{u}^T \mathbf{t} \, dA, \end{aligned} \quad (4.39)$$

in which all non-scalar quantities are represented as column vectors and in particular, the stress and strain vectors are given by Equations (4.32) and (4.33), respectively and the engineering shear strains are used. Note that $\dot{\mathbf{u}}^T \dot{\mathbf{u}} \equiv \dot{\mathbf{u}} \cdot \dot{\mathbf{u}}$, and similarly for other vector quantities. For completeness, the displacement and traction vectors are given by

$$\mathbf{u} = \begin{bmatrix} u_x \\ u_y \\ u_z \end{bmatrix} \quad \text{and} \quad \mathbf{t} = \begin{bmatrix} t_x \\ t_y \\ t_z \end{bmatrix}.$$

Hooke's law, from Equation (4.34), is written as

$$\boldsymbol{\sigma} = \mathbf{C} \boldsymbol{\varepsilon}^e. \quad (4.40)$$

The displacement within the particular finite element may be written in terms of the nodal displacements, \mathbf{u}_I , as we did in (4.29) so that

$$\mathbf{u} = \mathbf{N} \mathbf{u}_I \quad (4.41)$$

and the strains can be written, in general, in terms of the nodal displacements and the \mathbf{B} matrix, as we did for the truss element in Equation (4.30),

$$\boldsymbol{\varepsilon} = \mathbf{B} \mathbf{u}_I. \quad (4.42)$$

For the uniaxial truss element, $\boldsymbol{\varepsilon}$ becomes just the uniaxial, scalar, strain ε , but for other element types (in two and three dimensions), the other strain components are needed. We shall see an example of this later.

In applying Hamilton's principle, we shall start from the Lagrangian, L_m , for the single element

$$L_m = T_m - U_m + W_m = T_m = \frac{1}{2} \int_{\Omega} \rho \dot{\mathbf{u}}^T \dot{\mathbf{u}} \, dV - \frac{1}{2} \int_{\Omega} \boldsymbol{\varepsilon}^T \boldsymbol{\sigma} \, dV + \int_{\partial\Omega} \mathbf{u}^T \mathbf{t} \, dA$$

and substituting Equations (4.40)–(4.42) gives

$$L_m = \frac{1}{2} \dot{\mathbf{u}}_I^T \int_{\Omega} \rho \mathbf{N}^T \mathbf{N} \, dV \dot{\mathbf{u}}_I - \frac{1}{2} \mathbf{u}_I^T \int_{\Omega} \mathbf{B}^T \mathbf{C} \mathbf{B} \, dV \mathbf{u}_I + \mathbf{u}_I^T \int_{\partial\Omega} \mathbf{N}^T \mathbf{t} \, dA.$$

If we define element mass and stiffness matrices as

$$\mathbf{m} = \int_{\Omega} \rho \mathbf{N}^T \mathbf{N} \, dV \quad (4.43)$$

and

$$\mathbf{k} = \int_{\Omega} \mathbf{B}^T \mathbf{C} \mathbf{B} \, dV \quad (4.44)$$

and the vector of nodal forces as

$$\mathbf{f} = \int_{\partial\Omega} \mathbf{N}^T \mathbf{t} \, dA, \quad (4.45)$$

then the Lagrangian becomes

$$L_m = \frac{1}{2} \dot{\mathbf{u}}_I^T \mathbf{m} \dot{\mathbf{u}}_I - \frac{1}{2} \mathbf{u}_I^T \mathbf{k} \mathbf{u}_I + \mathbf{u}_I^T \mathbf{f}.$$

The J integral is, therefore

$$J = \int_{t_1}^{t_2} L_m \, dt = \int_{t_1}^{t_2} \left(\frac{1}{2} \dot{\mathbf{u}}_I^T \mathbf{m} \dot{\mathbf{u}}_I - \frac{1}{2} \mathbf{u}_I^T \mathbf{k} \mathbf{u}_I + \mathbf{u}_I^T \mathbf{f} \right) dt$$

and applying Hamilton's principle gives

$$\begin{aligned} \delta J &= \int_{t_1}^{t_2} \left(\frac{1}{2} \delta(\dot{\mathbf{u}}_I^T \mathbf{m} \dot{\mathbf{u}}_I) - \frac{1}{2} \delta(\mathbf{u}_I^T \mathbf{k} \mathbf{u}_I) + \delta(\mathbf{u}_I^T \mathbf{f}) \right) dt \\ &= \int_{t_1}^{t_2} \delta \mathbf{u}_I^T (-\mathbf{m} \ddot{\mathbf{u}}_I - \mathbf{k} \mathbf{u}_I + \mathbf{f}) \, dt = 0. \end{aligned}$$

Since $\delta \mathbf{u}_I$ is an arbitrary displacement, this gives for the equilibrium equation, for a single finite element

$$\mathbf{m} \ddot{\mathbf{u}}_I + \mathbf{k} \mathbf{u}_I = \mathbf{f}. \quad (4.46)$$

Equation (4.46) is the finite element equilibrium equation, or equation of motion, written in terms of nodal displacements, \mathbf{u}_I . In the absence of inertia forces, it reduces to the standard, quasi-static equation

$$\mathbf{k} \mathbf{u}_I = \mathbf{f}. \quad (4.47)$$

Some authors differentiate between *momentum balance equations* and *equilibrium equations*; those that are derived which include inertia (dynamic) effects—for example, that given in (4.46)—are often referred to as momentum balance equations, and those which do not include inertia effects (for quasi-static problems), are simply called equilibrium equations. In most cases in what follows, we shall simply refer to both types as equilibrium equations. In Section 4.4.2.1, we shall determine the mass and stiffness matrices for a truss element and examine a single-element problem.

4.4.2.1 Single truss element problem. Consider the uniform bar with cross-sectional area A , made of material with density ρ , and Young's modulus E , shown in Fig. 4.10(a).

This is discretized with a single, uniaxial truss element shown in Fig. 4.10(b). The shape functions are those given in (4.28),

$$N_1(\xi) = 1 - \xi, \quad N_2(\xi) = \xi$$

so that

$$\mathbf{N} = [1 - \xi \quad \xi].$$

From above, (4.31), the \mathbf{B} matrix is

$$\mathbf{B} = \frac{1}{L}[-1 \quad 1].$$

The mass matrix can then be determined from (4.43) as

$$\mathbf{m} = \int_{\Omega} \rho \mathbf{N}^T \mathbf{N} dV = \int_{x=0}^L \rho \begin{bmatrix} 1 - \xi \\ \xi \end{bmatrix} [1 - \xi \quad \xi] A dx.$$

This integral is currently given with respect to the deformed configuration, x , so it needs to be transformed to the local element reference frame, ξ . While trivial in this case, since $\xi = x/L$, in general we would need to obtain the Jacobian, mapping dV (or equivalently, dx) in the current configuration to dV' (or, $d\xi$) in the element reference

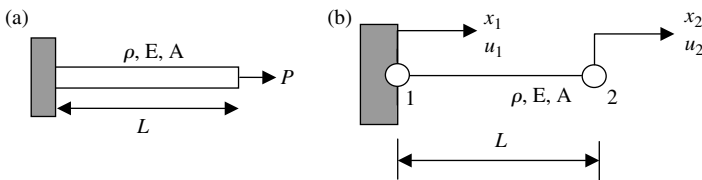


Fig. 4.10 (a) A uniform bar under axial force, P , and (b) its discretization using a single truss element.

frame, as we shall see later. For now, however,

$$\begin{aligned} \mathbf{m} &= \int_{x=0}^L \rho \begin{bmatrix} 1 - \xi \\ \xi \end{bmatrix} [1 - \xi \quad \xi] A \, dx = \int_{\xi=0}^1 \rho \begin{bmatrix} 1 - \xi \\ \xi \end{bmatrix} [1 - \xi \quad \xi] AL \, d\xi \\ &= \rho AL \int_0^1 \begin{pmatrix} (1 - \xi)^2 & \xi(1 - \xi) \\ \xi(1 - \xi) & \xi^2 \end{pmatrix} d\xi \end{aligned}$$

so

$$\mathbf{m} = \rho AL \begin{pmatrix} \frac{1}{3} & \frac{1}{6} \\ \frac{1}{6} & \frac{1}{3} \end{pmatrix}. \quad (4.48)$$

The stiffness matrix is, using (4.44)

$$\begin{aligned} \mathbf{k} &= \int_{\Omega} \mathbf{B}^T \mathbf{C} \mathbf{B} \, dV = \int_{x=0}^L \frac{1}{L} \begin{bmatrix} -1 \\ 1 \end{bmatrix} E \frac{1}{L} [-1 \quad 1] A \, dx \\ &= \int_{\xi=0}^1 \frac{E}{L^2} \begin{pmatrix} 1 & -1 \\ -1 & 1 \end{pmatrix} AL \, d\xi, \end{aligned}$$

where in this simple uniaxial case, the elasticity matrix \mathbf{C} is simply Young's modulus, E , so

$$\mathbf{k} = \frac{EA}{L} \begin{pmatrix} 1 & -1 \\ -1 & 1 \end{pmatrix} \quad (4.49)$$

and the nodal force vector, (4.45), for this problem is simply

$$\mathbf{f} = \begin{bmatrix} F_1 \\ P \end{bmatrix} \quad (4.50)$$

in which P is just the prescribed force at node 2 and F_1 the currently unknown reaction at node 1, and no integration over ξ is necessary. Note that because \mathbf{t} is a traction (stress vector), $\mathbf{t} \, dA$ is the force acting on the area dA at nodes 1 and 2. The integration of dA at the two ends therefore just gives A and is independent of ξ , so that $\mathbf{t} A$ at node 2 is P and that at node 1 is F_1 , both of which act in a direction parallel to \mathbf{t} ; that is, the x -direction. The equilibrium Equation (4.46) therefore gives

$$\rho AL \begin{pmatrix} \frac{1}{3} & \frac{1}{6} \\ \frac{1}{6} & \frac{1}{3} \end{pmatrix} \begin{bmatrix} \ddot{u}_1 \\ \ddot{u}_2 \end{bmatrix} + \frac{EA}{L} \begin{pmatrix} 1 & -1 \\ -1 & 1 \end{pmatrix} \begin{bmatrix} u_1 \\ u_2 \end{bmatrix} = \begin{bmatrix} F_1 \\ P \end{bmatrix}. \quad (4.51)$$

Let us assume inertia forces are negligible and that this is, therefore, a quasi-static problem so that we may eliminate the inertia term from (4.51) to give

$$\frac{EA}{L} \begin{pmatrix} 1 & -1 \\ -1 & 1 \end{pmatrix} \begin{bmatrix} u_1 \\ u_2 \end{bmatrix} = \begin{bmatrix} F_1 \\ P \end{bmatrix}.$$

With the boundary condition that $u_1 = 0$, these equations can be solved to give the expected result that

$$u_2 = \frac{PL}{EA}, \quad F_1 = -P$$

and using $\mathbf{u} = \mathbf{N}\mathbf{u}_I$, that

$$u_2 = [1 - \xi \quad \xi] \begin{bmatrix} 0 \\ u_2 \end{bmatrix} = \xi \frac{PL}{EA}.$$

where $0 \leq \xi \leq 1$. Despite using just a single element, these results are exact. This is only because, in this particular problem, we have been using a constant strain element to discretize what is, in any case, a constant strain problem.

In the following section, we shall give a more general description of the finite element method which includes the kinematics of large deformations and recognizes that the displacement of the nodes can become large; the problem then becomes *geometrically non-linear*. In addition, we need to give a fuller description of the mapping process between the current (and original) configuration and the local element reference frame. We will then look at several further examples.

4.4.3 General finite element approach

We will now return to the body in the initial and current configurations shown in Fig. 4.7. We will formulate the finite element equations with respect to the current, or deformed, configuration. When carried out incrementally, this is usually called an *updated Lagrangian formulation*. An alternative is to set up the equations with respect to the original configuration, in which case, it is called a *total Lagrangian formulation*. The initial position of the material particle P within the element shown can be specified as follows

$$\mathbf{X}(\boldsymbol{\xi}, t) \approx \sum_{I=1}^{\text{NNODE}} N_I(\boldsymbol{\xi}) \mathbf{X}_I(t), \quad (4.52)$$

where NNODE denotes the number of finite element nodes, $N_I(\boldsymbol{\xi})$ represents, as before, the element *shape functions* and \mathbf{X}_I indicates the *initial positions* of the finite element nodal points \mathbf{P}_I , which are given in terms of the local element reference, (ξ_1, ξ_2, ξ_3) shown in Fig. 4.8. Assuming that the material particle P remains attached to the same finite elements during the motion, the current positions of the material particles at the time t are specified by

$$\mathbf{x}(\boldsymbol{\xi}, t) \approx \sum_{I=1}^{\text{NNODE}} N_I(\boldsymbol{\xi}) \mathbf{x}_I(t) \quad (4.53)$$

where $\mathbf{x}_I(t)$ denotes the current positions of the finite element nodal points p_I . In the example in Section 4.4.2.1, the displacements were assumed to be small and there were no rigid body rotations. $\mathbf{X}(\boldsymbol{\xi}, t)$ and $\mathbf{x}(\boldsymbol{\xi}, t)$ were therefore identical and in addition, because the element considered was one-dimensional, $\boldsymbol{\xi}$ in Equations (4.52) and (4.53) was simply the scalar ξ . For two-dimensional elements, for example, two local reference frame independent variables are needed, (ξ_1, ξ_2) , to specify position. For the previous truss element example, $\mathbf{x}(\boldsymbol{\xi}, t)$ becomes

$$\mathbf{x}(\boldsymbol{\xi}, t) \approx \sum_{I=1}^2 N_I(\boldsymbol{\xi}) \mathbf{x}_I(t) = (1 - \xi) \mathbf{x}_1(t) + \xi \mathbf{x}_2(t). \quad (4.54)$$

Equation (4.54), and for the general case (4.53), therefore, maps any point within an element, specified by $\boldsymbol{\xi}$ with respect to the local element reference system, onto the corresponding position in the current configuration. The displacement and the velocity fields within each finite element are approximated as follows

$$\mathbf{u}(\boldsymbol{\xi}, t) \approx \sum_{I=1}^{\text{NNODE}} N_I(\boldsymbol{\xi}) \mathbf{u}_I(t), \quad (4.55)$$

$$\mathbf{v}(\boldsymbol{\xi}, t) \approx \sum_{I=1}^{\text{NNODE}} N_I(\boldsymbol{\xi}) \mathbf{v}_I(t). \quad (4.56)$$

In Equations (4.52)–(4.55), the same shape functions are used for interpolating position and displacement. Elements for which this holds true are called *isoparametric*. The deformation gradient tensor is obtained by differentiating Equation (4.53) with respect to the initial configuration as follows

$$\mathbf{F}(\boldsymbol{\xi}, t) \approx \sum_{I=1}^{\text{NNODE}} \mathbf{x}_I(t) \otimes \nabla_{\mathbf{X}} N_I(\boldsymbol{\xi}, t), \quad (4.57)$$

where

$$\nabla_{\mathbf{X}} N_I(\boldsymbol{\xi}, t) = \frac{\partial N_I(\boldsymbol{\xi})}{\partial \mathbf{X}(t)} = \left[\frac{\partial N_I}{\partial X} \quad \frac{\partial N_I}{\partial Y} \quad \frac{\partial N_I}{\partial Z} \right] \quad (4.58)$$

are the derivatives of the shape functions N_I . The gradient term, ∇ , and the *dyadic product*, \otimes , are explained in Appendix A. The derivative can be rewritten as follows

$$\nabla_{\mathbf{X}} N_I(\boldsymbol{\xi}, t) = \frac{\partial N_I(\boldsymbol{\xi})}{\partial \mathbf{X}(t)} = \frac{\partial N_I(\boldsymbol{\xi})}{\partial \boldsymbol{\xi}} \frac{\partial \boldsymbol{\xi}}{\partial \mathbf{X}(t)} = \frac{\partial N_I(\boldsymbol{\xi})}{\partial \boldsymbol{\xi}} \left(\frac{\partial \mathbf{X}(t)}{\partial \boldsymbol{\xi}} \right)^{-1}. \quad (4.59)$$

It is normally not possible to determine $\partial \boldsymbol{\xi} / \partial \mathbf{X}$ in Equation (4.59) directly since Equation (4.52) specifies \mathbf{X} in terms of $\boldsymbol{\xi}$. It is therefore necessary to determine $\partial \mathbf{X} / \partial \boldsymbol{\xi}$ instead and obtain the inverse. The derivative $\partial \mathbf{X} / \partial \boldsymbol{\xi}$ is called the *Jacobian* and relates

infinitesimal quantities in the material configuration to those in the local element coordinate system. We shall see this in several examples later. Using Equation (4.52),

$$\frac{\partial \mathbf{X}}{\partial \boldsymbol{\xi}} = \frac{\partial N_I(\boldsymbol{\xi})}{\partial \boldsymbol{\xi}} \mathbf{X}_I(t), \quad (4.60)$$

where the members of $\partial \mathbf{X}/\partial \boldsymbol{\xi}$ are given by

$$\frac{\partial X_i}{\partial \xi_j} = \sum_{I=1}^{\text{NNODE}} X_{iI} \frac{\partial N_I}{\partial \xi_j}. \quad (4.61)$$

The small strain tensor can be approximated

$$\boldsymbol{\varepsilon}(\boldsymbol{\xi}, t) = \frac{1}{2}[\nabla \mathbf{u} + (\nabla \mathbf{u})^T] \approx \frac{1}{2} \sum_{I=1}^{\text{NNODE}} [\mathbf{u}_I(t) \otimes \nabla_x N_I(\boldsymbol{\xi}) + \nabla_x N_I(\boldsymbol{\xi}) \otimes \mathbf{u}_I(t)]. \quad (4.62)$$

The velocity gradient is obtained as the spatial derivative of the velocity in Equation (4.56) as

$$\mathbf{L}(\boldsymbol{\xi}, t) \approx \sum_{I=1}^{\text{NNODE}} \mathbf{v}_I(t) \otimes \nabla_x N_I(\boldsymbol{\xi}, t)$$

and the rate of deformation tensor is obtained by using $\mathbf{D} = (1/2)(\mathbf{L} + \mathbf{L}^T)$ as follows

$$\mathbf{D}(\boldsymbol{\xi}, t) \approx \frac{1}{2} \sum_{I=1}^{\text{NNODE}} (\mathbf{v}_I(t) \otimes \nabla_x N_I(\boldsymbol{\xi}, t) + \nabla_x N_I(\boldsymbol{\xi}, t) \otimes \mathbf{v}_I(t)), \quad (4.63)$$

where

$$\nabla_x N_I(\boldsymbol{\xi}, t) = \frac{\partial N_I(\boldsymbol{\xi})}{\partial \mathbf{x}(t)} \quad (4.64)$$

are the spatial derivatives with respect to the current configuration, and are obtained from the shape functions as

$$\nabla_x N_I(\boldsymbol{\xi}, t) = \frac{\partial N_I(\boldsymbol{\xi})}{\partial \mathbf{x}(t)} = \frac{\partial N_I(\boldsymbol{\xi})}{\partial \boldsymbol{\xi}} \frac{\partial \boldsymbol{\xi}}{\partial \mathbf{x}(t)} = \frac{\partial N_I(\boldsymbol{\xi})}{\partial \boldsymbol{\xi}} \left(\frac{\partial \mathbf{x}(t)}{\partial \boldsymbol{\xi}} \right)^{-1}, \quad (4.65)$$

where members of the Jacobian, $\partial \mathbf{x}/\partial \boldsymbol{\xi}$, are given by

$$\frac{\partial x_i}{\partial \xi_j} = \sum_{I=1}^{\text{NNODE}} x_{iI} \frac{\partial N_I}{\partial \xi_j}. \quad (4.66)$$

We return now to the equilibrium Equation (4.20), obtained from Hamilton's principle, but write the increment in virtual work per unit volume and per unit time as

$$\delta W = \int_{\Omega} (\text{div}[\boldsymbol{\sigma}] - \rho \ddot{\mathbf{u}}) \cdot \delta \mathbf{v} \, dV = 0, \quad (4.67)$$

where $\delta \mathbf{v}$ is an arbitrary virtual velocity in the current configuration. By noting that

$$\begin{aligned} \operatorname{div}[\boldsymbol{\sigma} \cdot \delta \mathbf{v}] &= \operatorname{div}[\boldsymbol{\sigma}] \cdot \delta \mathbf{v} + \boldsymbol{\sigma} : \nabla \delta \mathbf{v}, \\ \mathbf{n} \cdot \boldsymbol{\sigma} \delta \mathbf{v} &= \delta \mathbf{v} \cdot \mathbf{t} \end{aligned} \quad (4.68)$$

that $\nabla \delta \mathbf{v} = \delta \mathbf{L}$ and that because $\boldsymbol{\sigma}$ is symmetric, it can be shown (with a little algebra) that $\boldsymbol{\sigma} : \delta \mathbf{L} = \boldsymbol{\sigma} : \delta \mathbf{D}$, substituting into (4.67) with the application of the divergence theorem gives

$$\delta W = \int_{\Omega} \rho \ddot{\mathbf{u}} \cdot \delta \mathbf{v} \, dV + \int_{\Omega} \boldsymbol{\sigma} : \delta \mathbf{D} \, dV - \int_{\partial \Omega} \mathbf{t} \cdot \delta \mathbf{v} \, dA = 0. \quad (4.69)$$

The second term in the right-hand side of (4.69) is the *internal work* per unit volume per second. A stress quantity is called *work conjugate* to the strain if their double contracted tensor product yields work. The co-rotational Cauchy, or true, stress is work conjugate to the rate of deformation.

The spatial virtual work equation, (4.69), which describes the dynamic equilibrium of the element can be rewritten in terms of the finite element discretization as follows

$$\begin{aligned} \delta W &\approx \int_{\Omega} \left(\rho \left(\sum_{I=1}^{\text{NNODE}} N_I \ddot{\mathbf{u}}_I \right) \right) \left(\sum_{I=1}^{\text{NNODE}} N_I \delta \mathbf{v}_I \right) dV \\ &\quad + \int_{\Omega} \boldsymbol{\sigma} : \frac{1}{2} \sum_{I=1}^{\text{NNODE}} (\delta \mathbf{v}_I \otimes \nabla_x N_I + \nabla_x N_I \otimes \delta \mathbf{v}_I) dV \\ &\quad - \int_{\partial \Omega} \mathbf{t} \cdot \left(\sum_{I=1}^{\text{NNODE}} N_I \delta \mathbf{v}_I \right) dA. \end{aligned} \quad (4.70)$$

As $\boldsymbol{\sigma}$ is a symmetric tensor, this reduces to

$$\begin{aligned} \delta W &\approx \int_{\Omega} \left(\rho \left(\sum_{I=1}^{\text{NNODE}} N_I \ddot{\mathbf{u}}_I \right) \right) \left(\sum_{I=1}^{\text{NNODE}} N_I \delta \mathbf{v}_I \right) dV \\ &\quad + \int_{\Omega} \boldsymbol{\sigma} : \sum_{I=1}^{\text{NNODE}} \delta \mathbf{v}_I \otimes \nabla_x N_I dV - \int_{\partial \Omega} \mathbf{t} \cdot \left(\sum_{I=1}^{\text{NNODE}} N_I \delta \mathbf{v}_I \right) dA \end{aligned}$$

and as the nodal virtual velocities are independent of the integration, this may be rewritten to give

$$\begin{aligned} \delta W &\approx \sum_{I=1}^{\text{NNODE}} \delta \mathbf{v}_I \cdot \int_{\Omega} N_I^T \rho \ddot{\mathbf{u}}_I [N_1, N_2, \dots, N_{\text{NNODE}}] dV \\ &\quad + \sum_{I=1}^{\text{NNODE}} \delta \mathbf{v}_I \cdot \int_{\Omega} \boldsymbol{\sigma} \nabla_x N_I dV - \sum_{I=1}^{\text{NNODE}} \delta \mathbf{v}_I \cdot \int_{\partial \Omega} N_I \mathbf{t} dA. \end{aligned} \quad (4.71)$$

112 Finite element method

The virtual work equation can finally be written in vector form as

$$dW \approx \sum_{I=1}^{\text{NNODE}} d\mathbf{v}_I \cdot (\mathbf{f}_I^{\text{inert}} + \mathbf{f}_I^{\text{int}} - \mathbf{f}_I^{\text{ext}}) \quad (4.72)$$

by introducing expressions for the equivalent element nodal force vectors as follows

$$\mathbf{f}_I^{\text{inert}} = \int_{\Omega} N_I^T \rho \ddot{\mathbf{u}}_I [N_1, N_2, \dots, N_{\text{NNODE}}] dV, \quad (4.73)$$

$$\mathbf{f}_I^{\text{int}} = \int_{\Omega} \boldsymbol{\sigma} \nabla_x N_I dV, \quad (4.74)$$

$$\mathbf{f}_I^{\text{ext}} = \int_{\partial\Omega} N_I \mathbf{t} dA, \quad (4.75)$$

where $\mathbf{f}_I^{\text{inert}}$, $\mathbf{f}_I^{\text{int}}$, and $\mathbf{f}_I^{\text{ext}}$ represent the inertial, the internal, and the external element nodal forces, respectively.

Since the discretized rate of virtual work, Equation (4.72) must be satisfied for all cases of the arbitrary virtual velocities, the element equation can be rewritten

$$\mathbf{f}_I^{\text{inert}} + \mathbf{f}_I^{\text{int}} - \mathbf{f}_I^{\text{ext}} = 0. \quad (4.76)$$

The nodal forces can be further *assembled* into *global* vectors (column matrices) by summing over all elements to give

$$\mathbf{F}^{\text{inert}} = \begin{bmatrix} \mathbf{f}_1^{\text{inert}} \\ \mathbf{f}_2^{\text{inert}} \\ \vdots \\ \mathbf{f}_n^{\text{inert}} \end{bmatrix}, \quad \mathbf{F}^{\text{int}} = \begin{bmatrix} \mathbf{f}_1^{\text{int}} \\ \mathbf{f}_2^{\text{int}} \\ \vdots \\ \mathbf{f}_n^{\text{int}} \end{bmatrix}, \quad \mathbf{F}^{\text{ext}} = \begin{bmatrix} \mathbf{f}_1^{\text{ext}} \\ \mathbf{f}_2^{\text{ext}} \\ \vdots \\ \mathbf{f}_n^{\text{ext}} \end{bmatrix}, \quad (4.77)$$

where n is the total number of points used in the discretization. Finally, the finite element discretization can be expressed by the set of non-linear equilibrium equations as follows:

$$\mathbf{F}^{\text{inert}}(\mathbf{u}) + \mathbf{F}^{\text{int}}(\mathbf{u}) - \mathbf{F}^{\text{ext}}(\mathbf{u}) = 0 \quad (4.78)$$

for the set (column matrix) of nodal displacements

$$\mathbf{u} = \begin{bmatrix} \mathbf{u}_1(t) \\ \mathbf{u}_2(t) \\ \vdots \\ \mathbf{u}_n(t) \end{bmatrix} \quad (4.79)$$

at time t .

We can rewrite Equation (4.76) in a more familiar way by considering the internal work term and writing it in terms of Voigt notation. We will assume small strain elasticity for simplicity. Returning to Equation (4.69), the internal work term originates from

$$\delta W^I = \int_{\Omega} \boldsymbol{\sigma} : \delta \mathbf{D} \, dV$$

and may be written using Voigt notation as

$$\delta W^I = \int_{\Omega} \boldsymbol{\sigma} : \delta \mathbf{D} \, dV = \int_{\Omega} \delta \mathbf{D}^T \boldsymbol{\sigma} \, dV, \quad (4.80)$$

where

$$\mathbf{D}^T = (D_{xx} \quad D_{yy} \quad D_{zz} \quad 2D_{xy} \quad 2D_{yz} \quad 2D_{zx})$$

in which the off-diagonal terms (shear terms) are doubled to satisfy work conjugacy as specified in (4.80). The rate of deformation is given in terms of nodal velocities in (4.63) by

$$\mathbf{D} = \frac{1}{2} \sum_{I=1}^{\text{NNODE}} (\mathbf{v}_I \otimes \nabla_x N_I + \nabla_x N_I \otimes \mathbf{v}_I).$$

After some algebra, this can be written in Voigt notation as

$$\mathbf{D} = \begin{bmatrix} D_{xx} \\ D_{yy} \\ D_{zz} \\ 2D_{xy} \\ 2D_{yz} \\ 2D_{zx} \end{bmatrix} = \sum_{I=1}^{\text{NNODE}} \mathbf{B}_I \cdot \mathbf{v}_I = \sum_{I=1}^{\text{NNODE}} \begin{bmatrix} \frac{\partial N_I}{\partial x} & 0 & 0 \\ 0 & \frac{\partial N_I}{\partial y} & 0 \\ 0 & 0 & \frac{\partial N_I}{\partial z} \\ \frac{\partial N_I}{\partial y} & \frac{\partial N_I}{\partial x} & 0 \\ 0 & \frac{\partial N_I}{\partial z} & \frac{\partial N_I}{\partial y} \\ \frac{\partial N_I}{\partial z} & 0 & \frac{\partial N_I}{\partial x} \end{bmatrix} \begin{bmatrix} v_{xI} \\ v_{yI} \\ v_{zI} \end{bmatrix} \quad (4.81)$$

so that from (4.80) the internal energy term becomes

$$\delta W^I = \int_{\Omega} \delta \mathbf{D}^T \boldsymbol{\sigma} \, dV = \int_{\Omega} \left(\sum_{I=1}^{\text{NNODE}} \mathbf{B}_I \, d\mathbf{v}_I \right)^T \boldsymbol{\sigma} \, dV. \quad (4.82)$$

If we assume purely elastic small deformation, then from (4.34), we may write

$$\begin{aligned} \delta W^I &= \int_{\Omega} \left(\sum_{I=1}^{\text{NNODE}} \mathbf{B}_I \delta \mathbf{v}_I \right)^T \mathbf{C} \boldsymbol{\varepsilon} dV \\ &= \int_{\Omega} \left(\sum_{I=1}^{\text{NNODE}} \mathbf{B}_I \delta \mathbf{v}_I \right)^T \mathbf{C} \left(\sum_{J=1}^{\text{NNODE}} \mathbf{B}_J \mathbf{u}_J \right) dV \end{aligned}$$

so that

$$\delta W^I = \delta \mathbf{v}_I^T \left(\sum_{I,J=1}^{\text{NNODE}} \int_{\Omega} \mathbf{B}_I^T \mathbf{C} \mathbf{B}_J dV \right) \mathbf{u}_J \quad (4.83)$$

since we may also write the small strains in terms of the nodal displacements as

$$\boldsymbol{\varepsilon} = \begin{bmatrix} \varepsilon_{xx} \\ \varepsilon_{yy} \\ \varepsilon_{zz} \\ 2\varepsilon_{xy} \\ 2\varepsilon_{yz} \\ 2\varepsilon_{zx} \end{bmatrix} = \sum_{I=1}^{\text{NNODE}} \mathbf{B}_I \cdot \mathbf{u}_I = \sum_{I=1}^{\text{NNODE}} \begin{bmatrix} \frac{\partial N_I}{\partial x} & 0 & 0 \\ 0 & \frac{\partial N_I}{\partial y} & 0 \\ 0 & 0 & \frac{\partial N_I}{\partial z} \\ \frac{\partial N_I}{\partial y} & \frac{\partial N_I}{\partial x} & 0 \\ 0 & \frac{\partial N_I}{\partial z} & \frac{\partial N_I}{\partial y} \\ \frac{\partial N_I}{\partial z} & 0 & \frac{\partial N_I}{\partial x} \end{bmatrix} \begin{bmatrix} u_{xI} \\ u_{yI} \\ u_{zI} \end{bmatrix}.$$

Equation (4.83) can be written as

$$\delta W^I = \delta \mathbf{v}_I^T \mathbf{k} \mathbf{u}_I,$$

where

$$\mathbf{k} = \sum_{I,J=1}^{\text{NNODE}} \int_{\Omega} \mathbf{B}_I^T \mathbf{C} \mathbf{B}_J dV. \quad (4.84)$$

When combined with (4.71) and considering an arbitrary virtual velocity, $\delta \mathbf{v}$, gives

$$\mathbf{m} \ddot{\mathbf{u}} + \mathbf{k} \mathbf{u} = \mathbf{f} \quad (4.85)$$

and for quasi-static problems,

$$\mathbf{k} \mathbf{u} = \mathbf{f}. \quad (4.86)$$

This equation, in general, is non-linear if the problem considered is geometrically non-linear. This is because the stiffness matrix, \mathbf{k} , depends upon the \mathbf{B} matrix which

contains the derivatives of the shape functions with respect to the spatial coordinates. In a geometrically non-linear problem, the spatial coordinates change so that the stiffness matrix also changes. For geometrically non-linear problems, Equation (4.86) therefore has to be solved incrementally, and at each increment, the stiffness matrix must be updated.

In the following sections, we look at a number of small deformation (geometrically linear) examples including a two-element axial vibration problem in which element assembly is addressed, a single-element and two-element bending problem in which beam elements are introduced, and a single square element static elastic problem in which linear four-noded (quad) elements are introduced.

4.4.3.1 Axial vibration of a beam using two truss elements. The uniform bar shown in Fig. 4.11(a) undergoes axial vibration. It is discretized using two truss elements shown in Fig. 4.11(b).

The truss element formulation, relative to the local element reference frame, is shown in Fig. 4.12.

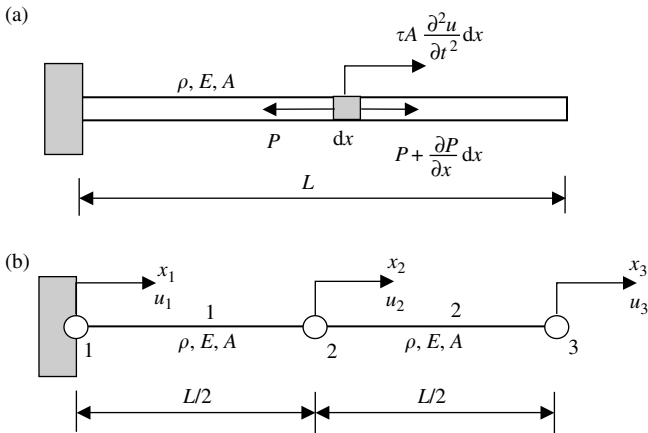


Fig. 4.11 A uniform bar undergoing axial vibration (a) shown schematically and (b) its discretization using two truss elements.

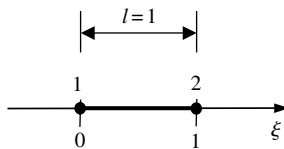


Fig. 4.12 Linear truss element formulation shown relative to the local element reference frame, ξ .

The shape functions are

$$N_1 = 1 - \xi, \quad N_2 = \xi$$

and in this problem, the two elements are identical so that their mass and stiffness matrices, respectively, are the same. Also, because this is a problem in which the displacements are infinitesimal, the current and original configurations are taken to be the same. We shall determine the mass and stiffness matrices for a single element, and then consider their assemblage.

The mass matrix given by (4.43) with respect to the spatial (which in this case coincides with the material) coordinate system is

$$\mathbf{m} = \int_{\Omega} \rho \mathbf{N}^T \mathbf{N} \, dV = \int_{X=0}^{L/2} \rho \mathbf{N}^T \mathbf{N} A \, dX$$

but of course, the shape functions are given with respect to the local element reference frame. Therefore, we write

$$\begin{aligned} \mathbf{m} &= \int_{X=0}^{L/2} \rho \mathbf{N}^T \mathbf{N} A \, dX = \int_{\xi=0}^1 \rho \mathbf{N}^T \mathbf{N} A \det(J) \, d\xi \\ &= \rho A \int_{\xi=0}^1 \begin{bmatrix} 1 - \xi \\ \xi \end{bmatrix} [1 - \xi \quad \xi] \det(J) \, d\xi \end{aligned} \quad (4.87)$$

in which J is the Jacobian, mapping the spatial coordinate system onto the local element reference frame. In this one-dimensional problem, the determinant of the Jacobian is just

$$\det(J) = \left| \frac{\partial X}{\partial \xi} \right| = \left| \frac{\partial}{\partial \xi} [N_1 \quad N_2] \begin{bmatrix} X_1 \\ X_2 \end{bmatrix} \right| = \left| \begin{bmatrix} \frac{\partial N_1}{\partial \xi} & \frac{\partial N_2}{\partial \xi} \end{bmatrix} \begin{bmatrix} X_1 \\ X_2 \end{bmatrix} \right|,$$

which is of the general form given in Equation (4.60). Using the shape functions, we obtain

$$\det(J) = \left| \begin{bmatrix} -1 & 1 \end{bmatrix} \begin{bmatrix} X_1 \\ X_2 \end{bmatrix} \right| = |[-X_1 + X_2]| = \left| \left[0 + \frac{L}{2} \right] \right| = \left| \left[\frac{L}{2} \right] \right| = \frac{L}{2}$$

so that the element mass matrix becomes

$$\mathbf{m} = \frac{\rho AL}{2} \int_{\xi=0}^1 \begin{pmatrix} 1 - 2\xi + \xi^2 & \xi - \xi^2 \\ \xi - \xi^2 & \xi^2 \end{pmatrix} d\xi = \frac{\rho AL}{2} \begin{pmatrix} \frac{1}{3} & \frac{1}{6} \\ \frac{1}{6} & \frac{1}{3} \end{pmatrix}. \quad (4.88)$$

Let us write the mass matrix for elements 1 and 2 as

$$\mathbf{m}_1 = \begin{bmatrix} m_{11}^1 & m_{12}^1 \\ m_{21}^1 & m_{22}^1 \end{bmatrix} = \frac{\rho AL}{2} \begin{bmatrix} \frac{1}{3} & \frac{1}{6} \\ \frac{1}{6} & \frac{1}{3} \end{bmatrix}, \quad \mathbf{m}_2 = \begin{bmatrix} m_{11}^2 & m_{12}^2 \\ m_{21}^2 & m_{22}^2 \end{bmatrix} = \frac{\rho AL}{2} \begin{bmatrix} \frac{1}{3} & \frac{1}{6} \\ \frac{1}{6} & \frac{1}{3} \end{bmatrix},$$

then the *global mass matrix* is given by

$$\mathbf{M} = \begin{bmatrix} m_{11}^1 & m_{12}^1 & 0 \\ m_{21}^1 & m_{22}^1 + m_{11}^2 & m_{12}^2 \\ 0 & m_{21}^2 & m_{22}^2 \end{bmatrix} = \rho A \frac{L}{2} \begin{bmatrix} \frac{1}{3} & \frac{1}{6} & 0 \\ \frac{1}{6} & \frac{2}{3} & \frac{1}{6} \\ 0 & \frac{1}{6} & \frac{1}{3} \end{bmatrix} = \rho AL \begin{bmatrix} \frac{1}{6} & \frac{1}{12} & 0 \\ \frac{1}{12} & \frac{1}{3} & \frac{1}{12} \\ 0 & \frac{1}{12} & \frac{1}{6} \end{bmatrix}. \quad (4.89)$$

The element stiffness matrix is given by (4.44) in terms of the spatial coordinates by

$$\mathbf{k} = \int_{\Omega} \mathbf{B}^T \mathbf{C} \mathbf{B} \, dV = \int_{X=0}^L \mathbf{B}^T \mathbf{C} \mathbf{B} A \, dX.$$

Introducing again the Jacobian in (4.87), the integral can be written with respect to the local element reference frame by

$$\mathbf{k} = \int_{\xi=0}^1 \mathbf{B}^T \mathbf{C} \mathbf{B} A \det(J) \, d\xi = \int_{\xi=0}^1 \mathbf{B}^T \mathbf{C} \mathbf{B} A \frac{L}{2} \, d\xi.$$

Because the truss elements are one-dimensional, the elasticity matrix, \mathbf{C} , becomes just the scalar Young's modulus, E , so

$$\mathbf{k} = \frac{EAL}{2} \int_{\xi=0}^1 \mathbf{B}^T \mathbf{B} \, d\xi.$$

The \mathbf{B} matrix contains the derivatives of the shape functions with respect to the spatial coordinates. We are assuming small displacements, however, and that the problem remains geometrically linear so that the spatial and material coordinates remain the same. Hence,

$$\mathbf{B} = \begin{bmatrix} \frac{\partial N_1}{\partial x} & \frac{\partial N_2}{\partial x} \end{bmatrix} \equiv \begin{bmatrix} \frac{\partial N_1}{\partial X} & \frac{\partial N_2}{\partial X} \end{bmatrix} = \begin{bmatrix} \frac{\partial N_1}{\partial \xi} \frac{\partial \xi}{\partial X} & \frac{\partial N_2}{\partial \xi} \frac{\partial \xi}{\partial X} \end{bmatrix}.$$

In general, $\partial \xi / \partial X$ cannot be determined directly, since we ordinarily know X in terms of ξ . In its most general form, the relationship is given by (4.52), and for the truss element in this problem, this is

$$X = [N_1 \quad N_2] \begin{bmatrix} X_1 \\ X_2 \end{bmatrix}.$$

We have already determined the Jacobian derivative, in (4.87), and note that this is the inverse of $\partial \xi / \partial X$. That is, therefore,

$$\frac{\partial \xi}{\partial X} = \left(\frac{\partial X}{\partial \xi} \right)^{-1} = J^{-1} = \left(\frac{L}{2} \right)^{-1} = \frac{2}{L}.$$

In general, therefore, the derivatives needed for the \mathbf{B} matrix are obtained from the inverse of the Jacobian. The \mathbf{B} matrix is, therefore,

$$\mathbf{B} = \begin{bmatrix} \frac{\partial N_1}{\partial \xi} \frac{\partial \xi}{\partial X} & \frac{\partial N_2}{\partial \xi} \frac{\partial \xi}{\partial X} \end{bmatrix} = \begin{bmatrix} -1 \times \frac{2}{L} & 1 \times \frac{2}{L} \end{bmatrix} = \frac{2}{L} \begin{bmatrix} -1 & 1 \end{bmatrix}$$

so that the element stiffness matrix becomes

$$\mathbf{k} = \frac{EAL}{2} \int_{\xi=0}^1 \left(\frac{2}{L}\right)^2 \begin{bmatrix} -1 \\ 1 \end{bmatrix} \begin{bmatrix} -1 & 1 \end{bmatrix} d\xi = \frac{2EA}{L} \begin{bmatrix} 1 & -1 \\ -1 & 1 \end{bmatrix}. \quad (4.90)$$

As for the mass matrices, we write the stiffness matrices for the two elements as

$$\mathbf{k}_1 = \begin{bmatrix} k_{11}^1 & k_{12}^1 \\ k_{21}^1 & k_{22}^1 \end{bmatrix} = \frac{2EA}{L} \begin{bmatrix} 1 & -1 \\ -1 & 1 \end{bmatrix}, \quad \mathbf{k}_2 = \begin{bmatrix} k_{11}^2 & k_{12}^2 \\ k_{21}^2 & k_{22}^2 \end{bmatrix} = \frac{2EA}{L} \begin{bmatrix} 1 & -1 \\ -1 & 1 \end{bmatrix}$$

so that the global stiffness matrix become

$$\mathbf{K} = \begin{bmatrix} k_{11}^1 & k_{12}^1 & 0 \\ k_{21}^1 & k_{22}^1 + k_{11}^2 & k_{12}^2 \\ 0 & k_{21}^2 & k_{22}^2 \end{bmatrix} = \frac{2EA}{L} \begin{bmatrix} 1 & -1 & 0 \\ -1 & 2 & -1 \\ 0 & -1 & 1 \end{bmatrix} = \frac{EA}{L} \begin{bmatrix} 2 & -2 & 0 \\ -2 & 4 & -2 \\ 0 & -2 & 2 \end{bmatrix}. \quad (4.91)$$

The finite element equilibrium equation, given in (4.46) and (4.85) then becomes

$$\mathbf{M}\ddot{\mathbf{u}} + \mathbf{K}\mathbf{u} = 0$$

so

$$\rho AL \begin{bmatrix} \frac{1}{6} & \frac{1}{12} & 0 \\ \frac{1}{12} & \frac{1}{3} & \frac{1}{12} \\ 0 & \frac{1}{12} & \frac{1}{6} \end{bmatrix} \begin{bmatrix} \ddot{u}_1 \\ \ddot{u}_2 \\ \ddot{u}_3 \end{bmatrix} + \frac{EA}{L} \begin{bmatrix} 2 & -2 & 0 \\ -2 & 4 & -2 \\ 0 & -2 & 2 \end{bmatrix} \begin{bmatrix} u_1 \\ u_2 \\ u_3 \end{bmatrix} = \begin{bmatrix} 0 \\ 0 \\ 0 \end{bmatrix}.$$

With the boundary condition $u_1 = 0$, this reduces to

$$\rho AL \begin{bmatrix} \frac{1}{3} & \frac{1}{12} \\ \frac{1}{12} & \frac{1}{6} \end{bmatrix} \begin{bmatrix} \ddot{u}_2 \\ \ddot{u}_3 \end{bmatrix} + \frac{EA}{L} \begin{bmatrix} 4 & -2 \\ -2 & 2 \end{bmatrix} \begin{bmatrix} u_2 \\ u_3 \end{bmatrix} = \begin{bmatrix} 0 \\ 0 \end{bmatrix}.$$

4.4.3.2 Cantilever beam in bending using a single element. The problem geometry and finite element discretization are shown in Figs 4.13 and 4.14.

The *Hermitian* shape functions in the element local coordinate system (note that $dx = L d\xi$) are obtained as follows:

$$N = a_0 + a_1\xi + a_2\xi^2 + a_3\xi^3.$$

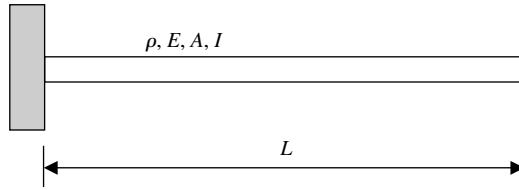


Fig. 4.13 Cantilever beam of uniform section with second moment of area I .

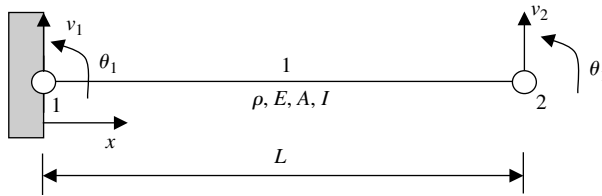


Fig. 4.14 Single beam element discretization of a cantilever. The element has four degrees of freedom; two translational and two rotational.

First degree of freedom (y_1)

$$\left. \begin{aligned} \xi = 0, N_1 = 1, \frac{dN_1}{d\xi} = 0 \\ \xi = 1, N_1 = 0, \frac{dN_1}{d\xi} = 0 \end{aligned} \right\} \Rightarrow N_1 = 1 - 3\xi^2 + 2\xi^3.$$

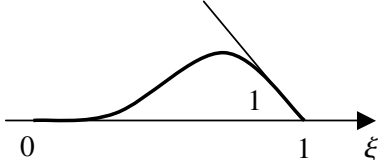
Second degree of freedom (θ_1)

$$\left. \begin{aligned} \xi = 0, N_2 = 0, \frac{dN_2}{d\xi} = 1 \\ \xi = 1, N_2 = 0, \frac{dN_2}{d\xi} = 0 \end{aligned} \right\} \Rightarrow N_2 = \xi - 2\xi^2 + \xi^3.$$

Third degree of freedom (y_2)

$$\left. \begin{aligned} \xi = 0, N_3 = 0, \frac{dN_3}{d\xi} = 0 \\ \xi = 1, N_3 = 1, \frac{dN_3}{d\xi} = 0 \end{aligned} \right\} \Rightarrow N_3 = 3\xi^2 - 2\xi^3.$$

Fourth degree of freedom (θ_2)

$$\left. \begin{array}{l} \xi = 0, \quad N_4 = 0, \quad \frac{dN_4}{d\xi} = 0 \\ \xi = 1, \quad N_4 = 0, \quad \frac{dN_4}{d\xi} = 1 \end{array} \right\} \Rightarrow N_4 = -\xi^2 + \xi^3.$$


We shall now apply Hamilton's principle in order to obtain the finite element equilibrium equations. For a beam in bending, we may write the kinetic, T , and potential (strain), U , energies as

$$T = \frac{1}{2} \int_0^L \rho A \left(\frac{\partial v}{\partial t} \right)^2 dx, \quad U = \frac{1}{2} \int_0^L EI \left(\frac{\partial^2 v}{\partial x^2} \right)^2 dx.$$

The finite element discretization is given by

$$\begin{aligned} v(x, t) &= N_1(\xi)v_1(t) + N_2(\xi)\theta_1(t) + N_3(\xi)v_2(t) + N_4(\xi)\theta_2(t) \\ &= N_1(\xi)v_1(t) + N_2(\xi)\frac{\partial v_1}{\partial \xi} + N_3(\xi)v_2(t) + N_4(\xi)\frac{\partial v_2}{\partial \xi} \\ &= N_1(\xi)v_1(t) + N_2(\xi)L\frac{\partial v_1}{\partial x} + N_3(\xi)v_2(t) + N_4(\xi)L\frac{\partial v_2}{\partial x}, \end{aligned}$$

which we shall write as

$$v = \mathbf{N}\mathbf{u} = [N_1(\xi) \quad N_2(\xi) \quad N_3(\xi) \quad N_4(\xi)] \begin{bmatrix} v_1 & \frac{\partial v_1}{\partial x} & v_2 & \frac{\partial v_2}{\partial x} \end{bmatrix}^T.$$

The derivatives in the strain energy term are given by

$$\begin{aligned} \frac{\partial^2 v}{\partial x^2} &= \frac{1}{L^2} \frac{\partial^2 v}{\partial \xi^2} = \frac{1}{L^2} \left[\frac{\partial^2 N_1}{\partial \xi^2} v_1 + \frac{\partial^2 N_2}{\partial \xi^2} L \frac{\partial v_1}{\partial x} + \frac{\partial^2 N_3}{\partial \xi^2} v_2 + \frac{\partial^2 N_4}{\partial \xi^2} L \frac{\partial v_2}{\partial x} \right] \\ &= \frac{1}{L^2} \begin{bmatrix} \frac{\partial^2 N_1}{\partial \xi^2} & \frac{\partial^2 N_2}{\partial \xi^2} L & \frac{\partial^2 N_3}{\partial \xi^2} & \frac{\partial^2 N_4}{\partial \xi^2} L \end{bmatrix} \begin{bmatrix} v_1 \\ \frac{\partial v_1}{\partial x} \\ v_2 \\ \frac{\partial v_2}{\partial x} \end{bmatrix} = \mathbf{B}\mathbf{u}. \end{aligned}$$

The element kinetic and strain energies are given by

$$T = \frac{1}{2} \int_0^L \rho A (\mathbf{N}\dot{\mathbf{u}})^T (\mathbf{N}\dot{\mathbf{u}}) dx = \frac{1}{2} \dot{\mathbf{u}}^T \left(\int_0^L \rho A \mathbf{N}^T \mathbf{N} dx \right) \dot{\mathbf{u}}$$

and

$$\begin{aligned}
 U &= \frac{1}{2} \int_0^L EI \left(\frac{\partial^2 \mathbf{N}}{\partial \xi^2} \mathbf{u} \right)^T \left(\frac{\partial^2 \mathbf{N}}{\partial \xi^2} \mathbf{u} \right) dx \\
 &= \frac{1}{2} \mathbf{u}^T \left(\int_0^L EI \left(\frac{\partial^2 \mathbf{N}}{\partial \xi^2} \right)^T \left(\frac{\partial^2 \mathbf{N}}{\partial \xi^2} \right) dx \right) \mathbf{u} \\
 &= \frac{1}{2} \mathbf{u}^T \left(\int_0^L EI \mathbf{B}^T \mathbf{B} dx \right) \mathbf{u}.
 \end{aligned}$$

The element Lagrangian, L , is

$$L = T - U = \frac{1}{2} \dot{\mathbf{u}}^T \mathbf{m} \dot{\mathbf{u}} - \frac{1}{2} \mathbf{u}^T \mathbf{k} \mathbf{u}, \quad (4.92)$$

where

$$\mathbf{m} = \int_0^L \rho A \mathbf{N}^T \mathbf{N} dx \quad (4.93)$$

and

$$\mathbf{k} = \int_0^L EI \mathbf{B}^T \mathbf{B} dx. \quad (4.94)$$

Integrating the Lagrangian with respect to time, and taking the first variation gives

$$\mathbf{m} \ddot{\mathbf{u}} + \mathbf{k} \mathbf{u} = \mathbf{0}.$$

The element mass matrix is

$$\begin{aligned}
 \mathbf{m} &= \begin{bmatrix} m_{11}^e & m_{12}^e & m_{13}^e & m_{14}^e \\ m_{21}^e & m_{22}^e & m_{23}^e & m_{24}^e \\ m_{31}^e & m_{32}^e & m_{33}^e & m_{34}^e \\ m_{41}^e & m_{42}^e & m_{43}^e & m_{44}^e \end{bmatrix} = \int_0^L \rho A \mathbf{N}^T \mathbf{N} dx \\
 &= \rho A \int_0^1 \begin{bmatrix} 1 - 3\xi^2 + 2\xi^3 \\ (\xi - 2\xi^2 + \xi^3)L \\ 3\xi^2 - 2\xi^3 \\ (-\xi^2 + \xi^3)L \end{bmatrix} \\
 &\quad \times \begin{bmatrix} 1 - 3\xi^2 + 2\xi^3 & (\xi - 2\xi^2 + \xi^3)L & 3\xi^2 - 2\xi^3 & (-\xi^2 + \xi^3)L \end{bmatrix} L d\xi \\
 &= \frac{\rho AL}{420} \begin{bmatrix} 156 & 22L & 54 & -13L \\ 22L & 4L^2 & 13L & -3L^2 \\ 54 & 13L & 156 & -22L \\ -13L & -3L^2 & -22L & 4L^2 \end{bmatrix}.
 \end{aligned}$$

The element stiffness matrix is given by

$$\begin{aligned}
 \mathbf{k} &= \begin{bmatrix} k_{11}^e & k_{12}^e & k_{13}^e & k_{14}^e \\ k_{21}^e & k_{22}^e & k_{23}^e & k_{24}^e \\ k_{31}^e & k_{32}^e & k_{33}^e & k_{34}^e \\ k_{41}^e & k_{42}^e & k_{43}^e & k_{44}^e \end{bmatrix} = \int_0^L EI \mathbf{B}^T \mathbf{B} \, dx \\
 &= \int_0^1 \frac{1}{L^2} \begin{bmatrix} -6 + 12\xi \\ (-4 + 6\xi)L \\ 6 - 12\xi \\ (-2 + 6\xi)L \end{bmatrix} EI \frac{1}{L^2} \\
 &\quad \times [-6 + 12\xi \quad (-4 + 6\xi)L \quad 6 - 12\xi \quad (-2 + 6\xi)L] L \, d\xi \\
 &= \frac{EI}{L^3} \begin{bmatrix} 12 & 6L & -12 & 6L \\ 6L & 4L^2 & -6L & 2L^2 \\ -12 & -6L & 12 & -6L \\ 6L & 2L^2 & -6L & 4L^2 \end{bmatrix}.
 \end{aligned}$$

The finite element equilibrium equation becomes

$$\begin{aligned}
 \frac{\rho AL}{420} \begin{bmatrix} 156 & 22L & 54 & -13L \\ 22L & 4L^2 & 13L & -3L^2 \\ 54 & 13L & 156 & -22L \\ -13L & -3L^2 & -22L & 4L^2 \end{bmatrix} \begin{bmatrix} \ddot{y}_1 \\ \ddot{\theta}_1 \\ \ddot{y}_2 \\ \ddot{\theta}_2 \end{bmatrix} \\
 + \frac{EI}{L^3} \begin{bmatrix} 12 & 6L & -12 & 6L \\ 6L & 4L^2 & -6L & 2L^2 \\ -12 & -6L & 12 & -6L \\ 6L & 2L^2 & -6L & 4L^2 \end{bmatrix} \begin{bmatrix} y_1 \\ \theta_1 \\ y_2 \\ \theta_2 \end{bmatrix} = \begin{bmatrix} 0 \\ 0 \\ 0 \\ 0 \end{bmatrix}.
 \end{aligned}$$

With the boundary conditions $v_1 = 0$ and $\theta_1 = 0$ at $x = 0$, the problem reduces to one with two degrees of freedom

$$\frac{\rho AL}{420} \begin{bmatrix} 156 & -22L \\ -22L & 4L^2 \end{bmatrix} \begin{bmatrix} \ddot{x}_2 \\ \ddot{\theta}_3 \end{bmatrix} + \frac{EI}{L^3} \begin{bmatrix} 12 & -6L \\ -6L & 4L^2 \end{bmatrix} \begin{bmatrix} x_2 \\ \theta_3 \end{bmatrix} = \begin{bmatrix} 0 \\ 0 \end{bmatrix}.$$

4.4.3.3 Free transverse vibration of a propped cantilever using two beam elements. A uniform, propped cantilever beam is shown in Fig. 4.15 and its finite element discretization using two beam elements in Fig. 4.16.

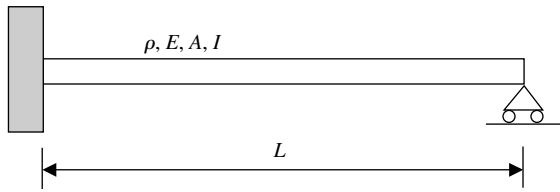


Fig. 4.15 A uniform propped cantilever beam.

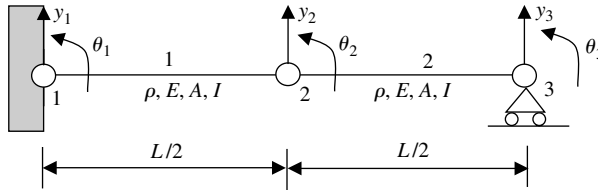


Fig. 4.16 Finite element discretization of a propped cantilever beam. The two beam elements are identical.

The element mass matrix (valid for both elements) is

$$m_e = \frac{\rho A(L/2)}{420} \begin{bmatrix} 156 & 22\frac{L}{2} & 54 & -13\frac{L}{2} \\ 22\frac{L}{2} & 4\left(\frac{L}{2}\right)^2 & 13\frac{L}{2} & -3\left(\frac{L}{2}\right)^2 \\ 54 & 13\frac{L}{2} & 156 & -22\frac{L}{2} \\ -13\frac{L}{2} & -3\left(\frac{L}{2}\right)^2 & -22\frac{L}{2} & 4\left(\frac{L}{2}\right)^2 \end{bmatrix}$$

and the stiffness matrix (valid for both elements) is

$$k_e = \frac{EI}{(L/2)^3} \begin{bmatrix} 12 & 6\frac{L}{2} & -12 & 6\frac{L}{2} \\ 6L & 4\left(\frac{L}{2}\right)^2 & -6\frac{L}{2} & 2\left(\frac{L}{2}\right)^2 \\ -12 & -6\frac{L}{2} & 12 & -6\frac{L}{2} \\ 6\frac{L}{2} & 2\left(\frac{L}{2}\right)^2 & -6\frac{L}{2} & 4\left(\frac{L}{2}\right)^2 \end{bmatrix}.$$

With the boundary conditions, we may write for the first element

$$\mathbf{u} = \begin{bmatrix} y_1 \\ \theta_1 \\ y_2 \\ \theta_2 \end{bmatrix} = \begin{bmatrix} 0 \\ 0 \\ y_2 \\ \theta_2 \end{bmatrix} \rightarrow \mathbf{k}_1 = \frac{EI}{(L/2)^3} \begin{bmatrix} X & X & X & X \\ X & X & X & X \\ X & X & 12 & -6\frac{L}{2} \\ X & X & -6\frac{L}{2} & 4\left(\frac{L}{2}\right)^2 \end{bmatrix}$$

and for element 2 that

$$\mathbf{u} = \begin{bmatrix} y_2 \\ \theta_2 \\ y_3 \\ \theta_3 \end{bmatrix} = \begin{bmatrix} y_2 \\ \theta_2 \\ 0 \\ \theta_3 \end{bmatrix} \rightarrow \mathbf{k}_2 = \frac{EI}{(L/2)^3} \begin{bmatrix} 12 & 6\frac{L}{2} & X & 6\frac{L}{2} \\ 6\frac{L}{2} & 4\left(\frac{L}{2}\right)^2 & X & 2\left(\frac{L}{2}\right)^2 \\ X & X & X & X \\ 6\frac{L}{2} & 2\left(\frac{L}{2}\right)^2 & X & 4\left(\frac{L}{2}\right)^2 \end{bmatrix}.$$

We proceed in a similar way for the mass matrix and obtain the finite element equilibrium equation

$$\mathbf{M}\ddot{\mathbf{u}} + \mathbf{K}\mathbf{u} = \mathbf{0}$$

to be

$$\frac{\rho AL}{420} \begin{bmatrix} 156 & 0 & -\frac{13}{4}L \\ 0 & L^2 & -\frac{3}{8}L^2 \\ -\frac{13}{4}L & -\frac{3}{8}L^2 & \frac{1}{2}L^2 \end{bmatrix} \begin{bmatrix} \ddot{y}_2 \\ \ddot{\theta}_2 \\ \ddot{\theta}_3 \end{bmatrix} + \frac{EI}{L^3} \begin{bmatrix} 172 & 0 & 24L \\ 0 & 16L^2 & 4L^2 \\ 24L & 4L^2 & 8L^2 \end{bmatrix} \begin{bmatrix} y_2 \\ \theta_2 \\ \theta_3 \end{bmatrix} = \begin{bmatrix} 0 \\ 0 \\ 0 \end{bmatrix}.$$

4.4.3.4 Static analysis of a single square element. We will examine one further example before moving on; a single, two-dimensional, four-noded, isoparametric element subjected to a static force. We take the material behaviour to be elastic, and assume conditions of plane strain. The problem is shown schematically in Fig. 4.17, together with the elastic constants.

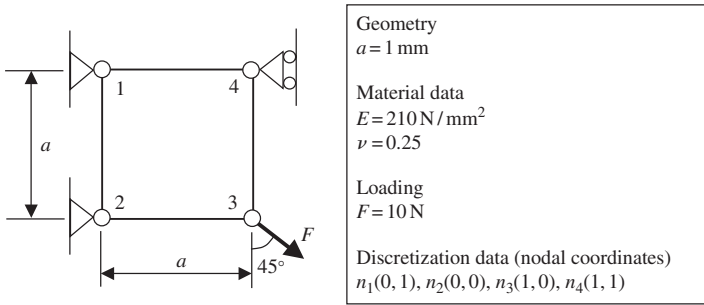


Fig. 4.17 Schematic diagram of a single, four-noded element subjected to force F directed at 45° to the vertical.

The shape functions for this element are as follows:

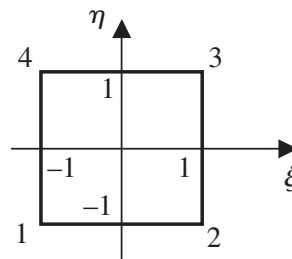
$$N_1(\xi, \eta) = \frac{1}{4}(1 - \xi)(1 - \eta),$$

$$N_2(\xi, \eta) = \frac{1}{4}(1 + \xi)(1 - \eta),$$

$$N_3(\xi, \eta) = \frac{1}{4}(1 + \xi)(1 + \eta),$$

$$N_4(\xi, \eta) = \frac{1}{4}(1 - \xi)(1 + \eta).$$

Element local coordinate system



We will find that we need to carry out integrations (in order to obtain the stiffness matrix) of the shape functions. Previously, we have been able to do the integrations analytically. Here, we will need to use a numerical technique. Often, in order to simplify the process, the integration is carried out with respect to a particular point in the element; this point is known as an *integration point*. The integration will be performed numerically using a single integration point at $P(\xi, \eta) = P(0, 0)$. Integrals over the element domain of the type

$$I = \int_{\Omega} f(\xi, \eta) dV$$

are expressed in the element local coordinate system by use of the Jacobian, \mathbf{J} , as

$$I = \int_{-1}^1 \int_{-1}^1 f(\xi, \eta) \det[\mathbf{J}] d\xi d\eta, \quad (4.95)$$

where the Jacobian for a two-dimensional problem is given by

$$\mathbf{J} = \begin{bmatrix} \frac{\partial X}{\partial \xi} & \frac{\partial X}{\partial \eta} \\ \frac{\partial Y}{\partial \xi} & \frac{\partial Y}{\partial \eta} \end{bmatrix}. \quad (4.96)$$

The integral in (4.95) will be approximated using *Gauss quadrature* (details may be found in any of the more specialized books on finite elements) by

$$I \approx \left(\int_{-1}^1 \int_{-1}^1 \det[J] d\xi d\eta \right) f(\xi, \eta).$$

The shape function derivatives at the integration point $P(\xi, \eta) = P(0, 0)$ are obtained from

$$\frac{\partial N}{\partial X} = \frac{\partial N}{\partial \xi} \frac{\partial \xi}{\partial X} = \frac{\partial N}{\partial \xi} \left(\frac{\partial X}{\partial \xi} \right)^{-1} \tag{4.97}$$

and the shape function derivatives with respect to element local coordinates are given by

$$\begin{aligned} \frac{\partial N(0, 0)}{\partial \xi} &= \begin{bmatrix} \frac{\partial N_1(0, 0)}{\partial \xi} & \frac{\partial N_1(0, 0)}{\partial \eta} \\ \frac{\partial N_2(0, 0)}{\partial \xi} & \frac{\partial N_2(0, 0)}{\partial \eta} \\ \frac{\partial N_3(0, 0)}{\partial \xi} & \frac{\partial N_3(0, 0)}{\partial \eta} \\ \frac{\partial N_4(0, 0)}{\partial \xi} & \frac{\partial N_4(0, 0)}{\partial \eta} \end{bmatrix} = \frac{1}{4} \begin{bmatrix} (-1)(1 - \eta)|_{(0,0)} & (1 - \xi)(-1)|_{(0,0)} \\ (1)(1 - \eta)|_{(0,0)} & (1 + \xi)(-1)|_{(0,0)} \\ (1)(1 + \eta)|_{(0,0)} & (1 + \xi)(1)|_{(0,0)} \\ (-1)(1 + \eta)|_{(0,0)} & (1 - \xi)(1)|_{(0,0)} \end{bmatrix} \\ &= \frac{1}{4} \begin{bmatrix} -1 & -1 \\ 1 & -1 \\ 1 & 1 \\ -1 & 1 \end{bmatrix}. \end{aligned}$$

In order to determine the Jacobian matrix $\partial X/\partial \xi$, let us first write down the relationship between element and nodal positions; that is,

$$\begin{aligned} X &= N_1 X_1 + N_2 X_2 + N_3 X_3 + N_4 X_4, \\ Y &= N_1 Y_1 + N_2 Y_2 + N_3 Y_3 + N_4 Y_4. \end{aligned}$$

We see, therefore, that

$$\frac{\partial X}{\partial \xi} = \frac{\partial N_1}{\partial \xi} X_1 + \frac{\partial N_2}{\partial \xi} X_2 + \frac{\partial N_3}{\partial \xi} X_3 + \frac{\partial N_4}{\partial \xi} X_4 = X_I \frac{\partial N_I}{\partial \xi}$$

and similarly for other terms. The Jacobian matrix, therefore, from (4.96) is

$$\begin{aligned} \mathbf{J} &= \begin{bmatrix} \frac{\partial X}{\partial \xi} & \frac{\partial X}{\partial \eta} \\ \frac{\partial Y}{\partial \xi} & \frac{\partial Y}{\partial \eta} \end{bmatrix} = \begin{bmatrix} X_I \frac{\partial N_I}{\partial \xi} & X_I \frac{\partial N_I}{\partial \eta} \\ Y_I \frac{\partial N_I}{\partial \xi} & Y_I \frac{\partial N_I}{\partial \eta} \end{bmatrix} \\ &= \begin{bmatrix} X_1 & X_2 & X_3 & X_4 \\ Y_1 & Y_2 & Y_3 & Y_4 \end{bmatrix} \begin{bmatrix} \frac{\partial N_1}{\partial \xi} & \frac{\partial N_1}{\partial \eta} \\ \frac{\partial N_2}{\partial \xi} & \frac{\partial N_2}{\partial \eta} \\ \frac{\partial N_3}{\partial \xi} & \frac{\partial N_3}{\partial \eta} \\ \frac{\partial N_4}{\partial \xi} & \frac{\partial N_4}{\partial \eta} \end{bmatrix}. \end{aligned}$$

This can be written in the general form given in Equation (4.61) as

$$\mathbf{J} = \mathbf{X} \frac{\partial \mathbf{N}}{\partial \boldsymbol{\xi}}.$$

With the shape functions given above, evaluated at the integration point, and the nodal coordinates, the Jacobian becomes

$$\begin{aligned} \frac{\partial \mathbf{X}}{\partial \boldsymbol{\xi}} &= \mathbf{X} \frac{\partial \mathbf{N}}{\partial \boldsymbol{\xi}} = \begin{bmatrix} X_1 & X_2 & X_3 & X_4 \\ Y_1 & Y_2 & Y_3 & Y_4 \end{bmatrix} \frac{1}{4} \begin{bmatrix} -1 & -1 \\ 1 & -1 \\ 1 & 1 \\ -1 & 1 \end{bmatrix} \\ &= \frac{1}{4} \begin{bmatrix} -X_1 + X_2 + X_3 - X_4 & -X_1 - X_2 + X_3 + X_4 \\ -Y_1 + Y_2 + Y_3 - Y_4 & -Y_1 - Y_2 + Y_3 + Y_4 \end{bmatrix} \\ &= \frac{1}{4} \begin{bmatrix} -0 + 0 + 1 - 1 & -0 - 0 + 1 + 1 \\ -1 + 0 + 0 - 1 & -1 - 0 + 0 + 1 \end{bmatrix} \\ &= \frac{1}{4} \begin{bmatrix} 0 & 2 \\ -2 & 0 \end{bmatrix} = \begin{bmatrix} 0 & 0.5 \\ -0.5 & 0 \end{bmatrix}. \end{aligned}$$

The determinant of the Jacobian is

$$\det[\mathbf{J}] = \det \left[\frac{\partial \mathbf{X}}{\partial \boldsymbol{\xi}} \right] = \det \begin{bmatrix} 0 & 0.5 \\ -0.5 & 0 \end{bmatrix} = 0.25$$

and its inverse is

$$\left(\frac{\partial \mathbf{X}}{\partial \boldsymbol{\xi}} \right)^{-1} = \begin{bmatrix} 0 & -2 \\ 2 & 0 \end{bmatrix}.$$

Finally, the shape function derivatives with respect to the spatial (here, equivalent to the material) coordinates are

$$\begin{aligned} \frac{\partial N}{\partial \mathbf{X}} &= \frac{\partial N}{\partial \xi} \left(\frac{\partial \mathbf{X}}{\partial \xi} \right)^{-1} = \frac{1}{4} \begin{bmatrix} -1 & -1 \\ 1 & -1 \\ 1 & 1 \\ -1 & 1 \end{bmatrix} \begin{bmatrix} 0 & -2 \\ 2 & 0 \end{bmatrix} \\ &= \frac{1}{4} \begin{bmatrix} -1 & -1 \\ 1 & -1 \\ 1 & 1 \\ -1 & 1 \end{bmatrix} \begin{bmatrix} 0 & -2 \\ 2 & 0 \end{bmatrix} = \begin{bmatrix} -1 & -1 \\ 1 & -1 \\ 1 & 1 \\ -1 & 1 \end{bmatrix} \begin{bmatrix} 0 & -0.5 \\ 0.5 & 0 \end{bmatrix} \\ &= \begin{bmatrix} -0.5 & 0.5 \\ -0.5 & -0.5 \\ 0.5 & -0.5 \\ 0.5 & 0.5 \end{bmatrix}. \end{aligned}$$

The \mathbf{B} matrix can now be obtained (for plane strain) from (4.81)

$$\mathbf{B}_I = \begin{bmatrix} \frac{\partial N_I(0,0)}{\partial x} & 0 \\ 0 & \frac{\partial N_I(0,0)}{\partial y} \\ \frac{\partial N_I(0,0)}{\partial y} & \frac{\partial N_I(0,0)}{\partial x} \end{bmatrix},$$

$$\mathbf{B} = \begin{bmatrix} -0.5 & 0 & -0.5 & 0 & 0.5 & 0 & 0.5 & 0 \\ 0 & 0.5 & 0 & -0.5 & 0 & -0.5 & 0 & 0.5 \\ 0.5 & -0.5 & -0.5 & -0.5 & -0.5 & 0.5 & 0.5 & 0.5 \end{bmatrix}.$$

The elasticity matrix for plane strain is

$$\mathbf{C} = \begin{bmatrix} \lambda + 2\mu & \lambda & 0 \\ \lambda & \lambda + 2\mu & 0 \\ 0 & 0 & \mu \end{bmatrix},$$

$$\lambda = \frac{\nu E}{(1 + \nu)(1 - 2\nu)} = 84 \text{ N/mm}^2,$$

$$\mu = G = \frac{E}{2(1 + \nu)} = 84 \text{ N/mm}^2,$$

$$\mathbf{C} = \begin{bmatrix} 252 & 84 & 0 \\ 84 & 252 & 0 \\ 0 & 0 & 84 \end{bmatrix} \text{ N/mm}^2.$$

The stiffness matrix can then be determined by using the approximate integration formula given above as

$$\begin{aligned}
 \mathbf{k} &= \int_V \mathbf{B}^T \mathbf{C} \mathbf{B} \, dV = \int_0^1 \int_0^1 \mathbf{B}^T \mathbf{C} \mathbf{B} \, dx \, dy = \int_{-1}^1 \int_{-1}^1 \mathbf{B}^T \mathbf{C} \mathbf{B} \, \det[\mathbf{J}] \, d\xi \, d\eta \\
 &\approx [\mathbf{B}(0, 0)]^T \mathbf{C} \mathbf{B}(0, 0) \det[\mathbf{J}(0, 0)]. \quad 2.2 \\
 &= \begin{bmatrix} -0.5 & 0 & 0.5 \\ 0 & 0.5 & -0.5 \\ -0.5 & 0 & -0.5 \\ 0 & -0.5 & -0.5 \\ 0.5 & 0 & -0.5 \\ 0 & -0.5 & 0.5 \\ 0.5 & 0 & 0.5 \\ 0 & 0.5 & 0.5 \end{bmatrix} \begin{bmatrix} 252 & 84 & 0 \\ 84 & 252 & 0 \\ 0 & 0 & 84 \end{bmatrix} \\
 &\times \begin{bmatrix} -0.5 & 0 & -0.5 & 0 & 0.5 & 0 & 0.5 & 0 \\ 0 & 0.5 & 0 & -0.5 & 0 & -0.5 & 0 & 0.5 \\ 0.5 & -0.5 & -0.5 & -0.5 & -0.5 & 0.5 & 0.5 & 0.5 \end{bmatrix} \frac{1}{4} \\
 &= \begin{bmatrix} 84 & -42 & 42 & 0 & -84 & 42 & -42 & 0 \\ -42 & 84 & 0 & -42 & 42 & -84 & 0 & 42 \\ 42 & 0 & 84 & 42 & -42 & 0 & -84 & -42 \\ 0 & -42 & 42 & 84 & 0 & 42 & -42 & -84 \\ -84 & 42 & -42 & 0 & 84 & -42 & 42 & 0 \\ 42 & -84 & 0 & 42 & -42 & 84 & 0 & -42 \\ -42 & 0 & -84 & -42 & 42 & 0 & 84 & 42 \\ 0 & 42 & -42 & -84 & 0 & -42 & 42 & 84 \end{bmatrix} \frac{1}{4} \\
 &= \begin{bmatrix} 84 & -42 & 42 & 0 & -84 & 42 & -42 & 0 \\ -42 & 84 & 0 & -42 & 42 & -84 & 0 & 42 \\ 42 & 0 & 84 & 42 & -42 & 0 & -84 & -42 \\ 0 & -42 & 42 & 84 & 0 & 42 & -42 & -84 \\ -84 & 42 & -42 & 0 & 84 & -42 & 42 & 0 \\ 42 & -84 & 0 & 42 & -42 & 84 & 0 & -42 \\ -42 & 0 & -84 & -42 & 42 & 0 & 84 & 42 \\ 0 & 42 & -42 & -84 & 0 & -42 & 42 & 84 \end{bmatrix}.
 \end{aligned}$$

The equilibrium equation for this quasi-static problem is

$$\mathbf{k} \mathbf{u} = \mathbf{f}, \quad (4.98)$$

$$\begin{bmatrix} 84 & -42 & 42 & 0 & -84 & 42 & -42 & 0 \\ -42 & 84 & 0 & -42 & 42 & -84 & 0 & 42 \\ 42 & 0 & 84 & 42 & -42 & 0 & -84 & -42 \\ 0 & -42 & 42 & 84 & 0 & 42 & -42 & -84 \\ -84 & 42 & -42 & 0 & 84 & -42 & 42 & 0 \\ 42 & -84 & 0 & 42 & -42 & 84 & 0 & -42 \\ -42 & 0 & -84 & -42 & 42 & 0 & 84 & 42 \\ 0 & 42 & -42 & -84 & 0 & -42 & 42 & 84 \end{bmatrix} \begin{bmatrix} 0 \\ 0 \\ 0 \\ 0 \\ u_{x3} \\ u_{y3} \\ 0 \\ u_{y4} \end{bmatrix} = \begin{bmatrix} R_{x1} \\ R_{y1} \\ R_{x2} \\ R_{y2} \\ F \cos \frac{\pi}{4} \\ -F \cos \frac{\pi}{4} \\ R_{x4} \\ 0 \end{bmatrix}$$

so that with the boundary conditions it simplifies to

$$\begin{bmatrix} 84 & -42 & 0 \\ -42 & 84 & -42 \\ 0 & -42 & 84 \end{bmatrix} \begin{bmatrix} u_{x3} \\ u_{y3} \\ u_{y4} \end{bmatrix} = \begin{bmatrix} 10\sqrt{2}/2 \\ -10\sqrt{2}/2 \\ 0 \end{bmatrix}.$$

The solution is obtained from

$$\mathbf{u} = \mathbf{k}^{-1} \mathbf{f},$$

$$\begin{bmatrix} u_{x3} \\ u_{y3} \\ u_{y4} \end{bmatrix} = \begin{bmatrix} 0.017857 & 0.011905 & 0.005952 \\ 0.011905 & 0.023810 & 0.011905 \\ 0.005952 & 0.011905 & 0.017857 \end{bmatrix} \begin{bmatrix} 10\sqrt{2}/2 \\ -10\sqrt{2}/2 \\ 0 \end{bmatrix},$$

$$\begin{bmatrix} u_{x3} \\ u_{y3} \\ u_{y4} \end{bmatrix} = \begin{bmatrix} 0.04209 \\ -0.08418 \\ -0.04209 \end{bmatrix} \text{ mm.}$$

The reactions can be obtained from

$$\begin{bmatrix} 84 & -42 & 42 & 0 & -84 & 42 & -42 & 0 \\ -42 & 84 & 0 & -42 & 42 & -84 & 0 & 42 \\ 42 & 0 & 84 & 42 & -42 & 0 & -84 & -42 \\ 0 & -42 & 42 & 84 & 0 & 42 & -42 & -84 \\ -84 & 42 & -42 & 0 & 84 & -42 & 42 & 0 \\ 42 & -84 & 0 & 42 & -42 & 84 & 0 & -42 \\ -42 & 0 & -84 & -42 & 42 & 0 & 84 & 42 \\ 0 & 42 & -42 & -84 & 0 & -42 & 42 & 84 \end{bmatrix} \begin{bmatrix} 0 \\ 0 \\ 0 \\ 0 \\ u_{x3} \\ u_{y3} \\ 0 \\ u_{y4} \end{bmatrix} = \begin{bmatrix} R_{x1} \\ R_{y1} \\ R_{x2} \\ R_{y2} \\ F \cos \frac{\pi}{4} \\ -F \cos \frac{\pi}{4} \\ R_{x4} \\ 0 \end{bmatrix},$$

$$R_{x1} = -84u_{x3} + 42u_{y3} + 0u_{y4} = -10\sqrt{2}/2N,$$

$$R_{y1} = 42u_{x3} - 84u_{y3} + 42u_{y4} = 10\sqrt{2}/2N,$$

$$R_{x2} = -42u_{x3} + 0u_{y3} - 42u_{y4} = 0,$$

$$R_{y2} = 0u_{x3} + 42u_{y3} - 84u_{y4} = 0,$$

$$R_{x4} = 42u_{x3} + 0u_{y3} + 42u_{y4} = 0.$$

We can carry out an equilibrium check as follows:

$$\sum F_x = R_{x1} + R_{x2} + R_{x4} + \frac{10\sqrt{2}}{2} = -\frac{10\sqrt{2}}{2} + 0 + 0 + \frac{10\sqrt{2}}{2} = 0,$$

$$\sum F_y = R_{y1} + R_{y2} - \frac{F\sqrt{2}}{2} = \frac{10\sqrt{2}}{2} + 0 - \frac{10\sqrt{2}}{2} = 0.$$

The element strains at the integration point may be determined as

$$\boldsymbol{\varepsilon}(\xi, \eta) = \boldsymbol{\varepsilon}(0, 0) \approx \sum_{I=1}^{\text{NNODE}} \mathbf{B}_I(0, 0) \cdot \mathbf{u}_I$$

$$= \begin{bmatrix} -0.5 & 0 & -0.5 & 0 & 0.5 & 0 & 0.5 & 0 \\ 0 & 0.5 & 0 & -0.5 & 0 & -0.5 & 0 & 0.5 \\ 0.5 & -0.5 & -0.5 & -0.5 & -0.5 & 0.5 & 0.5 & 0.5 \end{bmatrix} \begin{bmatrix} 0 \\ 0 \\ 0 \\ 0 \\ u_{x3} \\ u_{y3} \\ 0 \\ u_{y4} \end{bmatrix}$$

$$= \begin{bmatrix} -0.5 & 0 & -0.5 & 0 & 0.5 & 0 & 0.5 & 0 \\ 0 & 0.5 & 0 & -0.5 & 0 & -0.5 & 0 & 0.5 \\ 0.5 & -0.5 & -0.5 & -0.5 & -0.5 & 0.5 & 0.5 & 0.5 \end{bmatrix} \begin{bmatrix} 0 \\ 0 \\ 0 \\ 0 \\ 0.04209 \\ -0.08418 \\ 0 \\ -0.04209 \end{bmatrix}$$

$$= \begin{bmatrix} 0.021045 \\ 0.021045 \\ -0.08418 \end{bmatrix}$$

and the stresses are given by

$$\begin{aligned} \boldsymbol{\sigma}(\xi, \eta) &= \mathbf{C}\boldsymbol{\varepsilon}(\xi, \eta) = \begin{bmatrix} 252 & 84 & 0 \\ 84 & 252 & 0 \\ 0 & 0 & 84 \end{bmatrix} \begin{bmatrix} 0.021045 \\ 0.021045 \\ -0.08418 \end{bmatrix} \\ &= \begin{bmatrix} 7.071068 \\ 7.071068 \\ -7.071068 \end{bmatrix} = \begin{bmatrix} 10\sqrt{2}/2 \\ 10\sqrt{2}/2 \\ -10\sqrt{2}/2 \end{bmatrix} \text{ N/mm}^2. \end{aligned}$$

A further check is that the internal forces at nodal points must be equal to nodal external forces (note that the reactions are external forces too):

$$\begin{aligned} \mathbf{f}^{\text{int}} &= \begin{bmatrix} f_{x1}^{\text{int}} \\ f_{y1}^{\text{int}} \\ f_{x2}^{\text{int}} \\ f_{y2}^{\text{int}} \\ f_{x3}^{\text{int}} \\ f_{y3}^{\text{int}} \\ f_{x4}^{\text{int}} \\ f_{y4}^{\text{int}} \end{bmatrix} = \int_V \mathbf{B}^T \boldsymbol{\sigma} \, dV = \int_0^1 \int_0^1 \mathbf{B}^T \boldsymbol{\sigma} \, dx \, dy \\ &= \int_{-1}^1 \int_{-1}^1 \mathbf{B}^T \boldsymbol{\sigma} \det[\mathbf{J}] \, d\xi \, d\eta = \mathbf{B}^T \boldsymbol{\sigma} \frac{1}{4} \int_{-1}^1 \int_{-1}^1 d\xi \, d\eta \\ &= \mathbf{B}^T \boldsymbol{\sigma} \frac{1}{4} = \mathbf{B}^T \boldsymbol{\sigma} = \begin{bmatrix} -0.5 & 0 & 0.5 \\ 0 & 0.5 & -0.5 \\ -0.5 & 0 & -0.5 \\ 0 & -0.5 & -0.5 \\ 0.5 & 0 & -0.5 \\ 0 & -0.5 & 0.5 \\ 0.5 & 0 & 0.5 \\ 0 & 0.5 & 0.5 \end{bmatrix} \begin{bmatrix} 10\sqrt{2}/2 \\ 10\sqrt{2}/2 \\ -10\sqrt{2}/2 \end{bmatrix} = \begin{bmatrix} -10\sqrt{2}/2 \\ 10\sqrt{2}/2 \\ 0 \\ 0 \\ 10\sqrt{2}/2 \\ -10\sqrt{2}/2 \\ 0 \\ 0 \end{bmatrix} \text{ N}. \end{aligned}$$

We need to summarize a few important points before leaving this section. In all the examples considered, we have used only one or two finite elements. This is intended

to aid in the development of understanding of the finite element method rather than to suggest that practical problems can be solved in this way. Most engineering problems require very large numbers of finite elements in order to obtain an accurate representation and solution. Naturally, the calculations are then carried out on a computer. We should also note that we have gone on to determine solutions for only quasi-static problems. This required the solution of the Equation (4.98). However, we have set up the finite element equilibrium (also often known as *momentum balance*) equations for a number of dynamic problems which we have not attempted to solve. Solution of these problems requires in general the numerical integration of the momentum balance Equation (4.85), using, for example, the explicit central difference time integration scheme, which is introduced briefly later on, or an implicit scheme. So far, in this chapter, we have been concerned with both geometrically linear and non-linear problems in which the material behaviour has always been assumed to be linear (elasticity). We shall continue by introducing incremental finite element techniques for non-linear material behaviour; that is, in particular, for plasticity.

4.4.4 Finite element formulation for plasticity

The equilibrium equations derived in (4.71)–(4.75) from virtual work are applicable in general to linear and non-linear material behaviour. In order to address a particular example, we return to the equilibrium Equation (4.69) but for simplicity, assume quasi-static conditions and so ignore inertia terms, and we consider small deformations. Using Voigt notation the equation of virtual work becomes

$$\delta W = \int_{\Omega} \delta \mathbf{D}^T \boldsymbol{\sigma} \, dV - \int_{\partial\Omega} \mathbf{t} \cdot \delta \mathbf{v} \, dA = 0.$$

With the finite element discretization as before, the equation becomes

$$\delta W = \int_{\Omega} \left(\sum_{I=1}^{\text{NNODE}} \mathbf{B}_I \, d\mathbf{v}_I \right)^T \boldsymbol{\sigma} \, dV - \int_{\partial\Omega} \mathbf{t} \cdot \left(\sum_{I=1}^{\text{NNODE}} N_I \delta \mathbf{v}_I \right) \, dA.$$

For small strain elastic–plastic material behaviour, we

$$\boldsymbol{\sigma} = \mathbf{C} \boldsymbol{\varepsilon}^e = \mathbf{C} (\boldsymbol{\varepsilon} - \boldsymbol{\varepsilon}^p)$$

so

$$\delta W = \int_{\Omega} \left(\sum_{I=1}^{\text{NNODE}} \mathbf{B}_I \delta \mathbf{v}_I \right)^T \mathbf{C} (\boldsymbol{\varepsilon} - \boldsymbol{\varepsilon}^p) \, dV - \int_{\partial\Omega} \mathbf{t} \cdot \left(\sum_{I=1}^{\text{NNODE}} N_I \delta \mathbf{v}_I \right) \, dA$$

and with the finite element discretization for the strain presented in Section 4.4.3, this becomes

$$\begin{aligned} \delta W^I = \delta \mathbf{v}_I^T & \left(\sum_{I,J=1}^{\text{NNODE}} \int_{\Omega} \mathbf{B}_I^T \mathbf{C} \mathbf{B}_J dV \right) \mathbf{u}_J \\ & - \delta \mathbf{v}_I^T \sum_{I=1}^{\text{NNODE}} \int_{\Omega} \mathbf{B}_I^T \mathbf{C} \boldsymbol{\varepsilon}^P dV - \delta \mathbf{v}_I^T \sum_{I=1}^{\text{NNODE}} \int_{\partial\Omega} N_I \mathbf{t} dA. \end{aligned}$$

As before, for an arbitrary virtual velocity, we may then write the element equilibrium equation as

$$\mathbf{k} \mathbf{u} - \mathbf{f}^P = \mathbf{f}, \tag{4.99}$$

where

$$\mathbf{f}^P = \sum_{I=1}^{\text{NNODE}} \int_{\Omega} \mathbf{B}_I^T \mathbf{C} \boldsymbol{\varepsilon}^P dV.$$

In contrast to linear elastic problems in which there exists a unique relationship between stress and elastic strain, no such uniqueness holds for plasticity problems. An incremental approach to solving (4.99) is therefore almost always necessary, and to emphasize this, the displacement, plastic strain, and external force terms are written as increments so that

$$\mathbf{k} \Delta \mathbf{u} - \Delta \mathbf{f}^P = \Delta \mathbf{f} \tag{4.100}$$

and

$$\Delta \mathbf{f}^P = \sum_{I=1}^{\text{NNODE}} \int_{\Omega} \mathbf{B}_I^T \mathbf{C} \Delta \boldsymbol{\varepsilon}^P dV. \tag{4.101}$$

Equation (4.100) may alternatively be written as

$$\mathbf{k} \Delta \mathbf{u} = \Delta \mathbf{f}', \tag{4.102}$$

where

$$\Delta \mathbf{f}' = \Delta \mathbf{f}^P + \Delta \mathbf{f}.$$

4.4.4.1 Single truss element undergoing elastic–plastic deformation. We now return to the single truss element which we examined for the case of elastic material behaviour in Section 4.4.2.1. The problem is shown in Fig. 4.10(a) and the single element discretization in 4.10(b). For this problem, the \mathbf{B} matrix, and the stiffness matrix, \mathbf{k} , remain unchanged as

$$\mathbf{B} = \frac{1}{L} [-1 \quad 1], \quad \mathbf{k} = \frac{EA}{L} \begin{bmatrix} 1 & -1 \\ -1 & 1 \end{bmatrix}$$

and we write the incremental external force vector as

$$\Delta \mathbf{f} = \begin{bmatrix} \Delta F_1 \\ \Delta P \end{bmatrix}.$$

The plasticity ‘force’ is determined from (4.101) for this element as

$$\Delta \mathbf{f}^p = \int_{\Omega} \mathbf{B}^T \mathbf{C} \Delta \boldsymbol{\varepsilon}^p dV = \int_{\xi=0}^1 \frac{1}{L} \begin{bmatrix} -1 \\ 1 \end{bmatrix} E \Delta \boldsymbol{\varepsilon}^p A \det(J) d\xi = EA \Delta \boldsymbol{\varepsilon}^p \begin{bmatrix} -1 \\ 1 \end{bmatrix}$$

so that from (4.100) the equilibrium equation becomes

$$\frac{EA}{L} \begin{bmatrix} 1 & -1 \\ -1 & 1 \end{bmatrix} \begin{bmatrix} \Delta u_1 \\ \Delta u_2 \end{bmatrix} - EA \Delta \boldsymbol{\varepsilon}^p \begin{bmatrix} -1 \\ 1 \end{bmatrix} = \begin{bmatrix} \Delta F_1 \\ \Delta P \end{bmatrix}.$$

With the boundary condition that $u_1 = 0$, this reduces to

$$\frac{EA}{L} \Delta u_2 - EA \Delta \boldsymbol{\varepsilon}^p = \Delta P.$$

Rearranging gives

$$\Delta u_2 = \frac{\Delta PL}{EA} + L \Delta \boldsymbol{\varepsilon}^p. \quad (4.103)$$

In the absence of plasticity, this just gives us an incremental form of the expression we obtained before for elasticity in Section 4.4.2.1. For the case of plasticity, however, the increment in displacement now becomes that due to the elastic deformation together with that resulting from the plastic strain, which unsurprisingly in this small strain formulation has magnitude $L \Delta \boldsymbol{\varepsilon}^p$. To demonstrate further the need for an incremental approach, let us now assign elastic linear strain hardening plasticity properties to the rod material and determine the rod extension on application of a given force, P .

In Section 2.4.2, we saw that for uniaxial linear isotropic hardening the relation between the increment in uniaxial stress and plastic strain was given by

$$\Delta \boldsymbol{\varepsilon}^p = \frac{\Delta \sigma}{h}$$

in which h is the strain hardening constant. Writing $\Delta \sigma = \Delta P/A$ gives

$$\Delta \boldsymbol{\varepsilon}^p = \frac{\Delta P}{Ah}$$

and substituting into (4.102) gives

$$\Delta u_2 = \frac{\Delta PL}{EA} + \frac{L \Delta P}{Ah} = \frac{\Delta PL}{A} \left(\frac{1}{E} + \frac{1}{h} \right). \quad (4.104)$$

Therefore, the incremental displacement for elastic and elastic–plastic conditions becomes

$$\text{Elastic : } \sigma < \sigma_y, \quad \Delta u_2 = \frac{\Delta PL}{EA}.$$

$$\text{Elastic–plastic : } \sigma \geq \sigma_y, \quad \Delta u_2 = \frac{\Delta PL}{A} \left(\frac{1}{E} + \frac{1}{h} \right).$$

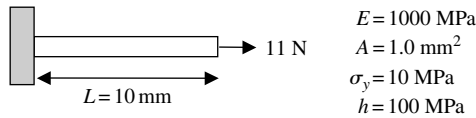


Fig. 4.18 A uniform bar under axial loading with the properties shown.

Let us analyse incrementally the problem shown in Fig. 4.18.

We will apply the load incrementally. The first load increment, however, will be chosen to cause first yield. That is, $\Delta P_1 = \sigma_y A = 10 \text{ N}$. The displacement increment is given by

$$\Delta u^{(1)} = \frac{\Delta PL}{EA} = \frac{10 \times 10}{1000 \times 1} = 0.1 \text{ mm}$$

so

$$u^{(1)} = u^{(0)} + \Delta u^{(1)} = 0 + 0.1 = 0.1 \text{ mm.}$$

Subsequent displacement increments must take account of the plasticity so that

$$\Delta u^{(2)} = \frac{\Delta PL}{EA} + \frac{L\Delta P}{Ah} = \frac{1 \times 10}{1000 \times 1} + \frac{10 \times 1}{1 \times 100} = 0.11 \text{ mm}$$

and

$$u^{(2)} = u^{(1)} + \Delta u^{(2)} = 0.1 + 0.11 = 0.21 \text{ mm.}$$

We see from Equation (4.104) that since the rate of hardening is constant (i.e. h is fixed), the displacement—load relationship becomes independent of increment size, once the material has yielded. However, were we to introduce non-linear hardening where, for example, h depends on plastic strain, Equation (4.104) shows that the displacement—load relationship then becomes dependent on the increment size.

4.5 Integration of momentum balance and equilibrium equations

4.5.1 Explicit integration using the central difference method

The finite element discretization of the momentum balance equation for a damped system can be expressed in matrix form as follows:

$$\mathbf{M}\ddot{\mathbf{u}} + \mathbf{C}\dot{\mathbf{u}} + \mathbf{F}^{\text{int}} = \mathbf{F}^{\text{ext}},$$

where \mathbf{M} is the mass matrix, \mathbf{F}^{int} the internal force vector, and \mathbf{F}^{ext} the external force vector. The integration of the equations can be carried out by means of the explicit *central difference time integration scheme*. The scheme is derived from Taylor series

expansions of the displacements, \mathbf{u} , as follows.

$$\mathbf{u}(t + \Delta t) = \mathbf{u}(t) + \dot{\mathbf{u}}(t)\Delta t + \ddot{\mathbf{u}}(t)\frac{\Delta t^2}{2} + \dots$$

$$\mathbf{u}(t - \Delta t) = \mathbf{u}(t) - \dot{\mathbf{u}}(t)\Delta t + \ddot{\mathbf{u}}(t)\frac{\Delta t^2}{2} - \dots$$

The central difference approximations are obtained taking the difference of the above expressions to give the velocity

$$\dot{\mathbf{u}}_N = \frac{\mathbf{u}_{N+1} - \mathbf{u}_{N-1}}{2\Delta t}$$

and by summing the expressions for the accelerations

$$\ddot{\mathbf{u}}_N = \frac{\mathbf{u}_{N+1} - 2\mathbf{u}_N + \mathbf{u}_{N-1}}{(\Delta t)^2},$$

where

$$\mathbf{u}_N = \mathbf{u}(t_N).$$

Assuming that the acceleration is constant between t_N and t_{N+1} the central difference approximations can be rearranged to give the following second-order integration scheme

$$\mathbf{u}_{N+1} = \mathbf{u}_N + \dot{\mathbf{u}}_N\Delta t + \frac{1}{2}\ddot{\mathbf{u}}_N(\Delta t)^2,$$

$$\dot{\mathbf{u}}_{N+1} = \dot{\mathbf{u}}_N + \frac{1}{2}(\ddot{\mathbf{u}}_N + \ddot{\mathbf{u}}_{N+1})\Delta t.$$

These are more commonly rewritten by defining the intermediate velocities based on the assumption that the acceleration is constant between t_0 and $t_{0+1/2}$ as well as between $t_{N-1/2}$ and $t_{N+1/2}$ so that

$$\dot{\mathbf{u}}_{1/2} = \dot{\mathbf{u}}_0 + \frac{1}{2}\ddot{\mathbf{u}}_0\Delta t$$

to give the *leap frog* explicit method

$$\dot{\mathbf{u}}_{N+1/2} = \dot{\mathbf{u}}_{N-1/2} + \ddot{\mathbf{u}}_N\Delta t,$$

$$\mathbf{u}_{N+1} = \mathbf{u}_N + \dot{\mathbf{u}}_{N+1/2}\Delta t.$$

The central difference method can be applied with a varying time increment (which is particularly important if the response of the continuum is non-linear), as illustrated in Fig. 4.19.

Let Δt_{N+1} be the time increment between t_N and t_{N+1} with $\mathbf{u}_N = \mathbf{u}(t_N)$ as illustrated in Fig. 4.19. The mid-step velocities are defined by

$$\dot{\mathbf{u}}_{N-1/2} = \dot{\mathbf{u}}(t_{N-1/2}), \quad \dot{\mathbf{u}}_{N+1/2} = \dot{\mathbf{u}}(t_{N+1/2}),$$

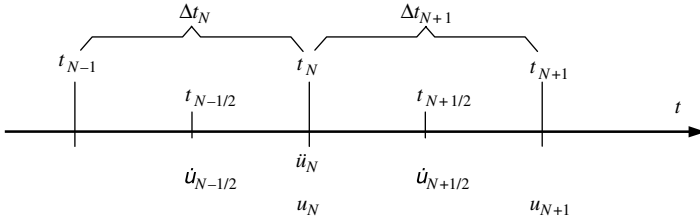


Fig. 4.19 Central difference integration scheme.

where

$$t_{N-1/2} = \frac{1}{2}(t_{N-1} + t_N), \quad t_{N+1/2} = \frac{1}{2}(t_N + t_{N+1}).$$

The central difference formula for velocity is

$$\dot{\mathbf{u}}_{N+1/2} = \frac{\mathbf{u}_{N+1} - \mathbf{u}_N}{\Delta t_{N+1}},$$

while the central difference formula for acceleration is

$$\ddot{\mathbf{u}}_N = \frac{\dot{\mathbf{u}}_{N+1/2} - \dot{\mathbf{u}}_{N-1/2}}{\Delta t_{N+1/2}},$$

where

$$\Delta t_{N+1/2} = \frac{1}{2}(\Delta t_N + \Delta t_{N+1}).$$

The discretization of the momentum balance equation for an undamped system can be obtained by substituting the acceleration term with its finite difference approximation as follows:

$$\mathbf{M} \frac{\dot{\mathbf{u}}_{N+1/2} - \dot{\mathbf{u}}_{N-1/2}}{\Delta t_{N+1/2}} + \mathbf{F}_N^{\text{int}} = \mathbf{F}_N^{\text{ext}},$$

which yields

$$\dot{\mathbf{u}}_{N+1/2} = \mathbf{M}^{-1}(\mathbf{F}^{\text{ext}} - \mathbf{F}^{\text{int}})\Delta t_{N+1/2} + \dot{\mathbf{u}}_{N-1/2}$$

and

$$\mathbf{u}_{N+1} = \mathbf{u}_N + \dot{\mathbf{u}}_{N+1/2}\Delta t_{N+1}.$$

Subsequently, the internal and external force vectors can be calculated as

$$\mathbf{F}_{N+1}^{\text{int}} = \mathbf{F}^{\text{int}}(\mathbf{u}_{N+1}), \quad \mathbf{F}_{N+1}^{\text{ext}} = \mathbf{F}^{\text{ext}}(\mathbf{u}_{N+1}),$$

which completes the N th time step. Furthermore, if the mass matrix is diagonalized the system of differential equations uncouples and can be solved independently for each degree of freedom (see, e.g. Newland).

4.5.1.1 Stability of the explicit time stepping scheme. The solution of a SDOF equilibrium equation

$$\ddot{u} + \omega^2 u = 0$$

can be obtained using the central difference time stepping scheme as follows

$$\ddot{u}_N = \frac{u_{N+1} - 2u_N + u_{N-1}}{(\Delta t)^2} = -\omega^2 u_N$$

giving the difference equation

$$u_{N+1} - (2 - \omega^2(\Delta t)^2)u_N + u_{N-1} = 0.$$

Trying solutions $u_N = A^n$ where A is the amplification factor gives

$$A^2 - (2 - \omega^2(\Delta t)^2)A + 1 = 0.$$

The roots of this polynomial are

$$A = \left(1 - \frac{\omega^2(\Delta t)^2}{2}\right) \pm \sqrt{\left(1 - \frac{\omega^2(\Delta t)^2}{2}\right)^2 - 1}.$$

For stability

$$|A| \leq 1,$$

which gives the stability condition as

$$\Delta t \leq \frac{2}{\omega}.$$

For a general multidegree of freedom system, the stability condition becomes

$$\Delta t \leq \frac{2}{\omega_{\max}},$$

where

$$\omega_{\max} = \max_i \{\omega_i\}$$

is the element maximum eigenvalue. A conservative estimate of the stable time increment is given by the following minimum taken over all the elements

$$\Delta t \leq \min \frac{L_c}{c_d},$$

where L_c is the characteristic element length and c_d is the current effective dilatational wave speed of the material.

4.5.2 Introduction to implicit integration

Implicit integration schemes are often preferred to their explicit counterparts since they involve the determination of a residual force at each step and iteration within the step to minimize the residual force to within a specified tolerance. We briefly introduce three techniques; the tangential stiffness method, the initial tangential stiffness method, and the Newton–Raphson method. We confine ourselves here to quasi-static problems so assume inertia effects are negligible.

4.5.2.1 Tangential stiffness method. The discretized static equilibrium equation given in (4.102), for example, will not generally be satisfied unless a convergence occurs which can be expressed in terms of residual forces as follows

$$\mathbf{k}(\mathbf{u})\mathbf{u} - \mathbf{f} = \Psi \neq 0.$$

The iteration starts from an initially guessed solution \mathbf{u}_0 and the corresponding *tangential stiffness matrix* $\mathbf{k}(\mathbf{u}_0)$. The residual forces are calculated from

$$\Psi^0 = \mathbf{k}(\mathbf{u}_0)\mathbf{u}_0 - \mathbf{f}.$$

The correction $\Delta\mathbf{u}$ is calculated as follows:

$$\Delta\mathbf{u}_n = [\mathbf{K}(\mathbf{u}_n)]^{-1}\Psi^n \quad (4.105)$$

and an improved solution is then obtained as follows:

$$\mathbf{u}_{n+1} = \mathbf{u}_n + \Delta\mathbf{u}_n.$$

The process continues until the residual forces Ψ^n are smaller than a specified tolerance.

4.5.2.2 Initial tangential stiffness method. The initial tangential stiffness method differs from the previous method only in that the correction to the displacement, given in Equation (4.105), is now calculated always based upon the initial tangential stiffness matrix so that

$$\Delta\mathbf{u}_n = [\mathbf{k}(\mathbf{u}_0)]^{-1}\Psi^n$$

and as before, the improved solution is obtained as

$$\mathbf{u}_{n+1} = \mathbf{u}_n + \Delta\mathbf{u}_n$$

and the process continues until the residual forces Ψ^n are smaller than a specified tolerance.

4.5.2.3 Newton–Raphson method. As in the previous methods, the residual force Ψ is determined from

$$\Psi = \mathbf{k}(\mathbf{u})\mathbf{u} - \mathbf{f} = 0. \quad (4.106)$$

Using a Taylor expansion, Ψ may be approximated by

$$\Psi(\mathbf{u}) + \frac{\partial \Psi(\mathbf{u})}{\partial \mathbf{u}} \Delta \mathbf{u} + O(\Delta \mathbf{u}^2) = 0. \quad (4.107)$$

The matrix $\mathbf{J} = \partial \Psi / \partial \mathbf{u}$ is called the Jacobian (which has nothing to do with the Jacobian introduced above for the mapping of spatial to local element configurations), or effective tangent stiffness, and from (4.106) it can be seen that this comprises a term corresponding to the internal forces, termed the *tangent stiffness matrix*, and a further term corresponding to the ‘external’ forces, called the *load stiffness matrix*. Equation (4.107) provides a linearization of (4.106) and may be written as

$$\Psi + \mathbf{J} \Delta \mathbf{u} = 0$$

so that

$$\mathbf{J}(\mathbf{u}_n) \Delta \mathbf{u}_n = -\Psi(\mathbf{u}_n)$$

and the displacement is updated by

$$\mathbf{u}_{n+1} = \mathbf{u}_n + \Delta \mathbf{u}_n.$$

The iteration continues until the tolerance limit on residual force is achieved.

The two schemes introduced above, namely explicit and implicit integration, may be used for the integration of the momentum balance, or equilibrium, finite element equations. In implementing plasticity models into finite element formulations, it is often necessary, in addition, to integrate a set of constitutive equations (e.g. to give the plastic strain increment). For this additional integration, it is also possible to employ either implicit or explicit integration methods. In the overall solution process, therefore, there are several possible combinations of implicit and explicit integration. Finite element methods which employ implicit schemes for the integration of the momentum balance, or equilibrium equations, regardless of whether the constitutive equations are integrated using implicit or explicit integration, are referred to as *implicit* finite element methods. Similarly, finite element methods which employ explicit schemes for the integration of the momentum balance, or equilibrium equations, are called *explicit* finite element methods. Both implicit and explicit formulations are available in ABAQUS. It can be seen that the implicit scheme offers the more robust overall approach, because of the iteration necessary in order to achieve convergence. Explicit schemes, however, can often produce more rapid solutions, and are more appropriate for dynamic analyses. Care has to be taken, however, in choosing time step size and ensuring the calculated solution does not drift away from the true solution. We shall examine this further in the context of integration of constitutive equations in Chapter 5.

Further reading

- Bathe, K.-J. (1996). *Finite Element Procedures*. Prentice Hall, New Jersey, revised edition.
- Belytschko, T., Liu, K.W., and Moran, B. (2000). *Non-linear Finite Element Analysis for Continua and Structures*. John Wiley & Sons, New York.
- Bonet, J. and Wood, R.D. (1997). *Non-linear Continuum Mechanics for Finite Element Analysis*. Cambridge University Press.
- Hinton, E. and Owen, D.R.J. (1979). *An Introduction to Finite Element Computations*. Pineridge Press, Swansea.
- Newland, D.E. (1989). *Mechanical Vibration Analysis and Computation*. Longman Scientific and Technical, John Wiley and Sons, New York.
- Owen, D.R.J. and Hinton, E. (1980). *Finite Elements in Plasticity: Theory and Practice*. Pineridge Press, Swansea.
- Timoshenko, S. and Goodier, J.N. (1983). *Theory of Elasticity*. McGraw-Hill, New York.
- Zienkiewicz, O.C. and Taylor, R.L. (1989). *The Finite Element Method*. McGraw-Hill, London, 4th edition.

5. Implicit and explicit integration of von Mises plasticity

5.1 Introduction

In this chapter, we shall return to the constitutive equations for plasticity introduced in Chapter 2 and see how they may be integrated and how the Jacobian or tangent stiffness may be obtained from them. We shall explore both implicit and explicit schemes for the integration of the constitutive equations. To start, we shall consider small strain, time-independent, linear isotropic hardening plasticity before looking at kinematic hardening and viscoplasticity. First, we return to the determination of the plastic multiplier.

5.2 Implicit and explicit integration of constitutive equations

We saw from Chapter 2 that the yield function for isotropic hardening can be written

$$f = \sigma_e - r - \sigma_y = \left(\frac{3}{2} \boldsymbol{\sigma}' : \boldsymbol{\sigma}' \right)^{1/2} - r - \sigma_y = 0 \quad (5.1)$$

and that the plastic multiplier, in principal stress space is given by

$$d\lambda = \frac{(\partial f / \partial \boldsymbol{\sigma}) \cdot \mathbf{C} \, d\boldsymbol{\epsilon}}{(\partial f / \partial \boldsymbol{\sigma}) \cdot \mathbf{C} (\partial f / \partial \boldsymbol{\sigma}) - (\partial f / \partial p) [(2/3)(\partial f / \partial \boldsymbol{\sigma}) \cdot (\partial f / \partial \boldsymbol{\sigma})]^{1/2}}, \quad (5.2)$$

where all terms are written in Voigt notation. Before proceeding, let us redetermine the plastic multiplier more generally, without the constraint of working in principal stress space. The consistency condition is written in terms of the stress tensor

$$df(\boldsymbol{\sigma}, p) = \frac{\partial f}{\partial \boldsymbol{\sigma}} : d\boldsymbol{\sigma} + \frac{\partial f}{\partial p} dp = 0.$$

If we write the tensor normal, \mathbf{n} , for a von Mises material

$$\mathbf{n} = \frac{\partial f}{\partial \boldsymbol{\sigma}} = \frac{3}{2} \frac{\boldsymbol{\sigma}'}{\sigma_e},$$

144 Implicit and explicit integration

the consistency condition becomes

$$df(\boldsymbol{\sigma}, p) = \mathbf{n} : d\boldsymbol{\sigma} + \frac{\partial f}{\partial p} dp = 0,$$

where without loss of generality, we assume out of plane shears are zero, so

$$\mathbf{n} = \begin{bmatrix} n_{11} & n_{12} & 0 \\ n_{12} & n_{22} & 0 \\ 0 & 0 & n_{33} \end{bmatrix}.$$

Let us also write, in Voigt notation, the vector normal, \mathbf{n} ,

$$\mathbf{n} = \begin{bmatrix} n_{11} \\ n_{22} \\ n_{33} \\ 2n_{12} \end{bmatrix}.$$

We can then see that

$$\mathbf{n} : d\boldsymbol{\sigma} = \begin{bmatrix} n_{11} & n_{12} & 0 \\ n_{12} & n_{22} & 0 \\ 0 & 0 & n_{33} \end{bmatrix} : \begin{bmatrix} d\sigma_{11} & d\sigma_{12} & 0 \\ d\sigma_{12} & d\sigma_{22} & 0 \\ 0 & 0 & d\sigma_{33} \end{bmatrix} = \begin{bmatrix} n_{11} \\ n_{22} \\ n_{33} \\ 2n_{12} \end{bmatrix} \cdot \begin{bmatrix} d\sigma_{11} \\ d\sigma_{22} \\ d\sigma_{33} \\ d\sigma_{12} \end{bmatrix} \equiv \mathbf{n} \cdot d\boldsymbol{\sigma}$$

so that, provided the normal vector, \mathbf{n} , in Voigt notation contains twice the tensorial normal shear terms, then

$$\mathbf{n} : d\boldsymbol{\sigma} \equiv \mathbf{n} \cdot d\boldsymbol{\sigma}$$

and the consistency condition becomes

$$df(\boldsymbol{\sigma}, p) = \mathbf{n} \cdot d\boldsymbol{\sigma} + \frac{\partial f}{\partial p} dp = 0.$$

We may now determine the plastic multiplier with Hooke's law written in Voigt notation, as before

$$d\boldsymbol{\sigma} = \mathbf{C}(d\boldsymbol{\varepsilon} - d\boldsymbol{\varepsilon}^P).$$

The increment in tensorial plastic strain is obtained from the normality hypothesis,

$$d\boldsymbol{\varepsilon}^P = d\lambda \frac{\partial f}{\partial \boldsymbol{\sigma}} = d\lambda \mathbf{n},$$

which we may write in Voigt notation as

$$d\boldsymbol{\varepsilon}^P = d\lambda \mathbf{n}$$

remembering that the shear strain terms in the Voigt strain vector are *engineering shears*; that is, twice the tensorial shears. Hooke's law then becomes

$$d\boldsymbol{\sigma} = \mathbf{C}(d\boldsymbol{\varepsilon} - d\lambda \mathbf{n})$$

and combining with the consistency condition, in which, for a von Mises material, $dp = d\lambda$, we obtain

$$\mathbf{n} \cdot \mathbf{C}(\mathbf{d}\boldsymbol{\varepsilon} - d\lambda\mathbf{n}) + \frac{\partial f}{\partial p} d\lambda = 0$$

so that the plastic multiplier is given by

$$d\lambda = \frac{\mathbf{n} \cdot \mathbf{C} \mathbf{d}\boldsymbol{\varepsilon}}{\mathbf{n} \cdot \mathbf{C}\mathbf{n} - (\partial f/\partial p)}.$$

For linear isotropic hardening, $r = hp$ so that $\partial f/\partial p = -\partial r/\partial p = -h$ and

$$d\lambda = \frac{\mathbf{n} \cdot \mathbf{C} \mathbf{d}\boldsymbol{\varepsilon}}{\mathbf{n} \cdot \mathbf{C}\mathbf{n} + h}. \quad (5.3)$$

Finally, the stress increment is given by

$$d\boldsymbol{\sigma} = \mathbf{C} \mathbf{d}\boldsymbol{\varepsilon}^e = \mathbf{C}(\mathbf{d}\boldsymbol{\varepsilon} - d\boldsymbol{\varepsilon}^p) = \mathbf{C}(\mathbf{d}\boldsymbol{\varepsilon} - d\lambda\mathbf{n}). \quad (5.4)$$

With knowledge of the total strain increment, $\mathbf{d}\boldsymbol{\varepsilon}$, together with the stress, $\boldsymbol{\sigma}$, Equation (5.3) allows the plastic multiplier to be determined so that the stress increment can be obtained from (5.4). The updated stress, $\boldsymbol{\sigma} + d\boldsymbol{\sigma}$ may then be obtained. This is called an *explicit integration* process. If we denote all quantities at time t with subscript t , and those at the next increment forward in time, $t + \Delta t$, in a similar way, then we may write

$$\begin{aligned} d\lambda_t &= \frac{\mathbf{n}_t \cdot \mathbf{C} \mathbf{d}\boldsymbol{\varepsilon}_t}{\mathbf{n}_t \cdot \mathbf{C}\mathbf{n}_t + h}, \\ d\boldsymbol{\sigma}_t &= \mathbf{C}(\mathbf{d}\boldsymbol{\varepsilon}_t - d\lambda_t\mathbf{n}_t), \\ dr &= h dp = h d\lambda_t. \end{aligned} \quad (5.5)$$

The integration to obtain all quantities at the end of the time step, Δt , may then be written as

$$\begin{aligned} \boldsymbol{\sigma}_{t+\Delta t} &= \boldsymbol{\sigma}_t + d\boldsymbol{\sigma}_t, \\ \boldsymbol{\varepsilon}_{t+\Delta t}^p &= \boldsymbol{\varepsilon}_t^p + d\boldsymbol{\varepsilon}_t^p, \\ r_{t+\Delta t} &= r_t + dr_t. \end{aligned} \quad (5.6)$$

This is called a *first-order forward Euler* explicit integration scheme. Its advantage is its simplicity and it is straightforward to implement as we shall see later. However, there are a number of disadvantages which need to be considered. First, because it is an explicit scheme, it is *conditionally stable*; that is, it may become unstable. Second, the accuracy of the integration depends, of course, on the time step size, Δt , chosen. Great care is therefore required in ensuring that the time step does not become too large such that erroneous results are obtained. Third, and perhaps most importantly,

the plastic multiplier given in Equation (5.5) was obtained to ensure that at time, t , the yield condition in (5.1) is satisfied. However, the forward integration process does not ensure that the yield condition is also satisfied at time $t + \Delta t$, and as a result, it is possible for the solution, over many time steps, to drift away from the yield surface. This is overcome by means of implicit integration of the equations which has the additional advantage of being *unconditionally stable*. The accuracy remains dependent, however, on the time step size. We introduce an implicit scheme, known as the *radial return method* for von Mises plasticity, in Section 5.2.1.

5.2.1 Implicit integration: the radial return method

Figure 5.1(a) shows a von Mises yield surface with a schematic representation of the explicit integration method described above. A step forward in time takes the updated stresses outside of the yield surface. Figure 5.1(b) shows a representation of an implicit scheme. A trial stress increment is chosen which again takes the updated stresses, $\sigma_{t+\Delta t}^{\text{tr}}$, outside of the yield surface. The stress is then updated with a *plastic correction* to bring it back onto the yield surface at time $t + \Delta t$. In deviatoric stress space, the plane stress von Mises ellipse becomes a circle, and the plastic correction term is always directed towards the centre of the yield surface (because of the normality condition). The technique has therefore come to be known as the *radial return method*.

In what follows, we shall take all quantities to be those at the end of a time step, $t + \Delta t$, unless specifically stated. So, the stress at $t + \Delta t$ is just σ and that at the beginning of the time step, at time t , is σ_t .

We may write Hooke's law in multiaxial form in terms of stress and strain tensors as

$$\sigma = 2G\epsilon^e + \lambda \text{Tr}(\epsilon^e)I.$$

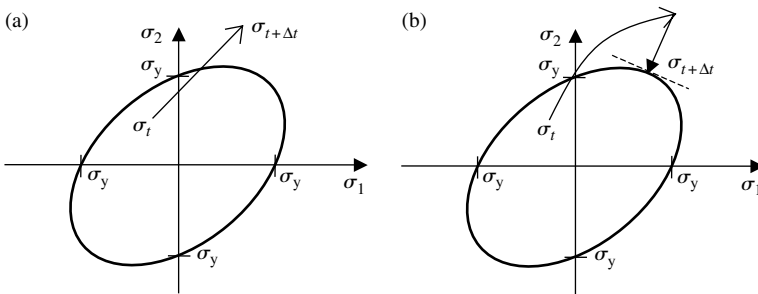


Fig. 5.1 Schematic representations of (a) explicit integration and (b) implicit integration, using the radial return method, of von Mises plasticity equations.

The elastic strain at the end of the time step may be written as

$$\boldsymbol{\varepsilon}^e = \boldsymbol{\varepsilon}_t^e + \Delta \boldsymbol{\varepsilon}^e = \boldsymbol{\varepsilon}_t^e + \Delta \boldsymbol{\varepsilon} - \Delta \boldsymbol{\varepsilon}^p$$

so that

$$\boldsymbol{\sigma} = 2G(\boldsymbol{\varepsilon}_t^e + \Delta \boldsymbol{\varepsilon} - \Delta \boldsymbol{\varepsilon}^p) + \lambda \text{Tr}(\boldsymbol{\varepsilon}_t^e + \Delta \boldsymbol{\varepsilon} - \Delta \boldsymbol{\varepsilon}^p) \mathbf{I}$$

and so

$$\boldsymbol{\sigma} = \underbrace{2G(\boldsymbol{\varepsilon}_t^e + \Delta \boldsymbol{\varepsilon}) + \lambda \text{Tr}(\boldsymbol{\varepsilon}_t^e + \Delta \boldsymbol{\varepsilon}) \mathbf{I}}_{\text{Elastic predictor}} - \underbrace{2G\Delta \boldsymbol{\varepsilon}^p}_{\text{Plastic corrector}} \quad (5.7)$$

since

$$\text{Tr}(\Delta \boldsymbol{\varepsilon}^p) = 0.$$

The elastic predictor, or trial stress, is denoted by

$$\boldsymbol{\sigma}^{\text{tr}} = 2G(\boldsymbol{\varepsilon}_t^e + \Delta \boldsymbol{\varepsilon}) + \lambda \text{Tr}(\boldsymbol{\varepsilon}_t^e + \Delta \boldsymbol{\varepsilon}) \mathbf{I} \quad (5.8)$$

so that from (5.7),

$$\boldsymbol{\sigma} = \boldsymbol{\sigma}^{\text{tr}} - 2G\Delta \boldsymbol{\varepsilon}^p = \boldsymbol{\sigma}^{\text{tr}} - 2G\Delta p \mathbf{n}, \quad (5.9)$$

which we may write as

$$\boldsymbol{\sigma} = \boldsymbol{\sigma}^{\text{tr}} - 2G\Delta p \frac{3}{2} \frac{\boldsymbol{\sigma}'}{\sigma_e}. \quad (5.10)$$

The stress may be expressed in terms of its deviatoric and mean as

$$\boldsymbol{\sigma} = \boldsymbol{\sigma}' + \frac{1}{3}(\boldsymbol{\sigma} : \mathbf{I}) \mathbf{I} \quad (5.11)$$

so that with (5.10) we obtain

$$\boldsymbol{\sigma}' + \frac{1}{3}(\boldsymbol{\sigma} : \mathbf{I}) \mathbf{I} = \boldsymbol{\sigma}^{\text{tr}} - 3G\Delta p \frac{\boldsymbol{\sigma}'}{\sigma_e} \quad (5.12)$$

and rearranging gives

$$\left(1 + 3G \frac{\Delta p}{\sigma_e}\right) \boldsymbol{\sigma}' = \boldsymbol{\sigma}^{\text{tr}} - \frac{1}{3}(\boldsymbol{\sigma} : \mathbf{I}) \mathbf{I}. \quad (5.13)$$

With some algebra, using Equation (5.8), we show that $\boldsymbol{\sigma}^{\text{tr}} - \frac{1}{3}(\boldsymbol{\sigma} : \mathbf{I}) \mathbf{I}$ is just the deviatoric of the trial stress, $\boldsymbol{\sigma}^{\text{tr}'}$ as follows, where K is the elastic bulk modulus.

$$\begin{aligned} \boldsymbol{\sigma}^{\text{tr}} - \frac{1}{3}(\boldsymbol{\sigma} : \mathbf{I}) \mathbf{I} &= 2G(\boldsymbol{\varepsilon}_t^e + \Delta \boldsymbol{\varepsilon}) + \lambda \mathbf{I}(\boldsymbol{\varepsilon}_t^e + \Delta \boldsymbol{\varepsilon}) : \mathbf{I} - K \boldsymbol{\varepsilon}^e : \mathbf{II} \\ &= 2G(\boldsymbol{\varepsilon}_t^e + \Delta \boldsymbol{\varepsilon}) + \lambda \mathbf{I}(\boldsymbol{\varepsilon}_t^e + \Delta \boldsymbol{\varepsilon}) : \mathbf{I} - K(\boldsymbol{\varepsilon}_t^e + \Delta \boldsymbol{\varepsilon} - \Delta \boldsymbol{\varepsilon}^p) : \mathbf{II} \\ &= 2G(\boldsymbol{\varepsilon}_t^e + \Delta \boldsymbol{\varepsilon}) + \lambda \mathbf{I}(\boldsymbol{\varepsilon}_t^e + \Delta \boldsymbol{\varepsilon}) : \mathbf{I} - K \mathbf{I}(\boldsymbol{\varepsilon}_t^e + \Delta \boldsymbol{\varepsilon}) : \mathbf{I} \\ &= 2G(\boldsymbol{\varepsilon}_t^e + \Delta \boldsymbol{\varepsilon}) + (\lambda - K) \mathbf{I}(\boldsymbol{\varepsilon}_t^e + \Delta \boldsymbol{\varepsilon}) : \mathbf{I} \equiv \boldsymbol{\sigma}^{\text{tr}'}. \end{aligned}$$

148 Implicit and explicit integration

We therefore obtain

$$\left(1 + 3G \frac{\Delta p}{\sigma_e}\right) \boldsymbol{\sigma}' = \boldsymbol{\sigma}^{\text{tr}'}. \quad (5.14)$$

If we take the contracted tensor product of each side of this with itself, we obtain

$$\left(1 + 3G \frac{\Delta p}{\sigma_e}\right)^2 \boldsymbol{\sigma}' : \boldsymbol{\sigma}' = \boldsymbol{\sigma}^{\text{tr}'} : \boldsymbol{\sigma}^{\text{tr}'}$$

or

$$\left(1 + 3G \frac{\Delta p}{\sigma_e}\right) \sigma_e = \left(\frac{3}{2} \boldsymbol{\sigma}^{\text{tr}'} : \boldsymbol{\sigma}^{\text{tr}'}\right)^{1/2} \equiv \sigma_e^{\text{tr}}. \quad (5.15)$$

This gives, finally,

$$\sigma_e + 3G \Delta p = \sigma_e^{\text{tr}}. \quad (5.16)$$

The multiaxial yield condition is

$$f = \sigma_e - r - \sigma_y = \sigma_e^{\text{tr}} - 3G \Delta p - r - \sigma_y = 0. \quad (5.17)$$

This is generally a non-linear equation in Δp which may be solved using Newton's method. We write

$$f + \frac{\partial f}{\partial \Delta p} d\Delta p + \dots = 0. \quad (5.18)$$

For linear hardening, $r = hp$ so that

$$\frac{\partial r}{\partial \Delta p} = \frac{\partial r}{\partial p} = h. \quad (5.19)$$

Substituting (5.17) into (5.18), using (5.19) therefore gives

$$\sigma_e^{\text{tr}} - 3G \Delta p - r - \sigma_y + (-3G - h) d\Delta p = 0.$$

Rearranging gives

$$d\Delta p = \frac{\sigma_e^{\text{tr}} - 3G \Delta p - r - \sigma_y}{3G + h}.$$

We may write the integration in iterative form then, as

$$\begin{aligned} r^{(k)} &= r_t + h \Delta p^{(k)}, \\ d\Delta p &= \frac{\sigma_e^{\text{tr}} - 3G \Delta p^{(k)} - r^{(k)} - \sigma_y}{3G + h}, \\ \Delta p^{(k+1)} &= \Delta p^{(k)} + d\Delta p. \end{aligned} \quad (5.20)$$

The effective stress may then be determined from (5.16); the deviatoric stress tensor from (5.14), so that the plastic strain tensor increment is

$$\Delta \boldsymbol{\epsilon}^p = \frac{3}{2} \Delta p \frac{\boldsymbol{\sigma}'}{\sigma_e} \equiv \frac{3}{2} \Delta p \frac{\boldsymbol{\sigma}^{\text{tr}'}}{\sigma_e^{\text{tr}}}$$

and the elastic increment

$$\Delta \boldsymbol{\varepsilon}^e = \Delta \boldsymbol{\varepsilon} - \Delta \boldsymbol{\varepsilon}^p$$

and the stress increment is given by

$$\Delta \boldsymbol{\sigma} = 2G \Delta \boldsymbol{\varepsilon}^e + \lambda I \Delta \boldsymbol{\varepsilon}^e : I.$$

We have now introduced both explicit and implicit integration of the plasticity constitutive equations. It is important to note that in the implicit scheme, all quantities are written at the end of the time increment. This ensures that the yield condition, given in Equation (5.17), is satisfied at the end of the time increment, therefore avoiding ‘drift’ from the yield surface which can occur in the explicit scheme. The implicit scheme, because it enables significantly larger time increments to be used, generally leads to much more rapid solutions.

In an implementation within implicit finite element code, we saw in Section 4.5.2.3 that the implicit integration of the momentum balance or equilibrium equations requires the determination of the Jacobian that comprises both the tangent stiffness matrix and the load stiffness matrix. The tangent stiffness matrix depends very much on the material behaviour, and hence on the constitutive equations. In the implementation of a plasticity model into implicit finite element code, it is therefore necessary to provide the material tangent stiffness matrix in addition to the integration of the plasticity constitutive equations. In explicit finite element code, however, which does not depend upon knowledge of the Jacobian, the tangent stiffness matrix is not required. The determination of the material Jacobian for implicit finite element code is very much bound up with the integration of the constitutive equations used. Typically, in implementing a plasticity model into commercial codes such as ABAQUS explicit or LSDyna (which is an explicit code), for example, we need to provide a subroutine which contains the integration of the plasticity constitutive equations (whether implicit or explicit). For implementations into implicit code, such as ABAQUS standard, we need to provide a subroutine which contains both the integration of the plasticity constitutive equations (whether implicit or explicit) together with the material Jacobian or tangent stiffness matrix. It is useful to note from Section 4.5.2.3 that the Jacobian is required in the iterative procedure in minimizing the force residual. If convergence occurs after a given number of iterations, the Jacobian does not influence the accuracy of the solution, but the rate at which convergence is achieved. It is for this reason that often approximate Jacobians are used (e.g. in the initial tangent stiffness method in Section 4.5.2.2). A further reason is that depending on the complexity of the plasticity model, the material Jacobian may not be derivable in analytical terms so that a numerical, approximate implementation has to be developed. *Perturbation methods* can allow the accurate numerical determination of the Jacobian. In the following section, we shall address first, the material Jacobian for an elastic material, and

then that for the time-independent linear strain isotropic hardening plasticity model for which the implicit integration scheme was presented in this section.

5.3 Material Jacobian

5.3.1 Isotropic elasticity

Hooke's law may be written incrementally as

$$\Delta\sigma = 2G\Delta\epsilon^e + \lambda I\Delta\epsilon^e : I, \tag{5.21}$$

which may be written more succinctly as

$$\Delta\sigma = (2GI + \lambda II) : \Delta\epsilon^e$$

in which I is the fourth-order identity tensor with the properties $I : I = I : I = I$ and $I : \Delta\epsilon = \Delta\epsilon : I = \Delta\epsilon$. We will define the material Jacobian here in the way it is required in the ABAQUS finite element code as $\partial\Delta\sigma/\partial\Delta\epsilon$ where

$$d\Delta\sigma = \frac{\partial\Delta\sigma}{\partial\Delta\epsilon} d\Delta\epsilon$$

in which the shear strains are taken to be engineering shears. For example,

$$\frac{\partial\Delta\sigma_{11}}{\partial\Delta\gamma_{12}} = \frac{\partial\Delta\sigma_{11}}{\partial\Delta\epsilon_{12}} \frac{\partial\Delta\epsilon_{12}}{\partial\Delta\gamma_{12}} = \frac{1}{2} \frac{\partial\Delta\sigma_{11}}{\partial\Delta\epsilon_{12}},$$

where $\partial\Delta\sigma_{11}/\partial\Delta\epsilon_{12}$ is obtained from Equation (5.21). The material Jacobian becomes, therefore, for conditions of plane strain or axial symmetry ($\Delta\gamma_{13} = \Delta\gamma_{23} = 0$),

$$\frac{\partial\Delta\sigma}{\partial\Delta\epsilon} = \begin{pmatrix} \frac{\partial\Delta\sigma_{11}}{\partial\Delta\epsilon_{11}} & \frac{\partial\Delta\sigma_{11}}{\partial\Delta\epsilon_{22}} & \frac{\partial\Delta\sigma_{11}}{\partial\Delta\epsilon_{33}} & \frac{\partial\Delta\sigma_{11}}{\partial\Delta\gamma_{12}} \\ \frac{\partial\Delta\sigma_{22}}{\partial\Delta\epsilon_{11}} & \frac{\partial\Delta\sigma_{22}}{\partial\Delta\epsilon_{22}} & \frac{\partial\Delta\sigma_{22}}{\partial\Delta\epsilon_{33}} & \frac{\partial\Delta\sigma_{22}}{\partial\Delta\gamma_{12}} \\ \frac{\partial\Delta\sigma_{33}}{\partial\Delta\epsilon_{11}} & \frac{\partial\Delta\sigma_{33}}{\partial\Delta\epsilon_{22}} & \frac{\partial\Delta\sigma_{33}}{\partial\Delta\epsilon_{33}} & \frac{\partial\Delta\sigma_{33}}{\partial\Delta\gamma_{12}} \\ \frac{\partial\Delta\sigma_{12}}{\partial\Delta\epsilon_{11}} & \frac{\partial\Delta\sigma_{12}}{\partial\Delta\epsilon_{22}} & \frac{\partial\Delta\sigma_{12}}{\partial\Delta\epsilon_{33}} & \frac{\partial\Delta\sigma_{12}}{\partial\Delta\gamma_{12}} \end{pmatrix} = \begin{pmatrix} 2G + \lambda & \lambda & \lambda & 0 \\ \lambda & 2G + \lambda & \lambda & 0 \\ \lambda & \lambda & 2G + \lambda & 0 \\ 0 & 0 & 0 & \frac{1}{2}2G \end{pmatrix}.$$

Note that in general, $\partial\Delta\sigma/\partial\Delta\epsilon$ and $\partial\sigma/\partial\epsilon$ are not the same thing; the former Jacobian quantity is required in ABAQUS, for example, for quadratic convergence. Unfortunately, the material Jacobian for plasticity is not quite so easy to obtain. It is derived in Section 5.3.2 for the plasticity model considered above; that is, for time-independent isotropic linear strain hardening plasticity.

5.3.2 Material Jacobian for time-independent isotropic linear strain hardening plasticity

We start from Equation (5.14) by applying the differential operator, δ (in a similar way as used to find the first variation of an integral in Chapter 4) so that we obtain

$$\left(1 + 3G \frac{\Delta p}{\sigma_e}\right) \delta \boldsymbol{\sigma}' + \frac{3G}{\sigma_e} \delta \Delta p \boldsymbol{\sigma}' - \frac{3G \Delta p}{\sigma_e^2} \delta \sigma_e \boldsymbol{\sigma}' = \delta \boldsymbol{\sigma}^{\text{tr}}. \quad (5.22)$$

Also, from (5.16), we may write

$$\delta \sigma_e + 3G \delta \Delta p = \delta \sigma_e^{\text{tr}}. \quad (5.23)$$

The yield condition is written as

$$\delta f = \delta \sigma_e - \delta r = 0$$

so that for linear hardening,

$$\delta \sigma_e = \delta r = h \delta p,$$

where δp is not the plastic strain in the increment, but an infinitesimal quantity, so that we may write

$$\delta \sigma_e = \delta r = h \delta \Delta p.$$

Combining with (5.23) gives

$$h \delta \Delta p + 3G \delta \Delta p = \delta \sigma_e^{\text{tr}}$$

so

$$\delta \Delta p = \frac{\delta \sigma_e^{\text{tr}}}{h + 3G}. \quad (5.24)$$

Combining with (5.23) gives

$$\delta \sigma_e = \delta \sigma_e^{\text{tr}} \left(1 - \frac{3G}{h + 3G}\right). \quad (5.25)$$

We now use (5.25), (5.24), and (5.19) in Equation (5.22) to eliminate $\delta \sigma_e$, $\delta \Delta p$, and Δp respectively to give (after some algebra)

$$\frac{\sigma_e^{\text{tr}}}{\sigma_e} \delta \boldsymbol{\sigma}' + \frac{\delta \sigma_e^{\text{tr}}}{\sigma_e \sigma_e} \left(\sigma_e - \frac{\sigma_e^{\text{tr}}}{1 + (3G/h)}\right) \boldsymbol{\sigma}' = \delta \boldsymbol{\sigma}^{\text{tr}}. \quad (5.26)$$

Consider the term,

$$\begin{aligned} \delta \sigma_e^{\text{tr}} &= \delta \left(\frac{3}{2} \boldsymbol{\sigma}^{\text{tr}'} : \boldsymbol{\sigma}^{\text{tr}'} \right)^{1/2} = \frac{1}{2} \left(\frac{3}{2} \boldsymbol{\sigma}^{\text{tr}'} : \boldsymbol{\sigma}^{\text{tr}'} \right)^{-1/2} \left(\frac{3}{2} \delta \boldsymbol{\sigma}^{\text{tr}'} : \boldsymbol{\sigma}^{\text{tr}'} + \frac{3}{2} \boldsymbol{\sigma}^{\text{tr}'} : \delta \boldsymbol{\sigma}^{\text{tr}'} \right) \\ &= \frac{3}{2} \frac{1}{\sigma_e^{\text{tr}}} \boldsymbol{\sigma}^{\text{tr}'} : \delta \boldsymbol{\sigma}^{\text{tr}'} . \end{aligned}$$

152 Implicit and explicit integration

Substituting this together with the expression for $\boldsymbol{\sigma}'$ in Equation (5.14) into (5.26) gives

$$\delta\boldsymbol{\sigma}' = \frac{3}{2} \left(\frac{1}{1 + (3G/h)} - \frac{\sigma_e}{\sigma_e^{\text{tr}}} \right) \frac{\boldsymbol{\sigma}^{\text{tr}'}}{\sigma_e^{\text{tr}}} \frac{\boldsymbol{\sigma}^{\text{tr}'}}{\sigma_e^{\text{tr}}} : \delta\boldsymbol{\sigma}^{\text{tr}'} + \frac{\sigma_e}{\sigma_e^{\text{tr}}} \delta\boldsymbol{\sigma}^{\text{tr}'}. \quad (5.27)$$

If we write

$$Q = \frac{3}{2} \left(\frac{1}{1 + (3G/h)} - \frac{\sigma_e}{\sigma_e^{\text{tr}}} \right) \quad \text{and} \quad R = \frac{\sigma_e}{\sigma_e^{\text{tr}}}$$

then (5.27) becomes

$$\delta\boldsymbol{\sigma}' = \left(Q \frac{\boldsymbol{\sigma}^{\text{tr}'}}{\sigma_e^{\text{tr}}} \frac{\boldsymbol{\sigma}^{\text{tr}'}}{\sigma_e^{\text{tr}}} + R\mathbf{I} \right) : \delta\boldsymbol{\sigma}^{\text{tr}'}. \quad (5.28)$$

Remember that in deriving the Jacobian, we are trying to relate $\delta\boldsymbol{\sigma}$ to $\delta\boldsymbol{\epsilon}$. We may write the deviatoric trial stress in terms of the deviatoric trial strain using Hooke's law (because the trial stress is obtained assuming elasticity) as

$$\delta\boldsymbol{\sigma}^{\text{tr}'} = 2G\delta\boldsymbol{\epsilon}^{\text{tr}'} = 2G \left(\delta\boldsymbol{\epsilon}^{\text{tr}'} - \frac{1}{3}\mathbf{II} : \delta\boldsymbol{\epsilon}^{\text{tr}'} \right)$$

and

$$\delta\boldsymbol{\epsilon}^{\text{tr}'} \equiv \delta\boldsymbol{\epsilon}$$

so

$$\delta\boldsymbol{\sigma}^{\text{tr}'} = 2G \left(\delta\boldsymbol{\epsilon} - \frac{1}{3}\mathbf{II} : \delta\boldsymbol{\epsilon} \right).$$

Substituting into Equation (5.28) gives

$$\begin{aligned} \delta\boldsymbol{\sigma}' &= \left(Q \frac{\boldsymbol{\sigma}^{\text{tr}'}}{\sigma_e^{\text{tr}}} \frac{\boldsymbol{\sigma}^{\text{tr}'}}{\sigma_e^{\text{tr}}} + R\mathbf{I} \right) : \left(2G \left(\delta\boldsymbol{\epsilon} - \frac{1}{3}\mathbf{II} : \delta\boldsymbol{\epsilon} \right) \right) \\ &= 2GQ \frac{\boldsymbol{\sigma}^{\text{tr}'}}{\sigma_e^{\text{tr}}} \frac{\boldsymbol{\sigma}^{\text{tr}'}}{\sigma_e^{\text{tr}}} : \delta\boldsymbol{\epsilon} - \frac{1}{3}Q \frac{\boldsymbol{\sigma}^{\text{tr}'}}{\sigma_e^{\text{tr}}} \frac{\boldsymbol{\sigma}^{\text{tr}'}}{\sigma_e^{\text{tr}}} : (\mathbf{II} : \delta\boldsymbol{\epsilon}) + 2GR\delta\boldsymbol{\epsilon} - \frac{2}{3}GR\mathbf{I} : (\mathbf{II} : \delta\boldsymbol{\epsilon}). \end{aligned}$$

The second term of the right-hand side is zero since $\boldsymbol{\sigma}^{\text{tr}'}$ is deviatoric so

$$\frac{\boldsymbol{\sigma}^{\text{tr}'}}{\sigma_e^{\text{tr}}} \frac{\boldsymbol{\sigma}^{\text{tr}'}}{\sigma_e^{\text{tr}}} : (\mathbf{II} : \delta\boldsymbol{\epsilon}) = \frac{\boldsymbol{\sigma}^{\text{tr}'}}{\sigma_e^{\text{tr}}} \frac{\boldsymbol{\sigma}^{\text{tr}'}}{\sigma_e^{\text{tr}}} : \mathbf{I} \text{Tr}(\delta\boldsymbol{\epsilon}) = 0$$

and therefore

$$\delta\boldsymbol{\sigma}' = 2GQ \frac{\boldsymbol{\sigma}^{\text{tr}'}}{\sigma_e^{\text{tr}}} \frac{\boldsymbol{\sigma}^{\text{tr}'}}{\sigma_e^{\text{tr}}} : \delta\boldsymbol{\epsilon} + 2GR\delta\boldsymbol{\epsilon} - \frac{2}{3}GR\mathbf{II} : \delta\boldsymbol{\epsilon} \quad (5.29)$$

since $\mathbf{I} : \mathbf{I} = \mathbf{I}$. Finally, the stress is given in terms of its deviatoric by

$$\begin{aligned} \delta\boldsymbol{\sigma} &= \delta\boldsymbol{\sigma}' + \frac{1}{3}\mathbf{II} : \delta\boldsymbol{\sigma} = \delta\boldsymbol{\sigma}' + K\mathbf{II} : \delta\boldsymbol{\epsilon}^e = \delta\boldsymbol{\sigma}' + K\mathbf{II} : (\delta\boldsymbol{\epsilon} - \delta\boldsymbol{\epsilon}^p) \\ &= \delta\boldsymbol{\sigma}' + K\mathbf{II} : \delta\boldsymbol{\epsilon}. \end{aligned}$$

Substituting into (5.29) gives

$$\delta \boldsymbol{\sigma} = 2GQ \frac{\boldsymbol{\sigma}^{\text{tr}'}}{\sigma_e^{\text{tr}}} \frac{\boldsymbol{\sigma}^{\text{tr}'}}{\sigma_e^{\text{tr}}} : \delta \boldsymbol{\varepsilon} + 2GR \delta \boldsymbol{\varepsilon} + \left(K - \frac{2}{3}GR \right) \mathbf{II} : \delta \boldsymbol{\varepsilon}. \quad (5.30)$$

We may write this in the shortened form as

$$\delta \boldsymbol{\sigma} = \left[2GQ \frac{\boldsymbol{\sigma}^{\text{tr}'}}{\sigma_e^{\text{tr}}} \frac{\boldsymbol{\sigma}^{\text{tr}'}}{\sigma_e^{\text{tr}}} + 2GRI + \left(K - \frac{2}{3}GR \right) \mathbf{II} \right] : \delta \boldsymbol{\varepsilon}. \quad (5.31)$$

Equation (5.30) provides the Jacobian or the material tangent stiffness matrix. In this case, because it has been derived from the implicit backward Euler integration scheme, which is used to integrate the plasticity constitutive equations, it is called the *consistent tangent stiffness*. Let us determine some of the terms using (5.30).

$$\begin{aligned} \delta \sigma_{11} &= 2GQ \frac{\sigma_{11}^{\text{tr}'}}{\sigma_e^{\text{tr}}} \frac{1}{\sigma_e^{\text{tr}}} \\ &\times (\sigma_{11}^{\text{tr}'} \delta \varepsilon_{11} + \sigma_{22}^{\text{tr}'} \delta \varepsilon_{22} + \sigma_{33}^{\text{tr}'} \delta \varepsilon_{33} + 2\sigma_{12}^{\text{tr}'} \delta \varepsilon_{12} + 2\sigma_{13}^{\text{tr}'} \delta \varepsilon_{13} + 2\sigma_{23}^{\text{tr}'} \delta \varepsilon_{23}) \\ &+ 2GR \delta \varepsilon_{11} + \left(K - \frac{2}{3}GR \right) (\delta \varepsilon_{11} + \delta \varepsilon_{22} + \delta \varepsilon_{33}). \end{aligned}$$

The first term of the Jacobian is, therefore,

$$D_{11} = \frac{\partial \delta \sigma_{11}}{\partial \delta \varepsilon_{11}} = 2GQ \frac{\sigma_{11}^{\text{tr}'}}{\sigma_e^{\text{tr}}} \frac{\sigma_{11}^{\text{tr}'}}{\sigma_e^{\text{tr}}} + 2GR + \left(K - \frac{2}{3}GR \right)$$

and the next is

$$D_{12} = \frac{\partial \delta \sigma_{11}}{\partial \delta \varepsilon_{22}} = 2GQ \frac{\sigma_{11}^{\text{tr}'}}{\sigma_e^{\text{tr}}} \frac{\sigma_{22}^{\text{tr}'}}{\sigma_e^{\text{tr}}} + \left(K - \frac{2}{3}GR \right)$$

and so on. A shear term is given by

$$D_{44} = \frac{\partial \delta \sigma_{12}}{\partial \delta \gamma_{12}} = \frac{1}{2} \frac{\partial \delta \sigma_{12}}{\partial \delta \varepsilon_{12}} = \frac{1}{2} \left[2GQ \frac{\sigma_{12}^{\text{tr}'}}{\sigma_e^{\text{tr}}} \frac{2\sigma_{12}^{\text{tr}'}}{\sigma_e^{\text{tr}}} + 2GR \right] = 2GQ \frac{\sigma_{12}^{\text{tr}'}}{\sigma_e^{\text{tr}}} \frac{\sigma_{12}^{\text{tr}'}}{\sigma_e^{\text{tr}}} + GR$$

and D_{14} is

$$D_{14} = \frac{\partial \delta \sigma_{11}}{\partial \delta \gamma_{12}} = \frac{1}{2} \frac{\partial \delta \sigma_{11}}{\partial \delta \varepsilon_{12}} = 2GQ \frac{\sigma_{11}^{\text{tr}'}}{\sigma_e^{\text{tr}}} \frac{\sigma_{12}^{\text{tr}'}}{\sigma_e^{\text{tr}}}.$$

For conditions of axial symmetry (so that the out of plane shears, σ_{13} , ε_{13} and σ_{23} , ε_{23} do not exist) therefore, the Jacobian is the symmetrical matrix

$$\frac{\partial \delta \boldsymbol{\sigma}}{\partial \delta \boldsymbol{\varepsilon}} = \begin{pmatrix} D_{11} & D_{12} & D_{13} & D_{14} \\ & D_{22} & D_{23} & D_{24} \\ & & D_{33} & D_{34} \\ & & & D_{44} \end{pmatrix}.$$

5.4 Kinematic hardening

In this section, we shall use implicit (backward Euler) integration for the case of linear kinematic hardening, and obtain the consistent tangent stiffness. We will then go on to address combined linear kinematic hardening with non-linear isotropic hardening, and to introduce combined non-linear kinematic and isotropic hardening. We will finish by introducing semi-implicit integration schemes for plasticity.

5.4.1 Linear kinematic hardening

With the backward Euler scheme, as given in Section 5.2.1.2 for isotropic hardening, Hooke's law may be written in its predictor–corrector form as

$$\boldsymbol{\sigma} = \boldsymbol{\sigma}^{\text{tr}} - 2G\Delta p\mathbf{n} \quad (5.32)$$

in which $\boldsymbol{\sigma}^{\text{tr}}$ is the elastic trial stress. We employ linear kinematic hardening so that the back stress increment is given by

$$\Delta \mathbf{x} = \frac{2}{3}c\Delta \boldsymbol{\varepsilon}^{\text{P}}$$

and as a result, if we write the back stress at time, t , as \mathbf{x}_t , then at the end of the time step, $t + \Delta t$, it becomes

$$\mathbf{x} = \mathbf{x}_t + \frac{2}{3}c\Delta \boldsymbol{\varepsilon}^{\text{P}} \quad (5.33)$$

and with the normality hypothesis for von Mises plasticity,

$$\mathbf{x} = \mathbf{x}_t + \frac{2}{3}c\Delta p\mathbf{n}, \quad (5.34)$$

where

$$\mathbf{n} = \frac{3}{2} \frac{\boldsymbol{\sigma}' - \mathbf{x}}{\sigma_{\text{e}}} \quad (5.35)$$

for kinematic hardening, in which \mathbf{x} is, of course, itself deviatoric, and Δp is the increment in effective plastic strain. Combining (5.35) and (5.34) gives

$$\boldsymbol{\sigma}' = \mathbf{x}_t + \frac{2}{3}\Delta p c\mathbf{n} + \frac{2}{3}\sigma_{\text{e}}\mathbf{n}. \quad (5.36)$$

The deviatoric stress is

$$\boldsymbol{\sigma}' = \boldsymbol{\sigma} - \frac{1}{3}\mathbf{II} : \boldsymbol{\sigma}$$

so that with (5.32), we may write (5.36) as

$$\boldsymbol{\sigma}^{\text{tr}} - 2G\Delta p\mathbf{n} - \frac{1}{3}\mathbf{II} : \boldsymbol{\sigma} = \mathbf{x}_t + \frac{2}{3}\Delta p c\mathbf{n} + \frac{2}{3}\sigma_{\text{e}}\mathbf{n}.$$

We saw earlier that we may write

$$\boldsymbol{\sigma}^{\text{tr}} - \frac{1}{3}\mathbf{II} : \boldsymbol{\sigma} \equiv \boldsymbol{\sigma}^{\text{tr}'}$$

so that

$$\boldsymbol{\sigma}^{\text{tr}'} - 2G\Delta p\mathbf{n} = \mathbf{x}_t + \frac{2}{3}\Delta pc\mathbf{n} + \frac{2}{3}\sigma_e\mathbf{n}. \quad (5.37)$$

Taking the contracted product of both sides of (5.37) with \mathbf{n} gives

$$(\boldsymbol{\sigma}^{\text{tr}'} - \mathbf{x}_t) : \mathbf{n} = \mathbf{n} : \mathbf{n} \left(2G\Delta p + \frac{2}{3}\Delta pc + \frac{2}{3}\sigma_e \right) \quad (5.38)$$

and

$$\mathbf{n} : \mathbf{n} = \frac{3}{2} \frac{\boldsymbol{\sigma}' - \mathbf{x}}{\sigma_e} : \frac{3}{2} \frac{\boldsymbol{\sigma}' - \mathbf{x}}{\sigma_e} = \frac{3}{2\sigma_e^2} \left[\frac{3}{2} (\boldsymbol{\sigma}' - \mathbf{x}) : (\boldsymbol{\sigma}' - \mathbf{x}) \right].$$

But the effective stress, σ_e , is defined by

$$\sigma_e = \left[\frac{3}{2} (\boldsymbol{\sigma}' - \mathbf{x}) : (\boldsymbol{\sigma}' - \mathbf{x}) \right]^{1/2}$$

so that

$$\mathbf{n} : \mathbf{n} = \frac{3}{2}.$$

Equation (5.38) therefore reduces to

$$(\boldsymbol{\sigma}^{\text{tr}'} - \mathbf{x}_t) : \mathbf{n} = 3G\Delta p + \Delta pc + \sigma_e. \quad (5.39)$$

From (5.32) we may write

$$\boldsymbol{\sigma}' = \boldsymbol{\sigma}^{\text{tr}'} - 2G\Delta p\mathbf{n}$$

so that from (5.35), we may write \mathbf{n} as

$$\mathbf{n} = \frac{3}{2} \left(\frac{\boldsymbol{\sigma}^{\text{tr}'} - 2G\Delta p\mathbf{n} - \mathbf{x}}{\sigma_e} \right) = \frac{3}{2} \left(\frac{\boldsymbol{\sigma}^{\text{tr}'} - 2G\Delta p\mathbf{n} - \mathbf{x}_t - (2/3)c\Delta p\mathbf{n}}{\sigma_e} \right).$$

Rearranging this equation for \mathbf{n} gives

$$\mathbf{n} = \frac{3}{2} \left(\frac{\boldsymbol{\sigma}^{\text{tr}'} - \mathbf{x}_t}{\sigma_e + 3G\Delta p + c\Delta p} \right) \quad (5.40)$$

and substituting into (5.39) gives

$$\left[\frac{3}{2} (\boldsymbol{\sigma}^{\text{tr}'} - \mathbf{x}_t) : (\boldsymbol{\sigma}^{\text{tr}'} - \mathbf{x}_t) \right]^{1/2} \equiv \sigma_e = 3G\Delta p + \Delta pc + \sigma_e. \quad (5.41)$$

Note that the effective trial stress is determined with respect to the back stress taken at time, t , rather than at the end of the time increment. Rearranging this equation gives

$$\Delta p = \frac{\sigma_e^{\text{tr}} - \sigma_e}{3G + c}. \quad (5.42)$$

The yield function for the case of kinematic hardening is

$$f = \sigma_e - \sigma_y = 0 \quad (5.43)$$

so that

$$\sigma_e = \sigma_y.$$

In Equation (5.42), therefore, for the case of linear kinematic hardening, none of the terms depends upon the effective plastic strain. Equation (5.42) is therefore an exact, closed-form expression for Δp and in this instance, no iteration is required for its determination. Plastic and elastic strains and the stress may then be updated using (5.42) to give

$$\mathbf{n} = \frac{3}{2} \left(\frac{\boldsymbol{\sigma}^{\text{tr}'} - \mathbf{x}_t}{\sigma_e^{\text{tr}}} \right).$$

$$\Delta \boldsymbol{\varepsilon}^{\text{P}} = \Delta p \mathbf{n},$$

$$\boldsymbol{\varepsilon}^{\text{P}} = \boldsymbol{\varepsilon}_t^{\text{P}} + \Delta \boldsymbol{\varepsilon}^{\text{P}},$$

$$\boldsymbol{\varepsilon}^{\text{e}} = \boldsymbol{\varepsilon}_t^{\text{e}} + \Delta \boldsymbol{\varepsilon}^{\text{e}} = \boldsymbol{\varepsilon}_t^{\text{e}} + \Delta \boldsymbol{\varepsilon} - \Delta \boldsymbol{\varepsilon}^{\text{P}},$$

$$\boldsymbol{\sigma} = 2G \boldsymbol{\varepsilon}^{\text{e}} + \lambda \mathbf{II} : \boldsymbol{\varepsilon}^{\text{e}}.$$

5.4.1.1 Consistent tangent stiffness for linear kinematic Hardening. In implicit finite element code, in addition to the integration of the plasticity constitutive equations, it is also necessary to provide the material Jacobian—the tangent stiffness matrix. Here, we determine the consistent (i.e. with the implicit integration given above) tangent stiffness for linear kinematic hardening.

Using (5.40) and (5.41), \mathbf{n} may be written as

$$\mathbf{n} = \frac{3}{2} \left(\frac{\boldsymbol{\sigma}^{\text{tr}'} - \mathbf{x}_t}{\sigma_e^{\text{tr}}} \right).$$

We have therefore

$$\boldsymbol{\sigma}' = \boldsymbol{\sigma}^{\text{tr}'} - 2G \Delta p \mathbf{n} = \boldsymbol{\sigma}^{\text{tr}'} - 2G \Delta p \frac{3}{2} \left(\frac{\boldsymbol{\sigma}^{\text{tr}'} - \mathbf{x}_t}{\sigma_e^{\text{tr}}} \right)$$

and substituting for Δp from (5.42) gives

$$\boldsymbol{\sigma}' = \boldsymbol{\sigma}^{\text{tr}'} - 2G \left(\frac{\sigma_e^{\text{tr}} - \sigma_e}{3G + c} \right) \frac{3}{2} \left(\frac{\boldsymbol{\sigma}^{\text{tr}'} - \mathbf{x}_t}{\sigma_e^{\text{tr}}} \right)$$

and after a little algebra, we obtain

$$\boldsymbol{\sigma}' = \boldsymbol{\sigma}^{\text{tr}'} \left(\frac{c/3G + \sigma_e/\sigma_e^{\text{tr}}}{1 + c/3G} \right) + \left(\frac{1 - \sigma_e/\sigma_e^{\text{tr}}}{1 + c/3G} \right) \mathbf{x}_t.$$

Applying the differential operator, and rearranging, we obtain

$$(1 + c/3G) \frac{\sigma_e^{\text{tr}}}{\sigma_e} \delta \boldsymbol{\sigma}' = \delta \boldsymbol{\sigma}^{\text{tr}'} (1 + (c/3G)(\sigma_e^{\text{tr}}/\sigma_e)) \\ + \boldsymbol{\sigma}^{\text{tr}'} (\delta \sigma_e / \sigma_e - \delta \sigma_e^{\text{tr}} / \sigma_e^{\text{tr}}) - (\delta \sigma_e / \sigma_e - \delta \sigma_e^{\text{tr}} / \sigma_e^{\text{tr}}) \mathbf{x}_t.$$

From the yield function in (5.43), $\delta f = \delta \sigma_e = 0$ so this reduces to

$$(1 + c/3G) \frac{\sigma_e^{\text{tr}}}{\sigma_e} \delta \boldsymbol{\sigma}' = \delta \boldsymbol{\sigma}^{\text{tr}'} (1 + (c/3G)(\sigma_e^{\text{tr}}/\sigma_e)) - (\boldsymbol{\sigma}^{\text{tr}'} - \mathbf{x}_t) (\delta \sigma_e^{\text{tr}} / \sigma_e^{\text{tr}}). \quad (5.44)$$

Now,

$$\sigma_e^{\text{tr}} = \left[\frac{3}{2} (\boldsymbol{\sigma}^{\text{tr}'} - \mathbf{x}_t) : (\boldsymbol{\sigma}^{\text{tr}'} - \mathbf{x}_t) \right]^{1/2}$$

so

$$\delta \sigma_e^{\text{tr}} = \frac{1}{2} \left[\frac{3}{2} (\boldsymbol{\sigma}^{\text{tr}'} - \mathbf{x}_t) : (\boldsymbol{\sigma}^{\text{tr}'} - \mathbf{x}_t) \right]^{-1/2} \left[\frac{3}{2} (\boldsymbol{\sigma}^{\text{tr}'} - \mathbf{x}_t) : \delta \boldsymbol{\sigma}^{\text{tr}'} + \frac{3}{2} \delta \boldsymbol{\sigma}^{\text{tr}'} : (\boldsymbol{\sigma}^{\text{tr}'} - \mathbf{x}_t) \right] \\ = \frac{1}{\sigma_e^{\text{tr}}} \frac{3}{2} (\boldsymbol{\sigma}^{\text{tr}'} - \mathbf{x}_t) : \delta \boldsymbol{\sigma}^{\text{tr}'}.$$

Substituting into (5.44), and writing

$$Q = \frac{\sigma_e / \sigma_e^{\text{tr}} + c/3G}{1 + c/3G} \quad R = -\frac{3}{2} \frac{\sigma_e}{\sigma_e^{\text{tr}}} \frac{1}{1 + c/3G}$$

gives

$$\delta \boldsymbol{\sigma}' = Q \delta \boldsymbol{\sigma}^{\text{tr}'} + R \frac{(\boldsymbol{\sigma}^{\text{tr}'} - \mathbf{x}_t)}{\sigma_e^{\text{tr}}} \frac{(\boldsymbol{\sigma}^{\text{tr}'} - \mathbf{x}_t)}{\sigma_e^{\text{tr}}} : \delta \boldsymbol{\sigma}^{\text{tr}'}.$$

As before,

$$\delta \boldsymbol{\sigma}^{\text{tr}'} = 2G \left(\delta \boldsymbol{\varepsilon} - \frac{1}{3} \mathbf{II} : \delta \boldsymbol{\varepsilon} \right)$$

so that

$$\delta \boldsymbol{\sigma}' = 2GQ \delta \boldsymbol{\varepsilon} + 2GR \frac{(\boldsymbol{\sigma}^{\text{tr}'} - \mathbf{x}_t)}{\sigma_e^{\text{tr}}} \frac{(\boldsymbol{\sigma}^{\text{tr}'} - \mathbf{x}_t)}{\sigma_e^{\text{tr}}} : \delta \boldsymbol{\varepsilon} - \frac{2}{3} GQ \mathbf{II} : \delta \boldsymbol{\varepsilon}$$

and finally,

$$\delta \boldsymbol{\sigma} = 2GQ \delta \boldsymbol{\varepsilon} + 2GR \frac{(\boldsymbol{\sigma}^{\text{tr}'} - \mathbf{x}_t)}{\sigma_e^{\text{tr}}} \frac{(\boldsymbol{\sigma}^{\text{tr}'} - \mathbf{x}_t)}{\sigma_e^{\text{tr}}} : \delta \boldsymbol{\varepsilon} - \left(K - \frac{2}{3} GQ \right) \mathbf{II} : \delta \boldsymbol{\varepsilon} \quad (5.45)$$

which gives the consistent tangent stiffness.

5.4.2 Combined isotropic and linear kinematic hardening

The isotropic hardening evolution equation is

$$dr = h dp$$

in which h can be a function of p so that r is not necessarily linear, and for the linear kinematic hardening,

$$d\mathbf{x} = \frac{2}{3}c d\boldsymbol{\epsilon}^p.$$

Because of the assumption of linearity, as before we may write

$$\mathbf{x} = \mathbf{x}_t + \frac{2}{3}c\Delta p\mathbf{n}$$

and from Section 5.4, we have

$$\sigma_e = \sigma_e^{\text{tr}} - (3G + c)\Delta p \quad (5.46)$$

in which σ_e^{tr} and σ_e are given by

$$\sigma_e^{\text{tr}} = \left[\frac{3}{2}(\boldsymbol{\sigma}^{\text{tr}'} - \mathbf{x}_t) : (\boldsymbol{\sigma}^{\text{tr}'} - \mathbf{x}_t) \right]^{1/2}, \quad \sigma_e = \left[\frac{3}{2}(\boldsymbol{\sigma}' - \mathbf{x}) : (\boldsymbol{\sigma}' - \mathbf{x}) \right]^{1/2}.$$

The yield function is

$$f = \sigma_e - r - \sigma_y = 0$$

which becomes, after substituting (5.46)

$$f = \sigma_e^{\text{tr}} - (3G + c)\Delta p - r - \sigma_y = 0. \quad (5.47)$$

In this case, r depends on h which may, for non-linear hardening, depend on p and the equation can be non-linear. We use Newton's method to solve it by writing

$$f + \frac{\partial f}{\partial \Delta p} d\Delta p = 0$$

and substituting (5.47) gives

$$d\Delta p = \frac{\sigma_e^{\text{tr}} - (3G + c)\Delta p - r - \sigma_y}{3G + c + h}. \quad (5.48)$$

Let us simplify it for the cases of linear kinematic hardening and isotropic hardening only to compare with the previous equations. If there is no isotropic hardening, then $r = h = 0$ and (5.48) becomes

$$d\Delta p = \frac{\sigma_e^{\text{tr}} - (3G + c)\Delta p - \sigma_y}{3G + c} \quad (5.49)$$

and for linear kinematic hardening, $\sigma_e = \sigma_e^{\text{tr}} - (3G + c)\Delta p$ and $\sigma_e = \sigma_y$ so (5.49) gives

$$d\Delta p = 0.$$

That is, there is no iteration required and Δp is given by

$$\Delta p = \frac{\sigma_e^{\text{tr}} - \sigma_y}{3G + c}$$

as before. If there is no kinematic hardening, $\mathbf{x} = 0$ and $c = 0$ so (5.49) becomes

$$d\Delta p = \frac{\sigma_e^{\text{tr}} - 3G\Delta p - r - \sigma_y}{3G + h},$$

where

$$\sigma_e^{\text{tr}} = \left[\frac{3}{2} \boldsymbol{\sigma}^{\text{tr}'} : \boldsymbol{\sigma}^{\text{tr}'} \right]^{1/2}$$

which is what we obtained before in Section 5.2.1.

5.4.3 Introduction to implicit integration of combined non-linear kinematic and isotropic hardening

In the previous sections in which we assumed linear kinematic hardening, we wrote the kinematic hardening variable in terms of its value at the start of the increment, \mathbf{x}_t , and the incremental value. As a result, subsequent equations were set up in terms of \mathbf{x}_t . Here, we will now introduce the more general case of non-linear kinematic hardening, and will find the equations depending on quantities at the end of the time increment.

As before, the deviatoric stress can be written in predictor–corrector form in terms of the trial stress and plastic return as

$$\boldsymbol{\sigma}' = \boldsymbol{\sigma}^{\text{tr}'} - 2G\Delta p \mathbf{n} \quad (5.50)$$

and the normal, \mathbf{n} , is given by

$$\mathbf{n} = \frac{3}{2} \frac{\boldsymbol{\sigma}' - \mathbf{x}}{\sigma_e}. \quad (5.51)$$

Combining these equations and after a little algebra, we obtain

$$(\boldsymbol{\sigma}^{\text{tr}'} - \mathbf{x}) : \mathbf{n} = \left(\frac{2}{3} \sigma_e + 2G\Delta p \right) \mathbf{n} : \mathbf{n}$$

and we have shown before that $\mathbf{n} : \mathbf{n} = \frac{3}{2}$, so

$$(\boldsymbol{\sigma}^{\text{tr}'} - \mathbf{x}) : \mathbf{n} = \sigma_e + 3G\Delta p. \quad (5.52)$$

160 Implicit and explicit integration

We can also obtain from (5.50) and (5.51)

$$\mathbf{n} = \frac{3 \boldsymbol{\sigma}^{\text{tr}'} - 2G \Delta p \mathbf{n} - \mathbf{x}}{2 \sigma_e}$$

so that rearranging,

$$\mathbf{n} = \frac{3 \boldsymbol{\sigma}^{\text{tr}'} - \mathbf{x}}{2 \sigma_e + 3G \Delta p}.$$

Combining with (5.52) gives

$$\sigma_e = \sigma_e^{\text{tr}} - 3G \Delta p, \quad (5.53)$$

where

$$\sigma_e^{\text{tr}} = \left[\frac{3}{2} (\boldsymbol{\sigma}^{\text{tr}'} - \mathbf{x}) : (\boldsymbol{\sigma}^{\text{tr}'} - \mathbf{x}) \right]^{1/2}. \quad (5.54)$$

The yield function is

$$f = \sigma_e - r - \sigma_y = \sigma_e^{\text{tr}} - 3G \Delta p - r - \sigma_y = 0 \quad (5.55)$$

with σ_e^{tr} given by (5.54). Note now that because \mathbf{x} depends on p (non-linearly for the case of non-linear kinematic hardening) as may r , Equation (5.55) is a non-linear equation in Δp for which we will need to use Newton's iterative solution method, for which we obtain

$$d\Delta p = \frac{\sigma_e^{\text{tr}(k)} - 3G \Delta p^{(k)} - r^{(k)} - \sigma_y}{3G + (\partial r^{(k)} / \partial \Delta p) - (\partial \sigma_e^{\text{tr}(k)} / \partial \Delta p)} \quad (5.56)$$

and

$$\Delta p^{(k+1)} = \Delta p^{(k)} + d\Delta p.$$

Both σ_e^{tr} and r are the two derivatives with respect to Δp need to be updated at every iteration for a fully implicit integration. Often, with complex plasticity hardening laws, this may be challenging. A simpler approach is to integrate the effective plastic strain implicitly but to update the normal \mathbf{n} and the internal variables—the isotropic and kinematic hardening—explicitly. Such an approach is called *semi-implicit* integration.

5.4.4 Semi-implicit integration of combined non-linear kinematic and isotropic hardening

In the semi-implicit scheme, Newton's method is used to determine the effective plastic strain increment using Equation (5.56) and the yield function (5.55) written at the end of the time increment ensures that drift from the yield surface does not occur. However, the updates of all other quantities are carried out explicitly as follows:

$$\Delta \boldsymbol{\epsilon}^{\text{p}(k+1)} = \Delta p^{(k+1)} \mathbf{n}_t,$$

where

$$\begin{aligned}
 \mathbf{n}_t &= \frac{3}{2} \frac{\boldsymbol{\sigma}'_t - \mathbf{x}_t}{\sigma_{e_t}}, \\
 \boldsymbol{\varepsilon}^{\text{p}(k+1)} &= \boldsymbol{\varepsilon}_t^{\text{p}} + \Delta \boldsymbol{\varepsilon}^{\text{p}(k+1)}, \\
 \boldsymbol{\varepsilon}^{\text{e}(k+1)} &= \boldsymbol{\varepsilon} - \boldsymbol{\varepsilon}^{\text{p}(k+1)}, \\
 \boldsymbol{\sigma}^{(k+1)} &= 2G \boldsymbol{\varepsilon}^{\text{e}(k+1)} + \lambda \mathbf{II} : \boldsymbol{\varepsilon}^{\text{e}(k+1)}, \\
 r^{(k+1)} &= r_t + \Delta r, \\
 \mathbf{x}^{(k+1)} &= \mathbf{x}_t + \Delta \mathbf{x},
 \end{aligned}$$

where, for example, the non-linear kinematic hardening increment, $\Delta \mathbf{x}$, is given by

$$\Delta \mathbf{x} = \frac{2}{3} c \Delta \boldsymbol{\varepsilon}^{\text{p}(k+1)} + \gamma \mathbf{x}_t \Delta p^{(k+1)}$$

and the isotropic hardening increment by

$$\Delta r = b(Q - r) \Delta p^{(k+1)}$$

if the non-linear evolution equations given in Chapter 2 are adopted, and

$$\sigma_e^{\text{tr}(k+1)} = \left[\frac{3}{2} (\boldsymbol{\sigma}^{\text{tr}'} - \mathbf{x}^{(k+1)}) : (\boldsymbol{\sigma}^{\text{tr}'} - \mathbf{x}^{(k+1)}) \right]^{1/2}.$$

The semi-implicit scheme is not unconditionally stable and we need to be concerned, therefore, about both stability and accuracy when using it.

5.5 Implicit integration in viscoplasticity

We saw in Chapter 2 that the plastic strain rate can be written, for a viscoplastic von Mises material, as

$$\dot{\boldsymbol{\varepsilon}}^{\text{p}} = \dot{p} \frac{\partial f}{\partial \boldsymbol{\sigma}}$$

in which, for viscoplasticity, \dot{p} is now specified by a constitutive equation (as opposed to being determined by the consistency condition) which, for both isotropic and kinematic hardening, can be written as

$$\dot{p} = \phi(\boldsymbol{\sigma}, \mathbf{x}, r).$$

We may write this incrementally as

$$\Delta p = \phi(\boldsymbol{\sigma}, \mathbf{x}, r) \Delta t = \phi \Delta t. \quad (5.57)$$

For both kinematic and isotropic hardening, the yield function is

$$f = J(\boldsymbol{\sigma}' - \mathbf{x}') - r - \sigma_y.$$

5.5.1 Uniaxial viscoplasticity equations

We will present implicit backward Euler integration for the uniaxial form of the equations first, for simplicity, and we start from the viscoplastic constitutive equation. Equation (5.57) may be written in uniaxial form, if we consider isotropic hardening only for now, as

$$\Delta p = \phi(\sigma_e, r) \Delta t \quad (5.58)$$

and we may write this in a form suitable for Newton's iterative solution as

$$\psi = \Delta p - \phi(\sigma_e, r) \Delta t = 0. \quad (5.59)$$

In preparation for differentiation, we may write the stress in terms of Δp by remembering (5.16)

$$\sigma_e + 3G \Delta p = \sigma_e^{\text{tr}} \quad (5.60)$$

so that (5.59) becomes

$$\psi(\Delta p, r) = \Delta p - \phi(\Delta p, r) \Delta t = 0. \quad (5.61)$$

Using Newton's method, we have

$$\psi + \frac{\partial \psi}{\partial \Delta p} d\Delta p + \frac{\partial \psi}{\partial r} dr = 0 \quad (5.62)$$

and differentiating (5.61) and substituting into (5.62) gives

$$\Delta p - \phi \Delta t + \left(1 - \frac{\partial \phi}{\partial \Delta p} \Delta t\right) d\Delta p - \frac{\partial \phi}{\partial r} \Delta t dr = 0. \quad (5.63)$$

We will write, from here on,

$$\phi_{\Delta p} = \frac{\partial \phi}{\partial \Delta p} \quad \text{and} \quad \phi_r = \frac{\partial \phi}{\partial r}$$

and similarly for other derivatives. If we assume for now linear isotropic hardening, then

$$dr = h dp = h d\Delta p.$$

Substituting into (5.63) and rearranging gives

$$d\Delta p = \frac{\phi(\Delta p, r) - \Delta p / \Delta t}{1 / \Delta t - \phi_{\Delta p} - h \phi_r}. \quad (5.64)$$

As an example, let us consider a particular viscoplasticity constitutive equation, given by

$$\dot{p} = \phi(\sigma_e, r) = \alpha \sinh \beta(\sigma_e - r - \sigma_y)$$

in which σ_y , α , and β are material constants. Using (5.59) this becomes

$$\dot{p} = \phi(\Delta p, r) = \alpha \sinh \beta(\sigma^{\text{tr}} - 3G \Delta p - r - \sigma_y)$$

and the required derivatives are

$$\phi_{\Delta p} = -3G\alpha\beta \cosh \beta(\sigma^{\text{tr}} - 3G\Delta p - r - \sigma_y)$$

and

$$\phi_r = -\alpha\beta \cosh \beta(\sigma^{\text{tr}} - 3G\Delta p - r - \sigma_y)$$

so that (5.64) gives

$d\Delta p$

$$= \frac{\alpha \sinh \beta(\sigma^{\text{tr}} - 3G\Delta p - r - \sigma_y) - \Delta p / \Delta t}{1/\Delta t + 3G\alpha\beta \cosh \beta(\sigma^{\text{tr}} - 3G\Delta p - r - \sigma_y) + h\alpha\beta \cosh \beta(\sigma^{\text{tr}} - 3G\Delta p - r - \sigma_y)}$$

with

$$r = r_t + h\Delta p.$$

As before in rate-independent plasticity, an iterative procedure is used to determine Δp from

$$\Delta p^{(k+1)} = \Delta p^{(k)} + d\Delta p.$$

5.5.2 Multiaxial viscoplasticity

For the case of isotropic hardening, Equation (5.64) still holds for the multiaxial case, and the plastic strain tensor increment can then be determined from

$$\Delta \boldsymbol{\epsilon}^p = \Delta p \mathbf{n} = \frac{3}{2} \Delta p \frac{\boldsymbol{\sigma}'}{\sigma_e} \equiv \frac{3}{2} \Delta p \frac{\boldsymbol{\sigma}^{\text{tr}'}}{\sigma_e^{\text{tr}'}}$$

so that the elastic strain and hence stress increments can be determined in the usual way.

We shall next consider combined multiaxial linear isotropic and kinematic hardening such that the constitutive equation is written as

$$\dot{p} = \phi(\Delta p, \mathbf{x}, r)$$

in which \mathbf{x} is the tensorial kinematic hardening variable. The problem may be written, as before,

$$\psi(\Delta p, \mathbf{x}, r) = \Delta p - \phi(\Delta p, \mathbf{x}, r)\Delta t = 0$$

and

$$\psi + \frac{\partial \psi}{\partial \Delta p} d\Delta p + \frac{\partial \psi}{\partial \mathbf{x}} : d\mathbf{x} + \frac{\partial \psi}{\partial r} dr = 0. \quad (5.65)$$

We may write the derivatives as

$$\frac{\partial \psi}{\partial \Delta p} = 1 - \phi_{\Delta p} \Delta t, \quad \frac{\partial \psi}{\partial \mathbf{x}} = -\boldsymbol{\phi}_x \Delta t, \quad \frac{\partial \psi}{\partial r} = -\phi_r \Delta t$$

164 Implicit and explicit integration

so that (5.65) becomes

$$\Delta p - \phi \Delta t + (1 - \phi_{\Delta p} \Delta t) d\Delta p - \phi_x : dx \Delta t - \phi_r dr \Delta t = 0. \quad (5.66)$$

Let us write the linear isotropic and kinematic hardening equations as

$$\begin{aligned} dr &= h dp = h d\Delta p, \\ dx &= \frac{2}{3} c d\epsilon_p = \frac{2}{3} c d\Delta p n \end{aligned}$$

so that substituting into (5.66) and rearranging gives

$$d\Delta p = \frac{\phi \Delta t - \Delta p}{1 - \phi_{\Delta p} \Delta t - h \phi_r \Delta t - (2/3)c \phi_x : n \Delta t}. \quad (5.67)$$

If we consider again a viscoplastic constitutive equation with kinematic and isotropic hardening of the form

$$\dot{p} = \phi(\sigma, x, r) = \alpha \sinh \beta (J(\sigma' - x') - r - \sigma_y) = \alpha \sinh \beta (\sigma_e - r - \sigma_y),$$

then

$$\phi_x = -\frac{\partial \phi}{\partial \sigma_e} \frac{\partial \sigma_e}{\partial x} = -\phi_{\sigma_e} \frac{3}{2} \frac{\sigma' - x'}{J(\sigma' - x')} = -\phi_{\sigma_e} n$$

and the term $\phi_x : n$ may be simplified to

$$\phi_x : n = -\phi_{\sigma_e} n : n = -\frac{3}{2} \phi_{\sigma_e}.$$

Substituting into (5.67) gives

$$d\Delta p = \frac{\phi - \Delta p / \Delta t}{1 / \Delta t - \phi_{\Delta p} - h \phi_r + c \phi_{\sigma_e}} \quad (5.68)$$

which is solved iteratively. The plastic strain increment is then determined from

$$\Delta \epsilon^p = \frac{3}{2} \Delta p \frac{\sigma' - x'}{J(\sigma' - x')} \equiv \frac{3}{2} \Delta p \frac{\sigma^{\text{tr}'} - x'}{\sigma_e^{\text{tr}}}.$$

5.5.3 Consistent tangent stiffness for viscoplasticity with isotropic hardening

The predictor–corrector form of the stress is

$$\sigma' = \sigma^{\text{tr}'} - 2G \Delta p n \quad \text{or} \quad \sigma = \sigma^{\text{tr}} - 2G \Delta p n, \quad (5.69)$$

where

$$n = \frac{3}{2} \frac{\sigma^{\text{tr}'}}{\sigma_e^{\text{tr}}} = \frac{3}{2} \frac{\sigma'}{\sigma_e} \quad (5.70)$$

and

$$\sigma_e = \sigma_e^{\text{tr}} - 3G\Delta p.$$

Rearranging (5.70) gives

$$\boldsymbol{\sigma}' = \frac{\sigma_e}{\sigma_e^{\text{tr}}} \boldsymbol{\sigma}^{\text{tr}'}$$

and applying the differential operator

$$\delta \boldsymbol{\sigma}' = \frac{\sigma_e}{\sigma_e^{\text{tr}}} \delta \boldsymbol{\sigma}^{\text{tr}'} + \left(\frac{\delta \sigma_e}{\sigma_e^{\text{tr}}} - \frac{\sigma_e}{\sigma_e^{\text{tr}}} \frac{\delta \sigma_e^{\text{tr}}}{\sigma_e^{\text{tr}}} \right) \boldsymbol{\sigma}^{\text{tr}'}. \quad (5.71)$$

Now,

$$\delta \sigma_e^{\text{tr}} = \frac{1}{\sigma_e^{\text{tr}}} \frac{3}{2} \boldsymbol{\sigma}^{\text{tr}'} : \delta \boldsymbol{\sigma}^{\text{tr}'} \quad (5.72)$$

and

$$\delta \sigma_e = \frac{1}{\sigma_e} \frac{3}{2} \boldsymbol{\sigma}' : \delta \boldsymbol{\sigma}'. \quad (5.73)$$

Substituting (5.72) and (5.73) into (5.71) and eliminating $\boldsymbol{\sigma}'$ using (5.70) gives

$$\delta \boldsymbol{\sigma}' = \frac{3}{2} \frac{\boldsymbol{\sigma}^{\text{tr}'}}{\sigma_e^{\text{tr}}} \frac{\boldsymbol{\sigma}^{\text{tr}'}}{\sigma_e^{\text{tr}}} : \delta \boldsymbol{\sigma}' + \frac{\sigma_e}{\sigma_e^{\text{tr}}} \delta \boldsymbol{\sigma}^{\text{tr}'} - \frac{\sigma_e}{\sigma_e^{\text{tr}}} \frac{3}{2} \frac{\boldsymbol{\sigma}^{\text{tr}'}}{\sigma_e^{\text{tr}}} \frac{\boldsymbol{\sigma}^{\text{tr}'}}{\sigma_e^{\text{tr}}} : \delta \boldsymbol{\sigma}^{\text{tr}'}$$

Because of the contracted product of $\delta \boldsymbol{\sigma}'$ in the first term on the right-hand side, we will substitute for this using the differential form of (5.50)

$$\delta \boldsymbol{\sigma}' = \delta \boldsymbol{\sigma}^{\text{tr}'} - 2G\delta \Delta p \mathbf{n}$$

to give

$$\begin{aligned} \delta \boldsymbol{\sigma}' &= \frac{3}{2} \frac{\boldsymbol{\sigma}^{\text{tr}'}}{\sigma_e^{\text{tr}}} \frac{\boldsymbol{\sigma}^{\text{tr}'}}{\sigma_e^{\text{tr}}} : (\delta \boldsymbol{\sigma}^{\text{tr}'} - 2G\delta \Delta p \mathbf{n}) + \frac{\sigma_e}{\sigma_e^{\text{tr}}} \delta \boldsymbol{\sigma}^{\text{tr}'} - \frac{\sigma_e}{\sigma_e^{\text{tr}}} \frac{3}{2} \frac{\boldsymbol{\sigma}^{\text{tr}'}}{\sigma_e^{\text{tr}}} \frac{\boldsymbol{\sigma}^{\text{tr}'}}{\sigma_e^{\text{tr}}} : \delta \boldsymbol{\sigma}^{\text{tr}'} \\ &= -\frac{3}{2} \frac{\boldsymbol{\sigma}^{\text{tr}'}}{\sigma_e^{\text{tr}}} \frac{\boldsymbol{\sigma}^{\text{tr}'}}{\sigma_e^{\text{tr}}} : 2G\delta \Delta p \mathbf{n} + \frac{\sigma_e}{\sigma_e^{\text{tr}}} \delta \boldsymbol{\sigma}^{\text{tr}'} + \left(1 - \frac{\sigma_e}{\sigma_e^{\text{tr}}} \right) \frac{3}{2} \frac{\boldsymbol{\sigma}^{\text{tr}'}}{\sigma_e^{\text{tr}}} \frac{\boldsymbol{\sigma}^{\text{tr}'}}{\sigma_e^{\text{tr}}} : \delta \boldsymbol{\sigma}^{\text{tr}'}. \end{aligned}$$

Now,

$$\frac{3}{2} \frac{\boldsymbol{\sigma}^{\text{tr}'}}{\sigma_e^{\text{tr}}} : \mathbf{n} = \mathbf{n} : \mathbf{n} = \frac{3}{2}$$

so

$$\delta \boldsymbol{\sigma}' = -\frac{\boldsymbol{\sigma}^{\text{tr}'}}{\sigma_e^{\text{tr}}} : 3G\delta \Delta p \mathbf{n} + \frac{\sigma_e}{\sigma_e^{\text{tr}}} \delta \boldsymbol{\sigma}^{\text{tr}'} + \left(1 - \frac{\sigma_e}{\sigma_e^{\text{tr}}} \right) \frac{3}{2} \frac{\boldsymbol{\sigma}^{\text{tr}'}}{\sigma_e^{\text{tr}}} \frac{\boldsymbol{\sigma}^{\text{tr}'}}{\sigma_e^{\text{tr}}} : \delta \boldsymbol{\sigma}^{\text{tr}'}. \quad (5.74)$$

The viscoplastic constitutive equation is written as, from (5.57),

$$\Delta p = \phi(\boldsymbol{\sigma}, r) \Delta t \quad (5.75)$$

166 Implicit and explicit integration

so that

$$\delta \Delta p = (\phi_\sigma : \delta \sigma + \phi_r \delta r) \Delta t. \quad (5.76)$$

Let us assume isotropic hardening of the form

$$\delta r = q(r) \delta p.$$

Because δp is again an infinitesimal increment in p (as opposed to the plastic strain increment), this can be written as

$$\delta r = q(r) \delta \Delta p. \quad (5.77)$$

Substituting this together with the second equation of (5.69) for $\delta \sigma$ into (5.76) gives

$$\delta \Delta p = (\phi_\sigma : (\delta \sigma^{\text{tr}} - 2G \delta \Delta p \mathbf{n}) + \phi_r q(r) \delta \Delta p) \Delta t$$

and rearranging

$$\delta \Delta p = \frac{\phi_\sigma : \delta \sigma^{\text{tr}}}{1/\Delta t + 2G \phi_\sigma : \mathbf{n} + \phi_r q(r)}. \quad (5.78)$$

Substituting into (5.74) gives

$$\delta \sigma' = -\frac{\sigma^{\text{tr}'}}{\sigma_e^{\text{tr}}} : 3G \frac{\phi_\sigma : \delta \sigma^{\text{tr}}}{1/\Delta t + 2G \phi_\sigma : \mathbf{n} + \phi_r q(r)} \mathbf{n} + \frac{\sigma_e}{\sigma_e^{\text{tr}}} \delta \sigma^{\text{tr}'} + \left(1 - \frac{\sigma_e}{\sigma_e^{\text{tr}}}\right) \frac{3}{2} \frac{\sigma^{\text{tr}'}}{\sigma_e^{\text{tr}}} \frac{\sigma^{\text{tr}'}}{\sigma_e^{\text{tr}}} : \delta \sigma^{\text{tr}'}. \quad (5.79)$$

Let us write

$$\alpha = -\frac{3G}{1/\Delta t + 2G \phi_\sigma : \mathbf{n} + \phi_r q(r)}, \quad \beta = \frac{\sigma_e}{\sigma_e^{\text{tr}}}, \quad \gamma = \frac{3}{2} \left(1 - \frac{\sigma_e}{\sigma_e^{\text{tr}}}\right),$$

then

$$\delta \sigma' = \alpha \frac{\sigma^{\text{tr}'}}{\sigma_e^{\text{tr}}} \phi_\sigma : \delta \sigma^{\text{tr}} + \beta \delta \sigma^{\text{tr}'} + \gamma \frac{\sigma^{\text{tr}'}}{\sigma_e^{\text{tr}}} \frac{\sigma^{\text{tr}'}}{\sigma_e^{\text{tr}}} : \delta \sigma^{\text{tr}'}. \quad (5.79)$$

Now,

$$\delta \sigma^{\text{tr}'} = 2G \delta \boldsymbol{\varepsilon}' = 2G \delta \boldsymbol{\varepsilon} - \frac{2}{3} G (\delta \boldsymbol{\varepsilon} : \mathbf{I}) \mathbf{I}.$$

Because ϕ is a function of the effective stress, its derivatives with respect to the stress components are deviatoric, and hence $\phi_\sigma : \delta \sigma^{\text{tr}} = \phi_\sigma : (\delta \sigma^{\text{tr}'} + (1/3) \delta \sigma^{\text{tr}} : \mathbf{I}) = \phi_\sigma : \delta \sigma^{\text{tr}'}$ since $\phi_\sigma : \mathbf{I} = 0$. In addition,

$$\delta \sigma = \delta \sigma' + K \mathbf{I} : \delta \boldsymbol{\varepsilon}$$

so that (5.79) becomes

$$\delta \sigma = \left[2G \alpha \frac{\sigma^{\text{tr}'}}{\sigma_e^{\text{tr}}} \phi_\sigma + \left(K - \frac{2}{3} G \beta\right) \mathbf{I} + 2G \gamma \frac{\sigma^{\text{tr}'}}{\sigma_e^{\text{tr}}} \frac{\sigma^{\text{tr}'}}{\sigma_e^{\text{tr}}} \right] : \delta \boldsymbol{\varepsilon} + 2G \beta \delta \boldsymbol{\varepsilon} \quad (5.80)$$

which gives the consistent tangent stiffness.

5.6 Incrementally objective integration for large deformations

So far, we have addressed the update of stress over a given time increment on the basis that there is no incremental rotation. In large deformation analyses, however, in which deformations and rigid body rotations can become large, we need to take account of the effect of incremental rotation on the determination of the updated stress. Figure 5.1 shows the representation of a body in its original configuration and then in deformed configurations at times t and $t + \Delta t$.

In the deformed configurations, the local material (or co-rotational) coordinate systems are shown indicating that an incremental rotation has occurred between the configurations at times t and $t + \Delta t$. We need to ensure that the stress update is carried out with respect to the same reference frame. For example, in using a user-defined subroutine for plasticity in ABAQUS, the user is supplied with the strains at the beginning and end of the time increment, together with the stress at the beginning of the time increment, but all these quantities and other tensor quantities have usually already been incrementally rotated to account for the incremental rigid body rotation. We shall return to this in Chapter 6. For now, however, we shall look at an incrementally objective stress update.

First, referring to Fig. 5.2, let us assume we know the stresses, σ_t , at time t with respect to the material reference frame, that is, the *undeformed* configuration at that time. Also, we have determined the spin, \mathbf{W} , given by the antisymmetric part of the velocity gradient.

The stress rate, $\dot{\sigma}$, with respect to the material reference frame, or undeformed configuration, at time t , taking full account of the incremental rigid body rotation, is

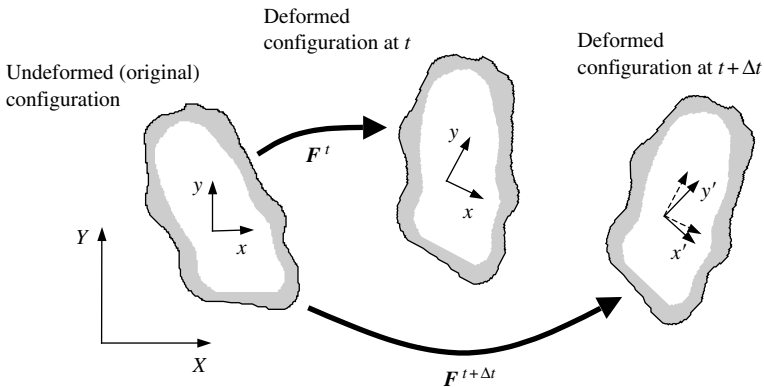


Fig. 5.2 A body in its original (undeformed) configuration and in deformed configurations at times t and $t + \Delta t$.

given by

$$\dot{\sigma} = \overset{\nabla}{\sigma} + \mathbf{W}_t \sigma_t - \sigma_t \mathbf{W}_t \quad (5.81)$$

so that the updated stress (written explicitly) with respect to the undeformed configuration at time t is simply

$$\sigma_{t+\Delta t} = \sigma + \dot{\sigma} \Delta t.$$

We can write Equation (5.81) in incremental form, if we wish, as

$$\Delta \sigma = \Delta \overset{\nabla}{\sigma} + (\mathbf{W}_t \sigma_t - \sigma_t \mathbf{W}_t) \Delta t \quad (5.82)$$

which we may also write as

$$\Delta \sigma = \Delta \overset{\nabla}{\sigma} + \mathbf{R} \sigma_t \mathbf{R}^T \quad (5.83)$$

in which $\Delta \overset{\nabla}{\sigma}$ is the increment in objective, or co-rotational, stress, and \mathbf{R} is a rotation to be determined.

We shall further consider these approaches in Chapter 6, concerned with the implementation of plasticity models into finite element code.

Further reading

- Bathe, K.-J. (1996). *Finite Element Procedures*. Prentice Hall, New Jersey, revised edition.
- Belytschko, T., Liu, K.W., and Moran, B. (2000). *Nonlinear Finite Element Analysis for Continua and Structures*. John Wiley & Sons, New York.
- Simo, J.C. and Hughes, T.J.R. (1998). *Computational Inelasticity*. Springer-Verlag, New York.
- Chaboche, J.-L. (1986). 'Time-independent constitutive theories for cyclic plasticity'. *International Journal of Plasticity*, 2(2), 149–188.
- Hughes, T.J.R. (1984). 'Numerical implementation of constitutive models: rate-independent deviatoric plasticity'. In Nemat Nasser S., Asaro R.J., and Hegemier G.A. (eds), *Theoretical Foundation for Large-Scale Computations of Non-linear Material Behaviour*, Martinus Nijhoff Publication, The Netherlands, 29–57.
- Krieg, R.D. and Key, S.W. (1976). 'Implementation of a time dependent plasticity theory into structural computer programs', In *Constitutive Equations in Viscoplasticity: Computational and Engineering Aspects* (eds) Stricklin J.A. and Saczalski K.J.), ASME.

6. Implementation of plasticity models into finite element code

6.1 Introduction

Several commercial finite element software packages (e.g. ABAQUS, LSDyna, and MARC) provide the facility for users to specify their own material models. In ABAQUS, the user is required to provide a Fortran subroutine called a ‘UMAT’. This chapter is concerned with the implementation of plasticity models into finite element code, which is carried out, by example, in using ABAQUS. In particular, we start by developing an ABAQUS UMAT for elasticity, and discuss the tests necessary to verify the model implementation into ABAQUS. We go on to consider isotropic hardening plasticity with explicit and implicit integration, with continuum and consistent tangent stiffnesses, large deformation formulations using rotated variables provided by ABAQUS, and from first principles using the deformation gradient. We use the problem of simple shear with elasticity to verify the large deformation implementations. We then present an implicit implementation for elasto-viscoplasticity (and creep). All the Fortran coding, together with the necessary ABAQUS input files, are available through the OUP website.

Finite element code is often modular in structure, whether it be commercial code or written in-house. An important module is that relating to material behaviour; in other words, the constitutive stress response of the material given prescribed conditions of deformation. In ABAQUS, but in a similar way for all codes, a range of information is passed into the material module relating to both the beginning and end of a time increment. In particular, stress, strain, and deformation gradient are provided at the beginning of the time increment. Strain and the deformation gradient are also provided at the end of the increment. Within the module, it is then necessary to execute three tasks. First, the stresses at the end of the time increment must be determined and, second, for the case of an implicit analysis (i.e. the finite element momentum balance or equilibrium equations are solved implicitly) using ABAQUS standard, for example, the material Jacobian, or tangent stiffness, must also be provided. Third, any state variables (such as the isotropic hardening variable or effective plastic strain) must

be updated to the end of the time increment. In fact, in coding an ABAQUS UMAT, a large range of information is provided, some of which will be referred to later. However, the job of the UMAT is clear: to update the stresses and state variables to the end of the time increment and to provide the Jacobian. We start by addressing elasticity.

6.2 Elasticity implementation

We discuss elasticity and its implementation into a UMAT for two main reasons. First, it provides a good introduction to writing and testing a UMAT subroutine for those who are new to the process. Second, it provides a basis from which elasto-plasticity models may be developed. For the latter reason, while is no way essential for elasticity, we use an incremental approach in implementing the linear elastic equations.

In Chapter 5, Hooke's law was given in an incremental form in Equation (5.21) together with the material Jacobian, for the case in which there are no out of plane shears (e.g. plane strain and axisymmetric problems). With knowledge of the increment in strains (provided to the UMAT), together with the specification of elastic constants (we shall take $E = 210$ GPa and $\nu = 0.3$ throughout), the stress increment is obtained either from Equation (5.21), or its equivalent written in Voigt notation,

$$\Delta\sigma = \mathbf{C}\Delta\epsilon^e = \begin{pmatrix} 2G + \lambda & \lambda & \lambda & 0 \\ \lambda & 2G + \lambda & \lambda & 0 \\ \lambda & \lambda & 2G + \lambda & 0 \\ 0 & 0 & 0 & G \end{pmatrix} \begin{pmatrix} \Delta\epsilon_{11} \\ \Delta\epsilon_{22} \\ \Delta\epsilon_{33} \\ \Delta\gamma_{12} \end{pmatrix}. \quad (6.1)$$

Because ABAQUS provides most tensor quantities in vector (Voigt) form, it may be more convenient to use Equation (6.1) than the tensor form given in (5.21). However, this is not always the case, and later we shall use the tensor form in preference, particularly where it is necessary to work from the deformation gradient. Note that the shear strain quantities provided by ABAQUS are always *engineering shears*, that is, twice the tensorial shear strains. It is also important to check the ordering of shear quantities, which can vary depending on element type used. Equation (6.1) is suitable for plane strain and axisymmetric problems, but not for problems of plane stress or three dimensions, for which different stiffness matrices are required. For linear elasticity, the material Jacobian is just the elastic stiffness matrix so that specification of the Jacobian in the UMAT is easy. The coding required for the UMAT for linear elasticity for plane strain, axisymmetric, and three-dimensional problems, is available through the OUP website. A complete list of all the UMAT coding, together with ABAQUS input files, is given in Appendix B.

6.3 Verification of implementations

The verification of the model implementation is vital. For complex material models, this requires the development of an independent solver (which will often be numerical) for uniaxial and pure shear problems so that direct comparison with the results obtained using the UMAT can be made. In addition, it is necessary to test the UMAT using a single, and where appropriate, multiple elements, for conditions of strain control and load control under uniaxial and pure shear conditions. If possible, perhaps by ‘switching off’ parts of the model implemented into the UMAT, make comparisons with a multiaxial problem with non-uniform strain and stress distributions for which the solution is known (either an independent solution or one obtained using an internal ABAQUS model). In this chapter, we shall not carry out all of the verification tests described for all the model implementations, but it is certainly advisable to do so for new model implementations into UMATs. Because of their importance, we go through some of the possible verification tests step by step.

1. *Single and multiple element uniaxial tests.* Figure 6.1 shows an axisymmetric single- and four-element unit square which is subjected to uniaxial displacement or force control in the z -direction producing uniform, uniaxial stress, σ_{zz} , and strain, ε_{zz} , with $\varepsilon_{rz} = \sigma_{rr} = \sigma_{\theta\theta} = \sigma_{rz} = 0$, which can be compared with independent closed-form solutions. The four-element problem is important since it introduces a ‘free’ node, which does not exist for the single four-noded axisymmetric element. The force controlled test is important for checking errors in the Jacobian.

2. *Single element simple shear test.* The uniaxial tests in (1) do not involve the shear terms at all, so it is important to include a problem which tests these terms, particularly because of the potential for errors with the use of engineering shear strains rather than their tensorial counterparts. Figure 6.2 shows a plane strain single-element unit square under simple shear loading. For small deformations, $\varepsilon_{xx} = \varepsilon_{yy} = \sigma_{xx} = \sigma_{yy} = 0$,

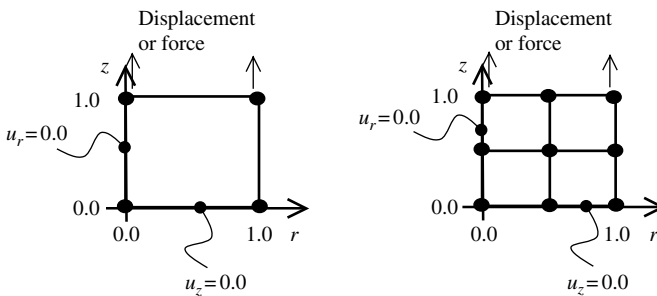


Fig. 6.1 Schematic diagram showing an axisymmetric single- and four-element unit square under uniaxial displacement or force controlled loading.

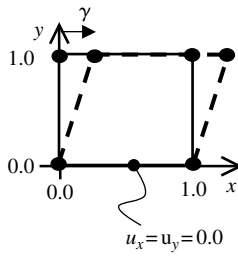


Fig. 6.2 Schematic diagram showing a plane strain single-element unit square under simple shear loading.

and uniform shear strain, γ_{xy} , and stress, σ_{xy} , are produced which can be compared with independent closed-form solutions.

3. *Non-uniform strain and stress field.* Often, a comparison test which generates non-uniform strain and stress fields will not be possible because a comparison may well not exist, and a closed-form solution is now no longer possible. However, it is sometimes possible to simplify the implemented plasticity model (e.g. by turning off the porosity in a Gurson-type porous plasticity model) such that a comparison with another solution (e.g. produced using one of the many built-in models contained within ABAQUS) is then possible. While this will not test all the features of the model implemented into the UMAT, it nonetheless may test a good number of them, and may therefore be worthwhile. Later in the chapter, both an implicit and explicit implementation of isotropic hardening plasticity are tested in this way by comparing the results obtained with those produced using the built-in ABAQUS model.

6.4 Isotropic hardening plasticity implementation

In Chapter 5, we presented both explicit and implicit integration of the equations for linear strain hardening isotropic plasticity, together with the consistent tangent stiffness for the implicit scheme. We will implement both integration schemes into ABAQUS UMATs and discuss the advantages and disadvantages of each. We start with the explicit scheme which was described at the beginning of Section 5.2, and introduce the *continuum Jacobian*.

6.4.1 Explicit integration for isotropic hardening plasticity with continuum Jacobian

We may summarize the implementation as follows. All quantities are assumed to be given at time, t , that is, at the start of the time increment, unless indicated

otherwise:

(i) Determine the yield function

$$f = \sigma_e - r - \sigma_y = \left(\frac{3}{2} \boldsymbol{\sigma}' : \boldsymbol{\sigma}' \right)^{1/2} - r - \sigma_y. \quad (6.2)$$

(ii) Determine if actively yielding

$$\text{Is } f > 0?$$

(iii) Determine the plastic multiplier

$$f > 0, \quad d\lambda = \frac{\mathbf{n} \cdot \mathbf{C} \, d\boldsymbol{\varepsilon}}{\mathbf{n} \cdot \mathbf{C} \mathbf{n} + h}, \quad (6.3)$$

$$f < 0, \quad d\lambda = 0.$$

(iv) Determine stress and isotropic hardening increments

$$d\boldsymbol{\sigma} = \mathbf{C} \, d\boldsymbol{\varepsilon}^e = \mathbf{C} (d\boldsymbol{\varepsilon} - d\lambda \mathbf{n}), \quad (6.4)$$

$$dr = h \, dp = h \, d\lambda.$$

(v) Update all quantities to the end of the time increment, using explicit integration

$$\boldsymbol{\sigma}_{t+\Delta t} = \boldsymbol{\sigma} + d\boldsymbol{\sigma},$$

$$\boldsymbol{\varepsilon}_{t+\Delta t}^p = \boldsymbol{\varepsilon}^p + d\boldsymbol{\varepsilon}^p, \quad (6.5)$$

$$r_{t+\Delta t} = r + dr.$$

(vi) Determine Jacobian.

(vii) End.

We now address the determination of the Jacobian. In Chapter 5, we derived the *consistent* tangent stiffness for the implicit integration scheme. For the purposes of the explicit integration considered here, we introduce what is sometimes referred to as the *continuum* Jacobian. That is, it is not derived explicitly on the basis of the integration scheme, but directly from the constitutive equations. We start from the stress–strain relationship written in Voigt notation

$$d\boldsymbol{\sigma} = \mathbf{C} \, d\boldsymbol{\varepsilon}^e = \mathbf{C} (d\boldsymbol{\varepsilon} - d\lambda \mathbf{n}), \quad (6.6)$$

which we may write out fully for conditions of axial symmetry or plane strain as

$$\begin{pmatrix} d\sigma_{11} \\ d\sigma_{22} \\ d\sigma_{33} \\ d\sigma_{12} \end{pmatrix} = \begin{pmatrix} d\sigma_1 \\ d\sigma_2 \\ d\sigma_3 \\ d\sigma_4 \end{pmatrix} = \begin{pmatrix} C_{11} & C_{12} & C_{13} & C_{14} \\ & C_{22} & C_{23} & C_{24} \\ & & C_{33} & C_{34} \\ \text{sym} & & & C_{44} \end{pmatrix} \left(\begin{pmatrix} d\varepsilon_1 \\ d\varepsilon_2 \\ d\varepsilon_3 \\ d\varepsilon_4 \end{pmatrix} - d\lambda \begin{pmatrix} n_1 \\ n_2 \\ n_3 \\ n_4 \end{pmatrix} \right). \quad (6.7)$$

174 Implementation of plasticity models

We may write the Jacobian (here symmetric) as

$$\mathbf{J} = \frac{\partial \mathbf{d}\boldsymbol{\sigma}}{\partial \mathbf{d}\boldsymbol{\varepsilon}} = \begin{pmatrix} J_{11} & J_{12} & J_{13} & J_{14} \\ & J_{22} & J_{23} & J_{24} \\ & & J_{33} & J_{34} \\ \text{sym} & & & J_{44} \end{pmatrix} \quad (6.8)$$

so that, for example, the first term is

$$J_{11} = \frac{\partial \mathbf{d}\sigma_1}{\partial \mathbf{d}\varepsilon_1} = C_{11} - \frac{\partial \mathbf{d}\lambda}{\partial \mathbf{d}\varepsilon_1} (C_{11}n_1 + C_{12}n_2 + C_{13}n_3 + C_{14}n_4).$$

With some algebra we may show, therefore, that

$$\mathbf{J} = \mathbf{C} - \mathbf{C}\mathbf{n} \otimes \frac{\partial \mathbf{d}\lambda}{\partial \mathbf{d}\boldsymbol{\varepsilon}}, \quad (6.9)$$

where \otimes is the dyadic product of two vectors, details of which may be found in Appendix A. In a similar way, by considering the numerator of the plastic multiplier given in Equation (6.3), we may show that

$$\frac{\partial \mathbf{d}\lambda}{\partial \mathbf{d}\boldsymbol{\varepsilon}} = \frac{\mathbf{C}\mathbf{n}}{\mathbf{n} \cdot \mathbf{C}\mathbf{n} + h}$$

so that the continuum Jacobian is

$$\mathbf{J} = \mathbf{C} - \frac{\mathbf{C}\mathbf{n} \otimes \mathbf{C}\mathbf{n}}{\mathbf{n} \cdot \mathbf{C}\mathbf{n} + h}. \quad (6.10)$$

The explicit integration and provision of Jacobian is then complete. An ABAQUS UMAT containing this formulation, together with various input files for uniaxial displacement and load control, together with a four-point beam bending problem, are available via the OUP website (full details are given in Appendix B). In addition, the very same problems are analysed using the built-in ABAQUS linear strain hardening plasticity model (chosen to represent a material with $E = 210,000$ GPa, $\nu = 0.3$, $\sigma_y = 240$ MPa, and $h = 1206$ MPa). In all the analyses using the explicit UMAT, the maximum time increment allowed in the analysis is carefully chosen to ensure stability and accuracy. Despite this, at the elastic–plastic transition, the stress at first yield is overestimated because the stress at the start of the increment was determined on the basis of elastic behaviour in the previous increment. With an explicit scheme, this is never corrected so that the stresses remain slightly overestimated throughout the analysis. The error in stress can be reduced by decreasing the time increment size, but at the cost of the computer CPU time and error accumulation. In any case, many more time increments are required using the explicit UMAT than are required using the built-in ABAQUS implicit plasticity integration. This is a further serious shortcoming of the explicit integration method, which needs to be weighed against the advantage

of simplicity, particularly for complex constitutive equations. However, despite considerably longer computer CPU times, the results obtained for the four-point bend simulation from the explicit UMAT and the built-in ABAQUS plasticity model are found to be near-identical. We consider an implicit implementation in Section 6.4.2.

6.4.2 Implicit integration for isotropic hardening plasticity with consistent Jacobian

We may summarize the implementation as follows. As opposed to the explicit case, all quantities are now assumed to be given at the end of the time increment, that is, at time $t + \Delta t$, unless otherwise indicated.

- (i) Determine the elastic trial stress

$$\boldsymbol{\sigma}^{\text{tr}} = \boldsymbol{\sigma}_t + 2G\Delta\boldsymbol{\epsilon} + \lambda I\Delta\boldsymbol{\epsilon} : \mathbf{I}. \quad (6.11)$$

- (ii) Determine the trial yield function

$$f = \sigma_e^{\text{tr}} - r - \sigma_y = \left(\frac{3}{2} \boldsymbol{\sigma}^{\text{tr}'} : \boldsymbol{\sigma}^{\text{tr}'} \right)^{1/2} - r - \sigma_y. \quad (6.12)$$

- (iii) Determine if actively yielding

$$\text{Is } f > 0?$$

- (iv) If yes, use Newton iteration to determine the effective plastic strain increment

$$\begin{aligned} r^{(k)} &= r_t + h\Delta p, \\ d\Delta p &= \frac{\sigma_e^{\text{tr}} - 3G\Delta p^{(k)} - r^{(k)} - \sigma_y}{3G + h}, \\ \Delta p^{(k+1)} &= \Delta p^{(k)} + d\Delta p. \end{aligned} \quad (6.13)$$

Otherwise,

$$\Delta p = 0.$$

- (v) Determine plastic and elastic strain and stress increments

$$\begin{aligned} \Delta\boldsymbol{\epsilon}^{\text{p}} &= \frac{3}{2} \Delta p \frac{\boldsymbol{\sigma}^{\text{tr}'}}{\sigma_e^{\text{tr}}}, \\ \Delta\boldsymbol{\epsilon}^{\text{e}} &= \Delta\boldsymbol{\epsilon} - \Delta\boldsymbol{\epsilon}^{\text{p}}, \\ \Delta\boldsymbol{\sigma} &= 2G\Delta\boldsymbol{\epsilon}^{\text{e}} + \lambda I\Delta\boldsymbol{\epsilon}^{\text{e}} : \mathbf{I}. \end{aligned} \quad (6.14)$$

- (vi) Update all quantities to the end of the time increment

$$\begin{aligned} \boldsymbol{\sigma} &= \boldsymbol{\sigma}_t + \Delta\boldsymbol{\sigma}, \\ p &= p_t + \Delta p. \end{aligned} \quad (6.15)$$

(vii) Determine consistent Jacobian

$$\delta\sigma = 2GQ \frac{\sigma^{\text{tr}'}}{\sigma_e^{\text{tr}}} \frac{\sigma^{\text{tr}'}}{\sigma_e^{\text{tr}}} : \delta\epsilon + 2GR\delta\epsilon + \left(K - \frac{2}{3}GR \right) \mathbf{II} : \delta\epsilon. \quad (6.16)$$

(viii) End.

An ABAQUS UMAT containing this formulation, together with various input files for uniaxial displacement and load control, together with a four-point beam bending problem, are available through the OUP website (full details are given in Appendix B). In addition, as before, the very same problems are analysed using the built-in ABAQUS linear strain hardening plasticity model. Using implicit integration with the consistent tangent stiffness eliminates the problem which occurred at the elastic–plastic transition when using explicit integration. In addition, the use of implicit integration enables much larger time increments to be used, therefore significantly reducing CPU times. The disadvantage of the implicit formulation is simply the difficulty in obtaining the consistent tangent stiffness for complex constitutive equations. Often, analytical forms are simply not obtainable, in which case a numerical procedure may be possible. The results obtained for the four-point bend simulation from the implicit UMAT and the built-in ABAQUS plasticity model are found to be identical.

6.5 Large deformation implementations

We have not yet differentiated between small and large deformation implementations in this chapter. In fact, the UMATs discussed above for both explicit and implicit schemes are suitable for both small and large deformation problems using ABAQUS. This is because the necessary rigid body rotations for the strains and stresses have already been carried out by ABAQUS before they are provided to the UMAT routine. That is, referring back to Section 5.6, the large deformation stress update necessary is

$$\Delta\sigma = \Delta\overset{\nabla}{\sigma} + (\mathbf{W}\sigma_t - \sigma_t\mathbf{W})\Delta t = \Delta\overset{\nabla}{\sigma} + \mathbf{R}\sigma_t\mathbf{R}^T \quad (6.17)$$

in which $\Delta\overset{\nabla}{\sigma}$ is the co-rotational stress increment. The stress, σ_t , at the start of the time increment (and the strain) has already been rotated by ABAQUS (i.e. the stress provided at the start of the time increment is effectively $\mathbf{R}\sigma_t\mathbf{R}^T$) so that all we need to do within the UMAT is to carry out the stress update. Sometimes, depending on the plasticity model employed, it is necessary to use internal variables which are also tensor quantities. An example is the back stress in a kinematic hardening model. The components of the back stress will need to be updated within the UMAT (just like the scalar isotropic hardening variable in the previous sections) and stored in what are called state variable arrays in ABAQUS. Because state variables are not modified

by ABAQUS, it is necessary for the user to carry out the rigid body rotations on tensorial state variables. In fact, ABAQUS provides a utility subroutine to simplify this process. If, for example, the tensorial variable recovered from the state variable array at the start of the increment is, say, \mathbf{x}_t , then the user must carry out the rigid body rotation $\mathbf{R}\mathbf{x}_t\mathbf{R}^T$ before updating \mathbf{x} to the end of the time increment within the UMAT. The rotation is carried out by a single call of the utility subroutine *rotsig* detailed in the ABAQUS manuals.

Sometimes, constitutive equations for elasticity and plasticity are formulated in terms of the deformation gradient, \mathbf{F} . Examples include hyperelasticity—large strain non-linear elasticity and crystal plasticity. It may be, however, that the user simply wishes to work from the deformation gradient rather than use the strain and stress quantities provided by ABAQUS to the UMAT subroutine. In Section 6.5.1, we present a large deformation implementation based on an explicit scheme.

6.5.1 Implementation using the deformation gradient

We may summarize the implementation as follows. In this explicit approach, all quantities are assumed to be given at time, t , that is, at the start of the time increment, unless indicated otherwise.

- (i) Determine the velocity gradient

$$\mathbf{L} = \dot{\mathbf{F}}\mathbf{F}^{-1}. \quad (6.18)$$

- (ii) Determine the rate of deformation and spin

$$\mathbf{D} = \frac{1}{2}(\mathbf{L} + \mathbf{L}^T), \quad \mathbf{W} = \frac{1}{2}(\mathbf{L} - \mathbf{L}^T). \quad (6.19)$$

- (iii) Determine the yield function

$$f = \sigma_e - r - \sigma_y = \left(\frac{3}{2} \boldsymbol{\sigma}' : \boldsymbol{\sigma}' \right)^{1/2} - r - \sigma_y. \quad (6.20)$$

- (iv) Determine if actively yielding

$$\text{Is } f > 0? \quad (6.21)$$

- (v) Determine rate of plastic deformation

$$\begin{aligned} f > 0, & \quad \mathbf{D}^P = \text{as specified by constitutive equation,} \\ f < 0, & \quad \mathbf{D}^P = 0. \end{aligned} \quad (6.22)$$

178 Implementation of plasticity models

- (vi) Determine rate of elastic deformation and Jaumann stress rate and isotropic hardening rate

$$\begin{aligned} \mathbf{D}^e &= \mathbf{D} - \mathbf{D}^p, \\ \overset{\nabla}{\boldsymbol{\sigma}} &= 2G\mathbf{D}^e + \lambda\mathbf{I}\mathbf{D}^e : \mathbf{I}, \\ \dot{r} &= h\dot{p}. \end{aligned} \quad (6.23)$$

- (vii) Determine stresses with respect to material reference

$$\dot{\boldsymbol{\sigma}} = \overset{\nabla}{\boldsymbol{\sigma}} + \mathbf{W}\boldsymbol{\sigma} - \boldsymbol{\sigma}\mathbf{W}. \quad (6.24)$$

- (viii) Update all quantities to the end of the time increment, using explicit integration

$$\begin{aligned} \boldsymbol{\sigma}_{t+\Delta t} &= \boldsymbol{\sigma} + \dot{\boldsymbol{\sigma}} \Delta t, \\ r_{t+\Delta t} &= r + \dot{r} \Delta t. \end{aligned} \quad (6.25)$$

- (ix) Determine Jacobian.

- (x) End.

We will next address the verification of a large deformation implementation, which is valid for both the implicit and explicit implementations in Sections 6.4.1 and 6.4.2. Note that uniaxial displacement or force controlled loading will not test whether the rigid body rotations are being calculated correctly, since for these cases, the continuum spin, \mathbf{W} , is zero. A good test, however, is provided in the form of simple shear if we allow the strains to become quite large. To simplify matters, we will ‘switch off’ the plasticity and allow elasticity only, since the test is being carried out to check the rigid body rotation calculation rather than the constitutive response.

We obtained the deformation gradient for simple shear in Section 3.5.1 as

$$\mathbf{F} = \begin{bmatrix} 1 & \delta \\ 0 & 1 \end{bmatrix}.$$

Considering a constant rate of shearing, $\dot{\delta}$, the velocity gradient is

$$\mathbf{L} = \begin{bmatrix} 0 & \dot{\delta} \\ 0 & 0 \end{bmatrix}$$

so that the rate of deformation and spin are

$$\mathbf{D} = \frac{1}{2} \begin{bmatrix} 0 & \dot{\delta} \\ \dot{\delta} & 0 \end{bmatrix}, \quad \mathbf{W} = \frac{1}{2} \begin{bmatrix} 0 & \dot{\delta} \\ -\dot{\delta} & 0 \end{bmatrix}.$$

Note that the spin is non-zero so that rigid body rotation, together with stretch, is occurring.

The Jaumann stress rate is given by

$$\overset{\nabla}{\boldsymbol{\sigma}} = 2G\mathbf{D} + \lambda\mathbf{ID} : \mathbf{I} = G \begin{bmatrix} 0 & \dot{\delta} \\ \dot{\delta} & 0 \end{bmatrix} \quad (6.26)$$

and the stress rate with respect to the material (undeformed) reference is

$$\dot{\boldsymbol{\sigma}} = \begin{bmatrix} \dot{\sigma}_{xx} & \dot{\sigma}_{xy} \\ \dot{\sigma}_{xy} & \dot{\sigma}_{yy} \end{bmatrix}, \quad (6.27)$$

which is given in terms of the Jaumann stress rate by

$$\dot{\boldsymbol{\sigma}} = \overset{\nabla}{\boldsymbol{\sigma}} + \mathbf{W}\boldsymbol{\sigma} - \boldsymbol{\sigma}\mathbf{W}$$

so that substituting for the spin and (6.26) and (6.27) gives

$$\begin{bmatrix} \dot{\sigma}_{xx} & \dot{\sigma}_{xy} \\ \dot{\sigma}_{xy} & \dot{\sigma}_{yy} \end{bmatrix} = G\dot{\delta} \begin{bmatrix} 0 & 1 \\ 1 & 0 \end{bmatrix} + \frac{1}{2}\dot{\delta} \begin{bmatrix} \sigma_{xy} & \sigma_{yy} \\ -\sigma_{xx} & -\sigma_{xy} \end{bmatrix} - \frac{1}{2}\delta \begin{bmatrix} -\sigma_{xy} & \sigma_{xx} \\ -\sigma_{yy} & \sigma_{xy} \end{bmatrix}$$

so that

$$\dot{\sigma}_{xy} = G\dot{\delta} + \frac{1}{2}\dot{\delta}(\sigma_{yy} - \sigma_{xx}), \quad (6.28)$$

$$\dot{\sigma}_{xx} = \dot{\delta}\sigma_{xy}, \quad (6.29)$$

$$\dot{\sigma}_{yy} = -\dot{\delta}\sigma_{xy}. \quad (6.30)$$

Equations (6.29) and (6.30) give, with the initial condition that all stresses are zero,

$$\sigma_{yy} = -\sigma_{xx}.$$

Differentiating (6.28) and substituting for (6.29) and (6.30) gives

$$\ddot{\sigma}_{xy} + \dot{\delta}^2\sigma_{xy} = 0,$$

which has solution

$$\sigma_{xy} = A \sin \dot{\delta}t + B \cos \dot{\delta}t.$$

The initial conditions require that $B = 0$. Solving for σ_{xx} and σ_{yy} using Equations (6.29) and (6.30) and imposing the initial conditions gives the solution

$$\sigma_{xy} = G \sin \dot{\delta}t, \quad \sigma_{xx} = -\sigma_{yy} = G(1 - \cos \dot{\delta}t). \quad (6.31)$$

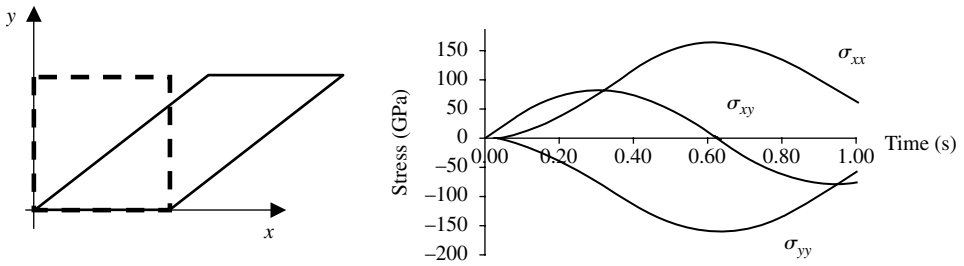


Fig. 6.3 Unit square under simple shear at a rate of 5.0 s^{-1} and the corresponding stresses.

For small strain, δ , at constant strain rate, these reduce to

$$\sigma_{xy} = G\delta \quad \text{and} \quad \sigma_{xx} = -\sigma_{yy} = 0. \quad (6.32)$$

The harmonic variation in (6.31) results from the large deformation, and in particular, the rigid body rotation taking place. This non-physical result arises because we are using a small strain, linear elasticity model under conditions of large deformation. Despite its non-physicality, it provides a good test of the calculation of the rigid body rotations in the large deformation UMAT. In order to do this, a single plane strain element, as shown in Fig. 6.2, has been subjected to simple shear to large strain. This has been carried out using the UMAT with elasticity described in Section 6.2, which uses ABAQUS-provided stresses and strains, a further UMAT based on the deformation gradient, described in this section, and using the built-in elasticity model in ABAQUS. The results obtained are identical and are shown in Fig. 6.3. The various UMATs, together with the ABAQUS input files, are detailed in Appendix B and are available via the OUP website.

6.6 Elasto-viscoplasticity implementation

Viscoplasticity, meaning rate-dependent plasticity in which the plastic multiplier is determined through the use of a viscoplastic constitutive equation as opposed to the use of the consistency condition, was introduced in Chapter 4. The radial return, implicit backward Euler integration for viscoplasticity was discussed in Chapter 5. Here, we present an implicit implementation for linear isotropic strain hardening elasto-viscoplasticity. Such an implementation can readily be simplified for the implicit analysis of creep. We employ a sinh-type viscoplastic constitutive equation and for simplicity, use the initial tangent stiffness (i.e. the elastic stiffness) for the material Jacobian.

The viscoplastic constitutive equation is taken to be

$$\dot{p} = \phi(\sigma_e, r) = \alpha \sinh \beta(\sigma_e - r - \sigma_y)$$

and the multiaxial plastic strain increments are given by

$$\Delta \boldsymbol{\epsilon}^p = \Delta p \mathbf{n} = \frac{3}{2} \Delta p \frac{\boldsymbol{\sigma}'}{\sigma_e'}$$

We determine the increment in effective plastic strain as described in Chapter 5 as follows. Note that all quantities are now assumed to be given at the end of the time increment, that is, at time $t + \Delta t$, unless otherwise indicated.

(i) Determine the elastic trial stress

$$\boldsymbol{\sigma}^{\text{tr}} = \boldsymbol{\sigma}_t + 2G\Delta\boldsymbol{\epsilon} + \lambda I\Delta\boldsymbol{\epsilon} : \mathbf{I}. \quad (6.33)$$

(ii) Determine the trial yield function

$$f = \sigma_e^{\text{tr}} - r - \sigma_y = \left(\frac{3}{2} \boldsymbol{\sigma}^{\text{tr}'} : \boldsymbol{\sigma}^{\text{tr}'} \right)^{1/2} - r - \sigma_y. \quad (6.34)$$

(iii) Determine if actively yielding

$$\text{Is } f > 0?$$

(iv) If yes, use Newton iteration to determine the effective plastic strain increment

$$\begin{aligned} \phi(\sigma_e, r) &= \alpha \sinh \beta (\sigma_e^{\text{tr}} - 3G\Delta p - r - \sigma_y), \\ \phi_{\Delta p} &= -3G\alpha\beta \cosh \beta (\sigma_e^{\text{tr}} - 3G\Delta p - r - \sigma_y), \\ \phi_r &= -\alpha\beta \cosh \beta (\sigma_e^{\text{tr}} - 3G\Delta p - r - \sigma_y), \\ r &= r_t + h\Delta p, \\ d\Delta p &= \frac{\phi(\Delta p, r) - (\Delta p/\Delta t)}{(1/\Delta t) - \phi_{\Delta p} - h\phi_r}, \\ \Delta p^{(k+1)} &= \Delta p^{(k)} + d\Delta p. \end{aligned} \quad (6.35)$$

(v) Determine plastic and elastic strain and stress increments

$$\begin{aligned} \Delta \boldsymbol{\epsilon}^p &= \frac{3}{2} \Delta p \frac{\boldsymbol{\sigma}^{\text{tr}'}}{\sigma_e^{\text{tr}}}, \\ \Delta \boldsymbol{\epsilon}^e &= \Delta \boldsymbol{\epsilon} - \Delta \boldsymbol{\epsilon}^p, \\ \Delta \boldsymbol{\sigma} &= 2G\Delta \boldsymbol{\epsilon}^e + \lambda I\Delta \boldsymbol{\epsilon}^e : \mathbf{I}. \end{aligned} \quad (6.36)$$

182 Implementation of plasticity models

(vi) Update all quantities to the end of the time increment

$$\begin{aligned}\boldsymbol{\sigma} &= \boldsymbol{\sigma}_t + \Delta\boldsymbol{\sigma}, \\ p &= p_t + \Delta p.\end{aligned}\tag{6.37}$$

(vii) Determine Jacobian.

(viii) End.

An ABAQUS UMAT containing this formulation, together with various input files for uniaxial displacement and load control, together with a four-point beam bending problem, are available via the OUP website (full details are given in Appendix B). In addition, uniaxial, closed form implicit and explicit solutions are provided in Fortran programs for verification of the implementation.

Part II. Plasticity models

This page intentionally left blank

7. Superplasticity

7.1 Introduction

Superplasticity is the ability of some materials to undergo very large, irreversible, tensile elongations without necking and failing. Generally, a very fine grain structure is required (a typical grain size will be of the order of $1\ \mu\text{m}$) and a deformation temperature of about $0.5 T_m$ is necessary to enable the appropriate superplastic deformation mechanisms to operate. Two common superplastically formed classes of material are aluminium and titanium alloys, which are used extensively in the aerospace and aero-engine industry. Superplastic forming exploits the ability of the material to undergo very large tensile elongations in metal sheet stretch forming and blow moulding processes, and has many advantages for the manufacture of complex shapes in sheet metal using simple low pressure pneumatic forming equipment.

In this chapter, we shall introduce superplasticity and its characteristics, constitutive equations for superplastic deformation which are coupled with the accompanying microstructural evolution, the multi-axial form of the equations, and an industrial application.

7.2 Some properties of superplastic alloys

Superplasticity is very much a viscoplastic process in the sense that the stress response is highly strain-rate dependent. The uniaxial response to variable constant true strain-controlled loading is simplified and schematically shown in Fig. 7.1.

There is often a very strong strain-rate sensitivity, and in addition, strain hardening is seen to occur. This results from a number of possible causes including the effect of grain growth which occurs in superplasticity, and from dislocation hardening processes. If we choose a particular strain in Fig. 7.1(b) and pick off the corresponding stress for each of the stress–strain curves at all the strain rates, we may then plot $\log(\text{stress})$ versus $\log(\text{strain rate})$, which often produces a curve of the form shown in Fig. 7.2.

Region (i) corresponds to very low strain rates in which diffusion processes dominate when the temperature is higher than $\sim 0.5 T_m$. Region (iii) corresponds to very high

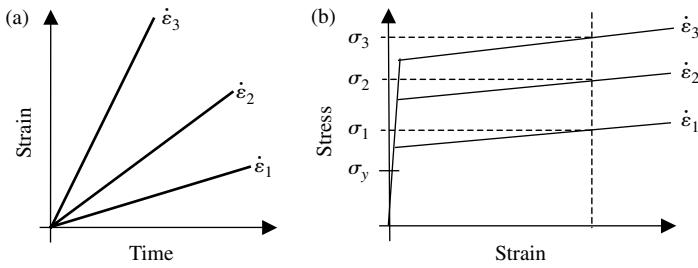


Fig. 7.1 Schematic showing simplified superplastic stress response which is dependent on strain rate.

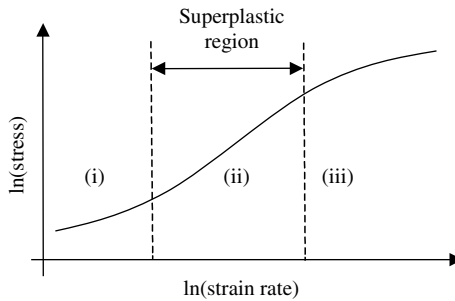


Fig. 7.2 $\log(\text{stress})$ versus $\log(\text{strain})$ showing the region usually considered to be superplastic.

strain rate at which diffusion is largely inhibited so that deformation occurs through dislocation motion, some of which is perhaps thermally activated, but diminishing with increasing strain rate. Region (ii) is that in which superplasticity takes place; that is, large tensile strains ($\sim 1-2$) are achievable which are many times larger than those obtainable in regions (i) and (iii).

Because of the approximate linearity in region (ii), the $\ln(\text{stress})-\ln(\text{strain rate})$ relationship can be written as

$$\ln(\sigma) = m \ln(\dot{\epsilon}) + k \tag{7.1}$$

in which m and k are constants. Rearranging (7.1) gives

$$\sigma = K \dot{\epsilon}^m \tag{7.2}$$

in which K is a further constant. In Equation (7.2), m is called the *strain-rate sensitivity* and is, of course, the gradient of the $\ln(\text{stress})$ versus $\ln(\text{strain rate})$ curve. In fact, the higher the value of m , the better the superplastic deformation, and the larger the tensile elongations achievable in the absence of necking and failure. Generally, for what would be described as superplastic deformation, $m > 0.35$. If, from Fig. 7.2, we now plot the strain-rate sensitivity versus $\ln(\text{strain rate})$, we will obtain the graph shown schematically in Fig. 7.3.

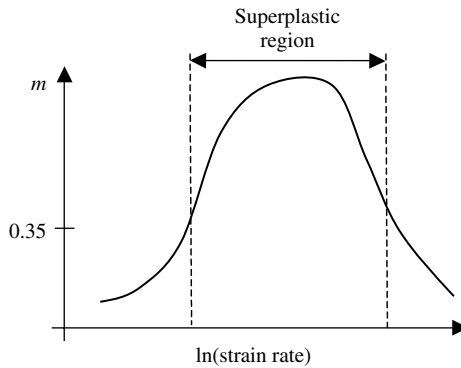


Fig. 7.3 Schematic representation of strain-rate sensitivity versus log(strain rate).

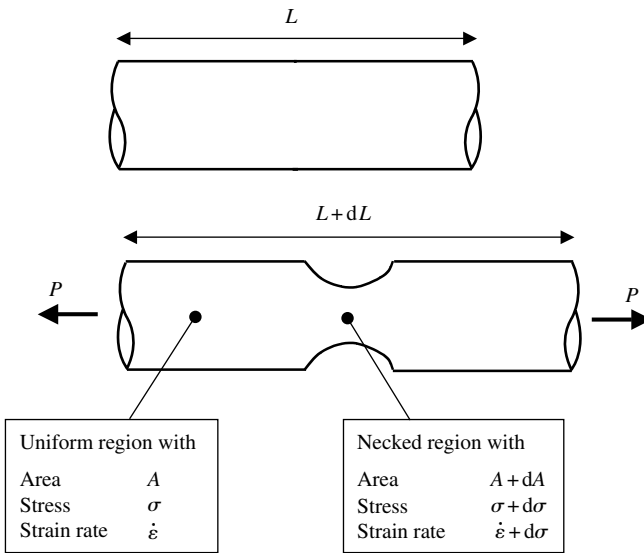


Fig. 7.4 Schematic diagram showing a uniform, circular test piece with cross-sectional area A under load P before and after the introduction of a neck.

We shall now examine further the significance of the strain-rate sensitivity, m , in superplasticity, by considering a uniform, uniaxial circular test piece containing a single, idealized neck shown schematically in Fig. 7.4. We employ the incompressibility condition, apply constant load, P , to the test piece during necking and assume the stress–strain rate relationship given in (7.2).

The incompressibility condition gives

$$AL = (A + dA)(L + dL) \approx AL + L dA + A dL$$

so that

$$\frac{dA}{A} = -\frac{dL}{L} = -d\varepsilon = -\dot{\varepsilon} dt$$

and

$$\frac{dA}{dt} = -\dot{\varepsilon} A \quad (7.3)$$

or, in the neck,

$$\frac{d(A + dA)}{dt} = -(\dot{\varepsilon} + d\dot{\varepsilon})(A + dA),$$

which, when combined with (7.3) gives

$$\frac{d}{dt}(dA) \approx -(A d\dot{\varepsilon} + \dot{\varepsilon} dA) = -dA\dot{\varepsilon} \left(\frac{A}{dA} \frac{d\dot{\varepsilon}}{\dot{\varepsilon}} + 1 \right). \quad (7.4)$$

The constancy of load, P , gives

$$\sigma A = (\sigma + d\sigma)(A + dA)$$

so that

$$\frac{d\sigma}{\sigma} = -\frac{dA}{A}. \quad (7.5)$$

The constitutive equation $\sigma = K\dot{\varepsilon}^m$ gives

$$\sigma + d\sigma = K(\dot{\varepsilon} + d\dot{\varepsilon})^m = K\dot{\varepsilon}^m \left(1 + \frac{d\dot{\varepsilon}}{\dot{\varepsilon}} \right)^m = K\dot{\varepsilon}^m \left[1 + m \frac{d\dot{\varepsilon}}{\dot{\varepsilon}} + \dots \right]$$

so that

$$\frac{d\sigma}{\sigma} \approx m \frac{d\dot{\varepsilon}}{\dot{\varepsilon}}. \quad (7.6)$$

Combining (7.6) and (7.5) gives

$$\frac{A}{dA} \frac{d\dot{\varepsilon}}{\dot{\varepsilon}} = -\frac{1}{m}$$

and substituting into (7.4) gives

$$\frac{d}{dt}(dA) \approx -dA\dot{\varepsilon} \left(1 - \frac{1}{m} \right). \quad (7.7)$$

This equation tells us that the rate of development of the neck depends upon the quantity $1 - (1/m)$. As the strain-rate sensitivity increases, and approaches unity, the rate of necking decreases to zero. We therefore see the significance of the strain-rate sensitivity in superplasticity; the higher the value of m , the more necking can be inhibited therefore allowing greater elongations prior to the onset of necking and failure. A much more complete introduction to superplasticity can be found in Pilling and Ridley (1989).

7.3 Constitutive equations for superplasticity

The constitutive equation in (7.2) is simple, but is often inadequate for simulating superplasticity processes because the $\ln(\text{stress})-\ln(\text{strain rate})$ relationship is not often linear, particularly over strain-rate regimes which occur in practical processing. In addition, it says nothing about the influence of changing microstructure during superplastic deformation, which is known to be important (Ghosh and Hamilton, 1979; Ghosh and Raj, 1981; Hamilton, 1984; Zhou and Dunne, 1996). We present here constitutive equations for superplasticity for the particular commercially important titanium alloy, Ti-6Al-4V. This alloy finds application in a range of aero-engine components, but for component manufacture using superplastic forming, the engine fan blades are perhaps the most important.

Uniaxial stress-strain curves for the Ti-6Al-4V alloy undergoing superplastic deformation at 927°C are shown in Fig. 7.5.

A strong strain-rate effect is seen together with significant strain hardening. The stresses required to cause the deformation are, however, really quite small but the tensile strains achieved during the superplastic deformation are large. The hardening is due to several processes; perhaps the most important is the increasing average grain size. The average grain size at the start of all the tests shown in Fig. 7.5 is $6.4\ \mu\text{m}$. At the end of the deformation, it has increased to about $10\ \mu\text{m}$, and depends on the rate of deformation. The evolution of the average grain size for each of the stress-strain curves shown in Fig. 7.5 is shown in Fig. 7.6.

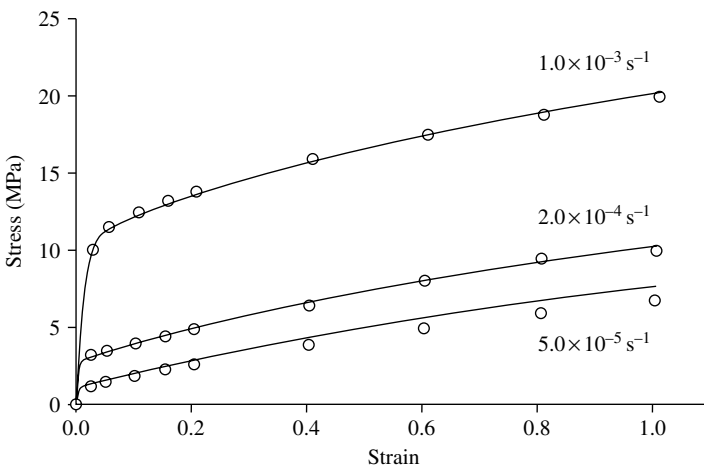


Fig. 7.5 Superplastic stress-strain curves for Ti-6Al-4V at 927°C at the strain rates shown. The initial grain size is $6.4\ \mu\text{m}$.

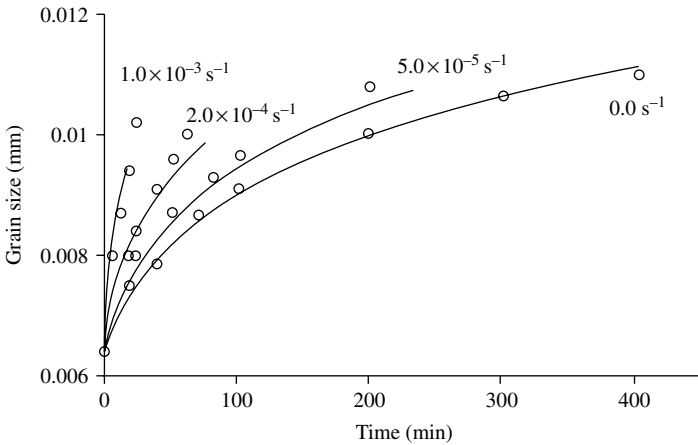


Fig. 7.6 Grain size versus time curves for Ti-6Al-4V at 927°C at the strain rates shown. The initial grain size is 6.4 μm.

An important feature is that for a strain rate of 0.0 s⁻¹, that is, a static test in which no deformation takes place, grain growth still takes place; this is called *static grain growth*. As the strain rate is increased, so the rate of growth of grain size increases. That part of the grain growth resulting from the straining is often referred to as *deformation-enhanced grain growth*. *Normal* grain growth (Shewmon, 1969) gives rise to a kinetic equation for static grain growth of the form

$$\dot{l} = \frac{\alpha_1}{l^\gamma} \tag{7.8}$$

in which l is the average grain size, and α_1 and γ are material constants. The deformation-enhanced grain growth is accounted for with an additional term so that the complete kinetic equation can be written as

$$\dot{l} = \frac{\alpha_1}{l^\gamma} + \beta_1 \dot{\rho} \tag{7.9}$$

in which β_1 is a further material constant and $\dot{\rho}$ is, as before, the effective plastic strain rate. The symbols in Fig. 7.5 are, in fact, experimental data and the lines result from fitting Equation (7.9) to the data. The material constants for this particular temperature of 927°C are given in Table 7.1 and assume grain size to be specified in millimetres. We now return to the microstructure–deformation coupling (Zhou and Dunne, 1996; Kim and Dunne, 1999) and employ the following elastic-viscoplastic constitutive equations

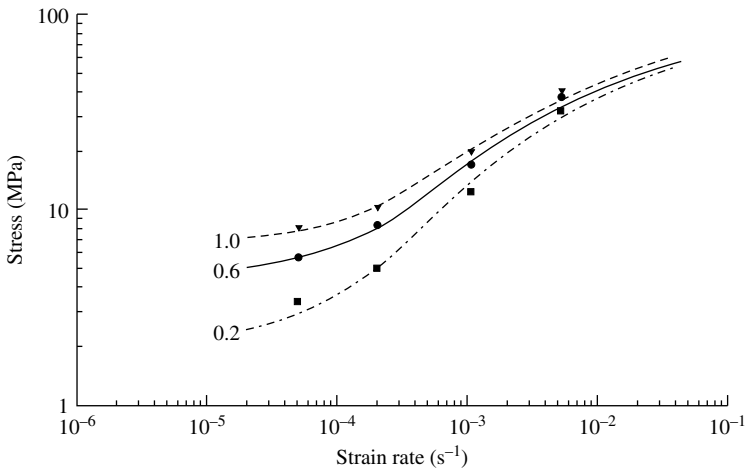
$$\dot{\epsilon}^p = \frac{\alpha}{l^\mu} \sinh \beta(\sigma - r - \sigma_y), \tag{7.10}$$

$$\dot{r} = (c_1 - \gamma_1 r) \dot{\rho}, \tag{7.11}$$

$$\dot{\sigma} = E(\dot{\epsilon} - \dot{\epsilon}^p), \tag{7.12}$$

Table 7.1 Material constants for Ti–6Al–4V at 927°C.

α	β	μ	σ_y (MPa)	E (MPa)
0.437×10^{-5}	0.0919	1.06	0.5	1000
c_1	γ_1	α_1	β_1	γ
8.397	0.666	0.128×10^{-16}	0.9625×10^{-13}	5.0


Fig. 7.7 Experimental (symbols) and predicted (lines) stress versus strain rate curves for Ti–6Al–4V at 927°C with an initial grain size of 6.4 μm for the strain levels shown.

which are coupled with the grain growth equation in (7.9). Equation (7.10) is the viscoplastic constitutive equation in which, as before, α and β are material constants, l is the current grain size, and μ the deformation–microstructure coupling constant. The hardening seen in Fig. 7.4 does not all result from the grain growth, although a substantial part of it does. A further isotropic hardening term, r , has therefore been introduced with evolution equation given in (7.11) in which c_1 and γ_1 are material constants. Equation (7.12) is Hooke’s law. Equations (7.9)–(7.12) constitute the uniaxial material model for superplasticity. With the material constants for the grain growth kinetic equation having been already determined, the unknown constants in Equations (7.10) and (7.11) are obtained by fitting the equations (Zhou and Dunne, 1996) to the experimental data in Fig. 7.5. The resulting computed stress–strain curves are given by the solid lines in the figure.

Comparisons of predicted and experimental $\log(\text{stress})$ versus $\log(\text{strain rate})$ behaviour for the Ti-alloy with an initial grain size of 6.4 μm obtained at the strain levels shown are given in Fig. 7.7, and the corresponding predicted variation of strain-rate sensitivity with strain rate (at a strain of 1.0) is shown in Fig. 7.8.

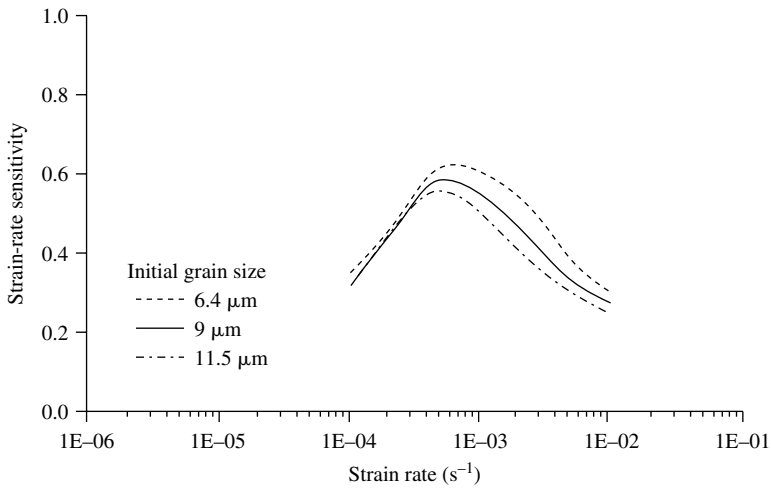


Fig. 7.8 Predicted variation of strain-rate sensitivity with strain rate for the initial grain sizes shown for Ti-6Al-4V at 927°C.

7.4 Multiaxial constitutive equations and applications

We may write the multiaxial equations within the framework of viscoplasticity by assuming the normality hypothesis and von Mises material behaviour. The multiaxial viscoplastic strain rate, given these assumptions, is

$$D^p = \frac{3}{2} \dot{p} \frac{\sigma'}{\sigma_e}, \tag{7.13}$$

where

$$\dot{p} = \frac{\alpha}{l\mu} \sinh \beta(\sigma_e - r - \sigma_y) \tag{7.14}$$

and Equations (7.9) and (7.11) remain unchanged. If considering large deformations (which is normally the case for superplasticity), the Jaumann stress rate is, as before,

$$\overset{\nabla}{\sigma} = \dot{\sigma} + \mathbf{W}\sigma - \sigma\mathbf{W}. \tag{7.15}$$

These equations, together with (7.9) and (7.11), have been implemented into ABAQUS by means of the CREEP routine, which is described in Chapter 8. This facilitates an easier implicit implementation, but a UMAT implementation would be carried out as described for viscoplasticity in Chapters 5 and 6, although if a plane stress implementation is required, additional problems would need to be addressed. The application we consider is the superplastic blow-forming of a rectangular-section box made from 1.25 mm thick Ti-6Al-4V sheet and processed at 900°C (Lin and Dunne, 2001, with thanks to Dr. Lin). The model is shown in Fig. 7.9 in which just one quarter

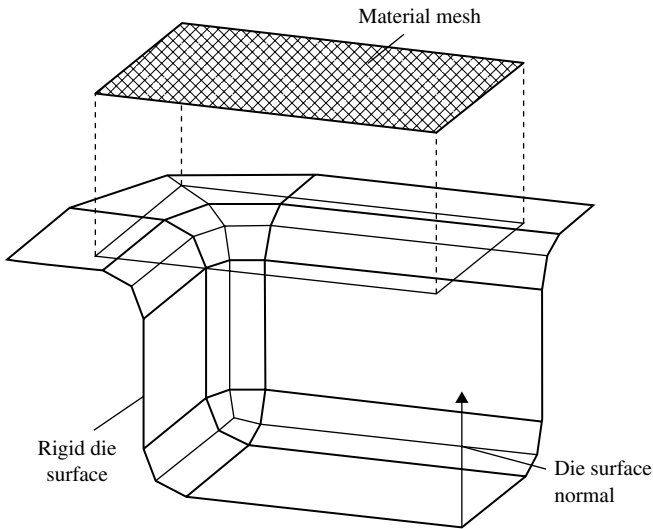


Fig. 7.9 Finite element model for the rectangular-section box die surface and the material blank.

is included, for reasons of symmetry, and both the initially flat sheet and the die surface are included.

The superplastic forming process consists of clamping the flat Ti-alloy sheet (modelled using shell elements) against the die, the surface of which forms a cavity in the shape required. Gas pressure is applied to the top face of the sheet, forcing it to acquire the die shape. In these analyses, the maximum strain rate over the deforming sheet is controlled to be close to the optimum deforming rate of the material; that is, the strain rate required to give the highest strain-rate sensitivity obtained from the equivalent of Fig. 7.7, but for 900°C . This is achieved by varying the applied gas pressure. The process is considered completed at a forming time, t_f , when all nodes on the deforming sheet are in contact with the die. Figure 7.10 shows the deformation of the superplastic metal sheet at three stages during the forming process at times $t/t_f = 0.1$, $t/t_f = 0.6$, and $t/t_f = 1.0$. The contours show the magnitude of the effective plastic strain rate. The maximum target strain rate specified for the analysis is $1.0 \times 10^{-5} \text{ s}^{-1}$ which is achieved by application of uniformly distributed gas pressure. Figure 7.10 shows that the distribution of effective plastic strain rate is highly non-uniform. This is typical of many practical superplastic forming processes; while ideally it is necessary to deform superplastically all points in the material at the same optimum strain rate (to maximize strain-rate sensitivity and hence elongation), this is rarely achievable in practice. It is possible, however, to ensure that a target maximum strain rate is not exceeded, and in this analysis, the gas pressure is varied to ensure a nominal maximum strain rate of $1.0 \times 10^{-5} \text{ s}^{-1}$. The variation of the maximum strain rate during the

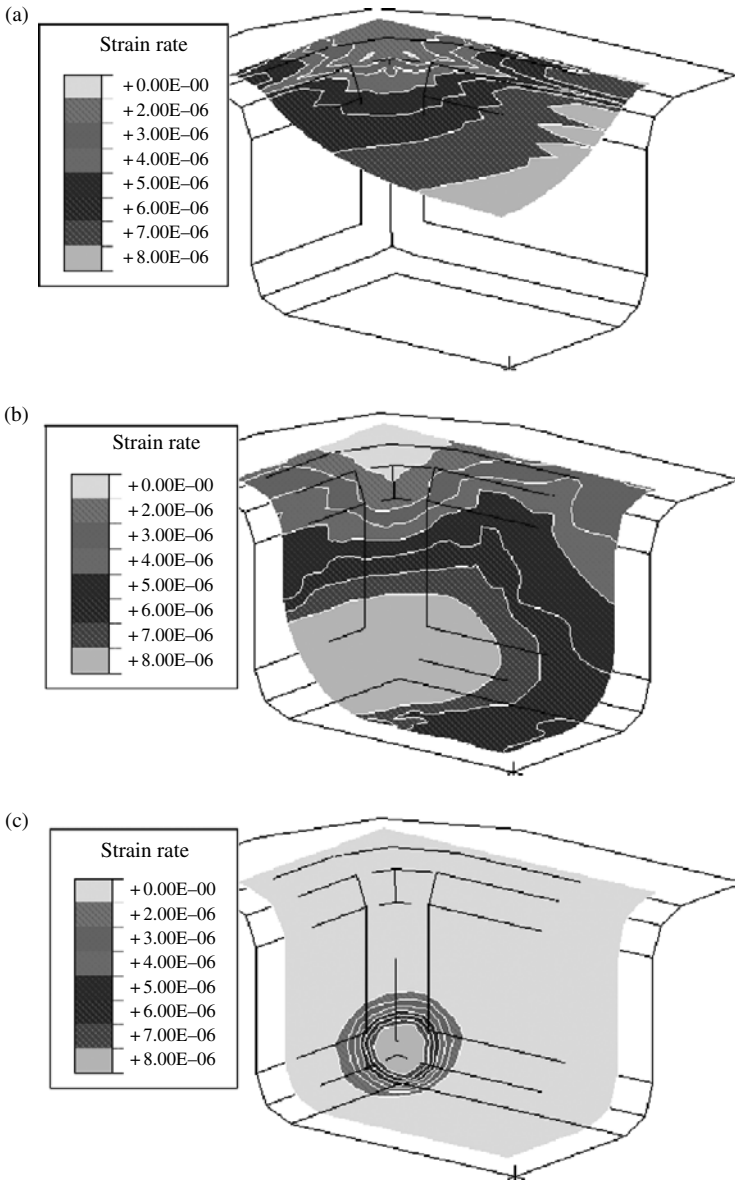


Fig. 7.10 The simulated superplastically deforming sheet showing the effective plastic strain rate at fractional processing times of $t/t_f = 0.1$, $t/t_f = 0.6$, and $t/t_f = 1.0$. (See also Plate 1.)

forming process is shown in Fig. 7.11 for target strain rates of both $1.0 \times 10^{-5} \text{ s}^{-1}$ and $1.0 \times 10^{-4} \text{ s}^{-1}$, and the corresponding variations in gas pressure to achieve these are given in Fig. 7.12. Higher gas pressure is needed for the higher target strain rate because of the higher flow stresses required. The gas pressure increases during the

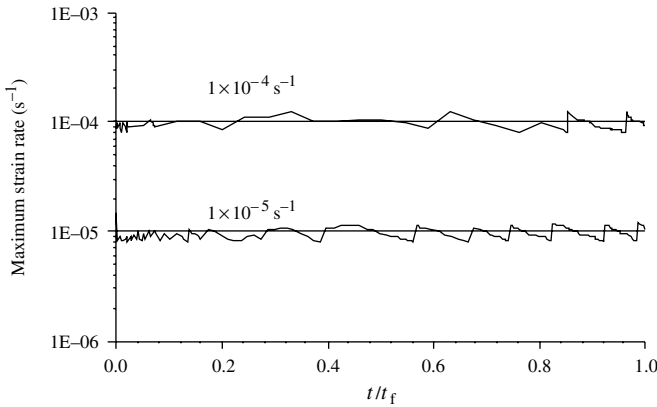


Fig. 7.11 Variation of the maximum strain rate over the deforming material blank during the superplastic forming process for the two target strain rates $\dot{\epsilon} = 1 \times 10^{-5}$ and $\dot{\epsilon} = 1 \times 10^{-4} \text{ s}^{-1}$.

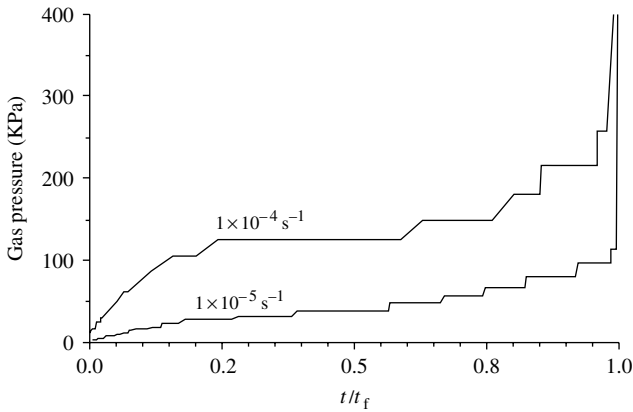


Fig. 7.12 Variation of gas pressure to ensure a maximum strain rate in the deforming sheet of 1.0×10^{-5} and $1.0 \times 10^{-4} \text{ s}^{-1}$.

superplastic forming because of increasing geometrical and frictional constraint and, in addition, because the material hardens during deformation which is due to the grain growth taking place. High gas pressure is required to fill the corner part of the die, which is the last stage of the forming process.

In Fig. 7.10, it is apparent that the last part of the sheet to be formed is the corner, which is also the area of maximum *thinning* and where tearing is most likely to occur. This is made clear by looking at the through-thickness strain fields which are shown for the two target strain rates of 1.0×10^{-5} and $1.0 \times 10^{-4} \text{ s}^{-1}$ in Fig. 7.13(a) and (b), respectively.

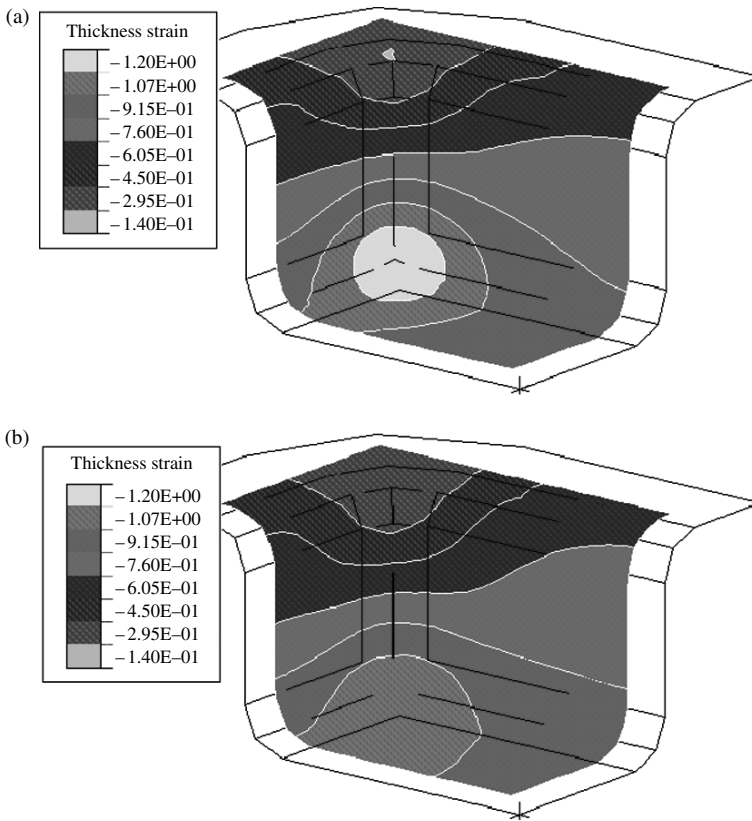


Fig. 7.13 Through-thickness strain fields at the end of the superplastic forming carried out with target maximum strain rates of (a) 1.0×10^{-5} and (b) $1.0 \times 10^{-4} \text{ s}^{-1}$. (See also Plate 2.)

The lower strain rate is seen to lead to a higher spatial variation in through-thickness strain; that is, *thinning*, which is often not desirable in practical processing. In fact, the ranges of out-of-plane strain for the low and high strain rates are 1.06 and 0.84, respectively. The reason for this becomes clear on looking at the grain size distributions, shown in Fig. 7.14.

At the lower target strain rate, the average grain size increase is larger than that at the higher strain rate because of static grain growth, which is inhibited in the latter. In addition, at the lower strain rate, the range of final grain size is less than that at the higher rate. For the case of the higher strain rate, therefore, the larger grain size in the deforming material in the corner (relative to that at the boundaries) leads to a higher stress in the corner region to generate the same strains seen for the lower strain rate. This inhibits straining in the corner region producing larger strains in the boundary regions. The net result is a more uniform strain distribution for the high strain rate, and a correspondingly more uniform thinning. This is generally preferable

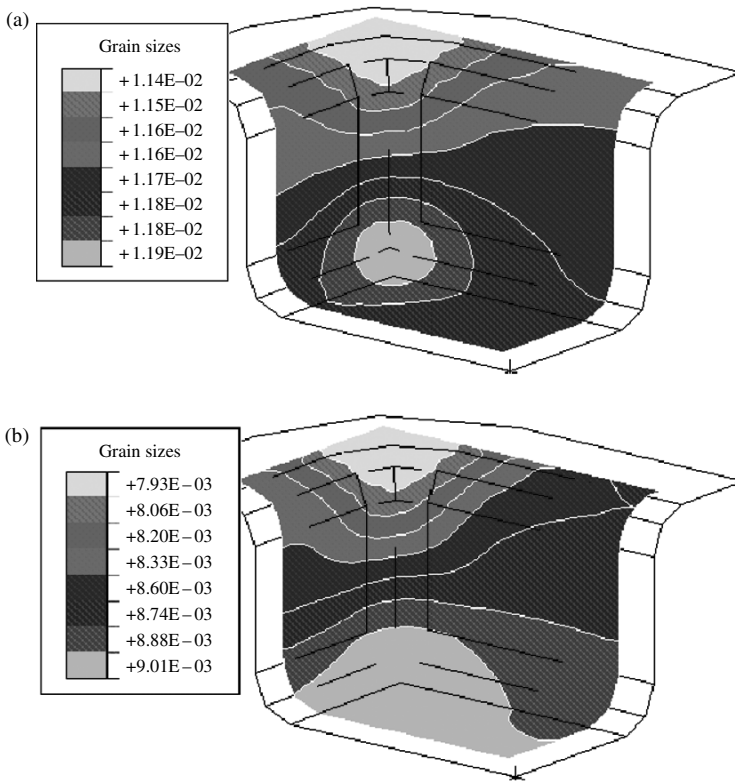


Fig. 7.14 Average grain size fields at the end of the superplastic forming carried out with target maximum strain rates of (a) 1.0×10^{-5} and (b) $1.0 \times 10^{-4} \text{ s}^{-1}$. (See also Plate 3.)

in practice, and results directly from the interactions of the superplastic deformation and microstructural evolution. These industrially important effects could not have been obtained without microstructurally based constitutive equations. An additional important effect is the distribution of grain size in commercial Ti-6Al-4V, which has not been addressed here. However, modelling techniques to incorporate it, its effects on strain-rate sensitivity and hence on necking and failure have been addressed by Kim and Dunne (1999), where further information may be found.

References

- Ghosh, A.K. and Hamilton, C.H. (1979). 'Mechanical behaviour and hardening characteristics of a superplastic Ti-6Al-4V alloy'. *Metallurgical Transactions*, 10, 699-706.
- Ghosh, A.K. and Raj, R. (1981). 'Grain size distribution effect in superplasticity'. *Acta Metallurgica*, 29, 607-616.

- Hamilton, C.H. (1984). 'Superplasticity in titanium alloys'. In Agrawal, S.P. (ed.), *Superplastic Forming, Proceedings of the Symposium*, California, March 13–22, American Society for Metals.
- Kim, T.-W. and Dunne, F.P.E. (1999). 'Modelling heterogeneous microstructures in superplasticity'. *Proceedings of the Royal Society*, 455, 701–718.
- Lin, J. and Dunne, F.P.E. (2001). 'Modelling grain growth evolution and necking in superplastic blow-forming'. *International Journal of Mechanical Science*, 43, 595–609.
- Pilling, J. and Ridley, N. (1989). *Superplasticity in Crystalline Solids*. The Institute of Metals, London.
- Shewmon, P.G. (1969). *Transformations in Metals*. McGraw-Hill, New York.
- Zhou, M. and Dunne, F.P.E. (1996). 'Mechanisms-based constitutive equations for the superplastic behaviour of a titanium alloy'. *Journal of Strain Analysis*, 31, 65–73.

8. Porous plasticity

8.1 Introduction

We have so far considered plasticity and viscoplasticity processes in which it has been assumed that the deforming material has been incompressible. There are some materials, however, for which this is not the case. An important example is in the processing of metal powders in which, generally at elevated temperature, the powder is consolidated by plastic deformation and the elimination of the porosity. During the process, significant volume changes occur because of the removal of the porosity. A further example of compressible or porous plasticity is that in which significant voiding develops in a material undergoing plastic deformation resulting from a damage process (e.g. creep cavitation). Again, while possibly small, volume changes occur during the deformation and the incompressibility condition no longer holds. A feature of the constitutive equations in porous plasticity is that there becomes a dependence on mean stress as we shall see shortly. In this chapter, we introduce the porous plasticity model of Duva and Crow and outline its implementation into ABAQUS using both a UMAT material subroutine and the simpler ABAQUS CREEP routine. For simplicity, within the UMAT, we use explicit integration of the constitutive equations and employ the initial stiffness as the material Jacobian.

A number of constitutive relations for the consolidation of metal powders have been developed. They have been used to predict the dependence of densification rate on consolidation pressure and temperature as well as volume fraction of voids. One of the first constitutive models for consolidation of metal powder was developed by Wilkinson and Ashby (1975). They analysed the creep collapse of a thick-walled spherical shell subjected to externally applied hydrostatic loading. In general, consolidation occurs under the action of a range of stress states that are not purely hydrostatic, for which the Wilkinson and Ashby model is therefore inappropriate. Subsequent research has therefore broadened the Wilkinson and Ashby model to more general loading conditions. The models have taken into account the effects of deviatoric and hydrostatic components of stress state by introducing potentials which make possible the

development of relationships between macroscopic strain rate and stress state (Cocks, 1989; Ponte Castaneda, 1991; Duva and Crow, 1992; Sofronis and McMeeking, 1992). The strain rate potential (ϕ) for a porous material can be written as a function of both deviatoric and hydrostatic stresses

$$\phi = \frac{\dot{\epsilon}_0 \sigma_0}{n+1} \left(\frac{S}{\sigma_0} \right)^{n+1}, \quad (8.1)$$

where

$$S^2 = a\sigma_e^2 + b\sigma_m^2, \quad (8.2)$$

$$\sigma_e^2 = \frac{3}{2} \boldsymbol{\sigma}' : \boldsymbol{\sigma}', \quad (8.3)$$

$$\sigma_m = \frac{1}{3} \mathbf{II} : \boldsymbol{\sigma}. \quad (8.4)$$

S is an *effective* effective stress (Duva and Crow, 1994) given in terms of the effective, σ_e , and hydrostatic, σ_m , stresses, n is the creep exponent, and the coefficients a and b are functions of current relative density, D , which is equivalent to the solid volume fraction of the porous material, a is associated with the deviatoric component and b with the hydrostatic component. The coefficients a and b are chosen such that, at the fully dense stage, that is, $D = 1$, the coefficient b becomes 0 and a becomes 1. The *effective* effective stress, S , is then reduced to σ_e . The various densification models for monolithic materials in the literature use different approaches to obtain the strain rate potential. This leads to different expressions for the coefficients a and b (Duva and Crow, 1994).

Duva and Crow (1994) proposed a strain rate potential for computing densification rates. Based on the strain rate potentials of Cocks (1989) and Ponte Castaneda (1991), the coefficients a and b were chosen to ensure that the potential gives densification rates identical to those of Wilkinson and Ashby (1975) in the hydrostatic load limit, and agree with both Cocks (1989) and Ponte Castaneda (1991) in the limit when the hydrostatic stress vanishes. The densification rates predicted by Duva and Crow's strain rate potential are consistent with their cell model calculations which were derived based on Hill's minimum principle for velocity. Duva and Crow predict densification rates which compare favourably with the prediction from the Wilkinson and Ashby model in the hydrostatic limit. The Duva and Crow potential also satisfies the lower bounds derived by both Cocks and Ponte Castaneda in the limit that the hydrostatic stress vanishes. The densification rate predicted from the Duva and Crow model, in the presence of a large deviatoric stress component, is closer to the experimental results than the predictions of Sofronis and McMeeking (1992).

8.2 Finite element implementation of the porous material constitutive equations

Strain rates are determined by differentiating the strain rate potential, ϕ , to give

$$\dot{\boldsymbol{\epsilon}} = \frac{\partial \phi}{\partial \boldsymbol{\sigma}} = AS^{n-1} \left(\frac{3}{2}a\boldsymbol{\sigma}' + \frac{1}{3}b\mathbf{I}\sigma_m \right) \quad (8.5)$$

in which

$$a = \frac{1 + (2/3)(1 - D)}{D^{2n/(n+1)}} \quad \text{and} \quad b = \left[\frac{n(1 - D)}{(1 - (1 - D)^{1/n})^n} \right]^{2/(n+1)} \left(\frac{3}{2n} \right)^2$$

and where A is a material parameter given by

$$A = \frac{\dot{\epsilon}_0}{\sigma_0^n}. \quad (8.6)$$

The dilatation rate can be obtained from

$$\dot{\epsilon}_{kk} = \dot{\epsilon}_{xx} + \dot{\epsilon}_{yy} + \dot{\epsilon}_{zz} \quad (8.7)$$

and hence, the densification rate is given as

$$\dot{D} = -D\dot{\epsilon}_{kk}, \quad (8.8)$$

where D is the relative density.

8.2.1 Implementation into ABAQUS UMAT

The constitutive equations for porous metals developed by Duva and Crow (1992) are implemented into the finite element software ABAQUS within a large deformation formulation using a UMAT subroutine. A simple, explicit, forward Euler integration is adopted. ABAQUS supplies to the UMAT subroutine the deformation gradient at the beginning and the end of each time step, \mathbf{F}^t and $\mathbf{F}^{t+\delta t}$. The user is required to supply the Cauchy stress at the end of the time step. The algorithms, first, need to define the rate of deformation gradient, $\dot{\mathbf{F}}$, which can be calculated, for small time steps, as

$$\dot{\mathbf{F}} = \frac{1}{\delta t}(\mathbf{F}^{t+\delta t} - \mathbf{F}^t). \quad (8.9)$$

Then, the velocity gradient, \mathbf{L} , is

$$\mathbf{L} = \mathbf{F}\mathbf{F}^{-1}. \quad (8.10)$$

The total rate of deformation, \mathbf{D} , and the spin tensor, \mathbf{W} , are given by

$$\mathbf{D} = \frac{1}{2}(\mathbf{L} + \mathbf{L}^T), \quad (8.11)$$

$$\mathbf{W} = \frac{1}{2}(\mathbf{L} - \mathbf{L}^T). \quad (8.12)$$

202 Porous plasticity

The strain components are calculated independently from

$$\boldsymbol{\varepsilon} = -\frac{1}{2} \ln(\mathbf{F}\mathbf{F}^T)^{-1}. \quad (8.13)$$

The dilatation rate, $\dot{\varepsilon}_{kk}$, and the densification rate, \dot{D} , can be calculated from Equations (8.7) and (8.8), respectively. The relative density at the end of each time step is determined using the first-order Euler integration scheme

$$D^{t+\delta t} = D^t + \dot{D}\delta t. \quad (8.14)$$

The co-rotational stress rate $\overset{\nabla}{\boldsymbol{\sigma}}$ is given by

$$\overset{\nabla}{\boldsymbol{\sigma}} = \frac{E}{(1+\nu)} \mathbf{D}^e + \frac{E\nu}{(1+\nu)(1-2\nu)} \mathbf{II} : \mathbf{D}^e, \quad (8.15)$$

where E is Young's modulus, ν is Poisson's ratio, and \mathbf{D}^e is the rate of elastic deformation given by

$$\mathbf{D}^e = \mathbf{D} - \mathbf{D}^p. \quad (8.16)$$

\mathbf{D}^p is the rate of plastic deformation as given in Equation (8.5). The stress increment, with respect to the material reference frame, is calculated as

$$\Delta \overset{\nabla}{\boldsymbol{\sigma}} = \Delta \overset{\nabla}{\boldsymbol{\sigma}} + \mathbf{R}\boldsymbol{\sigma}_t \mathbf{R}^t. \quad (8.17)$$

This, therefore, provides for an objective update of the stress with respect to a fixed coordinate system during the time step. The stress increment, $\Delta \overset{\nabla}{\boldsymbol{\sigma}}$, for each time step can be determined by utilizing the first-order Euler integration scheme

$$\Delta \boldsymbol{\sigma} = \overset{\nabla}{\boldsymbol{\sigma}} \Delta t. \quad (8.18)$$

The updated stress is returned to ABAQUS through the UMAT subroutine. Because here, we adopt an explicit first-order forward Euler integration, great care is necessary in choosing an appropriate time step, and in ensuring meaningful results are obtained.

8.2.2 Implementation into ABAQUS CREEP subroutine

The implementation of the Duva and Crow constitutive equations for consolidation is also carried out using the ABAQUS CREEP facility. This subroutine is suitable for constitutive equations in which the increments of inelastic strain are functions of the hydrostatic stress and the equivalent deviatoric stress described by Mises' or Hill's definitions, while the UMAT subroutine allows more general forms of constitutive laws to be implemented, and easier handling of internal state variables.

ABAQUS computes the incremental creep strain components as

$$\Delta \mathbf{e}^{\text{cr}} = \Delta \bar{\varepsilon}^{\text{cr}} \mathbf{n} + \frac{1}{3} \Delta \bar{\varepsilon}^{\text{sw}} \mathbf{I}, \quad (8.19)$$

where \mathbf{n} is the direction normal to the yield surface, given by

$$\mathbf{n} = \frac{\partial \sigma_e}{\partial \boldsymbol{\sigma}}. \quad (8.20)$$

$\Delta \bar{\varepsilon}^{\text{cr}}$ and $\Delta \bar{\varepsilon}^{\text{sw}}$ are the equivalent creep strains conjugate to the deviatoric stress and the mean stress, respectively. Therefore, $\Delta \bar{\varepsilon}^{\text{cr}}$ corresponds to the conventional deviatoric creep strain and $\Delta \bar{\varepsilon}^{\text{sw}}$ to the volumetric strain occurring because of void closure.

In order to implement the porous material constitutive equations using the CREEP subroutine, the plastic strain rate equation defined in Equation (8.5) has to be decomposed into two parts as follows

$$\dot{\mathbf{e}}^{\text{p}} = AS^{n-1} \frac{3}{2} a \boldsymbol{\sigma}' + \frac{1}{3} AS^{n-1} b \sigma_m \mathbf{I}. \quad (8.21)$$

The first part is associated with the deviatoric stress and the second with the mean stress. The user is required to provide $\Delta \bar{\varepsilon}^{\text{cr}}$, $\partial \Delta \bar{\varepsilon}^{\text{cr}} / \partial \sigma_e$, $\partial \Delta \bar{\varepsilon}^{\text{cr}} / \partial p$, $\Delta \bar{\varepsilon}^{\text{sw}}$, $\partial \Delta \bar{\varepsilon}^{\text{sw}} / \partial \sigma_e$, and $\partial \Delta \bar{\varepsilon}^{\text{sw}} / \partial p$, in which σ_e is the equivalent stress and p is the equivalent pressure stress given as

$$p = -\frac{1}{3}(\sigma_{xx} + \sigma_{yy} + \sigma_{zz}). \quad (8.22)$$

The variables are obtained as follows:

$$\Delta \bar{\varepsilon}^{\text{cr}} = AS^{n-1} a \sigma_e \Delta t, \quad (8.23)$$

$$\frac{\partial \Delta \bar{\varepsilon}^{\text{cr}}}{\partial \sigma_e} = \Delta \bar{\varepsilon}^{\text{cr}} \left(\frac{1}{\sigma_e} + \frac{(n-1)a\sigma_e}{S^2} \right), \quad (8.24)$$

$$\frac{\partial \Delta \bar{\varepsilon}^{\text{cr}}}{\partial p} = -\Delta \bar{\varepsilon}^{\text{cr}} \left(\frac{(n-1)b\sigma_m}{S^2} \right), \quad (8.25)$$

$$\Delta \bar{\varepsilon}^{\text{sw}} = Ab\sigma_m S^{n-1} \Delta t, \quad (8.26)$$

$$\frac{\partial \Delta \bar{\varepsilon}^{\text{sw}}}{\partial \sigma_e} = \Delta \bar{\varepsilon}^{\text{sw}} \left(\frac{(n-1)a\sigma_e}{S^2} \right), \quad (8.27)$$

$$\frac{\partial \Delta \bar{\varepsilon}^{\text{sw}}}{\partial p} = -\Delta \bar{\varepsilon}^{\text{sw}} \left(\frac{1}{\sigma_m} + \frac{(n-1)b\sigma_m}{S^2} \right). \quad (8.28)$$

In order to calculate σ_e and σ_m , the stress components are required. The CREEP subroutine does not provide these quantities, and therefore the USDFLD subroutine has to be utilized to access material point data and assign stress components to state variables, which are then passed into the CREEP subroutine. The densification rate

Table 8.1 Material parameters.

	$T < 750^{\circ}\text{C}$	$T \geq 750^{\circ}\text{C}$
A_0	8.49	95.67
n	2.18	1.53

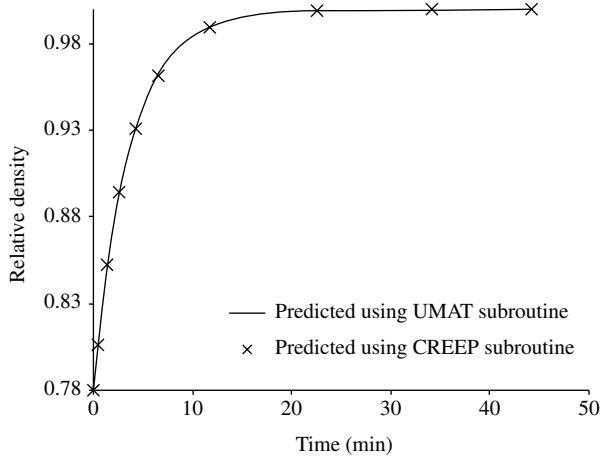


Fig. 8.1 Graph showing comparisons of relative density–time curves obtained from the porous plasticity material model utilizing both an ABAQUS UMAT subroutine and a CREEP subroutine.

can therefore be obtained from Equation (8.8). The relative density for each time increment can be determined by utilizing the first-order Euler integration as given in Equation (8.14).

The porous plasticity material model implemented using the CREEP subroutine was verified against that using the UMAT subroutine by simulating a simple compression process using a single plane strain element subjected to in-plane compressive load of 20 MPa at 925°C. The material constants, A_0 and n , used are given in Table 8.1, and A is calculated from

$$A = A_0 \exp\left(\frac{-Q}{RT}\right) \tag{8.29}$$

in which T is the temperature, R the gas constant, and Q activation energy.

Figure 8.1 shows comparisons of the relative density evolution over time calculated by the porous material model using the CREEP and the UMAT subroutines. The results can be seen to be identical.

The Duva and Crow porous plasticity model has been used (empirically) to approximate the behaviour in consolidation of continuous (SiC) fibre, (Ti) metal matrix

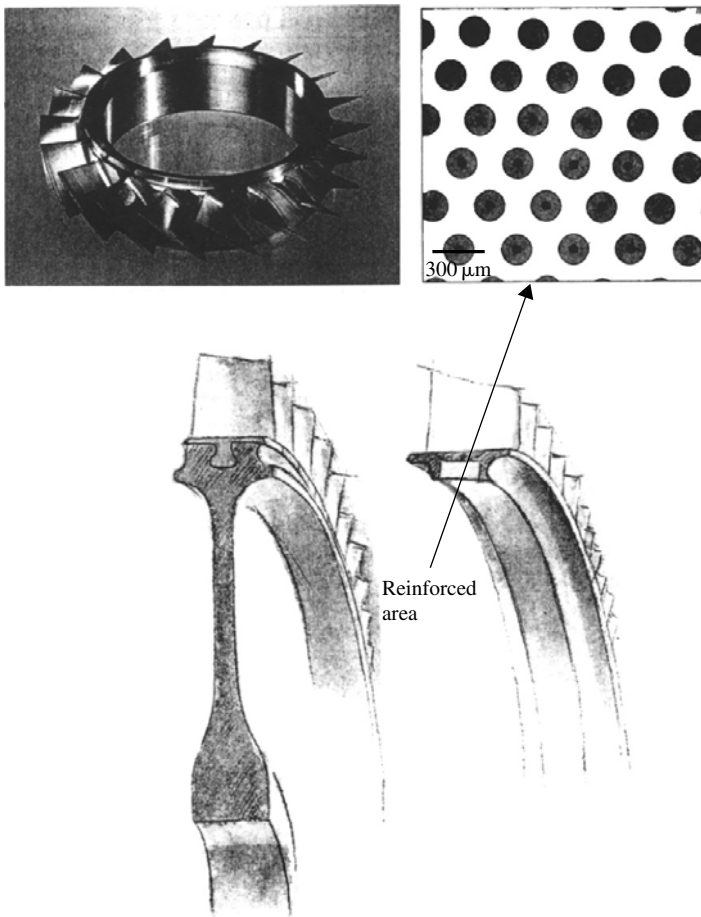


Fig. 8.2 Schematic diagram of an aero-engine bling showing region of reinforcement with Ti-MMC and a demonstrator disc (from King, 1998).

composite materials (Ti-MMCs) being developed for potential application to aero-engine components together with shafts, discs, brakes, and aircraft landing gear. Application to an aero-engine ‘bling’—a bladed ring—is shown in Fig. 8.2.

The Ti-MMC material in the unconsolidated and fully consolidated state is shown in Fig. 8.3(a) and (b), respectively.

8.3 Application to consolidation of Ti-MMCs

The simple consolidation model, which was implemented using the CREEP subroutine as described above, was set up to simulate (empirically) the consolidation of Ti-MMCs under a range of processing conditions. The consolidation process is

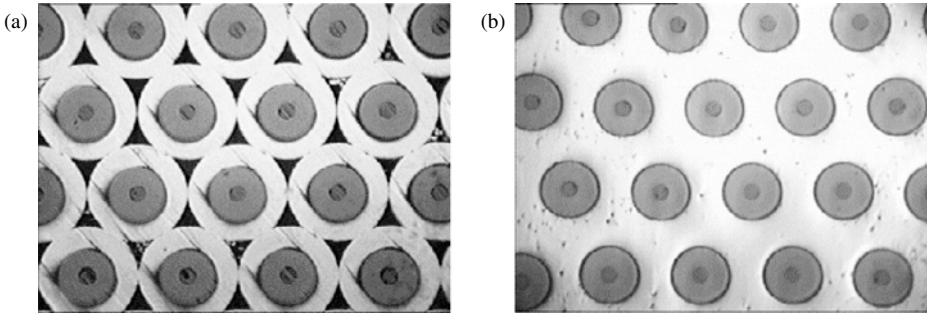


Fig. 8.3 Micrographs showing Ti-6Al-4V matrix, SiC continuous fibre composite material (a) unconsolidated and (b) consolidated at 925°C for 30 min at 15 MPa.

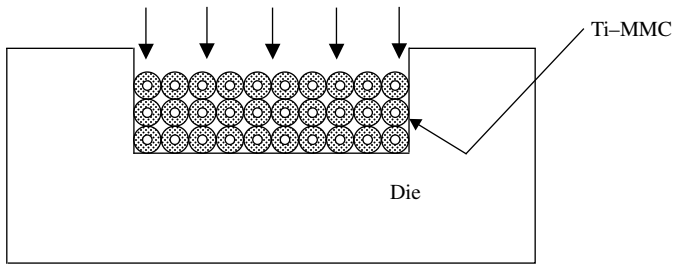


Fig. 8.4 Schematic diagram showing arrays of Ti-MMCs undergoing consolidation.

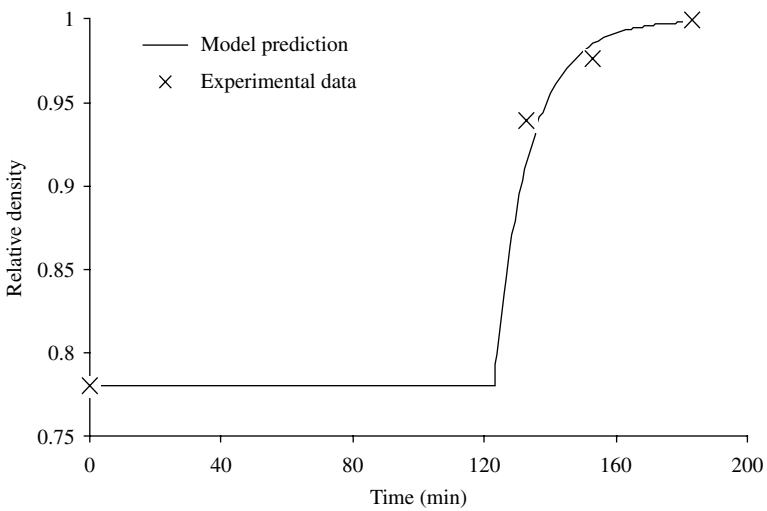


Fig. 8.5 Predicted and measured relative density evolution with time for Ti-6Al-4V/SiC composite consolidated at a constant temperature of 925°C with a pressure of 20 MPa.

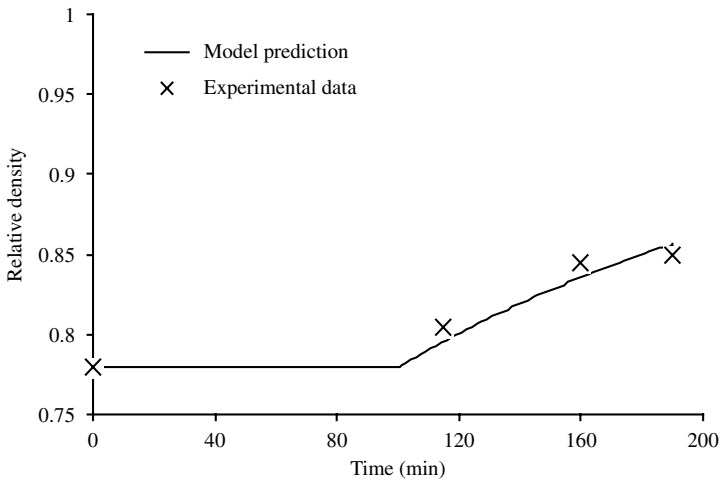


Fig. 8.6 Predicted and measured relative density evolution with time for Ti-6Al-4V/SiC composite consolidated at a constant temperature of 700°C with a pressure of 20 MPa.

shown schematically in Fig. 8.4. Generally, there are many more layers of fibres and the pressure is applied by means of a mechanical punch. The mechanical die ensures that the Ti-MMCs undergo plane strain compression.

Some of the results of the simulations, which were carried out at a constant temperature of 925°C under a pressure of 20 MPa, and at a temperature of 700°C under a constant pressure of 20 MPa, are shown in Figs 8.5 and 8.6, respectively, showing the important effect of temperature.

References

- Cocks, A.C.F. (1989). 'Inelastic deformation of porous materials'. *Journal of the Mechanics and Physics of Solids*, 37(6), 693.
- Duva, J.M. and Crow, P.D. (1992). 'The densification of powders by power-law creep during hot isostatic pressing'. *Acta Metallurgica*, 40(1), 31.
- Duva, J.M. and Crow, P.D. (1994). 'Analysis of consolidation of reinforced materials by power-law creep'. *Mechanics of Materials*, 17, 25.
- King, J. (1998). 'Composites take off without a parachute'. *Materials World*, 5(6), 324.
- Ponte Castaneda, P. (1991). 'The effective mechanical properties of nonlinear isotropic composites'. *Journal of the Mechanics and Physics of Solids*, 39(1), 45.
- Sofronis, P. and McMeeking, R.M. (1992). 'Creep of power-law material containing spherical voids'. *Journal of Applied Mechanics, Transactions of ASME*, 59(2), 88.
- Wilkinson, D.S. and Ashby, M.F. (1975). 'Pressure sintering by power law creep'. *Acta Metallurgica*, 23, 1277.

This page intentionally left blank

9. Creep in an aero-engine combustor material

9.1 Introduction

Aero-engine components operating under in-service conditions are often subjected to a range of complex cyclic mechanical and thermal loading, leading to combined creep and cyclic plasticity. The polycrystalline nickel-base superalloy (C263) is a commercial alloy used for stationary components in aero-engines such as combustion chambers, casings, liners, exhaust ducting, and bearing housings. It is a fine-precipitate strengthened alloy at 800°C, with a precipitate solvus temperature of 925°C (Betteridge and Heslop, 1974). Combustion chamber applications require the material to undergo temperature fluctuations between 20°C and 950°C, and the temperature range is therefore such that the precipitate solvus can be exceeded during in-service operation. Significant microstructural change is therefore likely to occur during ordinary operation, leading to quite profound changes in the creep mechanisms in the material, controlling both deformation and component life.

In this chapter, we shall introduce a physically based creep model which explicitly accounts for microstructural change, and its influence on creep deformation and failure, in polycrystalline nickel-base alloy C263 for temperatures both above and below the γ' solvus. The implementation into ABAQUS is carried out using a forward Euler integration scheme and we again use the initial stiffness as the material Jacobian for simplicity.

9.2 Physically based constitutive equations

Creep in nickel alloy C263 occurs through diffusion-activated dislocation climb and precipitate ‘cutting’, depending on the precipitate spacing, λ_p (or equivalently, size, r_s , for a given precipitate volume fraction, ϕ_p , which in turn depends on temperature, T). Above a critical particle spacing, λ_{pc} , dislocation climb dominates, whereas below the critical spacing, precipitate ‘cutting’ dominates. The material also undergoes *coarsening* at temperature such that the particle spacing increases with time.

All of these microstructural processes are embodied within creep constitutive equations. The creep strain rate, $\dot{\rho}_c$, also depends upon the density, ρ_n , of mobile dislocations which in turn depends on the accumulated creep strain. The constitutive equation set embodying all the mechanisms discussed above is given below. The activation volume, ΔV , depends on the active obstruction mechanism. In the case of dislocation pinning by precipitates, ΔV is dependent on the pinning distance, which in turn depends on the precipitate spacing. For precipitate cutting, the activation volume is ΔV_c . In the creep strain rate equation, the uniaxial strain rate, $\dot{\epsilon}_c$, in response to a uniaxial stress, σ , is determined from the corresponding shear values using the usual relationships (Dieter, 1988): $\dot{\epsilon} = \dot{\gamma}/\bar{M}$ and $\sigma = \bar{M}\tau$, in which \bar{M} is the Taylor factor. ΔF is the Helmholtz free energy, b the Burger's vector, ν the frequency of dislocation jumping energy barriers, k_b the Boltzman constant, and ρ_i the initial density of mobile dislocations.

$$\dot{\rho}_c = \frac{\rho_n \rho_i ([4\pi/3\phi_p]^{1/3} - 2)}{[4\pi/3\phi_p]^{1/3} \bar{M}} b^2 \nu \exp\left(\frac{-\Delta F}{k_b T}\right) \sinh\left(\frac{\sigma_e \Delta V}{k_b T \bar{M} (1 - \omega)}\right), \quad (9.1)$$

where

$$\begin{aligned} \Delta V &= \Delta V_c, & \text{if } \phi_p > 0 \text{ and } \lambda_p < \lambda_{pc} & \quad (\text{cutting}), \\ \Delta V &= \lambda_p b^2, & \text{if } \phi_p > 0, \lambda_p > \lambda_{pc} \text{ and } \lambda_p < \lambda_d & \quad (\text{climbing}), \\ \Delta V &= \lambda_d b^2, & \text{if } \phi_p = 0 & \quad (\text{dislocation network}) \end{aligned}$$

and

$$\lambda_p = r_s \left(\left[\frac{4\pi}{3\phi_p} \right]^{1/3} - 2 \right),$$

$$\dot{\rho}_n = \psi \dot{\epsilon}_c.$$

In Equation (9.1), ω is a scalar damage variable which has evolution equation

$$\dot{\omega} = \Omega \left(\frac{\sigma_1}{\sigma_e} \right)^\chi H(\sigma_1) \dot{\rho}_c \quad (9.2)$$

in which σ_1 is the maximum principal stress, H the Heaviside function, and Ω and χ are material constants (χ being the sensitivity of stress state parameter).

The equations contain just two unknown fitting constants, namely ψ and Ω associated with the multiplication of mobile dislocations and cavitation, occurring largely within the tertiary creep regime. All the other material constants are physical properties or measurable physical quantities.

Creep tests have been carried out by Rolls-Royce over the temperature range 700–750°C, and by Zhang and Knowles (2001) on C263 over the temperature range 800–950°C. Prior to creep testing, the material had been subjected to the standard

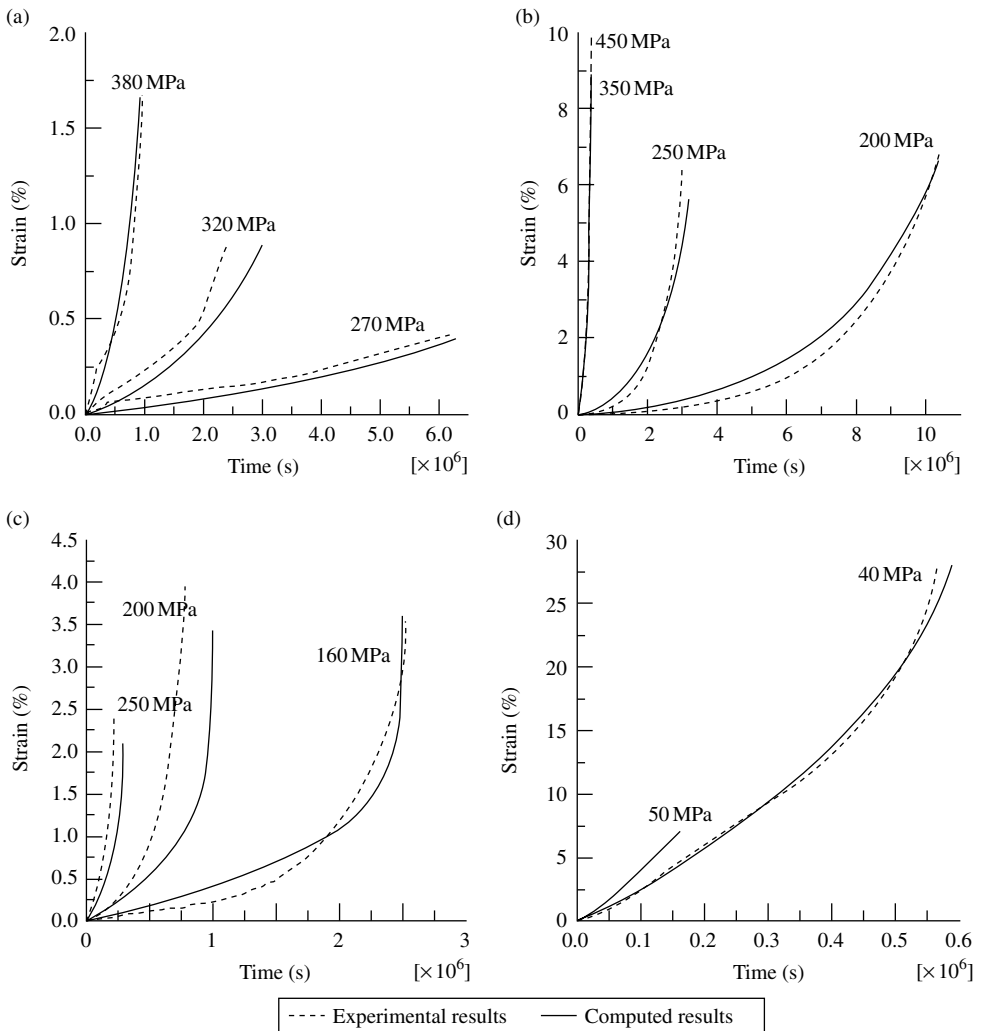


Fig. 9.1 Comparison of experimental and computed isothermal creep results at (a) 700°C, (b) 750°C, (c) 800°C, and (d) 950°C.

heat treatment. This involves solutioning at 1150°C for 2 h, quenching and ageing at 800°C for 8 h followed by air cooling. The results of the tests are shown in Fig. 9.1 by the broken lines.

The constants and constant groups appearing in the equations have been determined by standard optimization techniques. The volume fraction of γ' precipitate is known at each test temperature, Burger's vector for this material is taken as 2.5×10^{-10} m (Frost and Ashby, 1982), and the initial density of dislocations can be estimated to

Table 9.1 Physical constants determined from creep data by optimization.

ΔF (J/atom)	λ_{pc} (nm)	ΔV_c (m ³)	ν (s ⁻¹)	\bar{M}
7.4×10^{-19}	64.9	4.05×10^{-27}	15.1×10^{21}	3.57

be 10^{10} m^{-2} (Hull, 1975). The remaining temperature-independent physical properties can then be determined using the results of the optimization and the model equations. The results of this process are shown in Table 9.1, which includes the Helmholtz free energy, ΔF , the critical particle spacing, λ_{pc} , above which dislocation bowing dominates over particle cutting, the activation volume for cutting, ΔV_c , the frequency of dislocations jumping energy barriers, ν , and the Taylor factor. The temperature dependence of the two empirical constants for the evolution of multiplication of mobile dislocation density and cavitation is shown in Appendix 9.1. The computed creep curves resulting from the determination of the creep parameters are also shown in Fig. 9.1.

9.3 Multiaxial implementation into ABAQUS

We assume multiaxial creep deformation in nickel alloy C263 to obey von Mises behaviour; that is, the relationship between uniaxial creep strain rate and stress is identical to that between the effective creep strain rate and effective stress. Under multiaxial conditions, the creep strain rate ‘direction’ is taken to be normal to the dissipative surface, in an analogous way to that in plasticity, giving the multiaxial creep strain rate as

$$\dot{\epsilon}_c = \frac{3}{2} \dot{p}_c \frac{\boldsymbol{\sigma}'}{\sigma_e}$$

in which $\boldsymbol{\sigma}'$ is the deviatoric stress tensor, and σ_e the effective stress, given by

$$\sigma_e = \left(\frac{3}{2} \boldsymbol{\sigma}' : \boldsymbol{\sigma}' \right)^{1/2}$$

and the effective creep strain rate, \dot{p}_c , is given in Equation (9.1). The equations have been implemented into an ABAQUS UMAT using a simple forward Euler explicit integration scheme with the initial stiffness method; that is, the material Jacobian is specified simply as the elasticity matrix.

9.3.1 Finite element modelling of biaxial creep tests

A range of tests have been carried out on nickel alloy C263 in order to investigate its stress state sensitivity of creep failure. The tests have been carried out on thin-walled

Table 9.2 Summary of tests and loading conditions, and corresponding stress state.

	Shear stress (MPa)	Axial stress (MPa)	σ_1/σ_e
Tension	0	320	1.0
Tension–torsion	160	160	0.81
Torsion	184	0	0.58
Compression–torsion	160	–160	0.31

tubular specimens which have been subjected to uniaxial tension, tension–torsion, torsion, and compression–torsion. The material was subjected to the standard heat treatment such that its uniaxial creep behaviour, through to failure, is correctly modelled using the above constitutive equations with the material properties given in Manonukul *et al.* (2002). The test specimen gauge section has length 16 mm, with internal and external radii of 3.12 and 4.12 mm, respectively. The tests were carried out at 800°C such that the von Mises effective stress for each test was the same, namely 320 MPa. The loading conditions applied are summarized in Table 9.2.

The loads were increased linearly from zero to the maximum (to give the desired stresses) over 14 s, and were then held at the maximum value. The experimental test results are shown in Fig. 9.2(a). The quality of the creep data obtained for the torsion test is, unfortunately, not as good as desired because of problems with temperature control. However, the results do demonstrate the strong dependence of creep life on stress state. The stress state, given by σ_1/σ_e , for each test, is shown in Table 9.2. The test specimens were modelled by developing three-dimensional meshes of the gauge sections (i.e. uniform-section tubes). Because of the need to carry out compression tests, the wall thickness was constrained by buckling problems. As a result, the specimen wall thickness was such that an assumption of uniform shear strain and stress through the wall thickness would not have been appropriate. A two-dimensional finite element model was therefore necessitated. However, because of the ease of specification of torsional loading conditions using three-dimensional elements (as opposed to axisymmetric elements with ‘twist’ in ABAQUS), 240 eight-noded, three-dimensional solid elements were used so that the specimen thickness contained two elements. Geometrical non-linearity was accounted for using the standard ABAQUS large strain formulation. Under torsional loading, because of the radial variation of stress, the loads applied were chosen to ensure that the average effective stress through the thickness was that desired, that is, 320 MPa. The creep behaviour of the material was described by the constitutive equations given above. The only unknown parameter in the equations is the stress state sensitivity, χ . The four tests described above were simulated using the finite element model. Parametric studies were carried out in order

214 Creep in aero-engine components

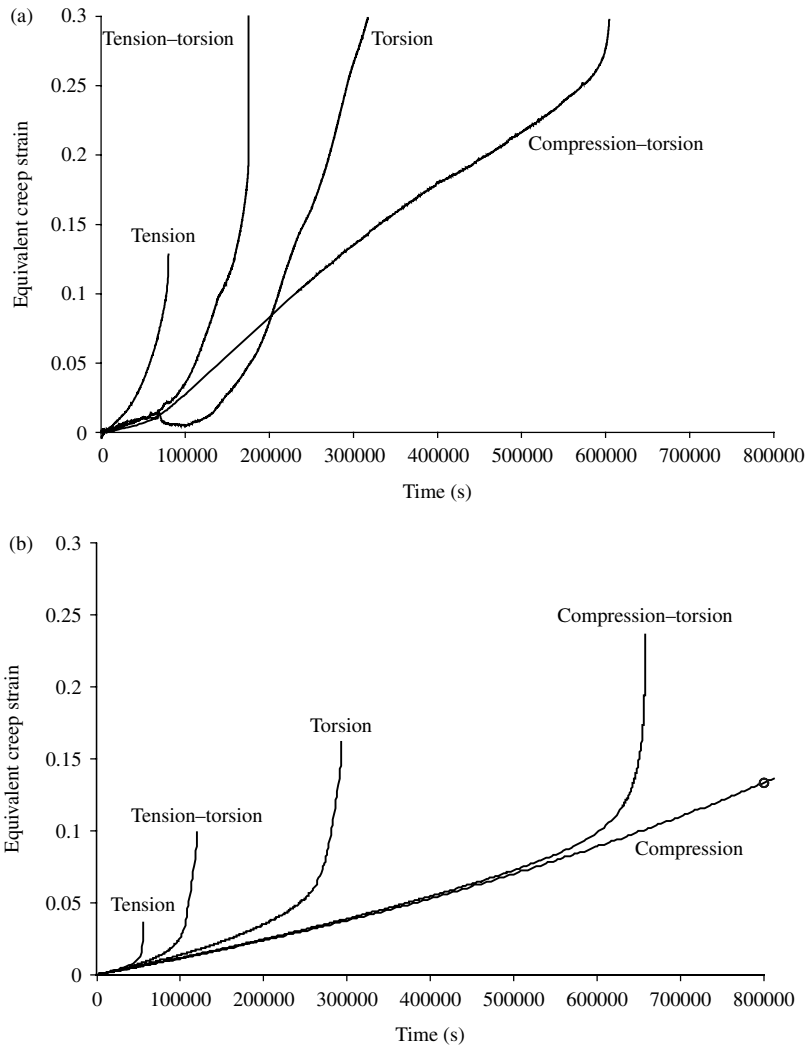


Fig. 9.2 (a) Experimental and (b) computed equivalent creep strain versus time for isothermal creep tests carried out at 800°C with effective stress 320 MPa for the loading conditions shown.

to determine χ . This was done by choosing that value of χ which provided computed results closest to those seen in the experiments. The computed results obtained using a value for χ of 0.38 are shown in Fig. 9.2(b). This value lies within the range for nickel alloys discussed by Dyson and Loveday (1981). Considerably different creep lives are seen to occur depending on the stress state, and this is captured well by the model. The computed creep curve for uniaxial compression shown in Fig. 9.2(b) can be seen to have a slowly increasing gradient, even though there is no creep cavitation

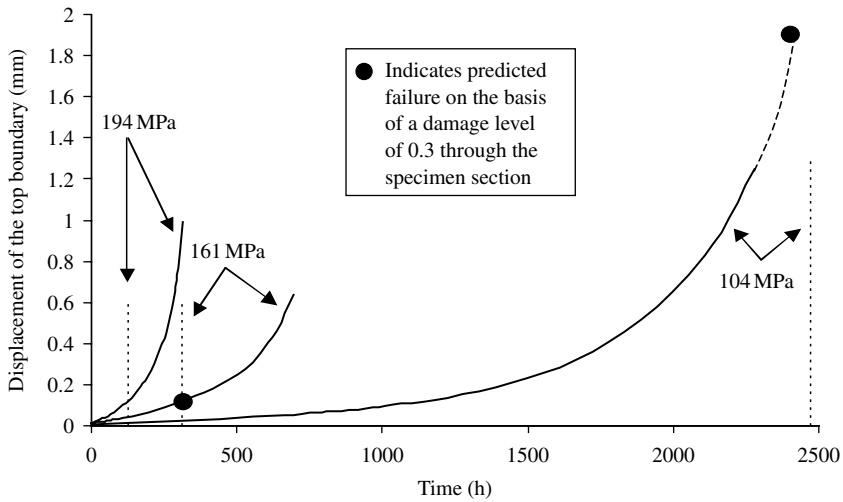


Fig. 9.3 Predicted displacement of the top boundary versus time (solid lines) for the double notch specimen subjected to the stresses shown. Broken straight lines indicate experimentally determined times to failure.

occurring. This results from both the precipitate coarsening and the multiplication of mobile dislocations, both of which are included in the model.

9.3.2 Prediction of notched bar creep behaviour

Three experimental tests have been carried out on double notched bar test specimens. The specimens have gauge length 25.4 mm and diameter 5.62 mm. The circular notches have diameter 1.12 mm and they are separated by 7 mm along the length of the specimen. The effect of the notches is to introduce multiaxial stress states local to the notches, which influence creep damage evolution, as discussed above. Uniaxial loading was applied to generate nominal section stresses of 104, 161, and 194 MPa, respectively. The test specimens were modelled using axisymmetric elements. Because of symmetry, just one quarter of the specimen section was modelled explicitly. The specimen lifetimes have been predicted and the lives compared with those obtained in the experiments.

The predicted displacements of the top boundary of the test specimen are shown for the three applied, nominal stresses of 104, 161, and 194 MPa in Fig. 9.3. The creep damage evolution for the case of the 161 MPa nominal stress is shown in Fig. 9.4(a). At this stress level, creep damage is predicted to initiate at the notch root after creeping for about 13 h. By the time creep has continued for 166 h, the damage has evolved right across the test specimen, in which the damage level is 0.26 or higher. This is

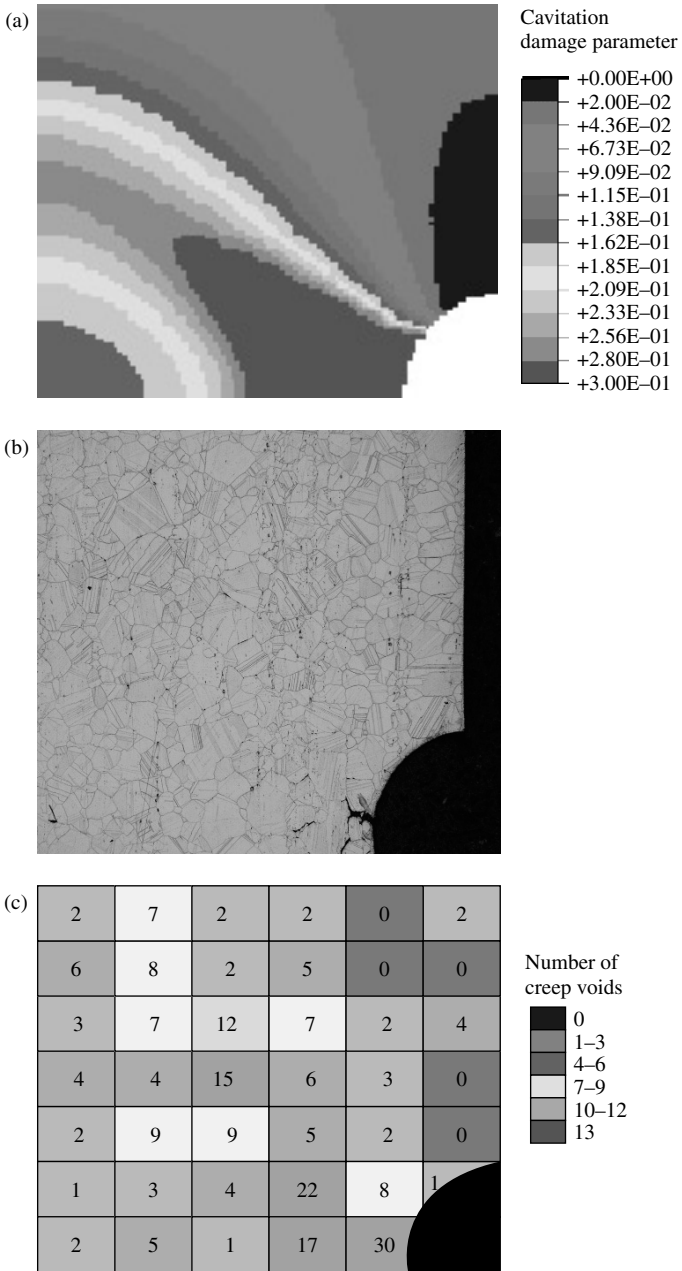


Fig. 9.4 Creep damage fields (a) predicted by the model, (b) observed in the microstructure, and (c) from a surface void count using the micrograph. (See also Plate 4.)

Table 9.3 Predicted and experimentally determined top boundary displacement at failure (defined as experimental specimen separation).

Stress (MPa)	Predicted displacement at failure (mm)	Experimental displacement at failure (mm)
104	1.9	1.97
161	0.1	0.11

shown in Fig. 9.4(a), together with a micrograph of the corresponding region of the test specimen in Fig. 9.4(b). Microcracking can be seen to initiate at the notch root at an angle of about 22° from the horizontal. A surface void count has been carried out and the results are shown in Fig. 9.4(c).

The damage fields in Fig. 9.4(a) can be seen to predict reasonably well both the site of major cracking and the distribution of experimentally observed creep cavitation. Dyson and McLean (1990) have argued that creep rupture occurs typically when the creep cavity damage achieves a value of about 0.3. This results from the coalescence of creep cavitation and the propagation of macroscopic creep cracking. The experimentally determined failure times are shown in Fig. 9.3 by the dashed lines. The measured and calculated displacements of the top boundary at failure, which show good agreement, are shown in Table 9.3. The predicted displacement at failure was determined as the predicted displacement when a damage level of about 0.3 had been achieved through the specimen section.

However, the analyses were not stopped once a creep damage level of 0.3 had been achieved across the specimen section, and hence Fig. 9.3 shows the calculated top boundary displacement continuing to increase as the damage level exceeds 0.3. A further reason for continuing the analysis is the difficulty of defining creep failure in the calculations. In the experiments, this is easier; it is simply the measured time until the specimen breaks. An alternative way to define calculated specimen rupture time is simply to examine the top boundary displacement rate, and to assume that rupture occurs once the rate becomes large. On this basis, the comparison of predicted and experimental time to rupture results shown in Fig. 9.3 is reasonable.

References

- Betteridge, W. and Heslop, J. (1974). *The Nimonic Alloys*. Edward Arnold, London, UK.
- Dyson, B.F. and Loveday, M.S. (1981). In Ponter, A.R.S. and Hayhurst, D.R. (eds), *Proceedings of the Creep in Structures IUTAM Symposium*, Springer, Berlin, 406–421.

- Dyson, B.F. and McLean, M. (1990). ‘Creep deformation of engineering alloys—development from physical modelling’. *Iron and Steel Institute of Japan International (ISIJ)*, 30, 802–811.
- Dieter, G.E. (1988). *Mechanical Metallurgy*. McGraw-Hill Book Co., London, UK.
- Frost, H.J. and Ashby, M.F. (1982). *Deformation-Mechanism Maps: The Plasticity and Creep of Metals and Ceramics*. Pergamon Press, Oxford, UK.
- Hull, D. (1975). *Introduction to Dislocations*, 2nd edition. Pergamon Press, Oxford, UK.
- Manonukul, A., Dunne, F.P.E., and Knowles, D. (2002). ‘Physically-based model for creep in nickel-base superalloy C263 both above and below the γ' solvus’. *Acta Materialia*, 50(11), 2917–2931.
- Zhang, Y.-H. and Knowles, D. (2001). ‘Deformation behaviour and development of microstructure during creep of a nickel-base superalloy’. In Parker, J.D. (ed.), *Proceedings of the 9th International Conference on Creep and Fracture of Engineering Materials and Structures*, April 2001, Gomer Press, UK.

Appendix 9.1

The dependence of precipitate volume fraction, ϕ , on temperature, T , in C263
 $\phi = -4.537 \times 10^{-9}T^3 + 1.261 \times 10^{-5}T^2 - 1.187 \times 10^{-2}T + 3.915$.

The dependence of constants Ω and Ψ on temperature.

	700°C	750°C	800°C	950°C
Ω	496.1	435.2	10.0	1.1×10^{-19}
ψ	1.58×10^{-2}	3.01×10^{-2}	18.62	19.84

10. Cyclic plasticity, creep, and TMF

10.1 Introduction

In Chapter 9, we examined creep in the aero-engine combustor material nickel-base superalloy C263. In this chapter, we address combined anisothermal cyclic plasticity and creep. We use time-independent cyclic plasticity with both isotropic and kinematic hardening which we combine with the physically based creep model described in Chapter 9. The plasticity model is implemented into ABAQUS Implicit by means of a UMAT subroutine which employs a simple first-order forward (explicit) integration scheme and the initial stiffness method. We then address isothermal cyclic plasticity and creep, followed by an examination of thermo-mechanical fatigue in nickel alloy C263.

10.2 Constitutive equations for cyclic plasticity

C263 is largely rate-independent and shows very limited creep response at temperatures below $\sim 600^\circ\text{C}$. During zero-mean, strain-controlled reversed plasticity below this temperature, the material exhibits both kinematic hardening within individual cycles, and isotropic strain softening/hardening over many cycles, depending on the temperature. The resulting stress–strain hysteresis loops show considerable change as plastic strain accumulates. Above $\sim 600^\circ\text{C}$, under similar loading, the material starts to exhibit strain-rate dependence. Viscoplastic constitutive equations for a polycrystalline nickel-base alloy have been presented by Yaguchi *et al.* (2002a,b), who considered uniaxial creep, isothermal, and anisothermal cyclic plasticity between 450°C and 950°C .

Because of the wide temperature range considered here ($20\text{--}950^\circ\text{C}$), a unified viscoplasticity-creep model is not adopted because of the numerical problems that can arise when using such a model for time-independent plasticity. In any case, it would, in addition, prevent the retention of the physical basis of the creep model to be used here, presented by Manonukul *et al.* (2002). A non-unified approach has therefore been adopted in which conventional time-independent reversed plasticity

theory for low-temperature deformation has been combined with the physically based creep model for elevated temperature deformation. The further justification for the separation of creep and time-independent plasticity terms is that at 20°C, for example, (thermally activated) creep simply does not occur. Deformation takes place by plastic slip which is not aided by thermally activated dislocation climb. Conversely, at 950°C, deformation is dominated by diffusion-controlled processes, and plastic slip, aided by thermal activation or otherwise, is negligible. At about 800°C, both sets of mechanisms operate, and a unified viscoplasticity theory would be appropriate. However, for the main application considered here—thermo-mechanical fatigue with considerable temperature variations, 20–950°C, our approach can be justified. It is therefore assumed that the elastic, $d\boldsymbol{\epsilon}^e$, time-independent plastic, $d\boldsymbol{\epsilon}^p$, creep, $d\boldsymbol{\epsilon}^c$, and thermal, $d\boldsymbol{\epsilon}^\theta$, strain increments may be additively decomposed such that the total strain, $d\boldsymbol{\epsilon}$, is given by

$$d\boldsymbol{\epsilon} = d\boldsymbol{\epsilon}^e + d\boldsymbol{\epsilon}^p + d\boldsymbol{\epsilon}^c + d\boldsymbol{\epsilon}^\theta. \quad (10.1)$$

There have been many developments in the modelling of kinematic hardening that take account, for example, of non-proportional loadings (Voyiadjis and Abu Al-Rub, 2003). However, for simplicity here, the Chaboche combined isotropic and kinematic hardening model (Lemaitre and Chaboche, 1990) is employed for time-independent plasticity.

The increment in non-linear kinematic hardening dx and the increment in isotropic hardening dr are given, respectively, by

$$dx = \frac{2}{3}c d\boldsymbol{\epsilon}^p - \gamma x dp \quad (10.2)$$

and

$$dr = b(Q - r) dp, \quad (10.3)$$

where

$$dp = \left(\frac{2}{3} d\boldsymbol{\epsilon}^p : d\boldsymbol{\epsilon}^p \right)^{1/2}. \quad (10.4)$$

Here, x is the kinematic hardening stress tensor, r the isotropic hardening stress, and b and Q are temperature dependent material parameters associated with isotropic hardening. Temperature and accumulated plastic strain dependent material parameters associated with kinematic hardening are c and γ , respectively. A large number of fully reversed cyclic plasticity tests have been carried out in order to determine the temperature-dependent material parameters arising in the kinematic hardening equations. dp is the effective time-independent plastic strain increment. The increment in plastic strain is determined in the conventional way assuming a von

Mises yield function, f , given by

$$f = \left[\frac{3}{2} (\boldsymbol{\sigma}' - \mathbf{x}') : (\boldsymbol{\sigma}' - \mathbf{x}') \right]^{1/2} - r - \sigma_y = 0$$

so that

$$d\boldsymbol{\varepsilon}^p = d\lambda \frac{\partial f}{\partial \boldsymbol{\sigma}} = \frac{3}{2} d\lambda \frac{\boldsymbol{\sigma}' - \mathbf{x}'}{\sigma_e} \quad (10.5)$$

in which $d\lambda$ is the plastic multiplier which, for combined isotropic and kinematic hardening, is given, using Voigt notation, by

$$\begin{aligned} d\lambda &= \frac{(\partial f / \partial \boldsymbol{\sigma}) \cdot \mathbf{C} d\boldsymbol{\varepsilon}}{(\partial f / \partial \boldsymbol{\sigma}) \cdot \{(2/3)c(\partial f / \partial \boldsymbol{\sigma}) - \gamma \mathbf{x}\} + b(Q - R) + (\partial f / \partial \boldsymbol{\sigma}) \cdot \mathbf{C} (\partial f / \partial \boldsymbol{\sigma})} \\ &= \left(\frac{(\frac{3}{2})(\boldsymbol{\sigma}' / \sigma_e) \cdot \mathbf{C} d\boldsymbol{\varepsilon}}{(\frac{3}{2})(\boldsymbol{\sigma}' / \sigma_e) \cdot \{(\frac{2}{3})c(\frac{3}{2})(\boldsymbol{\sigma}' / \sigma_e) - \gamma \mathbf{x}\} + b(Q - R) + (\frac{3}{2})(\boldsymbol{\sigma}' / \sigma_e) \cdot \mathbf{C} (\frac{3}{2})(\boldsymbol{\sigma}' / \sigma_e)} \right) \end{aligned} \quad (10.6)$$

The effective stress is, of course, given by

$$\sigma_e = \left[\frac{3}{2} (\boldsymbol{\sigma}' - \mathbf{x}') : (\boldsymbol{\sigma}' - \mathbf{x}') \right]^{1/2}.$$

The increment in thermal strain is calculated in the usual way as

$$d\boldsymbol{\varepsilon}^\theta = \alpha d\theta \mathbf{I} \quad (10.7)$$

in which α is the coefficient of thermal expansivity, $d\theta$ the increment in temperature, and \mathbf{I} the identity matrix.

The multiaxial constitutive equations presented above for creep and plasticity have been implemented into a UMAT user subroutine using the simple first-order explicit Euler forward integration scheme as follows

$$d\boldsymbol{\sigma}_t = \mathbf{C} \left(d\boldsymbol{\varepsilon}_t - \frac{3}{2} d\lambda \frac{\boldsymbol{\sigma}'}{\sigma_e} - d\boldsymbol{\varepsilon}^c - d\boldsymbol{\varepsilon}^\theta \right)$$

in which the increment in creep strain is obtained from Equation (9.33) and those in Table 9.1, and

$$\begin{aligned} \boldsymbol{\sigma}_{t+\Delta t} &= \boldsymbol{\sigma}_t + d\boldsymbol{\sigma}_t, \\ \mathbf{x}_{t+\Delta t} &= \mathbf{x}_t + d\mathbf{x}_t, \\ \boldsymbol{\varepsilon}_{t+\Delta t}^p &= \boldsymbol{\varepsilon}_t^p + d\boldsymbol{\varepsilon}_t^p, \\ r_{t+\Delta t} &= r_t + dr_t. \end{aligned}$$

10.3 Constitutive equations for C263 undergoing TMF

The thermo-mechanical loading cycles to which the nickel-base superalloy C263 is subjected in-service are such that the γ' solvus is exceeded so that the material is, in effect, solution treated. This has a profound effect on the behaviour of the material; under conditions of both creep and reversed plasticity. The rate-controlling mechanisms for creep deformation change from precipitate cutting and dislocation pinning at precipitates, and climb, to that of the pinning of dislocations through the establishment of a dislocation network. The physically based creep model employed here is able to capture these changes and to represent the micro- and macro-scale creep deformation. For a given temperature, the precipitate volume fraction is known, and because the precipitate coarsening kinetics has been quantified, both size and hence spacing of the precipitate is known. These quantities appear explicitly in the physically based creep model. The effect of solution treating on cyclic plastic response is also very significant and has been addressed. Cyclic plasticity tests between 20°C and 950°C have been carried out. With the combined creep–cyclic plasticity model described above, the temperature dependence of the isotropic and kinematic hardening constants have been determined (Manonukul *et al.*, 2001). The effect of precipitate volume fraction on cyclic plasticity behaviour is introduced into the model, therefore, through the temperature dependence of the material parameters for cyclic plasticity.

At temperatures of about 800°C and above, C263 creeps quite significantly. This appears in the cyclic plasticity response as a reduction in the overall stress level, occurring through relaxation. LCF tests have been carried out on C263 at 800°C and 950°C under fully reversed ($R = -1$), strain-controlled loading through to failure. The experimentally determined and calculated stress–strain hysteresis loops for the first and second cycles of the standard heat treated material are shown in Fig. 10.1. At 800°C, two strain rates have been used such that ramping times (the time over which the strain is applied linearly with time) of 1 and 10 s have been imposed resulting in the hysteresis loops shown in Fig. 10.1(a) and (b), respectively. Figure 10.1(c) shows the results for 950°C. In these cycles, a 1-s strain hold has been imposed at the tensile and compressive peak strains. At 800°C, this does not result in a distinctive stress relaxation, but this can be seen at 950°C in the computed result. However, the experiments show a much more progressive stress relaxation at the peak strains suggesting that the rate of relaxation is not well represented by the creep model. This occurs for a number of reasons. First, the creep model at 950°C was developed from experimental data obtained for a much lower stress level (a maximum of 50 MPa) whereas here, stresses of over 200 MPa are developed in the hysteresis loop. In addition, our cyclic plasticity model does not contain an explicit static recovery term,

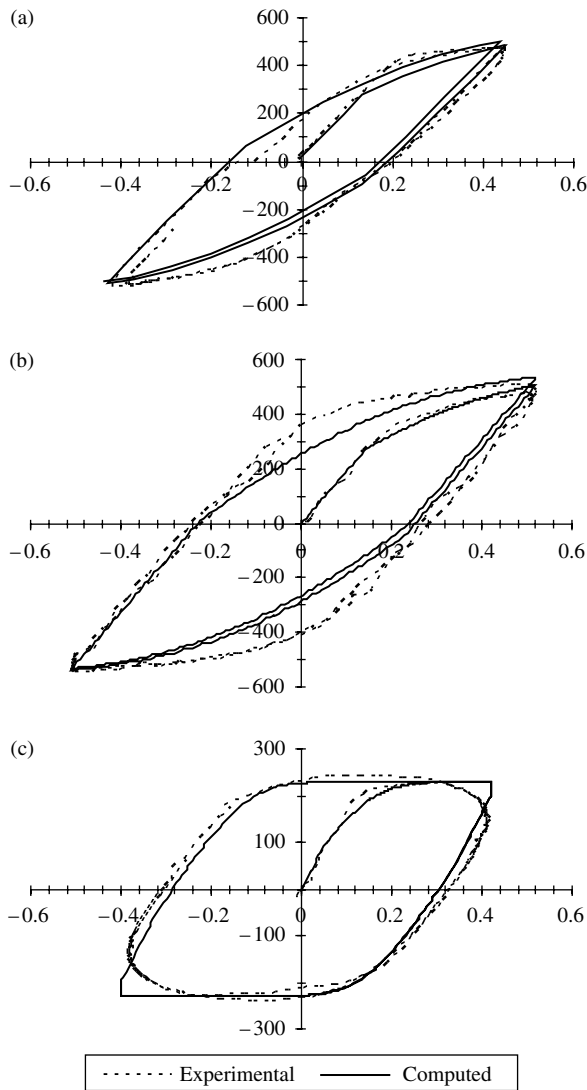


Fig. 10.1 Experimental and computed LCF stress–strain curves for the first and second cycles at (a) 800°C, 1 s ramping time, strain range 0.9%, (b) 800°C, 10 s ramping time, strain range 1%, and (c) 950°C, strain range 0.75%.

and further, the creep and plastic strain increments have, of course, been decoupled in the present work. Note that the microstructure of the material being loaded at 950°C is considerably different to that at 800°C because of the dissolution of the precipitate at the higher temperature. However, for both temperatures considered here, the peak stress levels are reasonably well predicted.

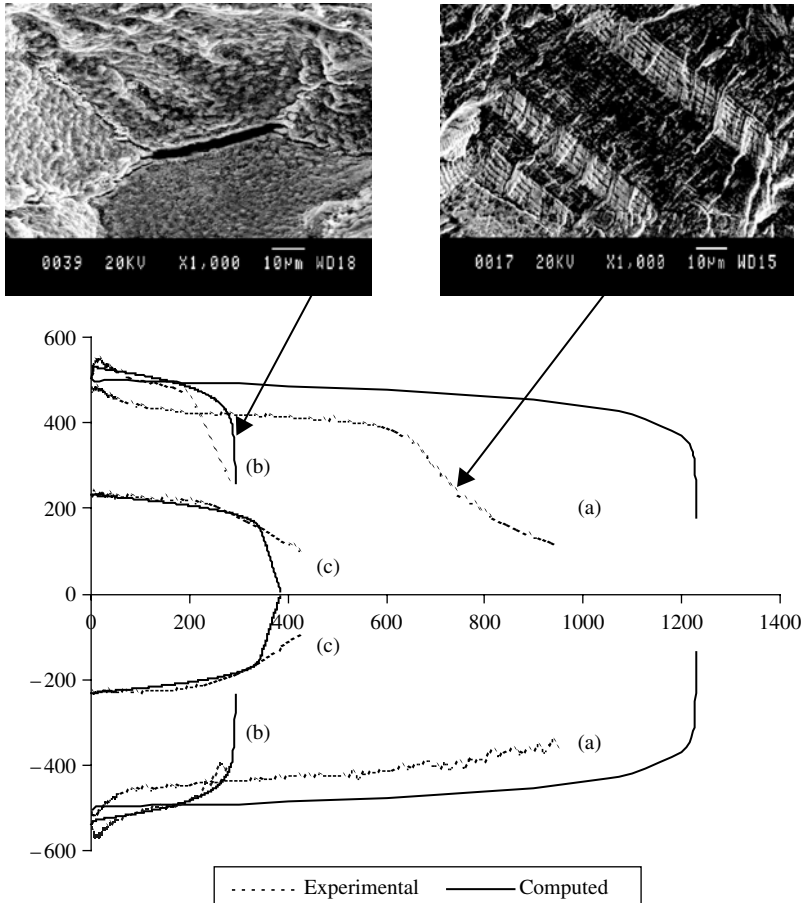


Fig. 10.2 Experimental and computed LCF peak stresses versus cycles at (a) 800°C, 1 s ramping time, strain range 0.9%, (b) 800°C, 10 s ramping time, strain range 1%, and (c) 950°C, strain range 0.75%.

Figure 10.2 shows the comparisons of computed and experimental peak stresses versus cycles for each of the cases (a), (b), and (c) in Fig. 10.1, through to failure. Good predictions of life can be seen to be achieved for (b) and (c) for which intergranular creep cavitation dominates. Intergranular creep damage typically observed under these conditions is shown in Fig. 10.2. The life is overpredicted for (a) since creep damage accumulation has ceased to be the dominant failure process. A micrograph for these conditions shows that transgranular fracture is now occurring.

Microstructural examination of specimens tested at 800°C and 950°C has been carried out after specimen failure. LCF tests carried out at 800°C, with 1-s ramp times, led to sample fracture surfaces showing transgranular cracking, as shown in Fig. 10.2, indicating that lifetime under these conditions is dominated by fatigue

processes. However, microstructural examination of specimens also tested at 800°C but with a considerably longer ramp time of 10 s showed the development of intergranular damage, which dominated in some regions of the material. The lifetime of the material under these conditions may well be influenced quite strongly by creep damage processes. Examination of microstructures of specimens tested at 950°C showed that intergranular cracking dominated at these temperatures, even for a ramp time of 1 s. The dominant failure process for these conditions is intergranular creep fracture. The results of the tests carried out at 800°C shown in Fig. 10.2(a) and (b) show the development of macrocracking towards the end of the test which influences the observed stress–strain response which becomes different in tension and compression because of crack closure effects.

The isotropic creep damage model used in the present work is not capable of predicting crack closure effects. The result at 950°C, however, which is dominated by creep softening and cavitation, does not show this effect.

10.3.1 TMF in C263 both above and below the γ' solvus

TMF tests have been carried out on C263 under conditions of both in and out of phase loading. Strain controlled tests have been carried out between strains of zero and a peak of 0.6%, in which the temperature is also varied between 300°C and 950°C. The strain and temperature loading imposed, together with the results obtained, are shown in Fig. 10.3. First, considering the in-phase loading shown in Fig. 10.3(a), the experimental results obtained for the initial loading, below the γ' solvus temperature, give stress levels that lie a little below that expected from both the solution treated and the standard treated material. After a time of 45 s, the temperature has exceeded 925°C, and in fact, the experimental results give stress levels that would be anticipated for such a material. It should be noted that prior to the imposition of the strain, the test specimen has undergone a prior temperature loading cycle. This is necessary to enable temperature compensation to be carried out on the TMF test rig. The consequence is that the material is, therefore, in effect in the solution treated state. The modelling of the behaviour has therefore been carried out with this assumption. For the cyclic plasticity modelling, two sets of material parameters were determined; one for the solution treated material (with the appropriate temperature dependence), and a further one for the standard treated material (i.e. for the material containing the precipitate volume fraction, which is dependent on temperature).

The model for the solution treated plasticity and creep behaviour give the computed behaviour also shown in Fig. 10.3(a). As the temperature increases, a number of processes are taking place. The volume fraction of precipitate is decreasing, and at 925°C, becomes zero. The creep rate becomes determined by dislocation network

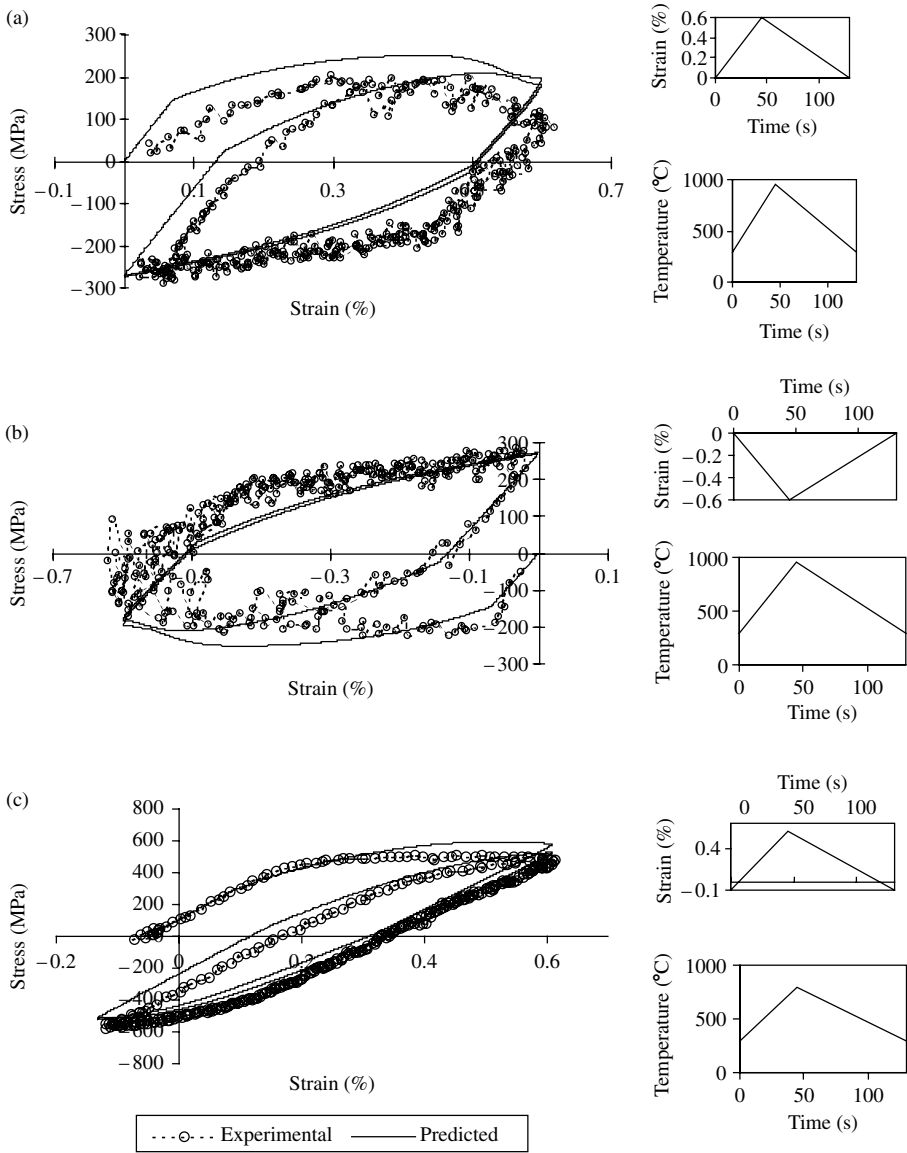


Fig. 10.3 Experimental and predicted stress–strain curves for (a) in-phase TMF at temperature range 300–950°C and (b) out-of-phase TMF at temperature range 300–950°C, and (c) in-phase TMF at temperature range 300–800°C .

pinning (Manonukul *et al.*, 2002) and increases as the temperature increases. The combined effects of these processes result in the predicted decreasing stress level. At a time of 45 s, both the strain and temperature loading are reversed, and a comparatively small elastic region (though creep deformation is still occurring) can be seen, which

is followed by a conventional plasticity region in which creep deformation becomes negligibly small as the temperature decreases towards 300°C. Note that the material continues to harden during this phase, with no stress relaxation occurring at the higher compressive stresses because of the elimination of creep. The stress levels measured and predicted by the model are those that would be anticipated from the solution treated material. The standard heat treated material would show considerably higher stresses. With the reversal of the loading again, a rather larger elastic region is observed because of the increased yield stress at lower temperature, and because of the existing hardening that has already taken place. The measured and predicted stresses developed with increasing plastic deformation show good agreement and, unlike the first quarter-cycle, are those that would be expected for the solution treated material.

The loading conditions and results obtained for out-of-phase TMF are shown in Fig. 10.3(b). In this case, the high tensile stresses occur during the low temperature parts of the loading cycle, and conventional plastic behaviour is observed. At the higher temperatures, the material is in compression, but again, stress relaxation can be seen to occur, and the features of the experimentally obtained results can be seen to be reasonably reproduced. For in-phase TMF with the same strain range, but with the temperature varying between 300°C and 800°C, the experimental and predicted results obtained are shown in Fig. 10.3(c). Good comparisons are achieved for these conditions.

References

- Lemaitre, J. and Chaboche, J.-L. (1990). *Mechanics of Solid Materials*. Cambridge University Press, Cambridge.
- Manonukul, A., Dunne, F.P.E., and Knowles, D. (2001). ‘Thermo-mechanical fatigue in nickel-base superalloy C263’. Internal Report, Department of Engineering Science, Oxford University, England.
- Manonukul, A., Dunne, F.P.E., and Knowles, D. (2002). ‘Physically-based model for creep in nickel-base superalloy C263 both above and below the γ' solvus’. *Acta Materialia*, 50, 2917–2931.
- Voyiadjis, G.Z. and Abu Al-Rub R.K. (2003). ‘Thermodynamic based model for the evolution equation of the backstress in cyclic plasticity’. *International Journal of Plasticity*, 19(12), 2121–2147.
- Yaguchi, M., Yamamoto, M., and Ogata, T. (2002a). ‘A viscoplastic constitutive model for nickel-base superalloy Part I: kinematic hardening rule of anisotropic dynamic recovery’. *International Journal of Plasticity*, 18(8), 1083–1109.
- Yaguchi, M., Yamamoto, M., and Ogata, T. (2002b). ‘A viscoplastic constitutive model for nickel-base superalloy Part II: modelling under anisothermal conditions’. *International Journal of Plasticity*, 18(8), 1111–1131.

This page intentionally left blank

Appendix A: Elements of tensor algebra

The dot (scalar) product of two first-order tensors (vectors) gives a scalar

$$\left(\text{NB. Einstein summation convention: } u_i v_i = \sum_{i=1}^n u_i v_i \right)$$

$$\mathbf{u} \cdot \mathbf{v} = u_i v_i = \sum_{i=1}^n u_i v_i, \quad (\text{A1})$$

$$\mathbf{v} \cdot \mathbf{u} = v_i u_i = \sum_{i=1}^n v_i u_i, \quad (\text{A2})$$

$$\mathbf{v} \cdot \mathbf{u} = \mathbf{u} \cdot \mathbf{v}. \quad (\text{A3})$$

Double contraction (double dot product) of two second-order tensors gives a scalar

$$\boldsymbol{\sigma} : \boldsymbol{\varepsilon} = \sigma_{ij} \varepsilon_{ij} = \sum_{i=1}^n \sum_{j=1}^n \sigma_{ij} \varepsilon_{ij}, \quad (\text{A4})$$

$$\boldsymbol{\varepsilon} : \boldsymbol{\sigma} = \varepsilon_{ij} \sigma_{ij} = \sum_{i=1}^n \sum_{j=1}^n \varepsilon_{ij} \sigma_{ij}, \quad (\text{A5})$$

$$\boldsymbol{\varepsilon} : \boldsymbol{\sigma} = \boldsymbol{\sigma} : \boldsymbol{\varepsilon}. \quad (\text{A6})$$

The dot product of a first-order tensor with a second-order tensor gives a first-order tensor

$$\boldsymbol{\sigma} \cdot \mathbf{n} \Rightarrow (\sigma_{ij} n_j)_i = \sum_{j=1}^n \sigma_{ij} n_j, \quad (\text{A7})$$

$$\mathbf{n} \cdot \boldsymbol{\sigma} \Rightarrow (n_j \sigma_{ji})_i = \sum_{j=1}^n n_j \sigma_{ji}, \quad (\text{A8})$$

230 Appendix A: Elements of tensor algebra

hence the expression

$$\mathbf{n} \cdot \boldsymbol{\sigma} = \boldsymbol{\sigma} \cdot \mathbf{n} \quad (\text{A9})$$

is valid only if $\boldsymbol{\sigma}$ is symmetric (i.e. if $\sigma_{ij} = \sigma_{ji}$ for any i, j).

The dyadic (direct) product of two first-order tensors gives a second-order tensor

$$\mathbf{u} \otimes \mathbf{v} \Rightarrow (\mathbf{u} \otimes \mathbf{v})_{ij} = u_i v_j. \quad (\text{A10})$$

For example, if

$$\mathbf{u} = \begin{bmatrix} u_1 \\ u_2 \\ u_3 \end{bmatrix} \quad \text{and} \quad \mathbf{v} = \begin{bmatrix} v_1 \\ v_2 \\ v_3 \end{bmatrix},$$

then

$$\mathbf{u} \otimes \mathbf{v} = \begin{pmatrix} u_1 v_1 & u_1 v_2 & u_1 v_3 \\ u_2 v_1 & u_2 v_2 & u_2 v_3 \\ u_3 v_1 & u_3 v_2 & u_3 v_3 \end{pmatrix}.$$

The product of two second-order tensors gives a second-order tensor

$$\mathbf{a} \cdot \mathbf{b} \Rightarrow (\mathbf{a} \cdot \mathbf{b})_{ij} = a_{ik} b_{kj} = \sum_{k=1}^n a_{ik} b_{kj}. \quad (\text{A11})$$

Double contraction (double dot product) of a third-order tensor with a second-order tensor gives a first-order tensor

$$\boldsymbol{\xi} : \boldsymbol{\sigma} = \sum_{i,j,k=1}^3 \xi_{ijk} \sigma_{jk} \mathbf{e}_i. \quad (\text{A12})$$

Double contraction (double dot product) of a fourth-order tensor with a second-order tensor gives a second-order tensor

$$\mathbf{c} : \boldsymbol{\varepsilon} \Rightarrow (\mathbf{c} : \boldsymbol{\varepsilon})_{ij} = c_{ijkl} \varepsilon_{kl} = \sum_{k=1}^n \sum_{l=1}^n c_{ijkl} \varepsilon_{kl} \quad (\text{A13})$$

hence the expression

$$\mathbf{c} : \boldsymbol{\varepsilon} = \boldsymbol{\varepsilon} : \mathbf{c} \quad (\text{A14})$$

is valid only if \mathbf{c} exhibits major symmetry (i.e. if $c_{ijkl} = c_{klij}$ for any i, j, k, l).

The dyadic (direct) product of two second-order tensors gives a fourth-order tensor

$$\mathbf{f} \otimes \mathbf{g} \Rightarrow (\mathbf{f} \otimes \mathbf{g})_{ijkl} = f_{ij} g_{kl}. \quad (\text{A15})$$

Kronecker delta—a special second-order tensor

$$\boldsymbol{\delta} \Rightarrow \delta_{ij} \quad \begin{cases} \delta_{ij} = 1, & \text{if } i = j, \\ \delta_{ij} = 0, & \text{if } i \neq j. \end{cases} \quad (\text{A16})$$

The unit fourth-order tensor (exhibits major but not minor symmetry)

$$\mathbf{I} \Rightarrow I_{ijkl} = \delta_{ik}\delta_{jl} \quad (\text{A17})$$

has the following important property

$$\mathbf{I} : \boldsymbol{\varepsilon} = \boldsymbol{\varepsilon} : \mathbf{I}, \quad (\text{A18})$$

which is valid for any second-order tensor $\boldsymbol{\varepsilon}$.

A symmetrized unit fourth-order tensor (exhibits both major and minor symmetry)

$$\mathbf{I}^s \Rightarrow I_{ijkl}^s = \frac{1}{2}(\delta_{ik}\delta_{jl} + \delta_{il}\delta_{jk}) \quad (\text{A19})$$

ensures the following identity

$$\mathbf{I}^s : \boldsymbol{\varepsilon} = \boldsymbol{\varepsilon} : \mathbf{I}^s, \quad (\text{A20})$$

which is valid only if the second-order tensor $\boldsymbol{\varepsilon}$ is symmetric.

Differentiation

Differentiation of a tensor valued function (e.g. \mathbf{u} , $\boldsymbol{\sigma}$) with respect to its tensorial argument (e.g. \mathbf{x} , $\boldsymbol{\varepsilon}$).

Example: Differentiation of the first-order tensor \mathbf{u} with respect to the first-order tensor \mathbf{x} gives the second-order tensor

$$\frac{\partial \mathbf{u}}{\partial \mathbf{x}} \Rightarrow \left(\frac{\partial u}{\partial x} \right)_{ij} = \frac{\partial u_i}{\partial x_j}. \quad (\text{A21})$$

Special case:

$$\frac{\partial \mathbf{u}}{\partial \mathbf{u}} \Rightarrow \left(\frac{\partial u}{\partial u} \right)_{ij} = \delta = \frac{\partial u_i}{\partial x_j} = \delta_{ij}. \quad (\text{A22})$$

Example: Differentiation of the second-order tensor $\boldsymbol{\sigma}$ with respect to the second-order tensor $\boldsymbol{\varepsilon}$ gives the fourth-order tensor

$$\frac{\partial \boldsymbol{\sigma}}{\partial \boldsymbol{\varepsilon}} \Rightarrow \left(\frac{\partial \sigma}{\partial \varepsilon} \right)_{ijkl} = \frac{\partial \sigma_{ij}}{\partial \varepsilon_{kl}}. \quad (\text{A23})$$

Special case:

$$\frac{\partial \boldsymbol{\sigma}}{\partial \boldsymbol{\sigma}} \Rightarrow \left(\frac{\partial \sigma}{\partial \sigma} \right)_{ijkl} = \mathbf{I} = \frac{\partial \sigma_{ij}}{\partial \sigma_{kl}} = I_{ijkl}. \quad (\text{A24})$$

The chain rule

Example: Second-order tensor f depends on a second-order tensor u and a scalar v

$$\frac{\partial f}{\partial x} = \frac{\partial f}{\partial u} : \frac{\partial u}{\partial x} + \frac{\partial f}{\partial v} \otimes \frac{\partial v}{\partial x} \Rightarrow \left(\frac{\partial f}{\partial x} \right)_{ijkl} = \frac{\partial f_{ij}}{\partial x_{kl}} = \frac{\partial f_{ij}}{\partial u_{mn}} \frac{\partial u_{mn}}{\partial x_{kl}} + \frac{\partial f_{ij}}{\partial v} \frac{\partial v}{\partial x_{kl}}. \tag{A25}$$

The gradient of a scalar field gives a first-order tensor

$$\nabla f \Rightarrow \frac{\partial f}{\partial x_i}. \tag{A26}$$

The gradient of a first-order tensor field gives a second-order tensor

$$\nabla v \Rightarrow \frac{\partial v_j}{\partial x_i}. \tag{A27}$$

The gradient of a second-order tensor field gives a first-order tensor with its components being second-order tensors

$$\nabla \sigma \Rightarrow (\nabla \sigma)_j = \frac{\partial \sigma_{ij}}{\partial x_i} = \frac{\partial \sigma_{ji}}{\partial x_i}. \tag{A28}$$

Hence,

$$\nabla \sigma = \begin{bmatrix} \left[\begin{array}{ccc} \frac{\partial \sigma_{xx}}{\partial x} & \frac{\partial \sigma_{xy}}{\partial x} & \frac{\partial \sigma_{xz}}{\partial x} \\ \frac{\partial \sigma_{xx}}{\partial y} & \frac{\partial \sigma_{xy}}{\partial y} & \frac{\partial \sigma_{xz}}{\partial y} \\ \frac{\partial \sigma_{xx}}{\partial z} & \frac{\partial \sigma_{xy}}{\partial z} & \frac{\partial \sigma_{xz}}{\partial z} \end{array} \right] \\ \left[\begin{array}{ccc} \frac{\partial \sigma_{yx}}{\partial x} & \frac{\partial \sigma_{yy}}{\partial x} & \frac{\partial \sigma_{yz}}{\partial x} \\ \frac{\partial \sigma_{yx}}{\partial y} & \frac{\partial \sigma_{yy}}{\partial y} & \frac{\partial \sigma_{yz}}{\partial y} \\ \frac{\partial \sigma_{yx}}{\partial z} & \frac{\partial \sigma_{yy}}{\partial z} & \frac{\partial \sigma_{yz}}{\partial z} \end{array} \right] \\ \left[\begin{array}{ccc} \frac{\partial \sigma_{zx}}{\partial x} & \frac{\partial \sigma_{zy}}{\partial x} & \frac{\partial \sigma_{zz}}{\partial x} \\ \frac{\partial \sigma_{zx}}{\partial y} & \frac{\partial \sigma_{zy}}{\partial y} & \frac{\partial \sigma_{zz}}{\partial y} \\ \frac{\partial \sigma_{zx}}{\partial z} & \frac{\partial \sigma_{zy}}{\partial z} & \frac{\partial \sigma_{zz}}{\partial z} \end{array} \right] \end{bmatrix}. \tag{A29}$$

The divergence of a second-order tensor gives a first-order tensor

$$\operatorname{div} \boldsymbol{\sigma} = \operatorname{Tr}[(\nabla \boldsymbol{\sigma})_i]. \quad (\text{A30})$$

Hence,

$$\operatorname{div} \boldsymbol{\sigma} = \begin{bmatrix} \operatorname{Tr} \left[\frac{\partial \sigma_{ij}}{\partial x_i} \right] \\ \operatorname{Tr} \left[\frac{\partial \sigma_{ij}}{\partial x_i} \right] \\ \operatorname{Tr} \left[\frac{\partial \sigma_{ij}}{\partial x_i} \right] \end{bmatrix} = \begin{bmatrix} \operatorname{Tr} \begin{bmatrix} \frac{\partial \sigma_{xx}}{\partial x} & \frac{\partial \sigma_{xy}}{\partial x} & \frac{\partial \sigma_{xz}}{\partial x} \\ \frac{\partial \sigma_{xx}}{\partial y} & \frac{\partial \sigma_{xy}}{\partial y} & \frac{\partial \sigma_{xz}}{\partial y} \\ \frac{\partial \sigma_{xx}}{\partial z} & \frac{\partial \sigma_{xy}}{\partial z} & \frac{\partial \sigma_{xz}}{\partial z} \end{bmatrix} \\ \operatorname{Tr} \begin{bmatrix} \frac{\partial \sigma_{yx}}{\partial x} & \frac{\partial \sigma_{yy}}{\partial x} & \frac{\partial \sigma_{yz}}{\partial x} \\ \frac{\partial \sigma_{yx}}{\partial y} & \frac{\partial \sigma_{yy}}{\partial y} & \frac{\partial \sigma_{yz}}{\partial y} \\ \frac{\partial \sigma_{yx}}{\partial z} & \frac{\partial \sigma_{yy}}{\partial z} & \frac{\partial \sigma_{yz}}{\partial z} \end{bmatrix} \\ \operatorname{Tr} \begin{bmatrix} \frac{\partial \sigma_{zx}}{\partial x} & \frac{\partial \sigma_{zy}}{\partial x} & \frac{\partial \sigma_{zz}}{\partial x} \\ \frac{\partial \sigma_{zx}}{\partial y} & \frac{\partial \sigma_{zy}}{\partial y} & \frac{\partial \sigma_{zz}}{\partial y} \\ \frac{\partial \sigma_{zx}}{\partial z} & \frac{\partial \sigma_{zy}}{\partial z} & \frac{\partial \sigma_{zz}}{\partial z} \end{bmatrix} \end{bmatrix} = \begin{bmatrix} \frac{\partial \sigma_{xx}}{\partial x} + \frac{\partial \sigma_{xy}}{\partial y} + \frac{\partial \sigma_{xz}}{\partial z} \\ \frac{\partial \sigma_{yx}}{\partial x} + \frac{\partial \sigma_{yy}}{\partial y} + \frac{\partial \sigma_{yz}}{\partial z} \\ \frac{\partial \sigma_{zx}}{\partial x} + \frac{\partial \sigma_{zy}}{\partial y} + \frac{\partial \sigma_{zz}}{\partial z} \end{bmatrix}. \quad (\text{A31})$$

Rotation

Finite rotation is mathematically described by the orthogonal second-order tensor

$$\mathbf{R}^{-1} = \mathbf{R}^T, \quad (\text{A32})$$

which transforms a first-order tensor as follows

$$\mathbf{x}' = \mathbf{R} \cdot \mathbf{x} \quad (\text{A33})$$

and a second-order tensor as follows

$$\boldsymbol{\sigma}' = \mathbf{R} \cdot \boldsymbol{\sigma} \cdot \mathbf{R}^T. \quad (\text{A34})$$

Successive finite rotations do not commute, that is,

$$\mathbf{R}_1 \cdot \mathbf{R}_2 \neq \mathbf{R}_2 \cdot \mathbf{R}_1. \quad (\text{A35})$$

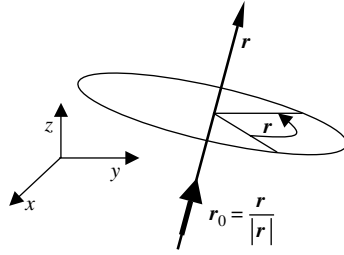


Fig. A.1 Finite rotation vector.

If the axis $\mathbf{r} = \begin{bmatrix} r_1 \\ r_2 \\ r_3 \end{bmatrix}$ and the magnitude $r = |\mathbf{r}|$ of a finite rotation are known the orthogonal second-order tensor which describes such rotation can be expressed in the form of an exponential function as follows:

$$\mathbf{R} = \exp[\hat{\mathbf{r}}] = \mathbf{I} + \hat{\mathbf{r}} + \frac{1}{2!}\hat{\mathbf{r}}^2 + \dots, \quad (\text{A36})$$

where $\hat{\mathbf{r}}$ is the associated skew-symmetric tensor

$$\hat{\mathbf{r}} = \begin{bmatrix} 0 & -r_3 & r_2 \\ r_3 & 0 & -r_1 \\ -r_2 & r_1 & 0 \end{bmatrix}, \quad (\text{A37})$$

which satisfies

$$\begin{aligned} \hat{\mathbf{r}} \cdot \mathbf{r} &= 0, \\ \hat{\mathbf{r}} \cdot \mathbf{x} &= \mathbf{r} \times \mathbf{x} \end{aligned} \quad (\text{A38})$$

as illustrated in Fig. A.1.

Small rotations can be approximated by

$$\mathbf{R} = \exp[\hat{\mathbf{r}}] = \mathbf{I} + \hat{\mathbf{r}} + \frac{1}{2!}\hat{\mathbf{r}}^2 + \dots \approx \mathbf{I} + \hat{\mathbf{r}} = \begin{bmatrix} 1 & 0 & 0 \\ 0 & 1 & 0 \\ 0 & 0 & 1 \end{bmatrix} + \begin{bmatrix} 0 & -r_3 & r_2 \\ r_3 & 0 & -r_1 \\ -r_2 & r_1 & 0 \end{bmatrix}, \quad (\text{A39})$$

which do commute

$$(\mathbf{I} + \hat{\mathbf{r}}_1) \cdot (\mathbf{I} + \hat{\mathbf{r}}_2) = (\mathbf{I} + \hat{\mathbf{r}}_2) \cdot (\mathbf{I} + \hat{\mathbf{r}}_1) = \mathbf{I} + \hat{\mathbf{r}}_1 + \hat{\mathbf{r}}_2 + \hat{\mathbf{r}}_1 \cdot \hat{\mathbf{r}}_2 \approx \mathbf{I} + \hat{\mathbf{r}}_1 + \hat{\mathbf{r}}_2. \quad (\text{A40})$$

Appendix B: Fortran coding available via the OUP website*

Directory/file	Description
elasticity	
elastic.f	UMAT for plane strain and axial symmetry for elastic behaviour using ABAQUS stress and strain quantities
elas_axidisp.inp	ABAQUS input file for single axisymmetric element under uniaxial displacement controlled loading, requiring UMAT elastic.f
elas_axiforce.inp	ABAQUS input file for single axisymmetric element under uniaxial force controlled loading, requiring UMAT elastic.f
plasticity_exp	
code_exp.f	UMAT for plane strain and axial symmetry for elastic, linear strain hardening plastic behaviour using explicit integration with continuum Jacobian, using ABAQUS stress and strain quantities. Suitable for large deformations
plas_exp_axidisp_abas.inp	ABAQUS input file for single axisymmetric element under uniaxial displacement controlled loading, using ABAQUS *PLASTIC
plas_exp_axiforce_abas.inp	ABAQUS input file for single axisymmetric element under uniaxial force controlled loading, using ABAQUS *PLASTIC

* www.oup.co.uk/isbn/0-19-856826-6

236 Appendix B: Fortran coding

plas_exp_axidisp.inp	ABAQUS input file for single axisymmetric element under uniaxial displacement controlled loading, requiring UMAT code_exp.f
plas_exp_axiforce.inp	ABAQUS input file for single axisymmetric element under uniaxial force controlled loading, requiring UMAT code_exp.f
plas_exp_beam_aba.inp	Four point bend loading using ABAQUS*PLASTIC, requiring mesh file beam_mesh.inp
plas_exp_beam.inp	Four point bend loading requiring UMAT code_exp.f, requiring mesh file beam_mesh.inp
plasticity_imp	
code_imp.f	UMAT for plane strain and axial symmetry for elastic, linear strain hardening plastic behaviour using implicit integration with consistent Jacobian, using ABAQUS stress and strain quantities. Suitable for large deformations
plas_imp_axidisp_aba.inp	ABAQUS input file for single axisymmetric element under uniaxial displacement controlled loading, using ABAQUS *PLASTIC
plas_imp_axiforce_aba.inp	ABAQUS input file for single axisymmetric element under uniaxial force controlled loading, using ABAQUS *PLASTIC
plas_imp_axidisp.inp	ABAQUS input file for single axisymmetric element under uniaxial displacement controlled loading, requiring UMAT code_imp.f
plas_imp_axiforce.inp	ABAQUS input file for single axisymmetric element under uniaxial force controlled loading, requiring UMAT code_imp.f
plas_imp_beam_aba.inp	Four point bend loading using ABAQUS*PLASTIC, requiring mesh file beam_mesh.inp
plas_imp_beam.inp	Four point bend loading requiring UMAT code_imp.f, requiring mesh file beam_mesh.inp

spin

spin_elastic.f	UMAT for three-dimensional, plane strain, and axial symmetry for elastic behaviour using ABAQUS stress and strain quantities
spin_elas_def.f	UMAT for three-dimensional, plane strain, and axial symmetry for elastic behaviour using the deformation gradient
spin_axidisp.inp	ABAQUS input file for single axisymmetric element under uniaxial displacement controlled loading, requiring UMAT spin_elas_def.f
spin_axiforce.inp	ABAQUS input file for single axisymmetric element under uniaxial force controlled loading, requiring UMAT spin_elas_def.f
spin_shear.inp	ABAQUS input file for a single plane strain element under simple shear, requiring UMAT spin_elas_def.f
spin_shear_aba.inp	ABAQUS input file for a single plane strain element under simple shear, using ABAQUS*ELASTIC

visco

uni_visco_imp.f	Closed form Fortran implicit solution for uniaxial elasto-viscoplasticity
uni_visco_exp.f	Closed form Fortran explicit solution for uniaxial elasto-viscoplasticity
visco_imp.f	UMAT for plane strain and axial symmetry for elastic, linear strain hardening viscoplastic behaviour using implicit integration using the initial tangent stiffness, using ABAQUS stress and strain quantities. Suitable for large deformations
visco_imp_axidisp.inp	ABAQUS input file for single axisymmetric element under uniaxial displacement controlled loading, requiring UMAT visco_imp.f

238 Appendix B: Fortran coding

visco_imp_axiforce.inp	ABAQUS input file for single axisymmetric element under uniaxial force controlled loading, requiring UMAT visco_imp.f
visco_imp_beam.inp	Four point bend loading requiring UMAT visco_beam.f, requiring mesh file beam_mesh.inp

Index

- ABAQUS 141, 149, 150, 167, 169, 235
- ABAQUS input files 169
- accumulated plastic strain 23
- Almansi strain 50
- angular velocity tensor 63
- anisothermal cyclic plasticity 220
- antisymmetric 51
- Armstrong–Frederick 21
- associated flow 18
- axial vibration 106, 115

- B** matrix 99
- back stress 29
- backward Euler integration 146, 161
- Bauschinger effect 28
- bcc 6
- biaxial creep tests 213
- bowing 212
- Burger's vector 8

- calculus of variations 85
- cantilever beam 118
- Cauchy stress 72
- Cauchy–Green tensor 49, 50
- cavitation 210
- central difference method 136
- Chaboche 31
- coarsening 209
- combustion chambers 209
- conservation of energy 84
- consistency condition 20
- consistent Jacobian 153
- consistent tangent stiffness 153
- consolidation 199
- constant strain element 99
- constitutive equations 40
- continuum tangent stiffness 172
- continuum damage 210
- continuum Jacobian 172
- continuum plasticity 10
- continuum spin 61
- contracted tensor product 15

- convergence 140
- co-rotational 73
- creep 209
- CREEP subroutine 202
- critical resolved shear stress 7
- crystal plasticity 5, 9
- crystallographic orientation 3
- crystallographic slip 5
- cyclic hardening 37
- cyclic plasticity 219

- deformation-enhanced grain growth 190
- deformation gradient 48
- deformed configuration 48
- densification rate 201
- deviatoric stress 14
- diagonalization 56
- differentiation of a tensor 231
- dilatation 201
- direction of plastic flow 19
- dislocation bowing 212
- dislocation density 210
- displacement-based finite element method 98
- divergence of a second-order tensor 233
- double contracted product 15
- Duva and Crow 200
- dyadic product 230
- dynamical path 84

- effective plastic strain rate 14
- effective stress 13
- elastic predictor 147
- elastic stiffness matrix 22, 100
- elastic–plastic deformation 11
- engineering shears 100
- equations of motion 90
- equilibrium 83
- equivalent stress 13
- Euler–Lagrange equation 86
- explicit finite element methods 1, 141
- explicit integration 136, 143

240 Index

- fcc 6
- finite element formulation for plasticity 133
- finite element method 83
- finite rotations 57
- first variation 87
- forward integration 145

- Gauss quadrature 126
- geometric non-linearity 108
- gradient of a first-order tensor 232
- gradient of a scalar 232
- gradient of a second-order tensor 232
- grain boundaries 3
- grain growth 190
- grain size 190

- Hamilton's principle 84
- hardening 23
- Helmholtz free energy 210
- Hooke's law 22, 170
- hydrostatic stress 14
- hysteresis 222

- identity tensor 42
- implicit 140, 143
- implicit finite element methods 143
- implicit implementation for elasto-viscoplasticity 161
- implicit integration 146
- implicit scheme 146
- incompressibility 3, 12
- incremental nature of plasticity 35
- incremental rotation 176
- initial tangential stiffness method 140
- integration point 126
- intergranular cracking 224
- intergranular creep fracture 217
- intermediate configuration 66
- internal variables 40
- isoparametric 109
- isotropic hardening 150

- J_2 plasticity 17
- Jacobian 150
- Jaumann stress rate 76
- J-integral 84

- Kinematic hardening 27
- kinematics 47
- kinetic energy 84

- Lagrangian 84
- Lame constant 42
- large deformation(s) 47
- leap frog explicit method 137

- mass and spring system 90
- mass matrix 105
- material objectivity 69
- material reference frame 48
- material stress rate 78
- mean stress 14
- microstructural evolution 190
- Mohr's circle 69
- momentum balance equations 106
- multiaxial creep strain rate 212
- multiaxial stress state 20, 212
- multiplicative decomposition 67

- necking 187
- Newton iteration 148
- Newton's method 148
- Newton-Raphson method 141
- nickel alloy C263 209
- nickel-base superalloy 209
- nodal force vector 112
- nodal forces 107
- non-conservative 84
- non-linear kinematic hardening 32
- norm 30
- normal grain growth 190
- normality hypothesis 18
- notched bar test 215

- objective stress 72
- objectivity 69
- one-dimensional rod element 99
- original configuration 48
- orthogonality 58
- out of phase loading 225
- over-stress 38

- particle cutting 209
- perfect plasticity 11
- plane stress 18
- plastic correction 146
- plastic deformation gradient 66
- plastic multiplier 19
- plastic strain rate tensor 14
- polar decomposition theorem 57
- polycrystal 3
- polycrystalline 3
- porosity 199
- porous plasticity 199
- potential energy 84
- potential function 45
- power-law creep 44
- Prager 29
- precipitate coarsening 209
- precipitate cutting 209
- precipitate spacing 210
- predictor-corrector 146
- principal coordinates 56

- principal stresses 13
- principle of virtual work 90

- quasi-static problems 105

- radial return method 146
- rate-dependent plasticity 38
- rate of deformation 60
- reaction 130
- reversed plasticity 28, 219
- rigid body rotation 57
- rotation 233
- rotation matrix 58

- Schmid's law 7
- second-order tensors 229
- second stress invariant 17
- semi-implicit integration 160
- shape functions 97
- shearing 3
- simple shear 58
- single and multiple element uniaxial tests 171
- single element simple shear test 178
- skew 51
- slip system 5
- solvus temperature 209
- spin 61
- stability of the explicit time stepping 139
- static grain growth 190
- stationary value 87
- stiffness matrix 105
- strain decomposition 11
- strain measure 49
- strain-rate sensitivity 39, 186
- strain tensor 100
- stress space 17
- stress tensor 14
- stress transformation 72
- stress vector 70
- stretch 48
- stretch ratios 54
- superplastic forming 192
- Superplasticity 185

- tangent stiffness 140, 150
- tangential stiffness matrix 150
- tension-torsion 213
- tensorial notation 229
- tensors 229
- thermo-mechanical fatigue 219
- thinning 195
- time-dependent plasticity 38
- time-independent plasticity 11
- Ti-MMCs 205
- titanium alloy, Ti-6Al-4V 189
- traction 70
- transformation of stress 72
- transverse vibration 118, 122
- Tresca 17
- trial stress 147
- true strain 53
- truss element 99

- UMAT 169
- undeformed configuration 48
- uniaxial loading 14, 42
- update of stress 143
- upsetting 42

- velocity gradient 60
- verification of the model implementation 171
- virtual work 90
- viscoplasticity 38
- viscous stress 39
- Voigt notation 19, 100
- volume changes 199
- von Mises 17

- weak formulation 83
- work conjugacy 111

- yield criteria 17
- yield function 17
- yielding 3

This page intentionally left blank

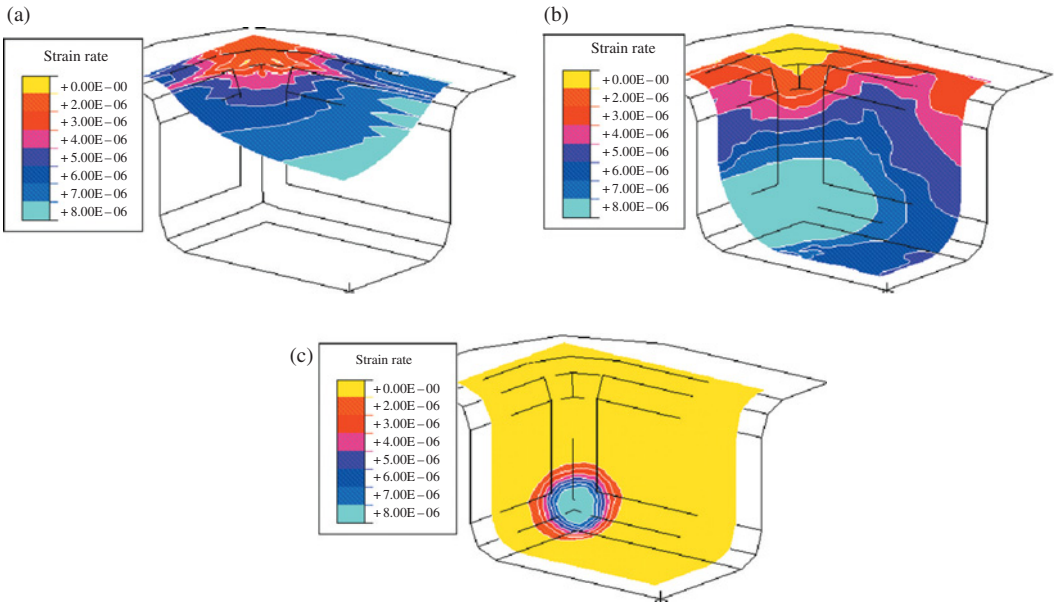


Plate 1 The simulated superplastically deforming sheet showing the effective plastic strain rate at fractional processing times of $t/t_f = 0.1$, $t/t_f = 0.6$, and $t/t_f = 1.0$.

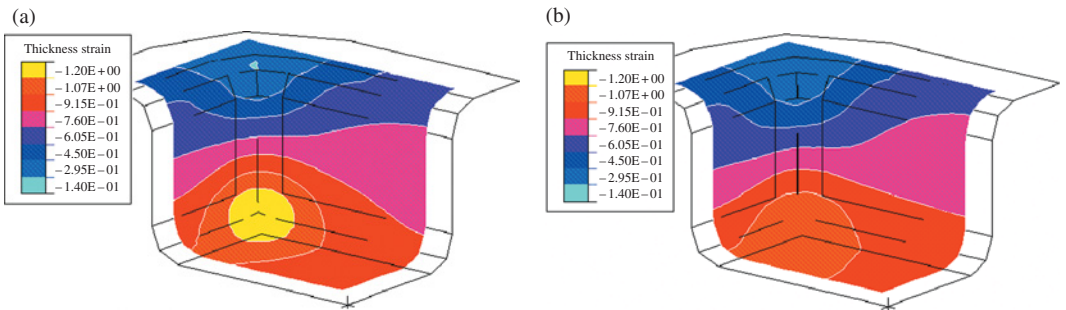


Plate 2 Through-thickness strain fields at the end of the superplastic forming carried out with target maximum strain rates of (a) 1.0×10^{-5} and (b) $1.0 \times 10^{-4} \text{ s}^{-1}$.

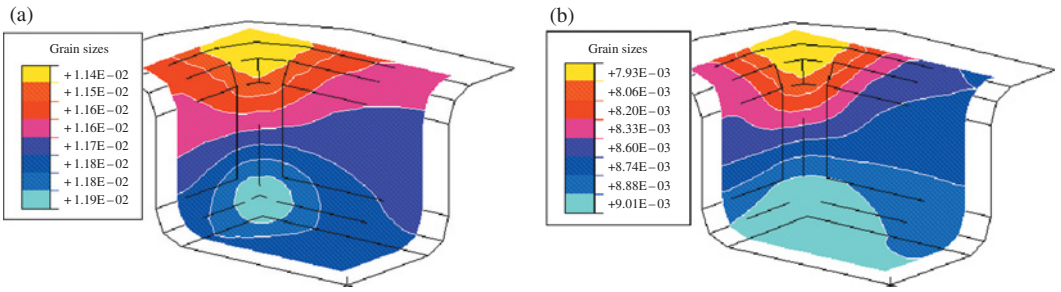


Plate 3 Average grain size fields at the end of the superplastic forming carried out with target maximum strain rates of (a) 1.0×10^{-5} and (b) $1.0 \times 10^{-4} \text{ s}^{-1}$.

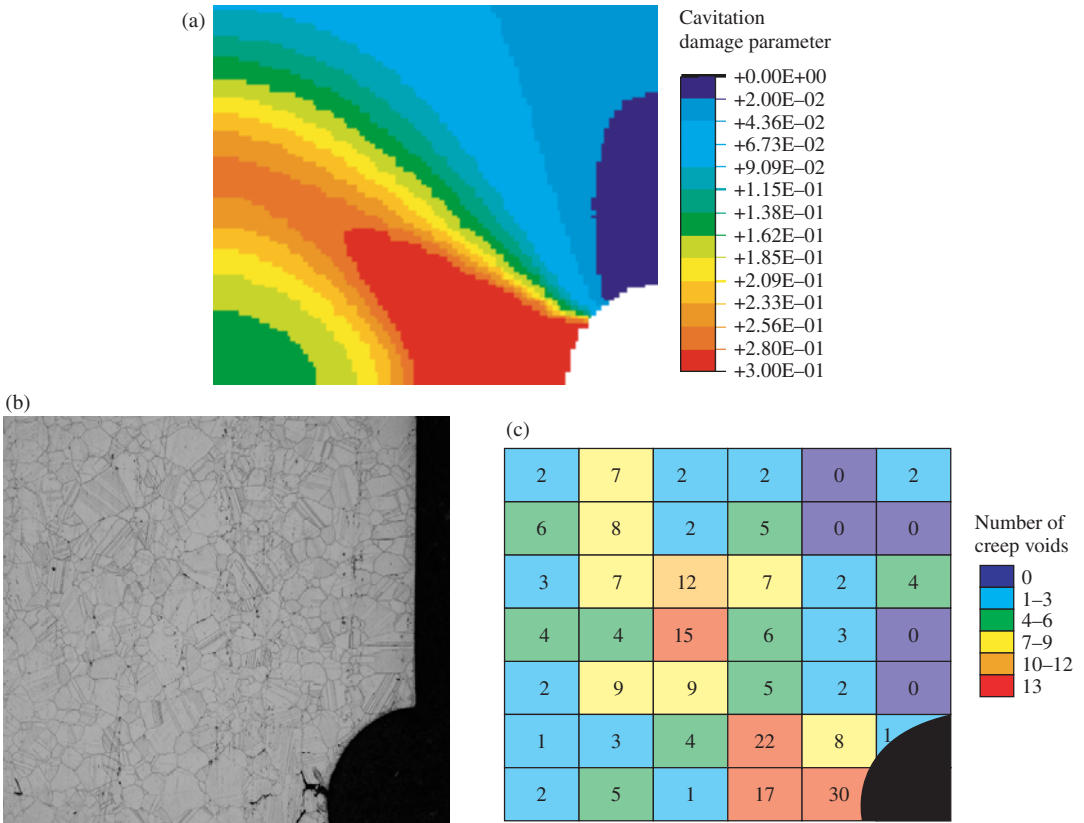


Plate 4 Creep damage fields (a) predicted by the model, (b) observed in the microstructure, and (c) from a surface void count using the micrograph.